Protein and Reaction Engineering of P450 Enzymes for Selective Oxidations

Joel Hoong Zhang Lee

Supervisors:

Assoc. Prof. Stephen G. Bell

Assoc. Prof. Keith E. Shearwin

Dr. Charlotte Williams

Thesis submitted for the degree of Doctor of Philosophy

THE UNIVERSITY of ADELAIDE

July 7, 2023

School of Physical Sciences

Contents

Abstract

Cytochrome P450 monooxygenase enzymes are versatile catalysts capable of selective C-H bond oxidation reactions. Mutation of the highly conserved active site threonine to a glutamate residue is able to convert P450 monooxygenases into peroxygenases that can utilise H_2O_2 alone for catalysis and without relying on expensive co-factors or electron transfer partner proteins. Mutant T252E of CYP199A4 is an engineered P450 peroxygenase and was first used in this thesis to study peroxide-driven activity with both H_2O_2 and a gentler chemical oxygen surrogate, urea-hydrogen peroxide (UHP). UHP and H_2O_2 both showed comparable levels of product formation when used by the T252E mutant for P450-catalysed *O*-demethylation of 4-methoxybenzoic acid. It was also demonstrated that the T252E mutant had higher stability towards H_2O_2 in the presence of a substrate that can undergo C-H bond abstraction. Deuterated substrates were used with both monooxygenase and peroxygenase pathways. It was found that no kinetic isotope effect was present in the C-H bond abstraction step of either pathway. A light-driven flavin system that generates H_2O_2 was then tested with T252E-CYP199A4 and a natural P450 peroxygenase, $P450_{BS\beta}$. Efficient product formation was observed using this light-driven system with both P450 peroxygenases.

Three different oxidase enzymes that generate H_2O_2, alditol oxidase (AldOx) from *Streptomyces coelicolor* A3(2), formate oxidase (AoFOx) from *Aspergillus oryzae* and an engineered choline oxidase (AcC06-AcChOx) from *Arthrobacter cholorphenolicus* were investigated for biocatalytic cascade reactions with P450 peroxygenases. Two of these oxidase enzymes, AldOx and AcC06-AcChox were expressed in sufficient yield in *E.coli* for further study. Both AldOx and AcC06-AcChox enzymes were able to generate H_2O_2 for T252E-CYP199A4 to drive P450 peroxygenase reactions. Reactions of T252E-CYP199A4 involving AldOx formed higher levels of P450 product compared to AcC06-AcChox. AldOx also allowed metabolite formation with $P450_{BS\beta}$ through peroxygenase activity.

Isothermal (Gibson) DNA assembly was then used to construct two-domain multifunctional fusion enzymes consisting of an oxidase joined by an amino acid linker to a P450 enzyme. Plasmids containing the DNA sequence of fusion enzymes of AldOx, AcC06-AcChOx and AoFOx linked to T252E-CYP199A4 were successfully constructed but production of these larger constructs in *E.coli* was poor. Peroxygenase reactions involving immobilising the T252E mutant of CYP199A4 to SOURCE15Q ion exchange media were undertaken. The immobilised T252E mutant was able to catalyse P450 peroxygenase activity levels comparable to the enzyme in free solution. Peroxygenase

activity remained even after the T252E mutant was immobilised for 100 h. Biocatalytic flow reactions were then performed using the T252E mutant immobilised to a bed of SOURCE15Q media within a chromotography column. Low levels of product formation were observed in these flow biocatalysis reactions.

The engineered P450 peroxygenase, T252E-CYP199A4 was crystallised with 4-methoxybenzoic acid and used for *in crystallo* peroxygenase reactions that were monitored through X-ray crystallography. Crystals of the substrate-bound T252E mutant were soaked in different concentrations of H_2O_2 for varying lengths of time. The structures of three of these H_2O_2-soaked crystals were solved and reported. *In crystallo* demethylation of the substrate to form 4-hydroxybenzoic was observed within these crystals to different degrees depending on the conditions tested. The active site structure of the enzyme in these crystals after soaking with H_2O_2 did not differ significantly from a previously reported structure of the T252E mutant. An X-ray crystal structure of T252E-CYP199A4 directly co-crystallised with 4-hydroxybenzoic acid was also solved and used for comparison.

CYP17A1 is steroid metabolising mammalian P450 enzyme capable of catalysing a challenging C-C bond cleavage reaction. Seeking to study the mechanism of C-C bond cleavage reactions in more detail using a microbial P450, α-hydroxy ketone probes were synthesised as substrates for the benzoic acid metabolising P450, CYP199A4. Low activity with these substrate probes was observed with WT CYP199A4 and mutagenesis was carried out to improve the C-C cleavage activity of this enzyme. The F182L mutant had the capability of enzyme-catalysed C-C bond cleavage with one of the α-hydroxy ketone substrates, JCM 1. Further experiments with the F182L mutant with other α-hydroxy ketone substrates generated in a one-pot reaction from initial ketone compounds also showed metabolite formation consistent with C-C cleavage activity. The C-C cleavage reaction of the F182L mutant with JCM 1 showed an inverse kinetic solvent isotope effect (KSIE), while hydroxylation reactions with this mutant showed a standard KSIE. This implies that the C-C cleavage step between JCM 1 and F182L-CYP199A4 would involve a different reaction intermediate than that of P450-catalysed hydroxylation. A crystal structure of the F182L mutant co-crystallised with JCM 1 was also solved. The structure of the active site revealed the (*S*)-enantiomer of JCM 1 was the preferred enantiomer and was held in a position that could mimic the topology of the C-C cleavage reaction of CYP17A1.

CYP199A4 was then used to explore P450-catalysed aromatic hydroxylations. WT CYP199A4 is unable to oxidise the aromatic substituent of 4-phenylbenzoic acid despite efficiently oxidising aliphatic C-H bonds on the similarly sized substrate, 4-

cyclohexylbenzoic acid. Co-crystallisation of this enzyme with 4-phenylbenzoic acid was carried out and its structure solved. The active site of this enzyme when bound to 4-phenylbenzoic acid was found to be similar to that of the same enzyme bound to 4-cyclohexylbenzoic acid. Based on the structure of WT CYP199A4 complexed with 4-phenybenzoic acid, the F182L mutant was tested and it was able to catalyse metabolite formation consistent with P450-dependent aromatic hydroxylation. A control reaction with the F182L mutant with 4-cyclohexylbenzoic acid showed aliphatic hydroxylation but there were changes in regioselectivity compared to the same reaction with the WT enzyme.

Declaration

I certify that this work contains no material which has been accepted for the award of any other degree or diploma in my name, in any university or other tertiary institution and, to the best of my knowledge and belief, contains no material previously published or written by another person, except where due reference has been made in the text. In addition, I certify that no part of this work will, in the future, be used in a submission in my name, for any other degree or diploma in any university or other tertiary institution without the prior approval of the University of Adelaide and where applicable, any partner institution responsible for the joint award of this degree. The author acknowledges that copyright of published works contained within the thesis resides with the copyright holder(s) of those works. I give permission for the digital version of my thesis to be made available on the web, via the University's digital research repository, the Library Search and also through web search engines, unless permission has been granted by the University to restrict access for a period of time.

I acknowledge the support I have received for my research through the provision of an Australian Government Research Training Program Scholarship and the CSIRO Synthetic Biology Future Science Platform for a PhD Supplementary Scholarship.

Joel Lee

July 7, 2023

Acknowledgements

This thesis was supported by the CSIRO Synthetic Biology Future Science Platform and I am immensely grateful for a PhD top-up scholarship provided by CSIRO. I also thank the University of Adelaide for providing me with the Constance Fraser Scholarship to support my studies.

This thesis would also not have been possible without my supervisor, A/Prof Stephen Bell. I first worked with him in 2014 and he has never stopped being a wealth of ideas, inspiration and motivation. Many thanks Stephen for giving me the chance to work with you and the support you have given me all this time. I would like to also thank Dr Charlotte Williams from CSIRO for being so immensely helpful with all the feedback, support and ideas through various points of my PhD. Your positivity and encouragement has been invaluable to me. Many thanks to A/Prof Keith Shearwin for being kind and supportive while also providing feedback on the Molecular Biology portions of this thesis. I would also like to thank Dr John Bruning for all the feedback and assistance with the crystallography portions of this thesis.

I am also immensely grateful for the support and friendship of all members of Bell group past and present. Thanks to Daniel Doherty for always willing to provide help whenever needed and for reading a chapter. Alecia Gee for assisting me during her placement with our lab, for reading a chapter and also being such a friendly and kind person. Amna Ghith for being so supportive, encouraging and fun to talk to through various stressful times in the lab. Jinia Akter for always organising outings for everyone and also sharing my interests in food and bubble tea. Matthew Podgorski for providing such detailed protocols whenever we ask for help. Many thanks to Alix Harlington for also reading another chapter of this thesis and for providing witty and friendly conversation whenever we meet. I would also like to thank Matthew Bull for all the work and effort he has put into maintaining all the analytical instruments I used throughout my PhD. You have always provided a welcoming environment for me to commiserate any troubles I've had over the past few years.

I could not have gotten through doing a PhD during a pandemic without the friendship and camaraderie of all the friends I have met since working in Level 3 of MLS. To Timothy Allen, my office writing buddy, thanks for the banter and for sending me home all the time. Thank you Claudia Neramitr for being a ray of sunshine and kindness whenever you drop by to our office. To Emily Kirby, Brooke Trowbridge and Xavier Montin for providing good, funny conversations with great company and taking care of me. Thanks Emily and Xavier for also sending me home. To Eunice Lee, thank

you for your friendship and heart-warming talks since our first year of university. To Byron Shue, your friendship and fun-loving ways have supported me so much these past few years and thanks for all the happiness and fun adventures.

This thesis was also blessed with support from friends in my home town of Ipoh, Malaysia. To the Morris siblings, Andrina, Alex and Alicia thank you for 15 years (probably more) years of friendship, support and sessions of " inspiration ". I am also immensely grateful to your parents, Angelica and Anthony for always being kind and welcoming to me. To the Jalleh family, Valarie, Julian, Martin and Terry, I am always very touched by your warmth, friendship and humour. To Terry especially, for being a kind, warm and gracious mother figure in my life. To Freddie Choong, we have known each for a long time and I cannot express how grateful I am of your friendship, support and banter. To Isaac Stephen, I am proud to call you my friend, your resilience and friendship will always hold a special place in my heart. To the late Brother Matthew Bay, thank you for the unspoken lessons on responsibility and what it means to lead through actions and not words. Thank you Br. Matt and Isaac for giving a quiet and lonely person like me, a place where he felt like he belonged.

To my mom, Francisca Lo, words cannot describe the sacrifice and hard work that you went through all my life to give me the future you never had. Thank you for the love and support. To my sister, Rachel Lee, thank you for keeping me company and the bubble tea you always buy me.

Finally, if you are reading this, thank you for taking the time to do so.

Abbreviations

AcCO6	Mutant S101A/D250G/F253R/V355T/F357R/M359R
ADH	Alcohol Dehydrogenase
AldOx	Alditol Oxidase from *Streptomyces coelicolor*
AcChOx	Choline Oxidase from *Arthrobacter cholorphenolicus*
AoFOx	Formate Oxidase from *Aspergillus oryzae*
DTT	Dithiothreitol
E.coli	*Escherichia Coli*
EtOH	Ethanol
EtOAc	Ethyl Acetate
GC-MS	Gas Chromatography-Mass Spectrometry
HCl	Hydrochloric Acid
HPLC	High Performance Liquid Chromatography
HS	High Spin
IPTG	Isopropyl β-D-thiogalactopyranoside
IS	Internal Standard
KIE	Kinetic Isotope Effect
KSIE	Kinetic Solvent Isotope Effect
LB	Luria-Bertani Medium
UHP	Urea-hydrogen peroxide
PDB	Protein Data Bank
NADH	Reduced form of Nicotinamide Adenine Dinucleotide
$NaHCO_3$	Sodium Bicarbonate
NMR	Nuclear Magnetic Resonance
SOC	Super Optimal Broth with Catabolite Repression
WT	Wild-Type enzyme
TIC	Total Ion Count

List of Figures

List of Tables

Publications

This thesis is based on the following publications (currently published and under preparation as of the 17th of April 2023) that detail some of the research undertaken during the period of candidature.

Lee, J.H.Z.; Podgorski, M.N.; Moir, M.; Gee,A. R.; Bell S. G., Selective Oxidations Using a Cytochrome P450 Enzyme Variant Driven with Surrogate Oxygen Donors and Light, *Chem. Eur. J.* **2022**, *28*.

Lee, J.H.Z.; Akter, J.; Harlington, A.C.; Whelan, F.; Bell, S.G., Regio- and Stereoselective Carbon-Hydrogen Bond Oxidations using an Oxidase and an Engineered Monooxygenase Cascade.

Lee, J.H.Z.; Bruning, J.B.; Bell, S.G., Evidence of *In Crystallo* Peroxygenase Reactions with T252E-CYP199A4.

Miller, J.C.*; **Lee, J.H.Z.***; Mclean, M.A.; Chao, R.R.; Stone, I.S.J.; Pukala, T.L.; Bruning, J.B.; De Voss, J.J.; Schuler, M.A.; Bell, S.G., Engineering C–C Bond Cleavage Activity into a P450 Monooxygenase Enzyme, *J. Am. Chem. Soc.* **2023**.

Coleman T.*; **Lee, J.H.Z.***; Podgorski, M.N.; Bruning, J.B.; De Voss, J.J.; Bell, S.G., Investigation of α-Hydroxycarbonyl Formation and Subsequent C-C Bond Cleavage by Cytochrome P450 Monooxygenase Enzymes.

Coleman T.; Kirk, A.M.; **Lee, J.H.Z.**; Doherty, D.Z.; Bruning, J.B.; Krenske, E.H.; De Voss, J.J.; Bell, S.G., Different Geometric Requirements for Cytochrome P450-Catalyzed Aliphatic Versus Aromatic Hydroxylation Results in Chemoselective Oxidation, *ACS Catal.* **2022**, *6*, 1-15.

Coleman, T.; **Lee, J.H.Z.**; Kirk, A.M.; Doherty, D.Z.; Podgorski, M.N.; Pinidiya, D.K.; Bruning, J.B.; De Voss, J.J.; Krenske, E.H.; Bell, S.G., Enabling Aromatic Hydroxylation in a Cytochrome P450 Monooxygenase Enzyme through Protein Engineering, *Chem. Eur. J.* **2022**, *28*.

*These authors contributed equally to this work.

This page is intentionally left blank

1 Introduction

1.1 Biocatalysis in Sustainable Chemistry

Biocatalysis is defined as the use of natural or biologically derived substances to enable a chemical reaction to occur at increased rates, these involve proteins known as enzymes.[1] Enzymes in particular have remarkable capability as catalysts. Different enzymes can accept a wide array of molecules with complex architectures as substrates and enzymatic reactions often occur with unparalleled regioselectivity and enantioselectivity.[2] This high selectivity provides a distinct advantage over organic synthesis, whereby tedious blocking and de-blocking steps to protect vital functional groups in conventional chemistry is common to achieve regio- and enantioselectivity. The lack of additional synthetic steps also results in highly efficient reactions with fewer by-products; this, alongside the mild reaction temperatures afforded with enzymes provide an environmentally friendly alternative to conventional chemistry.

Early use of enzymes in industry have primarily focused on the synthesis of chiral intermediates for pharmaceutical applications.[2,3] In the next decade, changing current chemical manufacturing processes towards greener and sustainable approaches will become vital and biocatalysis is an important route to achieve this change. Enzymes are typically used either as isolated proteins *in vitro*, or in whole-cell, *in vivo* systems. These two approaches to biocatalysis are both currently used in industry and are active areas of research. For example, the synthesis of trimethyl L-leucine, an important chiral intermediate for pharmaceutical applications has been achieved using isolated enzymes and whole-cell systems.[4] This intermediate is used as a precursor to synthesise anti-tumour, anti-viral, anti-inflammatory and anti-HIV drugs.[5–8] Trimethyl L-leucine is produced biocatalytically using leucine dehydrogenase from trimethyl pyruvic acid, an ammonium ion and NADH (Figure 1.1). A second enzyme, formate dehydrogenase regenerates the NADH used in the first enzymatic reaction for a further round of catalysis.[9,10]

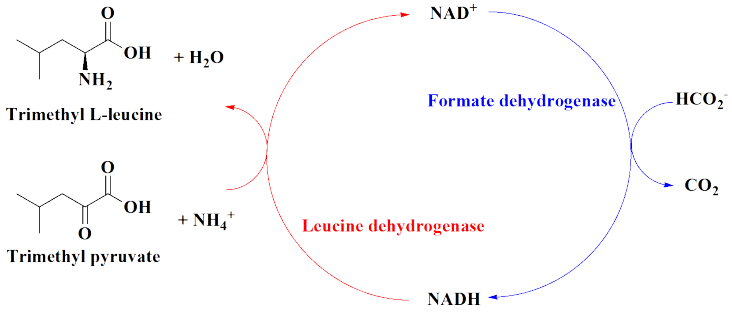

Figure 1.1: Enzymatic synthesis of L-tertiary leucine.

Despite the strong capability of enzyme biocatalysis, their stability, cost and need to engineer selectivity to non-physiological substrates via mutagenesis limits their use.[11,12] In recent years however, the availability of low cost synthetic genes have allowed for the rapid and affordable screening of libraries containing diverse enzyme variants and consequently enabled an acceleration in the development of biocatalysts.[11]

1.2 Heme-Dependent Oxygenases

Nature is able to carry out the numerous chemical transformations needed to sustain life through the use of protein-based enzymes that are made from polypeptide chains from the 20 genetically encoded amino acids.[13] The 3-dimensional folding of these polypeptide chains with the functional groups afforded by the amino acid residues already allows complex and diverse chemistry to be carried out by enzymes via simple acid-base catalysis.[13] However, many biological reactions often require metallic or organic cofactors which in concert with the spatial configuration of amino acid residues provide catalytic capabilities for reactions that can prove challenging for conventional chemistry.[13]

An important cofactor that supports life in our predominantly aerobic atmosphere is the iron-containing heme prophorphyrin IX cofactor (Figure 1.2). Redox active metals such as iron possess unpaired *d*-orbital electrons and can act as a mediator in the reductive activation of oxygen.[14] This allows metalloenzymes that contain heme to form metal-oxygen complexes.[14,15] These metal-oxygen complexes serve as intermediates within many biological pathways including aerobic respiration and photosynthesis.[15] For the purpose of biocatalysis, metalloenzymes with heme centres that are able to activate atmospheric oxygen and insert oxygen atoms into C-H bonds are known as oxygenases.

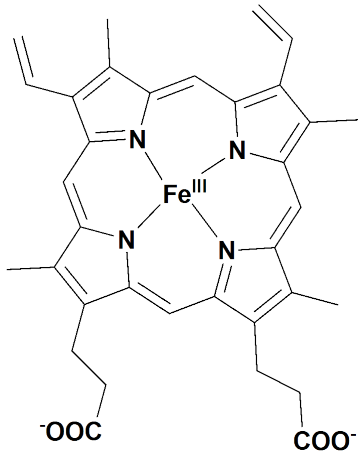

Figure 1.2: Structure of iron prophorphyrin IX.

Cytochrome P450 enzymes are a class of heme metalloenzymes which primarily func-

tion as monooxygenases (Section 1.3).[16] Chloroperoxidase (CPO) is another heme metalloenzyme that catalyses halogenation and monooxygenase reactions.[17]

1.3 Cytochrome P450 Enzymes

Cytochrome P450 (P450) enzymes are a ubiquitous superfamily of heme metalloenzymes with 300,000 catalogued P450 sequences (as of 2017) across all domains of life with more to be discovered.[18] The majority of these P450 enzymes function as monooxygenases that oxidise unactivated C-H bonds through the insertion of an oxygen atom (Equation 1.1). Oxidation of these bonds occur with high regio- and stereoselectivity.

$$\text{R-H} + \text{O}_2 + \text{H}^+ + \text{NAD(P)H} \rightarrow \text{R-OH} + \text{H}_2\text{O} + \text{NAD(P)}^+ \tag{1.1}$$

The primary reaction catalysed by P450s is hydroxylation. (Equation 1.1).[19] However, P450s have been studied extensively for decades[16] and have been observed to catalyse reactions including, but not limited to, epoxidation,[20,21] desaturation,[22,23] aromatic oxidation,[24,25] carbon-carbon bond cleavage,[26,27] Baeyer-Villiger oxidation,[28] heteroatom dealkylations and oxidations.[29,30]

P450 enzymes are categorised according to families and subfamilies. Family members share $\geq$ 40 % amino acid sequence similarity and subfamily members share $\geq$ 55 % similarity.[31] These enzymes are designated by the prefix CYP, that indicates it is a P450 enzyme, followed by its family number. For example, CYP1 - CYP49 are mammalian P450 families and CYP101 to CYP281 are bacterial families.[18] Following the family number, its subfamily is denoted by the subsequent letter and number.[31] For example, CYP101A1 from *Pseudomonas putida*,[32] is a member of family 101 and is the first member identified for subfamily A of this family.

All cytochrome P450 enzymes contain an iron protoporphyrin IX (heme) centre within the polypeptide structure.[33] This centre is similar to those found in hemoglobin and heme peroxidases such as horseradish peroxidase. The ferric iron centre when reduced to its ferrous form will bind strongly to O_2 but will preferentially bind CO. The heme proximal ligand binding site is bound to a highly conserved cysteine thiolate residue.[34,35] The formation of the ferrous-CO complex gives rise to a Soret maxima at $\sim$450 nm that is a defining spectral property for these enzymes of which the name "P450" comes from.[36] This Soret peak is attributed to the coordination of the heme to cysteine thiolate.[36]

The distal binding site contains a water ligand that is easily displaced upon the binding of a suitable substrate and is observed in most crystal structures of substrate-free P450.[16,34] Substrate binding will initiate the catalytic cycle of P450s in the presence of suitable redox partners and cofactors (Section 1.4).

1.4 The Catalytic Cycle of P450s

The catalytic reaction cycle of monooxygenase P450s and its various intermediates was first studied spectroscopically by Estabrook *et. al* in 1971 (Figure 1.3).[37]

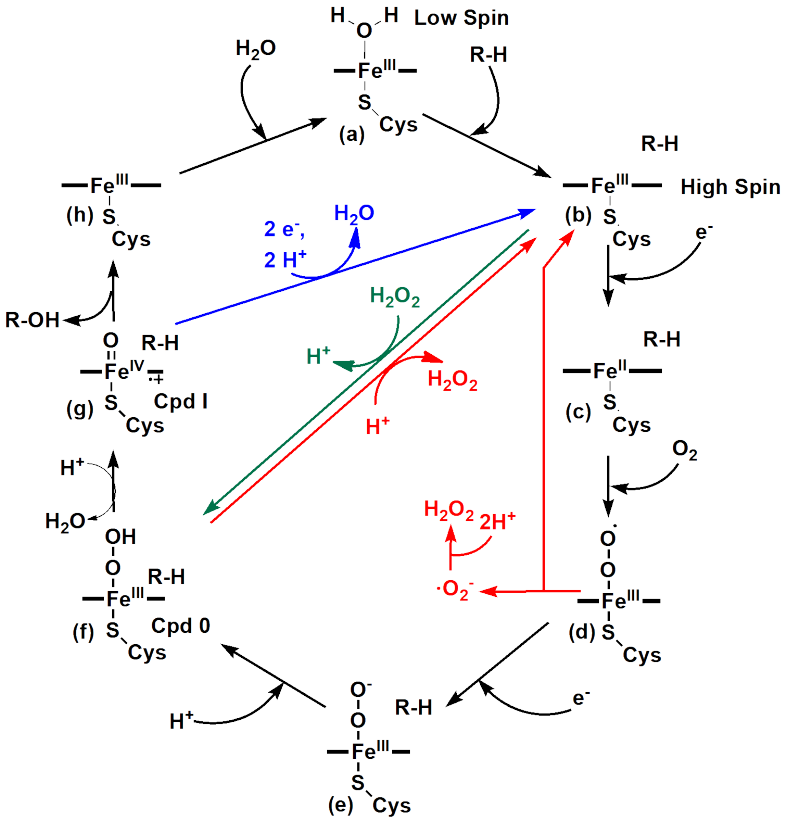

Figure 1.3: The catalytic cycle of P450 enzymes. The peroxide shunt pathway is shown in green while uncoupling reactions that generate hydrogen peroxide (H_2O_2) are shown in red.[33,38] The oxidase uncoupling pathway is shown in blue.[39]

This multi-step cycle (Figure 1.3)[40] is first initiated through the binding of substrate to displace the bound distal water ligand in its resting state (a). This causes the heme-iron complex to shift from low-spin to high-spin (b). The 5 coordinate high-spin complex is easily reduced and can accept an electron from NAD(P)H via electron transport partners that will reduce the ferric (Fe^{3+}) centre to the ferrous (Fe^{2+}) form (c). Subsequently, the binding of O_2 generates the ferrous dioxygen complex (d). This complex then accepts an electron to form the ferric-peroxo anion (e).[41] The delivery of a proton to complex (e) acting as a Lewis base forms the ferric-hydroperoxo complex

(f). This hydroperoxo complex is known as Compound 0 (Cpd 0). Cpd 0 then accepts another proton and its dioxygen bond undergoes heterolytic cleavage to form a water molecule and the active oxidant in this cycle, a ferryl-oxo-porphyrin-cation radical complex, Compound I (Cpd I) (g).[42]

Cpd I will undergo a radical rebound mechanism to insert its activated oxygen atom into the coordinated substrate (Figure 1.4).[43,44] The oxidised product then dissociates from the enzyme and a water molecule binds distally to the ferric centre to reform the resting state. This cycle is thought to be highly conserved across most members of the P450 superfamily.[45]

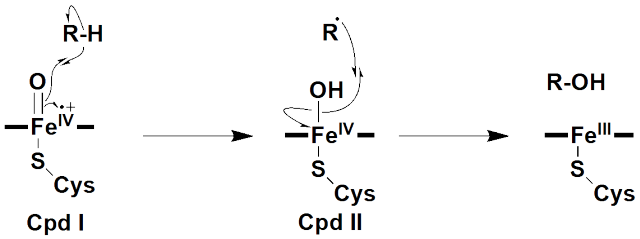

Figure 1.4: Radical rebound mechanism carried out by Compound I (Cpd I) within the catalytic cycle of P450 enzymes. Cpd I has a radical cation centre associated with the heme of the P450.[46] Cpd I first abstracts a hydrogen from the substrate to form Compound II (Cpd II) and the substrate radical.[46] Radical rebound then occurs to insert the activated oxygen atom from Cpd II into the substrate radical.

The displacement of the P450-bound water ligand by a substrate results in a shift from low spin (LS) to high spin (HS) ferric state. This is accompanied by a spectroscopically detectable shift from $\sim$ 418 nm (LS, substrate-free) to $\sim$ 390 nm (HS, substrate-bound).[47] This is known as a type I spectrum and the amplitude of this spectral shift can be used to determine the proportion of enzyme in the LS and HS state.[48] A type II spectrum can be observed when a red-shift from $\sim$ 418 nm to $\geq$ 420 nm occurs that is indicative of a ligand forming a 6-coordinate enzyme complex with a stronger field ligand than H_2O.[47] The presence of a type II shift is usually characteristic of an inhibitory ligand but type II inducing ligands can also be substrates.[49]

As observed in Figure 1.3, the reaction catalysed by the P450 is not necessarily productive. Uncoupling reactions can occur at several different points in the cycle. Uncoupling reactions in the catalytic cycle can generate H_2O_2 from the ferric-hydroperoxo complex (Figure 1.3, f) or the ferric-dioxygen complex (Figure 1.3, d). The electron transfer events occurring in the P450 catalytic cycle also requires the use of an electron transport chain system and electrons sourced from NAD(P)H. Cpd I is highly electron deficient and capable of being reduced by electrons from NAD(P)H.[50] The reaction of Cpd I with electrons will reduce the heme-bound oxygen to form water and is known as the oxidase uncoupling pathway.[39] These uncoupling reactions are unproductive

pathways that lowers efficiency of P450 systems in large scale-syntheses.[51]

1.5 Oxidants in P450 Reactions

One of the major functions of P450 enzymes in humans is the detoxification of xenobiotics through hydroxylation occurring in the liver.[52] The introduction of an alcohol group renders xenobiotics more soluble and susceptible to further modification for later metabolism and elimination. In particular, CYP3A4 in humans is responsible for the metabolism of half of all currently used drugs.[52] P450s are also responsible for the biosynthesis of steroidal compounds.[52]

Activation of a C-H bond is difficult to achieve chemically due to the high energy requirements in cleaving this bond ($\sim$ 100 kcal mol^{-1}).[53,54] The radical rebound mechanism that was primarily developed from the work of Groves *et.al*,[44] uses Cpd I (Figure 1.3 and Figure 1.4) as the oxidant in this mechanism.[33] The radical rebound mechanism proceeds via a two-step H atom abstraction/oxygen rebound mechanism (Figure 1.4).[44] The H-atom abstraction of an alkyl substrate first proceeds to generate a Fe(IV)-OH complex and the substrate radical (Figure 1.4). The substrate radical then recombines with the hydroxyl radical from the Fe(IV)-OH complex to form the hydroxylated product (Figure 1.4).

Cpd I has been established as the main oxidant in most P450 reactions.[55,56] Different reaction intermediates within the general P450 catalytic cycle are also theorised to be capable of catalysing certain oxidation reactions depending on the type of substrate (Figure 1.5).[55–57] For example, the ferric-peroxo species (Figure 1.5) has been proposed to be responsible for oxidative C-C cleavage in CYP17A1, which plays a significant role in steroidal biosynthesis.[58–61]

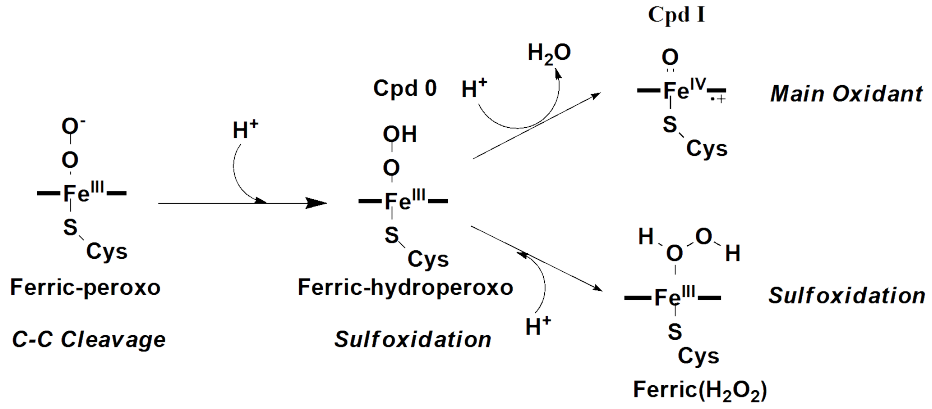

Figure 1.5: Different intermediates of the P450 catalytic cycle and possible reactions catalysed shown in *italics*.

1.5.1 P450 Hydroxylations

The role of Cpd I in P450 hydroxylations has been extensively studied. Green *et. al* reported the long-sought isolation and capture of Cpd I of CYP119A1 through reaction of the ferric P450 with *meta*-chloroperoxybenzoic acid (*m*CPBA).[43] The captured Cpd I was characterised using Mössbauer and EPR spectroscopy, whereby its spectral properties matched the spectra elicited by Cpd I of chloroperoxidase (CPO). The isolated Cpd I of CYP119A1 was directly observed to hydroxylate lauric acid.[43]

Radical clock studies have been used in determining the lifetime of the radical intermediate in the P450 rebound mechanism (Figure 1.4).[62] Radical clock substrates contain strained cyclic structures such as cyclopropyl, bonded to an adjacent carbon atom from which the C-H bond is abstracted. This adjacent carbon atom will then undergo H-atom abstraction by the P450 to become a radical centre that forms a cyclopropylcarbinyl radical. The strained ring structure of the radical can irreversibly rearrange to form the corresponding homoallylic radical.[33] The cyclopropylcarbinyl and homoallylic radical can both be hydroxylated by the P450 forming hydroxylation products for two alternate routes.

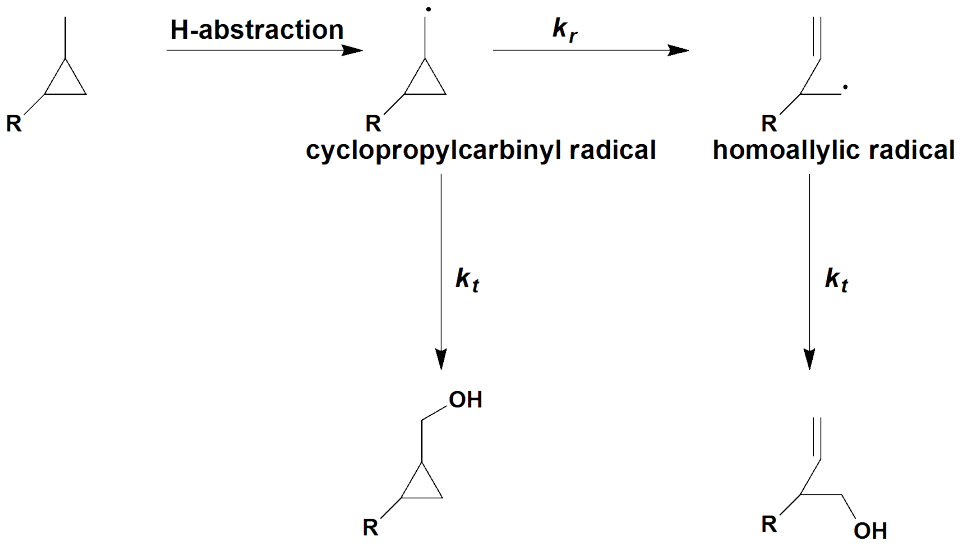

Figure 1.6: Radical trapping of P450 hydroxylation. Strained cyclopropyl substrates after H-abstraction can be trapped (k_t) by P450 hydroxylation or undergo rearrangement (k_r) before hydroxylation.

The ratio between the amount of products from two different hydroxylation pathways can then be used to calculate the lifetime of the radical intermediate.[33,62] Early trapping experiments for the P450 rebound mechanism gave radical lifetimes consistent with reaction intermediates (50 ps).[62] But, these reactions with later ultrafast radical clock substrates were significantly shorter (70 - 200 fs).[62–68] These shorter radical lifetimes were more consistent with that of transition states being used in P450 hydroxylation

rather than reaction intermediates as previously theorised.[64]

Newcomb *et. al* also employed bespoke radical clock substrates designed to distinguish between radical or carbocation intermediates based on the rearrangement products.[65,67] The hydroxylation products formed from P450 reactions with these newly-designed substrates gave evidence of a carbocation intermediate being involved in P450-mediated hydroxylation.[65] The short radical lifetimes and evidence for carbocation intermediates cast doubt on the radical rebound mechanism for P450 hydroxylation reactions and it was theorised that oxidants other than Cpd I were involved in hydroxylation.[65] Cpd 0 was initially theorised to be able to catalyse hydroxylation through direct insertion of a hydronium ion (H_3O^+) that forms a carbocation intermediate with the substrate (Figure 1.7).[65] The proposal that multiple oxidants are involved in P450 reactions is known as the "two-oxidant" theory, where the more abundant oxidant species (Cpd I or Cpd 0) dictates product distribution.[69]

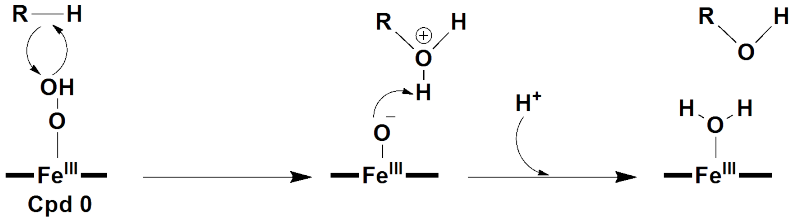

Figure 1.7: Proposed reaction mechanism for Cpd 0 mediated hydroxylation.[65]

Theoretical studies that involve the use of density functional theory (DFT) and quantum mechanical/molecular mechanical (QM/MM) calculations showed that Cpd 0 is too weak an oxidant to facilitate C-H hydroxylation.[70] Shaik *et. al* then proposed an alternate to the two-oxidant theory that relies upon two spin states of Cpd I that were determined using QM/MM calculations.[71,72] In Cpd I, the $3d\pi^*$ (π^*_{FeO}) of the heme-iron centre has two unpaired electrons and one electron in the porphyrin ($a_{2u}\pi^*$) (Figure 1.8, inset).[73] In the quartet high spin state ($^4A_{2u}$), all three electrons are parallel but in the doublet low spin state ($^2A_{2u}$) the electron in the porphyrin $a_{2u}\pi^*$ orbital is inverted (Figure 1.8, inset).[73]

The two spin-states have relatively the same energy requirements for the initial hydrogen abstraction step (Figure 1.8).[74] The quartet $^4A_{2u}$ pathway has high energy barrier during radical rebound that could lead to a carbocation intermediate as determined by DFT calculations.[72] The doublet $^2A_{2u}$ pathway has no significant energy barrier for radical rebound and proceeds directly to the hydroxylated product (Figure 1.8).[74]

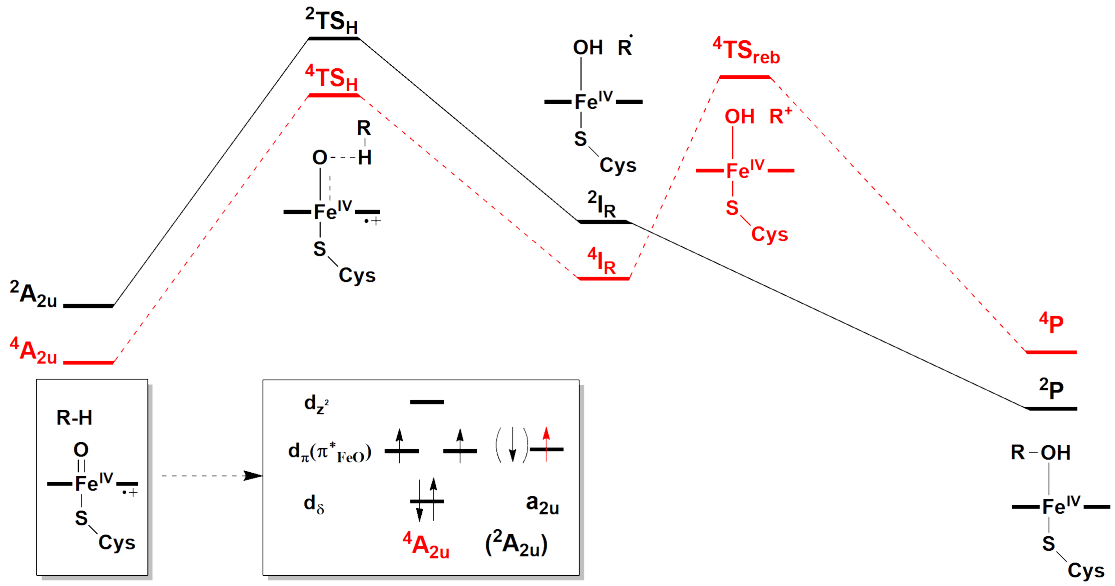

Figure 1.8: Two-state reactivity model for P450 hydroxylation begins with Cpd I in either the quartet $^4A_{2u}$ (red) or doublet $^2A_{2u}$ spin state (black). The electronic configuration of Cpd 1 is shown inset. The two spin-states leads into the transition state for hydrogen abstraction, TS_H, followed by the hydrogen abstraction intermediate (I). The quartet $^4A_{2u}$ pathway possesses an additional higher energy cation intermediate during radical rebound (R^+, TS_{reb}). The two pathways will eventually end with a hydroxylation product (P).

The "barrierless" doublet pathway provides an explanation of the short-radical lifetimes observed by previous radical clock experiments. While the large energy barrier in the quartet pathway that possesses an additional cationic intermediate which would explain the longer radical lifetimes and cationic rearrangement products as discovered in previous experiments.[63,65] This proposed theory is known as the "two-state" reactivity model, and the intermediates (radical or cation) formed depends on the dominant spin-state of Cpd I.[74] The dominance and distribution of the spin-state of Cpd I will depend on the residues surrounding the heme and also the substrate being oxidised.[75–77]

1.5.2 P450 Sulfoxidations

P450 enzymes have also been observed to oxidise organic sulfide molecules either through sulfur dealkylation or direct sulfur oxidation (sulfoxidation).[78] It has been observed both experimentally and through theoretical calculations that the sulfoxidation pathway of sulfide is more favourable over (*S*)-dealkylation with heme-containing enzymes.[30,56,79,80]

Sulfoxidation reactions by P450s have been theorised to involve either Cpd I or Cpd 0. The ferryl oxygen of Cpd I could react directly with the sulfur heteroatom in sulfides (Figure 1.9).[78] Cpd I can also abstract a single electron from the sulfur atom to form a cation radical and oxygen transfer from the ferryl centre to the sulfur occurs to give

the sulfoxide product (Figure 1.9).[78]

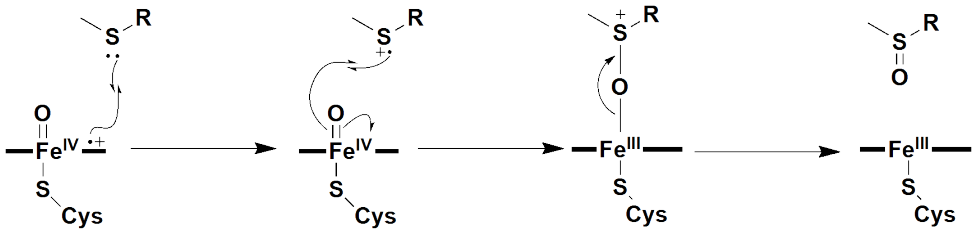

Figure 1.9: Proposed reaction mechanism for Cpd 1 mediated sulfoxidation that proceeds via single-electron transfer from the sulfur atom to heme-iron centre to form a sulfur cation radical.

The ferric-hydroperoxo intermerdiate, Cpd 0 has also been implicated in P450 sulfoxidation.[70,81,82] Mutagenesis studies with CYP102A1 ($P450_{BM3}$) designed to hinder Cpd I but promote Cpd 0 formation by mutating an active site threonine (T268) to an alanine (Mutant T268A) were carried out to investigate the oxidants involved in P450 sulfoxidation reactions.[81,82] Volz *et. al* used dimethyl-(4-methylsulfanylphenyl)amine that can undergo either sulfoxidation (Cpd 0 mediated) or *N*-dealkylation (Cpd I mediated) (Figure 1.10).[82] The T268A mutant of $P450_{BM3}$ was shown to favour sulfoxidation products 60 times more over dealkylation products.[82] Cryle *et. al* have also used the same T268A mutant of $P450_{BM3}$ to investigate the oxidation of thia fatty acids and found sulfoxidation rates were not decreased with this mutation.[81] They also found sulfoxidation of thia fatty acids and equivalent hydroxylation of fatty acids by $P450_{BM3}$ displayed completely opposite enantioselectivity.[81] This once again infers that alternate oxidants may be involved in sulfoxidation.

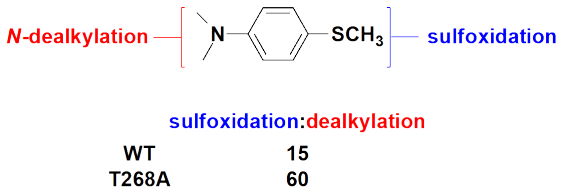

Figure 1.10: Sulfoxidation or *N*-demethylation of dimethyl-(4-methylsulfanylphenyl)amine by $P450_{BM3}$ conducted by Volz *et. al*.[82]

These mutagenesis studies strongly imply that Cpd 0 is involved in sulfoxidation reactions but theoretical calculations have shown that Cpd 0 is a weak oxidant.[70] Shaik have proposed another possible oxidant in P450 sulfoxidation reactions which uses a Fe^{III}-H_2O_2 complex.[83] Theoretical calculations have shown that this complex is an efficient oxidant for P450 sulfoxidation reactions and could oxidise sulfur at a faster rate than Cpd I.[83] The mechanism for this complex begins with the sulfur heteroatom of the substrate undergoing nucleophilic attack by the distal oxygen of heme bound H_2O_2 (Figure 1.11). This is followed by heterolytic O-O bond cleavage of the heme-bound H_2O_2 and proton transfer to insert an oxygen atom into the substrate (Figure 1.11).[83]

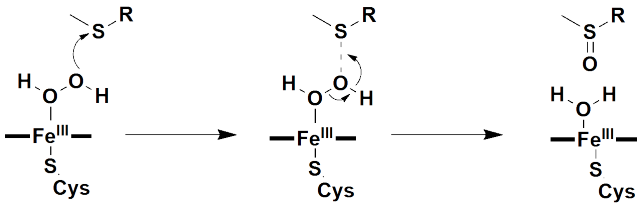

Figure 1.11: Sulfoxidation mechanism of P450s proposed using the Fe^{III}-H_2O_2 complex.

1.5.3 P450 C-C Bond Cleavage Reactions

The capability of cytochrome P450s as powerful oxidants is none more apparent in their ability to catalyse the cleavage of carbon-carbon (C-C) bonds. These P450 catalysed C-C cleavage reactions (lyase reactions) can sometimes involve significant rearrangements of the substrate architecture, multistep oxidative transformations and substrate fragmentation.[84] P450 lyase reactions are usually involved in biosynthetic pathways that generate secondary metabolites such as steroidal compounds (Figure 1.12).[61] Known C-C cleavage reactions in mammals include: side-chain cleavage of cholesterol to form pregnenolone (CYP11A1, Figure 1.12a), 17α-hydroxylation/lyase reaction of pregnenolone (CYP17A1, Figure 1.12b) and 14α-demethylation of lanosterol (CYP51A1, Figure 1.12c).[85,86] CYP17A1 reactions are of significant interest as a target of drug inhibition in the growth of tumours of certain cancers.[87–89]

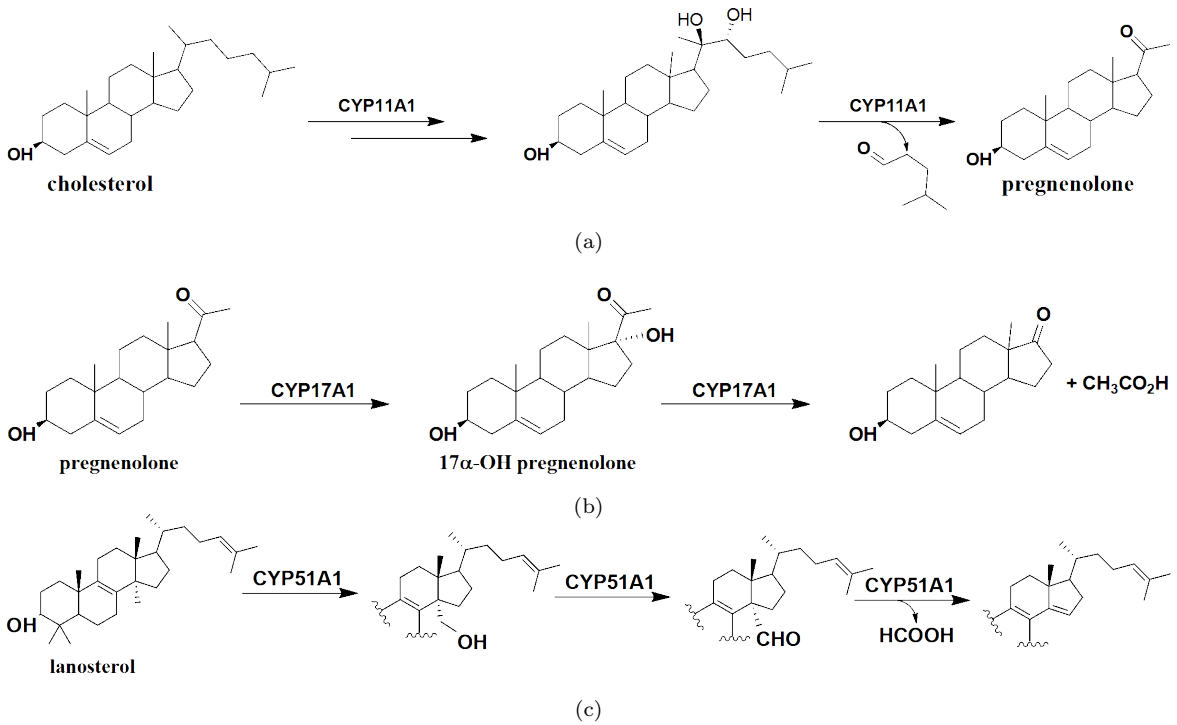

Figure 1.12: P450 C-C cleavage reactions involved in steroid biosynthesis. (a) Side-chain cleavage of cholesterol by CYP11A1. (b) 17α-hydroxylation and subsequent lyase reaction of pregnenolone by CYP17A1.(c) 14α-demethylation of lanosterol by CYP51.[90]

The C-C cleavage reactions for these P450 systems require different oxidised carbon-carbon bonds. CYP11A1 carries out sequential oxidation steps to produce a *vicinal*-diol centre of which the bond between the hydroxylated centres is cleaved by the P450 to form pregnenolone and an isocaproic aldehyde (Figure 1.12a).[84,91,92] Pregnenolone is also a substrate of CYP17A1, where this P450 will first hydroxylate its C17 centre to generate an α-hydroxy ketone moiety. This moiety is then cleaved by CYP17A1 to form a new ketone centre and acetic acid (Figure 1.12b).[93,94] Lastly, CYP51A1 first hydroxylates lanosterol at the C14 position to form an OH group and this is further oxidised to generate an aldehyde through *gem*-diol formation. The aldehyde carbon centre then undergoes C-C cleavage to form a ring alkene and formic acid (Figure 1.12c).[84,95]

The P450 oxidants and reaction mechanisms involved in the various C-C cleavage reactions described in Figure 1.12 are varied depending on the individual P450 system.[90] For CYP11A1, electron paramagnetic spectroscopy (EPR) experiments with Cpd I derived from γ-irradiated CYP11A1 showed both the hydroxylation and C-C cleavage steps were catalysed by Cpd I.[96] The reaction mechanism by which the Cpd I of CYP11A1 catalyses the lyase step is still unconfirmed but ^{18}O isotopic labelling studies have proposed two different lyase mechanisms for this P450 (Figure 1.13).[84,97,98] The first mechanism involves Cpd I acting as an electrophilic species to allow nucleophilic attack by one of the vicinal hydroxy groups to form a Fe-hydroperoxide adduct. The diol carbons undergo heterolytic cleavage to generate the resultant carbonyl compounds (Figure 1.13).[97] The second mechanism involves initial H-abstraction from a vicinal hydroxyl group and the resultant radical species undergoes homolytic cleavage across the diol carbon bonds to generate a new radical centre (Figure 1.13).[90,98] This new centre will undergo radical rebound (Figure 1.4) with the protonated Cpd I complex to form a *gem*-diol compound that will undergo dehydration to form the observed carbonyl compounds (Figure 1.13).[90]

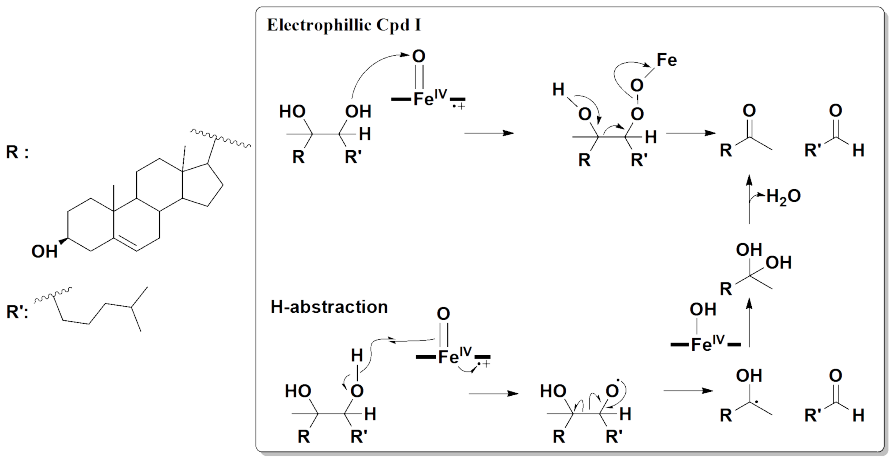

Figure 1.13: Proposed mechanisms for CYP11A1 lyase activity with vicinal diol carbon centres.[90]

^{18}O isotopic labelling studies were used to investigate CYP17A1's reaction pathway and the key oxidative species in the cleavage of hydroxylated pregnenolone.[58,99] It is proposed that the ferric-peroxo anion of CYP17A1 will attack the C=O centre of the α-hydroxy carbonyl group to form a peroxo adduct. This peroxo-adduct can then undergo different Baeyer Villiger oxidative cleavage reactions (Figure 1.14) to form the final ketone product and acetic acid.[60,100] CYP17 that has been enriched with the ^{18}O isotope (Figure 1.14) incorporates the ^{18}O label into the acetic acid cleavage product.[94,99] This provides evidence that the CYP17 ferric peroxo species was involved as a nucleophile in Baeyer Villiger type reactions.[94,99]

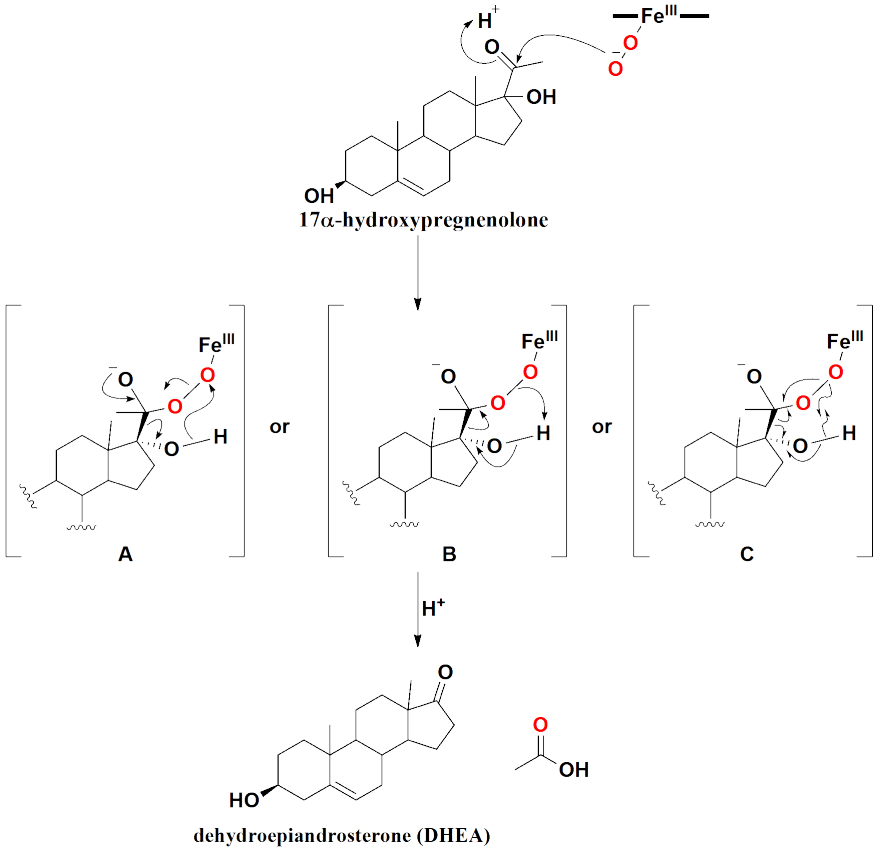

Figure 1.14: Proposed mechanism for CYP17A1 lyase activity. ^{18}O labelling studies showed the ^{18}O (red) is incorporated into the acetic acid product that supports a Baeyer-Villiger mechanism with the ferric-peroxo form of CYP17A1.

CYP51A1 was also used in NMR and ^{18}O isotope labelling experiments to determine the main oxidant and reaction mechanism involved in the C-C cleavage reaction of this P450 enzyme.[95,101] Isolation of a 14α-formyloxy compound by Fisher *et. al* has led to the proposal of another Baeyer-Villiger like mechanism for C-C cleavage by CYP51A1 that arises from the addition of a P450 ferric-peroxo anion to the electrophilic aldehyde centre (Figure 1.15).[84,95] Akhtar *et. al* also proposed an alternate mechanism involving O-O homolytic cleavage to form a radical intermediate that will undergo decomposition to form the cleavage product.[60]

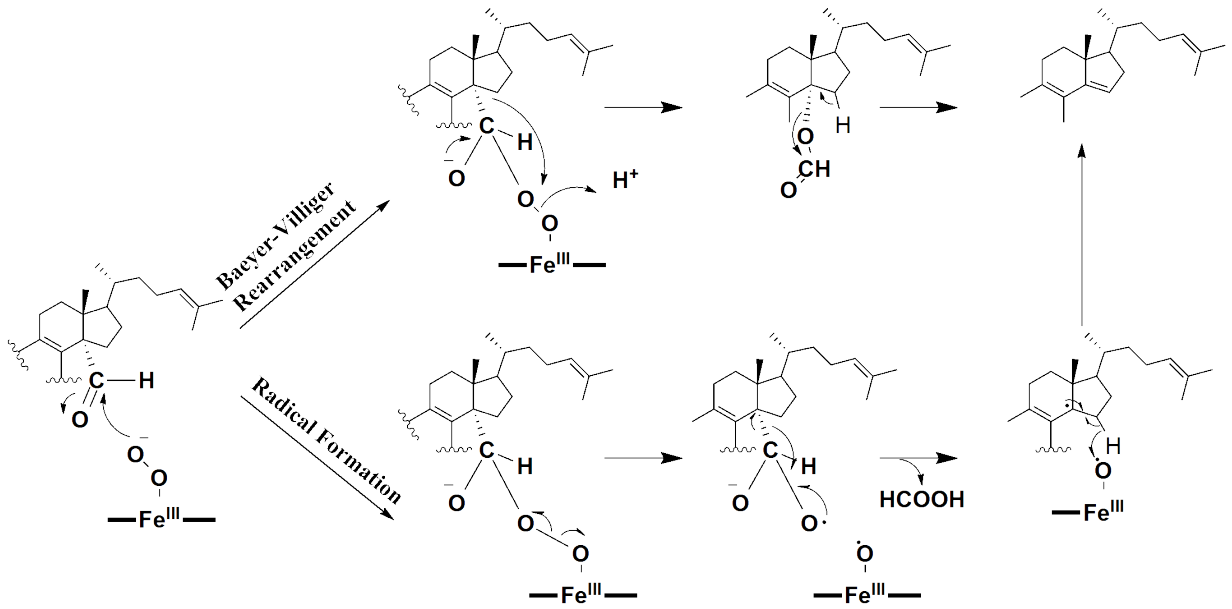

Figure 1.15: Proposed mechanisms for CYP51A1 C-C cleavage activity.[60]

1.6 P450 Electron Transport Systems

In the P450 catalytic cycle (Figure 1.3), NAD(P)H or NADH serves an electron source through the donation of a hydride ion but the catalytic cycle requires two sequential single electron transfer steps (Figure 1.3). Electron transfer systems are therefore needed to convert a hydride derived from NAD(P)H into electrons and relay these one at a time to the P450 for oxidation activity.

Ten different classes of electron transport chains have been identified in the literature and are classified according to the topology of the proteins involved in the electron relay.[102] These chains can be found in different species ranging from bacterial, mitochondrial, fungi and mammalian systems.[103–105]

The complete P450 systems can be classified into either one, two or three component systems (Figure 1.16).[102] The multi-component systems utilise reductase enzymes that contain flavin cofactors (FAD or FMN) that catalyse the oxidation of NAD(P)H and allows for subsequent electron relay to another electron transfer centre or the P450 heme centre.[38,102] Three-component systems can also contain an iron-sulfur [2Fe-2S] ferredoxin that relay the electrons needed from the reductase to the P450.[103] A well-known example of a three-component system is that of CYP101A1 ($P450_{cam}$) from *Pseudomonas putida* that consists of putidaredoxin and putidaredoxin reductase, which shuttles electrons from NADH to $P450_{cam}$ for hydroxylation reactions.[106]

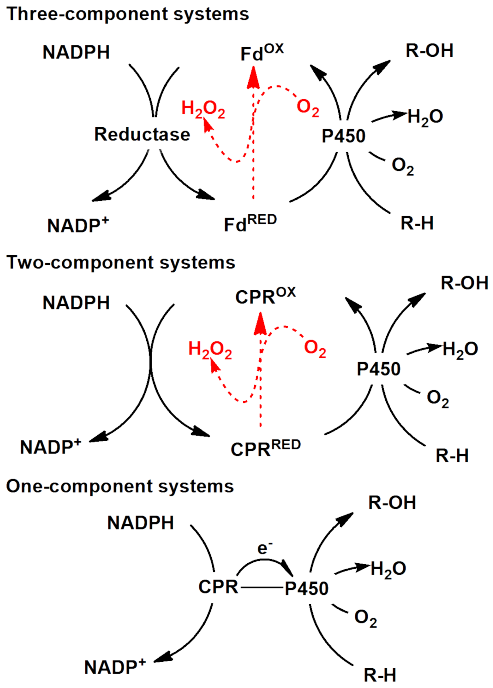

Figure 1.16: Electron transfer systems of P450s. Fd: Ferredoxin. CPR: Cytochrome P450 reductase. Uncoupling reactions that generate H_2O_2 is shown in red.

Multicomponent P450 systems require specific redox protein partners to enable electron transfer activity to the P450 centre. For example, CYP101A1 will only accept electrons from putidaredoxin, its physiological redox partner.[107] The need to pair specific redox partners to individual P450s hampers widespread use of these enzymes on a larger scale.

A separate but well-known issue with multicomponent electron transfer systems is that reduced electron transfer proteins such as the reductase or ferredoxin can be highly sensitive to oxygen and temperature.[38] Reactions of these reduced proteins with oxygen can result in uncoupling, to produce H_2O_2 that will therefore result in an unproductive reaction (Figure 1.16).[38,108] The uncoupling reactions within the P450 electron transport chain and alongside those occurring in the P450 catalytic cycle diverts the reducing power of NADPH cofactors away from the desired oxidative reactions and towards futile side reactions that produce reactive oxygen species (ROS) such as H_2O_2.[102] The effects of ROS and its role in the damage of proteins is well-known, whereby it impacts cell viability and enzyme stability/lifetime in biocatalytic systems.[109]

Enzymes that function as ROS-scavengers such as catalases and superoxide dismutatases have been employed with *in vitro* biocatalytic systems to remove said reactive species. While this alleviates the immediate issue with uncoupling reactions, further scale up of biocatalytic monooxygenase systems would introduce further problems, such as additional amounts of ROS-scavengers and the need for a molar surplus of

NAD(P)H to mitigate unproductive uncoupling reactions to drive substrate conversion to completion.[102]

NAD(P)H cofactors have high costs associated with their production and therefore are too expensive for use as stoichiometric agents but these cofactors can be regenerated *in situ*. Whole-cell systems are often used when co-factor regeneration is needed but regeneration with *in vitro* systems is possible also.[110] These regeneration methods often make use of additional enzymes such glucose and/or alcohol dehydrogenases and sacrificial substrates (isopropanol/glucose) that can generate superstoichiometric quantities of carbon waste and will often require continuous pH monitoring and adjustment.[110,111]

These issues related to uncoupling and NAD(P)H use alongside the need to co-express electron transport proteins makes P450 monooxygenase systems less appealing for large scale industrial applications. An alternative to the monooxygenase system is the use of peroxygenases. Peroxygenases utilise readily available hydrogen peroxide as an electron source that is cheaper[112] and therefore more cost-effective.

1.7 H_2O_2 Peroxygenases

In nature, there are heme enzymes that are capable of binding H_2O_2 or other reactive oxygen species, these include catalases and peroxidases which function as ROS scavengers through cleavage of the peroxide bond to form water.[113,114] Another class of H_2O_2-dependent heme enzymes are the peroxygenases, which functionalise the C-H bonds of organic substrates using H_2O_2.[108] These include P450 peroxygenases and the related unspecific fungal peroxygenases.[108,115]

The heme centre of peroygenases forms the active oxidant, Cpd I through the use of a peroxide shunt pathway (Figure 1.3 and 1.17).[33] This pathway involves the binding of hydrogen peroxide to the heme to directly form the hydroperoxo species which subsequently forms Cpd I for substrate oxidation.[33,116]

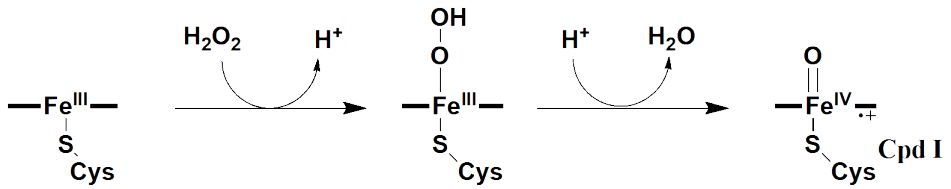

Figure 1.17: Peroxide Shunt Pathway of P450 or peroxygenase enzymes. The binding of hydrogen peroxide to the 5-coordinate high-spin complex allows the direct formation of Cpd I without the need for electron transfer steps.[33]

Hydrogen peroxide and organic surrogates such as cumene hydroperoxide and iodosylbenzene can utilise this peroxide shunt pathway or through direct transfer of an oxygen atom to the heme centre.[117] These oxygen surrogates bypasses the need for cofactors and electron transfer partner proteins in P450 reactions.[118] The oxyfunctionalisation reactions catalysed by P450 peroxygenases will introduce an oxygen atom from the bound peroxide rather from dioxygen.[119,120]

Unspecific fungal peroxygenases (UPO) are a distinct class of peroxygenases exclusively found in fungal species.[121] These peroxygenases possess a heme thiolate centre similar to P450s (Figure 1.18) but differ significantly in that these fungal enzymes are secreted into extracellular space as opposed to P450s that are expressed within intracellular environments.[108] The reactions catalysed by UPOs are similar to those of P450s and include aliphatic hydroxylations, alkene epoxidation, aromatic oxidation and dealkylations.[122] The physiological role UPOs play in the fungal species is not known, though their catalytic versatility may play a role in unspecific oxidation and detoxification of xenobiotics that is likened to an extracellular "fungal liver".[123]

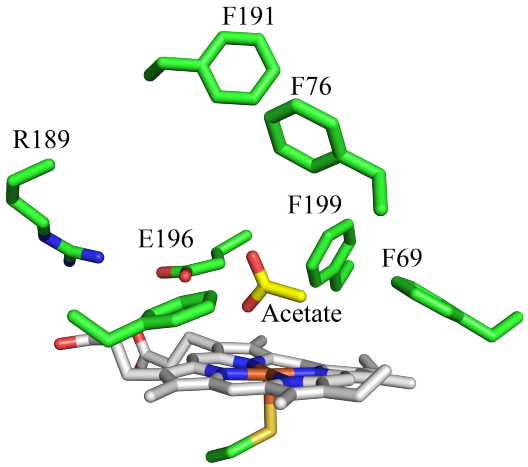

Figure 1.18: Crystal structure of *Aae*APO from *Agrocybe aegerita* showing its active site and heme-centre (PDB: 2YP1).[123] The heme-thiolate structure is similar to those in P450s and it is noted that a glutamine residue (E196) is present above the heme on the distal side. An acetate molecule was present in the active site as substrate.

While UPOs offer greater stability as extracellular proteins, they offer poor yields when expressed in conventional recombinant expression systems, which is due to host expression systems that lack capability for post-translational modifications and missing chaperones.[122] Therefore, reported expression of UPOs in the literature often require extensive host strain engineering and directed evolution campaigns to achieve high expression.[108,124] The most successful example of UPO engineering and expression is *Aae*UPO from *Agrocybe aegerita* which underwent several rounds of laboratory directed evolution to achieve high expression (200 mg L^{-1}) in *P.pastoris*.[124,125]

Natural P450 peroxygenases that have been discovered primarily come from the CYP152 family, such CYP152A1 ($P450_{BS\beta}$), CYP152B1 ($P450_{SP\alpha}$), CYP152A2 ($P450_{CLA}$), CYP152K6, CYP152N1 and CYP152L1 ($P450_{OleT}$).[126–130] These P450 enzymes primarily bind and hydroxylate fatty acids driven by the presence of H_2O_2. Decarboxylation of these fatty acids to form alkenes have also been observed with P450 peroxygenaseses.[131] $P450_{BS\beta}$ primarily hydroxylates long chain fatty acids at the β (3-hydroxy) position while $P450_{SP\alpha}$ hydroxlates at the α (2-hydroxy) position. The turnover activity of $P450_{BS\beta}$ with the hydroxylation of myristic acid is reported to be 1400 min^{-1} and has high affinity towards H_2O_2 with a K_M value of 32 µM that indicates these enzymes can function as efficient peroxygenases at low H_2O_2 levels.[132,133]

The majority of P450 monooxygenase enzymes possess a highly conserved acid-alcohol pair within the active site that function as proton relays to the iron-oxygen species during the catalytic cycle, for example D251 and T252 in both CYP101A1 ($P450_{cam}$)[16] and CYP199A4 (Figure 1.19a).[134] The substrate-bound crystal structures of various P450 peroxygenases in the CYP152 family,[132,135,136] revealed their active sites instead contain carboxylate binding arginine and proline residues, such as R241 and P242 in $P450_{SP\alpha}$ or R242 and P243 in $P450_{BS\beta}$ (Figure 1.19b and 1.19c).[132,135] The guanidinium of the arginine residue (Figure 1.19b and 1.19c) in particular forms a strong bidentate interaction with the carboxylate group of the substrate.[135]

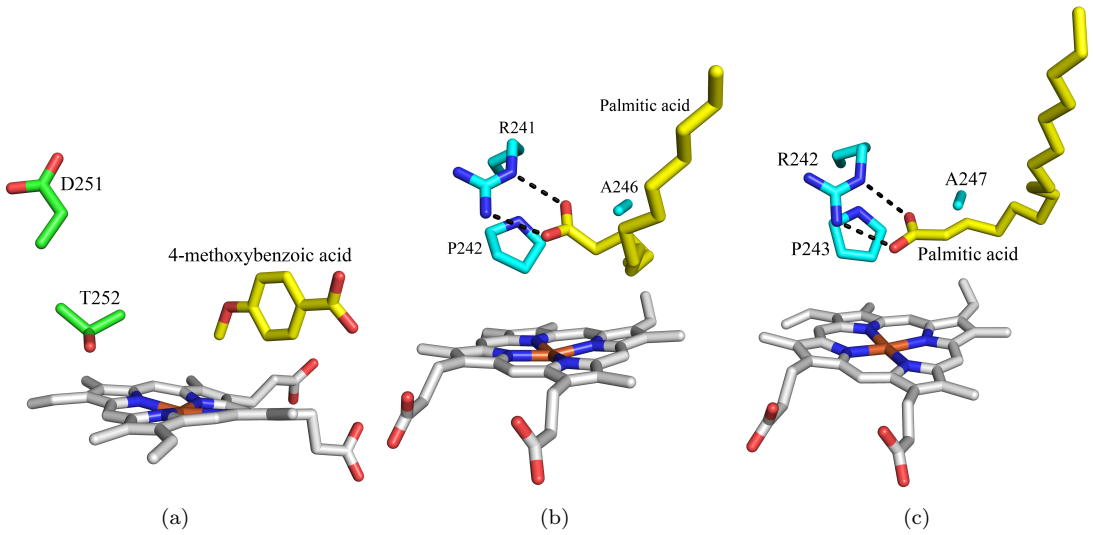

Figure 1.19: (a) Crystal structure of CYP199A4 (PDB: 4DO1)[137] bound to 4-methoxybenzoic acid, whereby the D251 and T252 residue are the acid-alcohol pair conserved in P450 monooxygenases. b) Crystal structure of CYP152B1 ($P450_{SP\alpha}$, PDB: 3AWM) bound to palmitic acid.[132] (c) Crystal structure of CYP152A1 ($P450_{BS\beta}$, PDB: 1IZO)[135] bound to palmitic acid.[132]

Crystal structures of P450 peroxygenases (Figure 1.19) showed that the interaction of the arginine residue (R241 in Figure 1.19b) with the fatty acid carboxylate is similar to that of interactions between active site histidine and glutamate residues of the

chloroperoxidase (CPO) enzyme from *Caldariomyces fumago*.[17] CPO exhibits catalase, peroxidase and P450-like activity with H_2O_2.[17] The reaction mechanism of CPO involves the active site glutamate (E183) functioning as an acid-base catalyst for O-O bond cleavage of H_2O_2 and an adjacent histidine residue modulates the basicity of the glutamate through hydrogen bonding (Figure 1.20).[138]

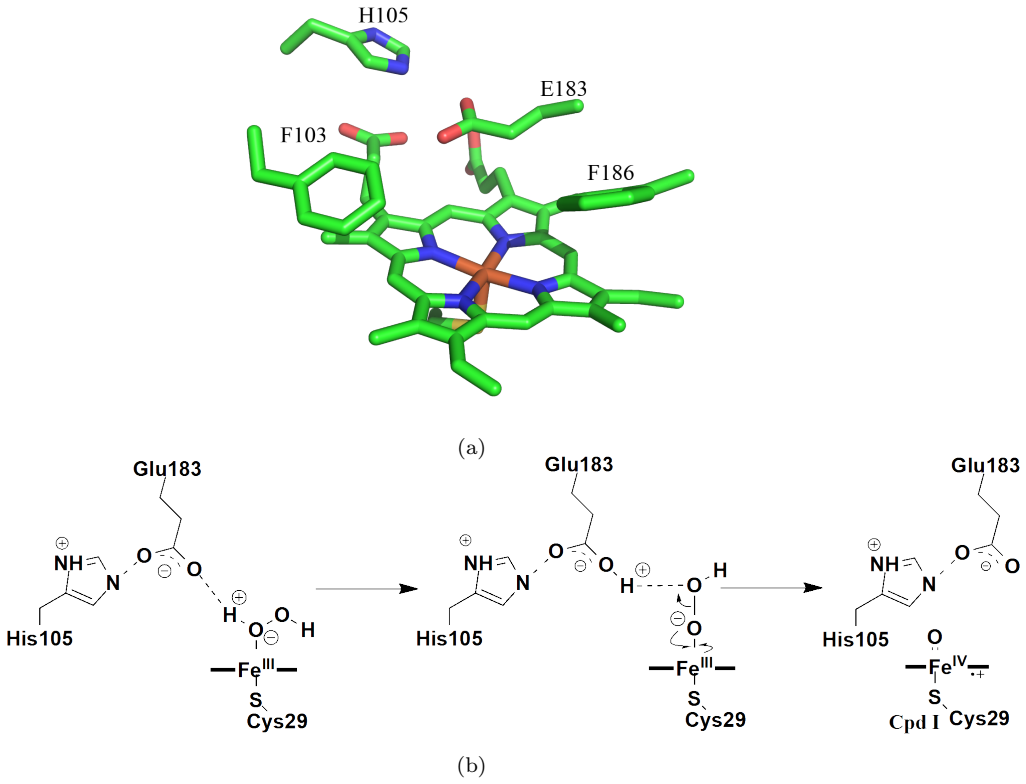

Figure 1.20: (a) Crystal structure of chloroperoxidase (CPO) from *Caldariomyces fumago*. (b) H105 and E183 form acid-base interactions during Cpd I formation of CPO with H_2O_2.

Using CPO as a mechanistic basis (Figure 1.20b), Lee *et. al* proposed a similar molecular mechanism for P450 peroxygenase reactions whereby the active site arginine (R241 in $P450_{SP\alpha}$) will modulate the basicity of the substrate carboxylate and allow it to act as an acid-base catalyst.[135] This was confirmed by Shoji *et. al* using decoy molecules and crystallography, whereby the addition of short alkyl chain molecules that contain carboxylate groups allowed $P450_{SP\alpha}$ to oxidise non-native substrates such as styrene, and highlights the importance of this substrate carboxylate for catalytic function.[135,139]

The proposed mechanism for Cpd I formation with these P450 peroxygenases is shown in Figure 1.21. The peroxygenase mechanism begins after the displacement of the distal water ligand by the substrate. Subsequently, the substrate carboxylate abstracts a proton from H_2O_2 (Figure 1.21) forming a peroxide anion. The peroxide anion binds to the heme ferric centre to form the hydroperoxo complex (Figure 1.21). The hydroperoxo

complex then abstracts a proton from the substrate to undergo O-O cleavage to form Cpd I (Figure 1.21).[135,139,140]

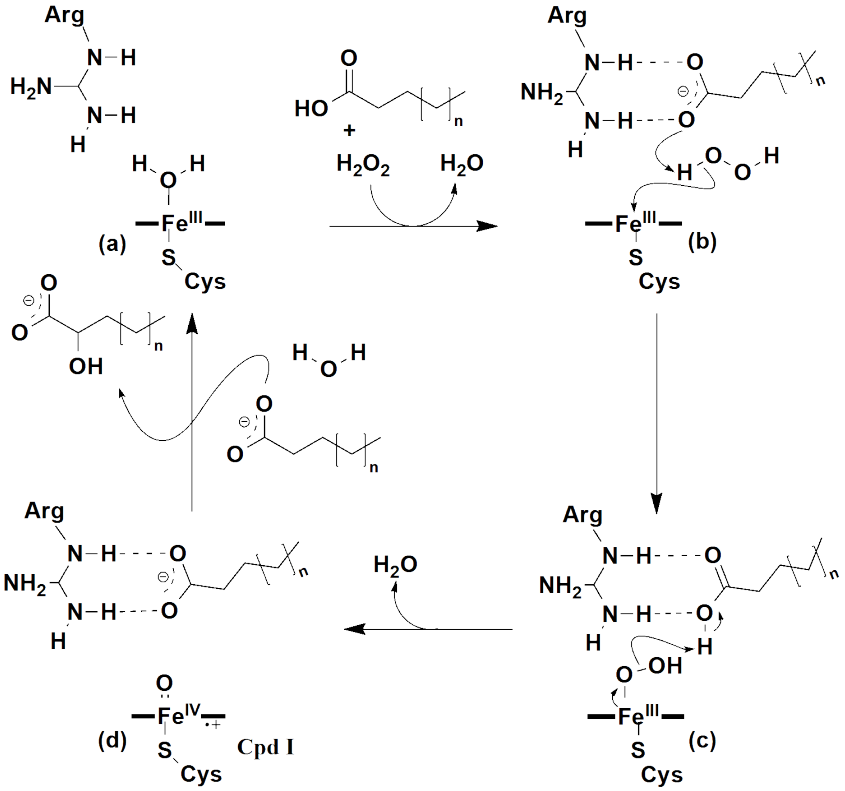

Figure 1.21: The proposed catalytic reaction mechanism of P450 peroxygenases in the hydroxylation of long chain fatty acids.

An alternate mechanism for heme enzyme peroxygenase reactions has also been proposed by Shaik *et. al* shown in Figure 1.22.[141,142] This mechanism proposed by Shaik *et. al* involves the formation of a Fe^{III}-H_2O_2 complex (Figure 1.22) that is stabilised by the substrate carboxylate. The O-O bond of the peroxide undergoes homolytic cleavage to form a hydroxyl radical and a Fe^{IV}-OH. The hydroxyl radical is stabilised by interactions with the substrate carboxylate and a free water molecule, which would then lead to the radical abstracting a proton from Fe^{IV}-OH to form Cpd I.[143]

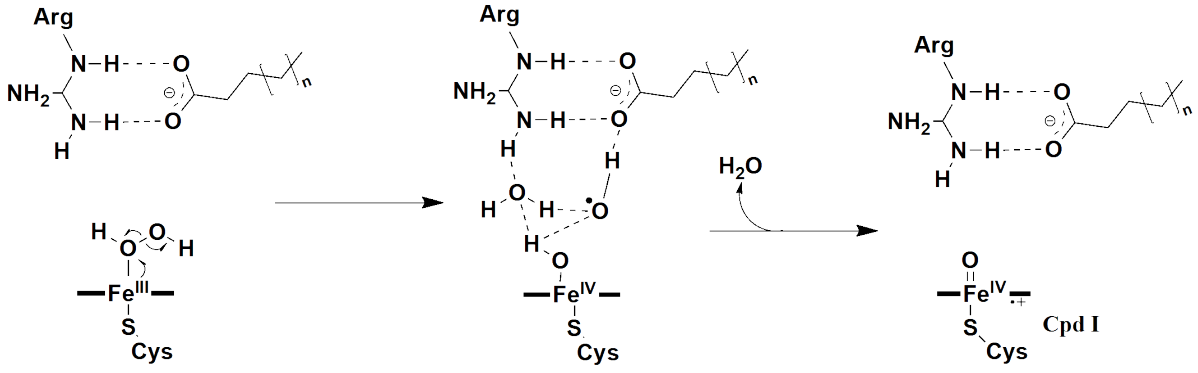

Figure 1.22: An alternate catalytic reaction mechanism of P450 peroxygenases to form Cpd I. This mechanism involves a O-O homolytic cleavage of the hydrogen peroxide.

Natural P450 peroxygenases are self-sufficient catalysts without any of the dependencies on external partner proteins required by monooxygenases. However, the importance of the substrate carboxylate group in the catalytic mechanism of the CYP152 family peroxygenases limits their substrate range almost exclusively to fatty acids and hampers their use in more useful oxidative reactions. The use of decoy molecules could expand their substrate range but requires bespoke molecules for specific substrate/enzyme combinations. Thus, efforts have been undertaken by Shoji *et. al* to engineer peroxygenase activity in natural P450 monooxygenases.[135,139,140]

Shoji *et. al* achieved this through the introduction of an acidic glutamate residue in the active site of P450 monooxygenases such as $P450_{cam}$, CYP102A1 ($P450_{BM3}$), CYP119 and also within a natural peroxygenase, $P450_{SP\alpha}$. Single-point mutagenesis of a highly conserved active site threonine to a glutamate residue in these monooxygenases was able to introduce peroxygenase activity in these P450s. An equivalent residue in $P450_{SP\alpha}$, A245, was mutated also (Figure 1.19c). The introduction of an acidic glutamate near the heme centre of these P450s would mimic the effect of the substrate carboxylate in the CYP152 family of natural P450 peroxygenases such as in $P450_{SP\alpha}$ and $P450_{BS\beta}$. Mutant A245E-$P450_{SP\alpha}$ showed significantly improved peroxygenase activity in the oxidation of styrene with a turnover rate of 280 min^{-1} without the use of decoy molecules.[140] Mutants T252E-$P450_{cam}$ and T268E-$P450_{BM3}$ both showed improved turnover activity towards their natural substrates in the presence of H_2O_2 over their wild-type (WT) counterparts, with the latter displaying a turnover rate of 110 min^{-1} with styrene and H_2O_2.

Other efforts undertaken to convert P450 monooxygenases to peroxygenases including single-point mutagenesis of the F87 residue of $P450_{BM3}$ to an alanine or glycine residue resulted in increased peroxygenase function for $P450_{BM3}$ but still showed rapid destruction towards H_2O_2.[144–146] An extensive directed evolution campaign was also carried out to improve peroxygenase activity with $P450_{cam}$.[147]

I propose to use this single-point mutagenesis approach, in this thesis to study P450 peroxygenase reactions.

1.8 CYP199A4 from *Rhodopseudomonas palustris* HaA2

CYP199A4 was discovered within strain HaA2 of the bacterium, *Rhodopseudomonas palustris*.[148] This bacterium is gram-negative and has been found in many diverse environments including swine waste lagoons, pond water and earthworm droppings.[149] The wide range of environments they can survive in is owed to its incredible metabolic di-

versity that allows them to grow and adapt using energy from any of the following pathways: photoautotrophic and photoheterotrophic (energy from light and CO_2/organic compounds as a carbon source), chemoautotrophic and chemoheterotrophic (carbon and energy from inorganic/organic compounds and CO_2).[149]

There are different strains of *R. palustris* that possess differing genomes depending on the micro-environment of the strain. The vast metabolic diversity of this bacterium has led to different strains containing a number of different P450s for varied metabolic function. Strain CGA009 of *R. palustris* contained 7 P450 genes within its genome that belong to at least 4 different P450 families, whereby four of these P450s (CYP195A2, CYP199A2, CYP203A1, and CYP153A5) have been expressed in *Escherichia coli* (*E.coli*).[150] CYP199A2 has been reconstitued *in vitro* with palustrisredoxin A and putidaredoxin reductase of the $P450_{cam}$ system.[150] Ferredoxin and ferredoxin reductase gene sequences were also found in the genome of strain CGA009 that are likely part of the electron transfer chain system with some of these P450s.[150]

CYP199A4 was discovered in strain HaA2 of *R. palustris*.[148] This strain was found in the sediment of a pool of rainwater near Haren, the Netherlands.[151] Initial genomic analyses of this strain found that it is more suited for oxidative aerobic metabolism rather than phototrophic or anaerobic metabolism.[151,152] CYP199A4 alongside a ferredoxin (HaPux) and ferredoxin reductase (HaPuR) were identified from its genome after BLAST searches using the amino acid sequences of CYP199A2 and the related electron transfer partners from strain CGA009 were undertaken.[148] Furthermore, CYP199A4, HaPux and HaPuR were expressed in *E.coli* and successfully purified in high-yield.[148] It is noted that CYP199A4 and HaPux are purified in greater yield (> 5-fold) than the equivalent proteins of CYP199A2. Enzyme activity has been successfully reconstituted with CYP199A4 with HaPux and HaPuR using NADH as an electron source.[150]

CYP199A4 and CYP199A2 are closely related P450s that are able to bind *para*-substituted benzoic acids (Figure 1.23) and catalyse their oxidation.[30,48,137,153,154] CYP199A4 strongly prefers this *para*-substituted benzoic framework as *meta* substituents are often oxidised less efficiently compared their *para* counterparts, for example 3-methoxybenzoic acid with CYP199A4 produces a NADH consumption rate of 498 min^{-1} but no product formation is observed.[155] This is in contrast to 4-methoxybenzoic acid, whereby CYP199A4 has significantly higher NADH consumption and product formation rates (> 1000 min^{-1}), as well as a coupling efficiency (ratio of product formed : NADH added) of 91 % (Figure 1.23).[30]

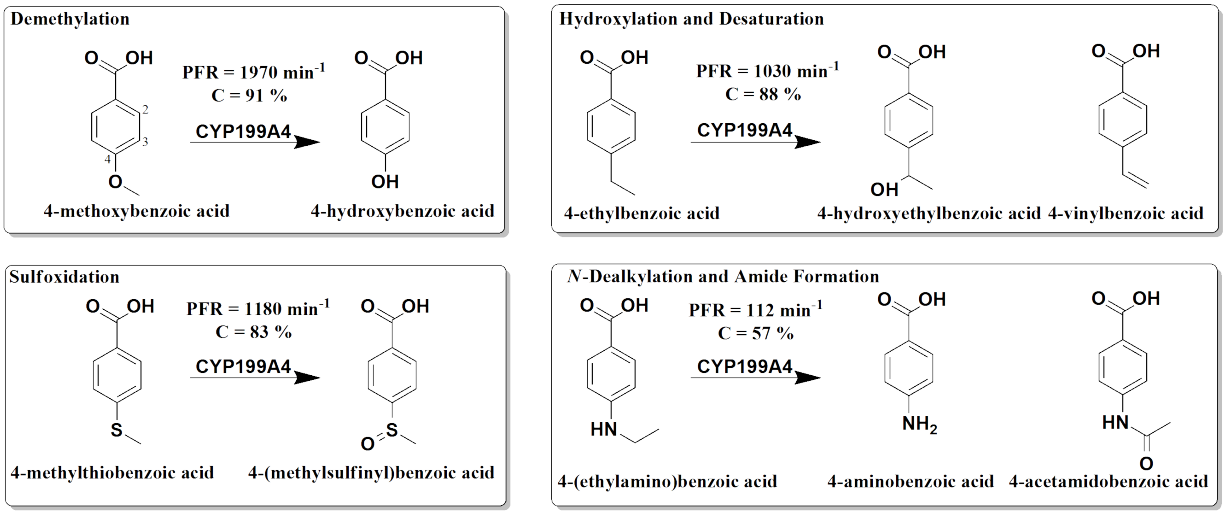

Figure 1.23: Enzymatic reactions catalysed by CYP199A4 with *para*-substituted benzoic acids.

Several crystal structures with CYP199A4 have been solved.[30,134,153,155,156] These crystal structures have been used to elucidate its binding modes and preference towards the *para*-substituted benzoic acids.[157]

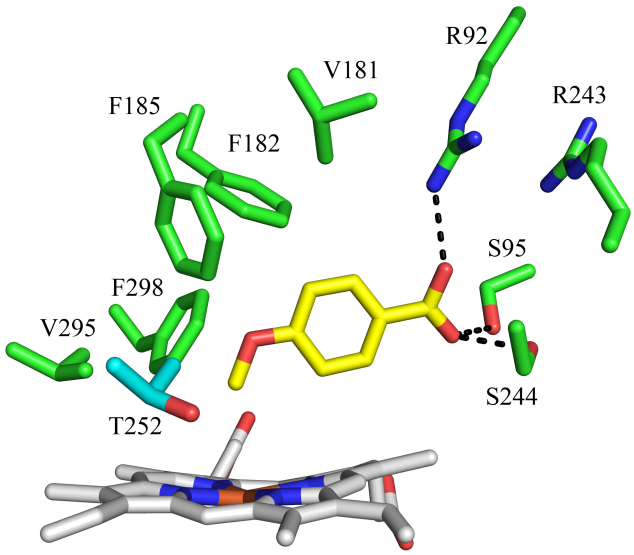

Figure 1.24: Crystal structure of the active site of CYP199A4 complexed with 4-methoxybenzoic acid (PDB: 4DO1). The carboxylate moiety of the substrate is essential for tight binding with this enzyme owing to interactions with polar residues (R92, R243, S95 and S244) surrounding the moiety.[157] The T252 residue is highlighted in cyan.

The high yield expression and purification of CYP199A4 and its electron transfer partners, HaPux and HaPuR from recombinant *E.coli* coupled with easy access to crystal structures allows this enzyme to be used as a model system and therefore detailed mechanistic studies for P450 reactions.[48] The relatively simple *para*-substituted benzoic acid architecture enables a variety of different P450 monooxygenase reactions to be studied with this enzyme with enantiomerically available compounds.

CYP199A4 has been used as a model system to study P450 reactions such as sulfoxidation, *N*-dealkylation and amide formation (Figure 1.23).[30] CYP199A4 also catalyses hydroxylation and desaturation reactions with 4-ethylbenzoic acid to produce a mixture of products from both reactions.[48] Protein engineering approaches in conjunction with crystal structures complexed with 4-ethylbenzoic acid have been used to investigate the partition between reaction pathways of hydroxylation and desaturation.[48] Mutation of active site residue, F185 to a less bulky isoleucine (F185I) residue favoured the desaturation pathway (100% desaturation product). This was hypothesised to be due to the additional space in the active site caused by the mutation, which positions the substrate alkyl carbons further away from the heme centre during the catalytic cycle. The further distance hinders the radical rebound mechanism that favours hydroxylation.[48]

Initial efforts to convert CYP199A4 into a peroxygenase have been done based on the work of Shoji *et al.*.[140,156] This was achieved through mutagenesis of the conserved threonine (T252, Figure 1.24) residue to a glutamate residue to introduce an acid-base catalyst within the active site of CYP199A4.[156] The glutamate residue mimics the conditions necessary for P450 peroxygenase reactions to occur (Figure 1.21).[140] As a result, peroxygenase activity was successfully introduced in CYP199A4. Reactions with 4-methoxybenzoic acid yielded turnover numbers (> 100) comparable to P450 peroxygenases with their respective substrates.[156] The T252E mutant also exhibited poor catalytic efficiency while oxidising 4-methoxybenzoic acid using $NADH/O_2$ and electron transfer partners, with product formation rates (0.8 min^{-1}) and coupling efficiencies (10%) significantly lower than the WT enzyme (1971 min^{-1} and 91 % respectively).[156]

Substrate binding studies of T252E-CYP199A4 showed only 5 % type I shift with 4-methoxybenzoic acid which is in contrast to the $\geqslant$ 95 % shift observed with WT-CYP199A4.[148] This indicates that the distal water ligand has not been displaced by the substrate.[156] The crystal structure of T252E-CYP199A4 reveals that the sixth water ligand in this mutant has not been displaced upon substrate binding (Figure 1.25a, PDB: 7REH). This is likely due to the carboxylate of residue E252 interacting with the heme-bound water which prevents its displacement when substrate binds.[156] There were additional changes observed in the oxygen binding groove of the T252E mutant compared to the WT and the orientation of the D251 residue was also slightly altered (Figure 1.25b).[156]

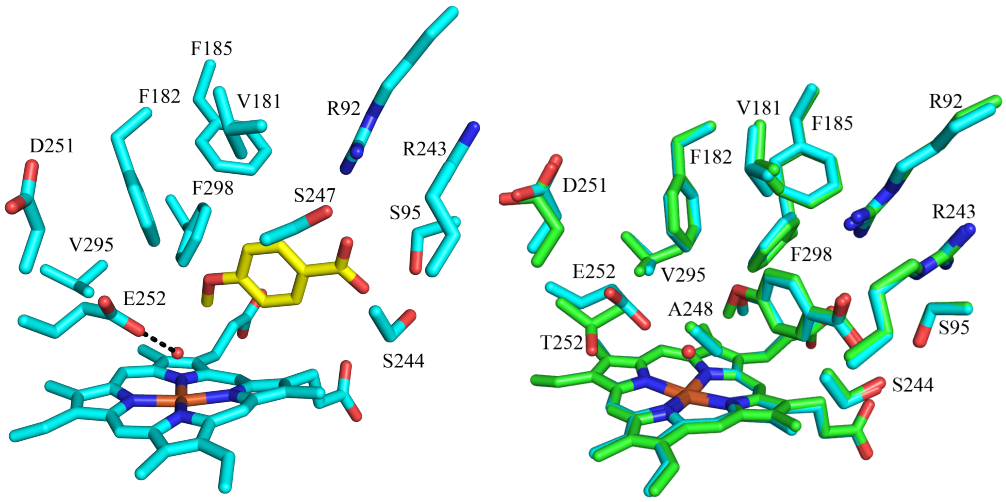

Figure 1.25: (a) The active site of T252E-CYP199A4 (PDB: 7REH). The heme distal water ligand is not displaced by substrate binding and has a strong interaction with E252. (b) Superimposed active site structures of WT (green) and T252E (cyan) variants of CYP199A4. The 4-methoxy moiety of the substrate was angled away from the heme centre in the T252E mutant.

T252E-CYP199A4 can be used as a model system to study P450 peroxygenase reactions. Efforts have been made to understand the sulfoxidation reaction mechanism in P450s using this mutant.[158] The T252E mutant showed greater sulfoxidation activity over *O*-demethylation using the peroxygenase pathway but the WT enzyme showed no preference for either reaction when using the monooxygenase pathway. Given that Cpd I, the proposed active oxidant, is formed in both pathways (Figure 1.17 and Figure 1.3), the results imply that the peroxygenase pathway likely involved another oxidative intermediate involved in the sulfoxidation reaction. It was proposed that the Fe^{III}-H_2O_2 complex (Figure 1.22) originally theorised by Shaik *et. al* is the likely oxidant that can also catalyse sulfoxidation reactions in P450s.[143,158]

A significant drawback suffered by these peroxygenases is that H_2O_2 can deactivate the heme centre.[108] Indeed, the binding affinity (K_M) of H_2O_2 with T252E-CYP199A4 was 15 mM[156] and lowering this value will be ideal to allow lower H_2O_2 concentrations to be used to drive peroxygenase activity.[143] Another approach to drive peroxygenase activity in these enzymes is generating H_2O_2 *in situ*.

1.9 *In situ* H_2O_2 Generation for Peroxygenase Reactions

An approach that generates H_2O_2 *in situ* could mitigate damage to the heme centre through slowly exposing the peroxygenase to low but replenishing levels of H_2O_2. Initial work that demonstrates this by Sheldon *et. al* uses a H_2O_2 sensor that continually monitors and maintains the low H_2O_2 levels (50 µM) in reaction with CPO.[159] This

approach enabled improved stability over time and greater substrate conversion.[159]

Efforts have also been undertaken to use reduced flavin molecules that are highly reactive to molecular oxygen to produce H_2O_2. Different ways to generate reduced flavins include the use of visible light and EDTA (Figure 1.26a)[160] and a synthetic NADH analogue, 1-benzyl-1,4-dihydronicotinamide (BNAH) (Figure 1.26b).[161]

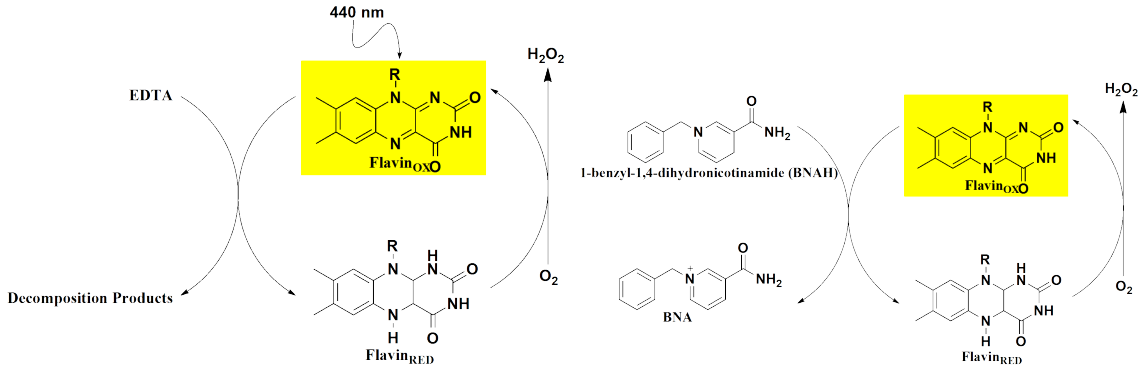

Figure 1.26: *In situ* generation of H_2O_2 using free flavins with (a) light-activation alongside EDTA and (b) synthetic NADH analogues.

Girhard *et. al* demonstrated that flavins in the presence of visible light and EDTA can be reduced and reacts with oxygen to generate H_2O_2.[160] Paul *et. al* showed the NADH analogue, BNAH, was able to reduce flavins with greater reactivity than its natural counterpart and generate H_2O_2. Both approaches were used with peroxygenases of the CYP152 family and were successful in demonstrating substrate conversion with these P450s.[160–162] Further optimisation of reaction conditions would be needed to maximise reaction rates while minimising enzyme deactivation by H_2O_2. The photochemical method using light and EDTA have also been used to drive H_2O_2 dependent activity in chloroperoxidase (CPO) and *Agrocybe aegerita* aromatic peroxygenase (*AaeAPO*).[163,164]

A chemical approach to generate H_2O_2 was developed by Karmee *et al.* that used supercritical carbon dioxide ($scCO_2$) (Figure 1.27a).[165] Liquid $scCO_2$ was used as medium to produce H_2O_2 directly from H_2 and O_2 with Palladium (Pd) as a catalyst (Figure 1.27a). This method produced H_2O_2 for CPO to generate an optically enriched (*R*)-sulfoxide through sulfoxidation.[165] A similar sulfoxidation reaction with CPO was achieved through electrochemical approaches, whereby electrodes containing catalysts that converts oxygen to H_2O_2 were used to drive sulfoxidation activity with CPO (Figure 1.27b).[166,167] Zhang *et. al* used gold and palladium (Au-Pd) nanoparticles loaded on TiO_2 to generate H_2O_2 for peroxygenase reactions with an unspecific peroxygenase (UPO).[168] The heterogenous Au-Pd-TiO_2 catalyst generates H_2O_2 from oxidising hydrogen gas and reducing O_2, where the H_2O_2 generated is then be supplied

to UPO.[168]

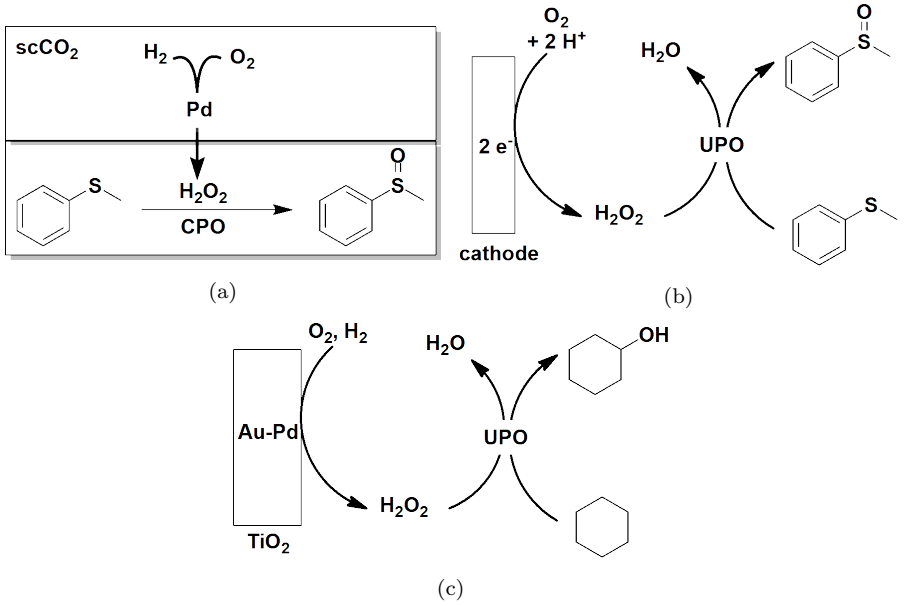

Figure 1.27: *In situ* generation of H_2O_2 using (a) supercritical CO_2, (b) an electrochemical approach and (c) Au-Pd catalysts supported on TiO_2.

Oxidase enzymes that can generate H_2O_2 enzymatically have also been used to supply H_2O_2 to CYP152 enzymes.[131,169] Gandomkar *et. al* employed an α-hydroxyacid oxidase in solution with $P450_{CLA}$ to drive peroxygenase activity.[169] Munro *et.al* produced an unnatural fusion enzyme where alditol oxidase was attached to $P450_{OleT_{JE}}$ via a short amino acid linker to generate H_2O_2 in close proximity to the P450 peroxygenase.[131] A less conventional application of these oxidases involved the use of natural deep eutectic solvents (NADES).[51] Li *et. al* successfully employed a eutectic solvent of choline-chloride and urea with a choline oxidase (ChOx), where the solvent acted as a co-substrate for the oxidase to generate and supply H_2O_2 to a UPO enzyme for sulfoxidation.[51]

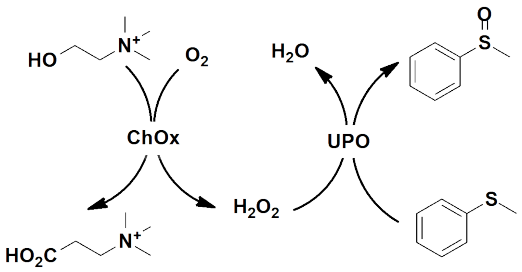

Figure 1.28: The use of a natural deep eutectic solvent (NADES) in the *in situ* generation of H_2O_2 for peroxygenase reactions.

1.10 Enzyme Immobilisation

Peroxygenases presents a more cost-effective and sustainable method to achieving large scale biocatalytic reactions for green and sustainable chemical production. Industrial applications of peroxygenases and enzymes in general would be hindered through poor long-term operational stability, challenging enzyme recovery and re-use.[170] Operational stability in particular is a significant issue for peroxygenases due to enzyme deactivation by H_2O_2. These issues can be overcome through enzyme immobilisation,[170–172] through which different approaches exist for biocatalysis. These approaches include binding to a carrier or encapsulation (Figure 1.29).[170]

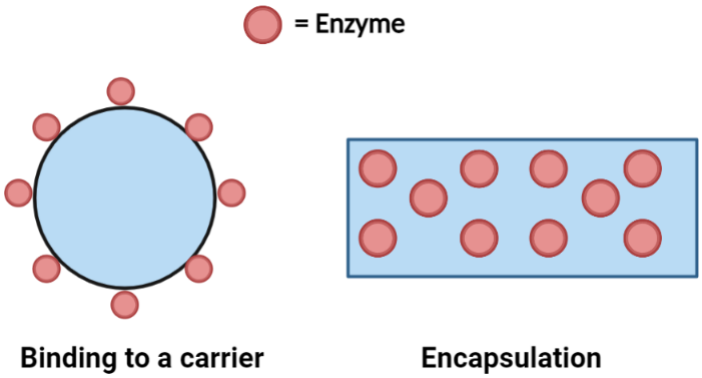

Figure 1.29: Different approaches to immobilising enzymes.

Immobilising the enzyme onto a solid surface allows for more convenient handling and recovery of the enzyme.[170] This will also minimise contamination by the enzyme into the final enzymatic product owing to the ease of separation of solid enzyme from liquid reaction mixtures. Facile enzyme separation also allows for efficient recovery and re-use of the enzyme to extend its operational lifetime.[172]

Binding to a carrier involves attaching the enzyme to solid support either through physical, ionic or covalent interactions.[173] Carriers that have been used include synthetic organic polymers, natural polymers and inorganic polymers.[170] Natural polymers used for enzyme immobilisation consists of water-insoluble polysaccharides such as cellulose, starch and chitin.[170] A well-known example of this employed commercially is the Tanabe process that is used in the production of L-amino acids through resolution of racemic acylamino acids by an aminoacylase.[174] The aminoacylase is immobilised on to cellulose modified with diethylaminoethyl groups (DEAE-Sephadex).

Inorganic polymers such as silica have been used to immobilise different enzymes such as CPO from *Caldariomyces fumago*[175] and lipases.[176,177] The silica used in these examples were epoxy-functionalised silica. The epoxide functional group on the silica

beads will react with the the enzyme's terminal amino group and attach itself to the silica bead surface (Figure 1.30).

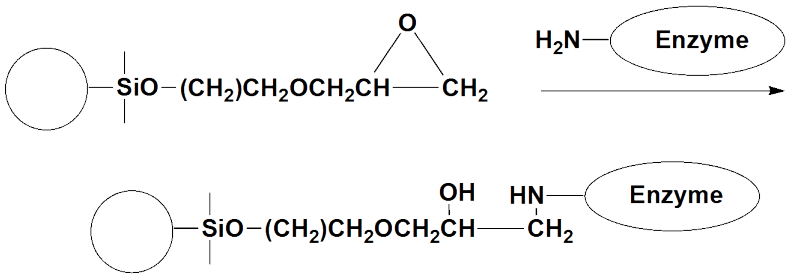

Figure 1.30: Functionalisation of epoxy-silica beads with enzyme.

1.11 Thesis Aims

CYP199A4 has demonstrated considerable use as model system for P450 reactions owing to its robust heterologous in recombinant *E. coli* and ease of crystallisation for structural studies. Initially, the T252E mutant of CYP199A4 will be expressed and purified. In Chapter 2, this mutant will be tested with different methods to generate H_2O_2 *in situ* such as oxygen surrogates and photochemical flavin-based reactions. Reaction conditions will be optimised to drive and maximise product formation with T252E-CYP199A4. Insights gleaned from these methods with T252E-CYP199A4 will be applied to other P450 peroxygenase enzymes such as CYP152A1 ($P450_{BS\beta}$). Deuterated *para*-substituted benzoic acids will also be used to study the peroxygenase and monooxygenase pathways of CYP199A4 to ascertain if a kinetic isotope effect is present in the C-H bond abstraction step in either pathway.

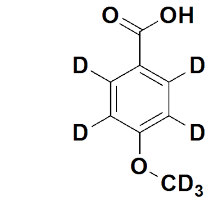

4-(-methoxy-d_3)benzoic acid-d_4

Figure 1.31: Deuterated 4-methoxybenzoic acid used to probe kinetic isotope effects of C-H abstraction with CYP199A4.

In Chapter 3, enzymatic approaches to generate H_2O_2 *in situ* for P450 reactions will also be explored through the use of different oxidases. Oxidase enzymes are able to generate H_2O_2 in the presence of a suitable substrate and O_2, such oxidases include alditol oxidase,[178] choline oxidase[179] and formate oxidase.[180] The oxidases will also be fused to P450 peroxygenases to generate two-domain fusion protein that will have both H_2O_2-generating and peroxygenase functions. Optimisation of these oxidase-P450 reactions will be carried out with T252E-CYP199A4 and other P450 peroxygenases to determine the viability of this approach. The immobilisation of P450 peroxygenases onto solid surfaces will also be tested to explore future use of flow chemistry with these P450s.

P450 peroxygenases only require H_2O_2 for catalytic activity. In Chapter 4, crystals of T252E-CYP199A4 will be co-crystallised with substrate bound to the active site. These crystals will be soaked with different concentrations of H_2O_2 with the aim of driving an enzymatic reaction within the crystallised enzyme. Crystal structures of these soaked P450 crystals will be solved to access if any *in crystallo* enzymatic reaction has occurred.

In Chapter 5, CYP199A4 will be used as a model system to investigate carbon-carbon (C-C) bond cleavage reactions catalysed by P450 enzymes. These bond cleavage reactions are of significant interest in the human steroidogenic pathway and its reaction mechanism is not completely understood. Site-directed mutagenesis will also be used to generate mutants of CYP199A4 with the aim of introducing C-C cleavage activity with suitable α-hydroxyketone compounds. These compounds are designed after similar substrates in physiological C-C cleavage reactions. X-ray structures of mutants that are able to catalyse C-C cleavage reactions will be determined to rationalise any activity observed.

In Chapter 6, CYP199A4 will be used to explore P450 aromatic oxidations. Crystals of CYP199A4 complexed with an aromatic substrate will be presented. Mutagenesis approaches will be used to enable aromatic oxidation with CYP199A4.

Finally, Chapter 7 will discuss concluding remarks and possible future directions of the insights gleaned from this thesis.

2 Selective Oxidations Using a Cytochrome P450 Enzyme Variant Driven with Surrogate Oxygen Donors and Light

Accepted for publication in Chemistry: A European Journal.

Lee, J.H.Z.; Podgorski, M.N.; Moir, M.; Gee,A. R.; Bell S. G., Selective Oxidations Using a Cytochrome P450 Enzyme Variant Driven with Surrogate Oxygen Donors and Light, *Chem. Eur. J.* 2022.

Contributions

This chapter presents research contributions by the candidate that first includes expression and purification of T252E-CYP199A4. This P450 enzyme was then used by the candidate for heme-bleaching assays with 4-trifluoromethoxybenzoic acid and 4-methoxybenzoic acid. A structure of T252E-CYP199A4 in complex with 4-trifluoromethoxybenzoic acid was also crystallised and solved. Peroxygenase reactions of T252E-CYP199A4 were then optimised by the candidate using H_2O_2 and urea-hydrogen peroxide. Further experiments were performed using deuterated substrates to assess if a kinetic isotope effect was present with peroxygenase and monooxygenase reactions of CYP199A4. Light-driven reactions using flavin molecules were also carried out by the candidate to drive peroxygenase reactions with T252E-CYP199A4.

Statement of Authorship

Title of Paper	Selective Oxidations Using a Cytochrome P450 Enzyme Variant Driven with Surrogate Oxygen Donors and Light
Publication Status	☑ Published ☐ Accepted for Publication ☐ Submitted for Publication ☐ Unpublished and Unsubmitted work written in manuscript style
Publication Details	Lee, J. H. Z.; Podgorski, M. N.; Moir, M.; Gee, A. R.; Bell, S. G. Selective Oxidations Using a Cytochrome P450 Enzyme Variant Driven with Surrogate Oxygen Donors and Light. *Chem. Eur. J.* **2022**, *28*

Principal Author

Name of Principal Author (Candidate)	Joel Hoong Zhang Lee		
Contribution to the Paper	Expression and Purification of P450 enzymes, light-driven and chemical surrogate reactions with P450s, heme-bleaching assays, P450 reactions with deuterated substrates, Crystallisation and crystal data processing of T252E-CYP1994+4-trifluoromethoxybenzoic acid, data analysis and initial drafting.		
Overall percentage (%)	70		
Certification:	This paper reports on original research I conducted during the period of my Higher Degree by Research candidature and is not subject to any obligations or contractual agreements with a third party that would constrain its inclusion in this thesis. I am the primary author of this paper.		
Signature		Date	18/04/2023

Co-Author Contributions

By signing the Statement of Authorship, each author certifies that:

i. the candidate's stated contribution to the publication is accurate (as detailed above);

ii. permission is granted for the candidate in include the publication in the thesis; and

iii. the sum of all co-author contributions is equal to 100% less the candidate's stated contribution.

Name of Co-Author	Michael Moir		
Contribution to the Paper	Synthesis of deuterated substrates		
Signature		Date	20/02/2023

Name of Co-Author	Alecia Gee		
Contribution to the Paper	Carried out light-driven P450 reactions		
Signature		Date	17/2/23

Please cut and paste additional co-autho

Name of Co-Author	Matthew Podgorski
Contribution to the Paper	Carried out P450 reactions assessing enantioselectivity and product yield with peroxide shunt pathway
Signature	Date 26/3/23

Name of Co-Author	Stephen Bell
Contribution to the Paper	Conceptualisation of experiments and drafting of publication
Signature	Date 17/2/2023

Chemistry–A European Journal
Research Article
doi.org/10.1002/chem.202201366
Chemistry Europe
European Chemical Societies Publishing
www.chemeurj.org

Selective Oxidations Using a Cytochrome P450 Enzyme Variant Driven with Surrogate Oxygen Donors and Light

Joel H. Z. Lee,[a] Matthew N. Podgorski,[a] Michael Moir,[b] Alecia R. Gee,[a] and Stephen G. Bell*[a]

Abstract: Cytochrome P450 monooxygenase enzymes are versatile catalysts, which have been adapted for multiple applications in chemical synthesis. Mutation of a highly conserved active site threonine to a glutamate can convert these enzymes into peroxygenases that utilise hydrogen peroxide (H_2O_2). Here, we use the T252E-CYP199A4 variant to study peroxide-driven oxidation activity by using H_2O_2 and urea-hydrogen peroxide (UHP). We demonstrate that the T252E variant has a higher stability to H_2O_2 in the presence of substrate that can undergo carbon-hydrogen abstraction. This peroxygenase variant could efficiently catalyse *O*-demethylation and an enantioselective epoxidation reaction (94% *ee*). Neither the monooxygenase nor peroxygenase pathways of the P450 demonstrated a significant kinetic isotope effect (KIE) for the oxidation of deuterated substrates. These new peroxygenase variants offer the possibility of simpler cytochrome P450 systems for selective oxidations. To demonstrate this, a light driven H_2O_2 generating system was used to support efficient product formation with this peroxygenase enzyme.

Introduction

Cytochromes P450 (P450s) are a family of heme monooxygenase enzymes that carry out oxidative transformations including the hydroxylation of carbon-hydrogen bonds and the epoxidation of alkenes.[1] These enzyme-catalysed transformations offer advantages over synthetic methods in that highly selective carbon-hydrogen bonds can be functionalised under mild conditions and in a single step.[2] The high-valent iron-oxo radical cation intermediate, Compound 1 (Cpd 1) is the reactive intermediate which abstracts a hydrogen from the substrate before undergoing an oxygen rebound step to form the carbon-oxygen bond.[3–4] The multi-step catalytic cycle of these monooxygenases involve substrate binding, electron transfer, binding of dioxygen, and electron and proton delivery to enable Cpd I formation (Scheme 1).

The electrons used to drive oxygen activation are derived from a nicotinamide cofactor (NAD(P)H) and are delivered via electron transfer partners.[5] In most CYP enzymes, proton delivery and oxygen activation is controlled by specific residues within the I-helix.[6–10] The requirement for electron transfer proteins and expensive cofactors hampers the use of many of these P450 enzymes as biocatalysts.[11] If the need for both could be removed it could result in the simpler application, and more widespread use of these enzymes.[12–18] An alternative

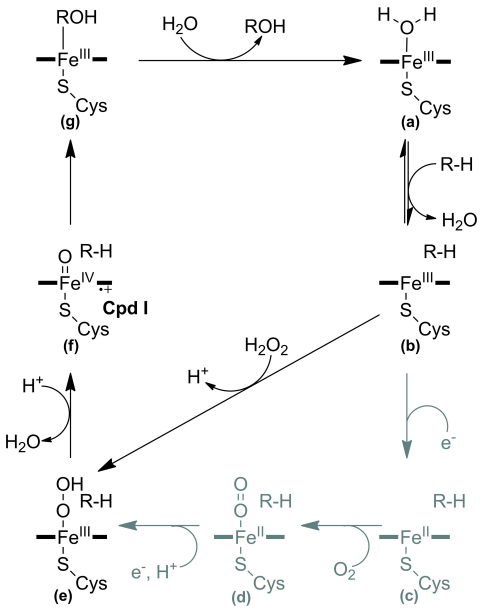

Scheme 1. Catalytic cycle of P450 monooxygenases. The peroxide shunt pathway which enables the enzyme to bypass the electron transfer steps is highlighted.

[a] *J. H. Z. Lee, M. N. Podgorski, A. R. Gee, Dr. S. G. Bell*
Department of Chemistry
University of Adelaide
Adelaide, SA 5005 (Australia)
E-mail: stephen.bell@adelaide.edu.au

[b] *Dr. M. Moir*
National Deuteration Facility
Australian Nuclear Science and Technology Organisation (ANSTO)
Lucas Heights, Sydney, NSW 2232 (Australia)

Supporting information for this article is available on the WWW under https://doi.org/10.1002/chem.202201366

method is to use hydrogen peroxide (H_2O_2) via the peroxide shunt mechanism (Scheme 1).[12]

A select number of P450 family members have evolved to naturally function as peroxygenases. The CYP152 family of enzymes, whose members include CYP152A1 (P450BSβ) can oxidise fatty acids using H_2O_2 by making use of the carboxylate group of the substrate to generate Cpd I with hydrogen peroxide.[19–22] Cytochrome P450 heme monooxygenase enzymes have been converted to peroxygenases by introducing a single mutation, changing the active site threonine of the I-helix (part of the acid-alcohol pair involved in dioxygen activation) to a glutamate.[6–10,23–25] Alternatively molecules, which place an acid/base functional group close to the heme, can also introduce peroxygenase activity, though this requires significant synthetic effort and design of these bespoke molecules for each enzyme/substrate combination.[26]

Here we use the threonine-252 to glutamate variant (T252E) of the P450 enzyme CYP199A4, from *Rhodopseudomonas palustris* HaA2,[24] to explore how such engineered peroxygenases can be used for catalytic oxidations using hydrogen peroxide and urea-hydrogen peroxide (UHP) with *para*-substituted benzoic acids. The mechanism of enzyme action is investigated using fluorinated and deuterated substrates. The oxidation of *para*-substituted benzoic acids is demonstrated using a light-activated system that generates hydrogen peroxide using flavin.

Results and Discussion

The activity and stability of the T252E mutant of CYP199A4, which converts this enzyme into a H_2O_2 utilising peroxygenase, was tested using the oxidation of 4-methoxybenzoic acid as substrate by H_2O_2. First, we tested the stability of both the T252E and wild type (WT) CYP199A4 enzymes to hydrogen peroxide in the presence and absence of 4-methoxybenzoic acid. In the presence of $\geq$10 mM H_2O_2, the heme of the substrate-free T252E mutant was rapidly bleached. Higher H_2O_2 concentrations resulted in faster heme bleaching (Figure 1, Figure S1). This occurred more rapidly with the mutant than with the WT CYP199A4 (Figure S2).

The addition of 4-methoxybenzoic acid significantly reduced the rate of heme destruction in the T252E peroxygenase mutant (Figure 1). The fluorinated substrate 4-trifluoromethoxybenzoic acid, which is not oxidised by T252E-CYP199A4 (or WT CYP199A4) due to the strong C–F bonds,[27] was demonstrated to hinder bleaching of the enzyme by H_2O_2 compared to the absence of a substrate (Figure 1). However, the rate of bleaching was slower in the presence of 4-methoxybenzoic acid. 4-Trifluoromethoxybenzoic acid did not induce a spin state change on addition to the T252E mutant (Figure S3). However, we were able to determine a crystal structure of T252E-CYP199A4 with this substrate bound (Figures 2 and S4, Tables S1 and S2). This demonstrated that 4-trifluoromethoxybenzoic acid was bound to the peroxygenase variant in a similar fashion to 4-methoxybenzoic acid in the T252E variant. Importantly the glutamate residue maintains a strong interaction with the heme aqua ligand which is not displaced on substrate binding explaining the lack of a change in the UV-vis spectrum on substrate addition.

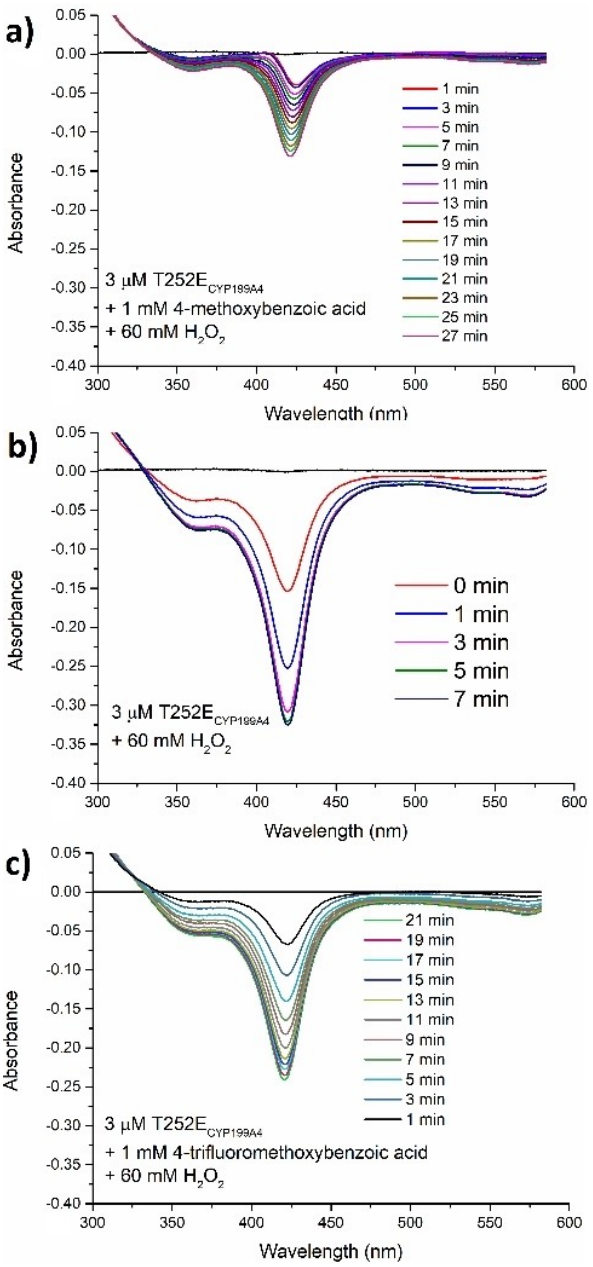

Figure 1. Rate of heme bleaching of the T252E-CYP199A4 enzyme (3 μM) exposed to 60 mM H_2O_2 with (a) 1 mM 4-methoxybenzoic acid, (b) in the absence of substrate and (c) 1 mM 4-trifluoromethoxybenzoic acid. After 1 minute spectra were recorded at 2 minute intervals.

We propose that quenching of reactive intermediates through substrate oxidation is partly responsible for preventing rapid heme destruction. We demonstrated that after bleaching

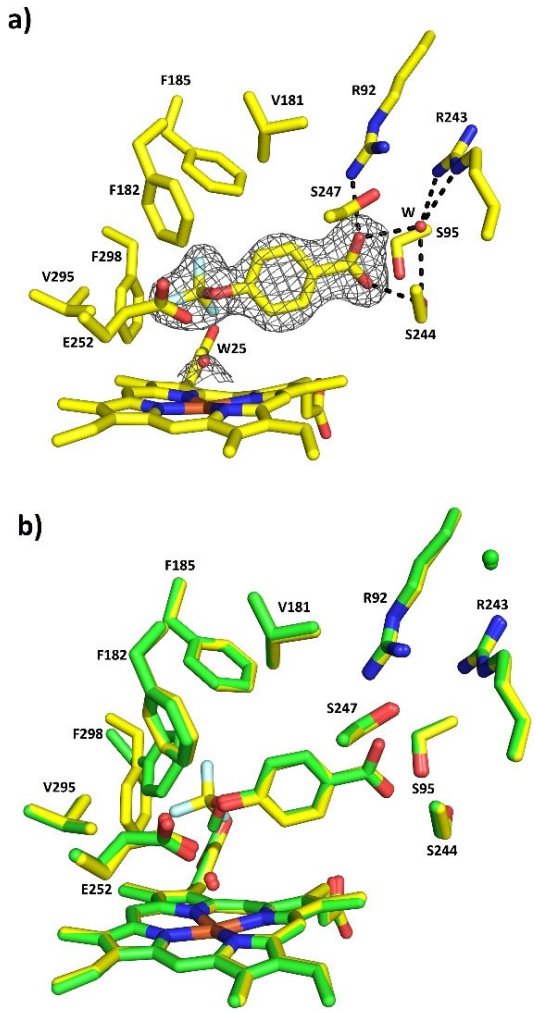

Figure 2. Crystal structure of 4-trifluoromethoxybenzoic acid bound to T252E-CYP199A5 solved at 1.95 Å. A composite omit map of the 4-trifluoromethoxybenzoic acid substrate is shown as a grey mesh contoured at 1.0 (1.5 Å carve). b) The superimposed crystal structures of T252E-CYP199A4 bound to 4-trifluoromethoxybenzoic acid (yellow) and 4-methoxybenzoic acid (green). When bound to the fluorinated substrate, the F298 residue moves away from the heme centre compared to 4-methoxybenzoic acid to accommodate the trifluoro moiety.

through exposure to H_2O_2 the enzyme was inactivated, and no product formation was observed (Figure S5). Recently P450 peroxygenases have been demonstrated to display catalase activity.[28–29] This catalase activity has also been linked to protection against heme degradation and it was shown that in the presence of suitable substrates it acts as a scavenger pathway preventing heme degradation. Despite the similar binding modes of the fluorinated substrate and 4-methoxybenzoic acid we yet cannot rule out that the interaction of peroxide with the heme is weaker in the presence of this ligand.[30]

Next, we optimised the peroxygenase activity of T252E-CYP199A4 by varying the concentrations of enzyme, H_2O_2 or urea-hydrogen peroxide (UHP), and the temperature. UHP is a crystalline solid that slowly yields free hydrogen peroxide when added to an aqueous solution.[31–32] 4-Methoxybenzoic acid was oxidised with 1, 3 or 5 μM T252E-CYP199A4 and 1 to 64 mM H_2O_2 or 16 to 64 mM UHP (Scheme 2). The differences in the levels of product formation when using UHP and H_2O_2 were moderate (Figure 3). Increasing the concentration of both to 32 mM and 64 mM yielded the highest levels of oxidised metabolite (Figure 3). The highest total turnover numbers were achieved with 3 μM enzyme, 1 mM substrate and at 30 °C rather than 16 °C (Figure S6).

Previous experimental evidence and theory suggests the P450 CYP152 family peroxygenases use the Cpd I intermediate to catalyse hydroxylations and *O*-demethylations.[33–34] To investigate if this was the case in the engineered T252E variant, we synthesised the deuterated substrate, 4-(methoxy-d_3)benzoic-d_4 acid (see Experimental Section for details). This deuterated substrate could be used to measure if there was a kinetic isotope effect during the peroxygenase reactions of T252E-CYP199A4.

The deuterated substrate bound to WT CYP199A4 and induced a complete change in the spin-state of the heme from low-spin to high-spin as measured using UV-vis spectroscopy (Figure S7). In contrast a minimal change in the spectrum was observed on addition of 4-(methoxy-d_3) benzoic-d_4 acid to the T252E variant (Figure 4). This is consistent with what has been observed for 4-methoxybenzoic acid and is related to the occupancy of the heme aqua ligand which is retained in the T252E variant as it interacts with the introduced glutamate residue.[24]

This was compared to the monooxygenase reactions of WT-CYP199A4 in which electron transfer is the rate determining step in bacterial P450s.[35] Comparative oxidation reactions were performed with deuterated and non-deuterated 4-methoxybenzoic acid individually and as a mixture (Figure S7–S10). For both monooxygenase and peroxygenase systems there was not a significant difference in the levels of product arising from the deuterated or non-deuterated substrates or in the turnover rate of the catalytic cycle (Figure 4, Table S3 and Figures S7–S10). There was also no change in the proportion of the deuterated versus non-deuterated substrate over the time of the reactions (Figure S11, Table S4). The comparable results across both the monooxygenase and peroxygenase systems

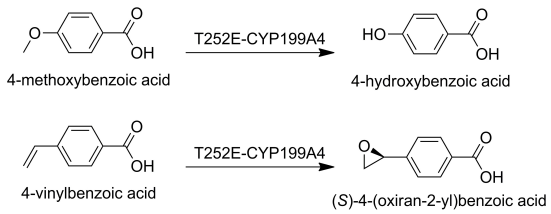

Scheme 2. Oxidation of *para*-substituted benzoic acids carried out by T252E-CYP199A4.

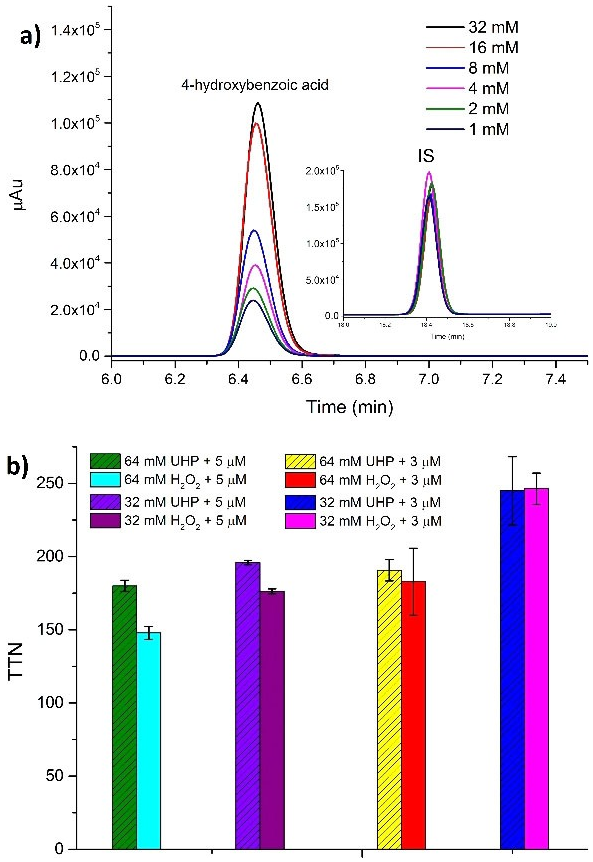

Figure 3. (a) HPLC analysis of 4-methoxybenzoic acid *O*-demethylation by T252E-CYP199A4 (1 μM) using different concentrations of H_2O_2. Products are labelled as is the internal standard (IS). (b) A comparison of the total turnover numbers (TTN) obtained with T252E-CYP199A4 (5 μM or 3 μM) in the presence of 1 mM 4-methoxybenzoic acid and different concentrations of UHP and H_2O_2 (32 mM or 64 mM). Reactions were conducted at 30 °C and left for 24 h.

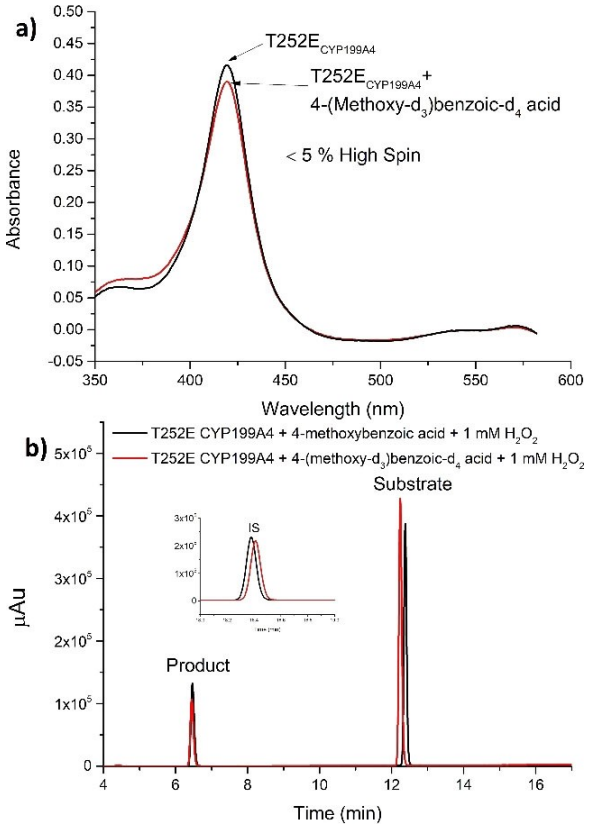

Figure 4. (a) Spin state shift analysis of 4-(methoxy-d_3) benzoic-d_4 acid with T252E-CYP199A4. (b) HPLC analysis of 4-methoxybenzoic acid (black) and 4-(methoxy-d_3) benzoic-d_4 acid (red) with T252E-CP199A4 in the presence of 1 mM H_2O_2 after 24 h of incubation at 16 °C and 70 RPM. Substrate concentration used was 100 μM.

were indicative that C–H bond abstraction is not involved in the rate determining step of either the peroxygenase or monooxygenase reaction mechanisms. This would be consistent with both C–H bond activation steps in these *O*-demethylation reactions proceeding via the radical rebound mechanism using Cpd I which is known to be fast.[36–37]

We next investigated if the peroxygenase activity of the T252E variant could catalyse the epoxidation of 4-vinylbenzoic acid. WT CYP199A4 has been demonstrated to catalyse this reaction with high enantioselectivity for the (*S*)-enantiomer (99% ee).[38] The T252E peroxygenase enzyme was able to epoxidise 4-vinylbenzoic acid using H_2O_2 more efficiently than the WT enzyme (Figure 5). The high enantioselectivity for the (*S*)-enantiomer was also maintained in these peroxygenase reactions (94% ee, by HPLC Scheme 2).

The T252E peroxygenase variant of CYP199A4 opens the possibility of using new methods to drive C–H bond activation by cytochrome P450 enzymes. We wanted to assess if the catalytic activity of the system could be supported by generating H_2O_2 over time using light, flavin mononucleotide (FMN), and the electron donor ethylenediaminetetraacetate (EDTA).[39]

To assess the efficiency of this method, control reactions were performed, using the natural CYP152 family peroxygenase enzyme P450Bsβ. This enzyme is reported to catalyse the α- and β-hydroxylation of fatty acids.[40] GC-MS analysis of the reaction of this enzyme with tetradecanoic acid demonstrated the formation of a complex mix of metabolites (Figures 6 and S12a–d). This included metabolites arising from α- and β-hydroxylation but also from α-oxidative decarboxylation to yield shorter-alkyl-chain fatty acids including tridecanoic, dodecanoic, undecanoic and decanoic acid (Scheme 3).[41] Extensive further oxidation of these shorter chain fatty acids also occurred (Figure 6). This control reaction highlighted that the light driven system could generate enough H_2O_2 to support these peroxygenase enzymes.

We then applied this system to T252E-CYP199A4 to assess if it could drive C–H bond activation. We were able to demon-

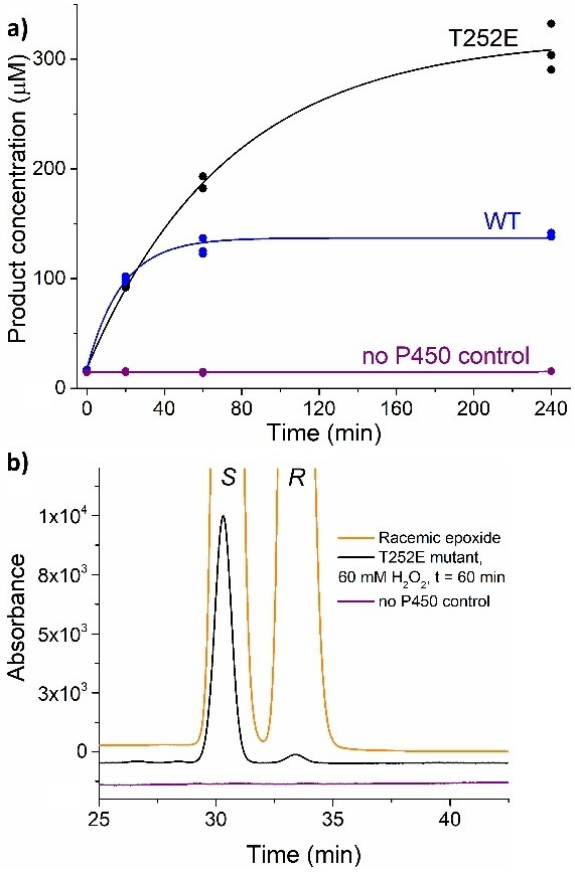

Figure 5. (a) Time course of 4-vinylbenzoic acid conversion into the corresponding epoxide by peroxygenase activity of WT and T252E CYP199A4 isoforms (b) Enantioselective HPLC analysis of the epoxide generated by the T252E mutant in a H_2O_2-driven reaction (60 mM H_2O_2) over a 60-minute period (black). In purple is a control reaction omitting the P450.

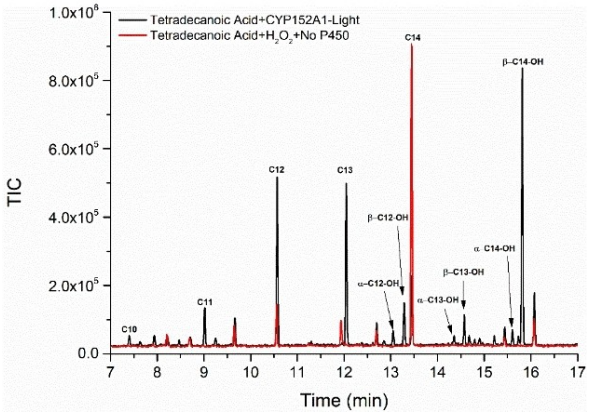

Figure 6. GC-MS Analysis of light driven oxidation of tetradecanoic acid (C14) by CYP152A1 (black, P450BSβ). In red is a control reaction with 10 mM H_2O_2 and no P450 added. Conditions used are 5 μM P450, 200 μM FMN, 1 mM EDTA and 100 μM substrate for the light-driven reaction. Other metabolites were indicated by the length of the fatty acid chain (i.e., C10 for decanoic acid) and by α or β hydroxylation (i.e., α-C14-OH for α-hydroxy tetradecanoic acid).

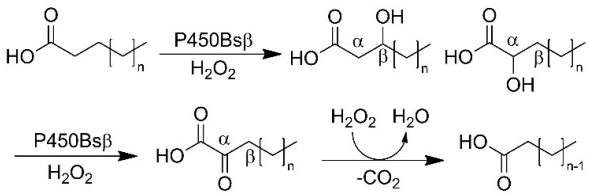

Scheme 3. Reaction scheme for the hydroxylation of fatty acids by P450Bsβ and subsequent α-keto decarboxylation.

strate the oxidative demethylation of 4-methoxybenzoic acid using light (Figure 7).

Optimisation of the system by varying the enzyme and substrate concentration resulted in complete conversion of 200 μM substrate with 2.5% molar equivalents of enzyme as the biocatalyst (40 TTN). While these turnover numbers need to be improved for practical applications, we have been able to show complete conversion of substrate to product using a system that can generate H_2O_2 *in situ*. This should enable greater control of the conditions that enable productive enzyme activity versus catalyst degradation. We were also able to demonstrate that T252E-CYP199A4 with FMN and light was able to epoxidise 4-vinylbenzoic acid (Figure S14).

Conclusion

The T252E-CYP199A4 peroxygenase variant could catalyse the oxidative demethylation of 4-methoxybenzoic acid and the stereoselective epoxidation of 4-vinylbenzoic acid by using H_2O_2 supplied directly, in the form of urea-hydrogen peroxide or generated by using a light-driven flavin/EDTA-based system. The selectivity of the WT enzyme for these reactions was maintained when using the T252E peroxygenase variant. The lack of a kinetic isotope effect in our experiments demonstrates that C–H bond abstraction is not involved in a rate determining step of the mechanism for the peroxygenase pathway. This would agree with both peroxygenase and monooxygenase pathways by using Cpd I as the reactive intermediate. Further studies with bespoke substrate/enzyme combinations could enable the measurement of an intrinsic kinetic isotope effect that would facilitate a more complete analysis. This peroxygenase system is a step towards generating simpler biocatalysts for selective hydroxylation reactions and eliminating the requirement for nicotinamide cofactors and electron transfer partners. The equivalent mutation in other P450s would enable peroxygenase activity to be conferred for selective oxidations across a range of substrates by using these enzymes. Further optimisation of the systems, by rational protein engineering or directed evolution, could also be undertaken to improve the catalytic activity and the stability. Flow chemistry methods to

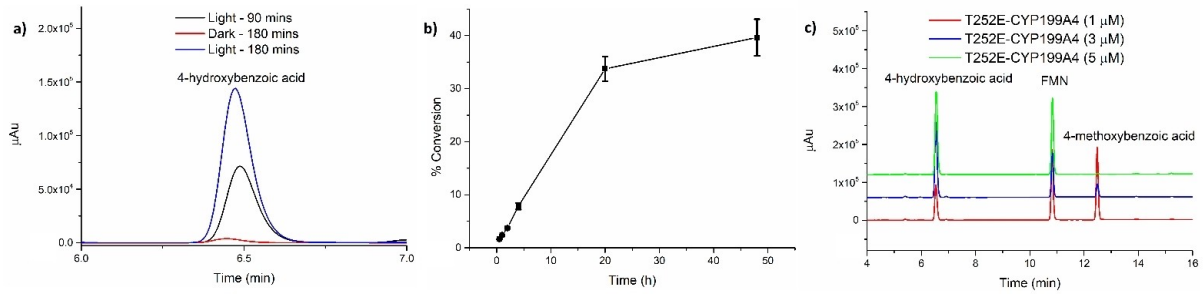

Figure 7. (a) Light driven turnovers of T252E-CYP199A4 (1 μM) and substrate (200 μM) with a control reaction in the dark. (b) Time course experiments of light activated T252E-CYP199A4 reaction with 4-methoxybenzoic acid. Conditions used are CYP199A4-T252E (3 μM), FMN (200 μM), EDTA (1 mM) and 4-methoxyBA (200 μM). (c) Optimisation of light-activated systems were then carried out with different enzyme concentrations (1 μM, 3 μM and 5 μM) with 200 μM FMN Reaction time was 20 hr at room temperature).

deliver the H_2O_2 cofactor over an immobilised enzyme could also be used to improve the catalyst lifetime and therefore the yield.[42]

Experimental Section

Enzymology - General: General reagents and organics were purchased from Sigma-Aldrich. Isopropyl-β-D-thiogalactopyranoside (IPTG) and buffer components were obtained from Astral Scientific (Australia). UV/Vis spectroscopy was performed on an Agilent Cary 60 spectrophotometer.

Analytical high performance liquid chromatography (HPLC) was performed on a Shimadzu LC-20AD equipped with a Phenomenex Kinetex 5u XB–C18 100 A column (250 mm x 4.6 mm, 5 μM), SIL-20 A autosampler, CTO-20 A, SPD-20 A UV detector and CBM-20Alite communications module. A gradient of 20–95% acetonitrile in water (both containing trifluoroacetic acid, TFA, 0.1%) was run at a flow rate of 1 mL min^{-1} over 30 minutes and detector wavelength was set at 254 nm.

Chiral HPLC analysis was carried using the same system as above using a Lux Cellulose-1 chiral column (1000 Å pore size, 100× 4.6 mm, 3 μm; Phenomenex) using isocratic elution with 20% Acetonitrile in H_2O (0.1% TFA) at a flow rate of 0.4 mL min^{-1}.

GC-MS analysis was performed using a Shimadzu GC-2010 gas chromatograph equipped with an autoinjector and a GCMS-QP2010S detector; the column used was again a DB-5MS UI column. The interface and injection port temperatures were held at 280 and 250 °C. The column was held at 120 °C for 3 min, and the temperature was then increased to 240 °C at a rate of 7.5 °C min^{-1} and held at 240 °C for 6 min.

Production and purification of enzymes: HaPux, HaPuR, CYP199A4 and its variants were all produced, and purified as described previously.[24] A pET28 plasmid containing the gene for CYP152 A1 (P450BSβ) with 6 x Histag residues at the N-terminus and a silica binding amino acid sequence (MPGRARAQRQSSRGR)[43] at the C-terminus was purchased commercially from Twist Biosciences. This plasmid was transformed into *E. coli* BL21 (DE3) competent cells (New England Biolabs) and the bacteria were incubated overnight at 37 °C on an LB agar plate containing kanamycin (30 mg L^{-1}). Colonies of the bacteria were used to inoculate 1 mL of LB with kanamycin (30 mg L^{-1}) and left for 5 h at 37 °C and 200 RPM to generate a starter culture. The starter culture (50 μL) was used to inoculate 2 x 750 mL volumes of LB broth containing kanamycin (30 mg L^{-1}) and the larger cultures were incubated for 8 h at 37 °C and 120 RPM. This was followed by incubation at 18 °C and 90 RPM, while 2% w/v EtOH, 0.02% w/v of benzyl alcohol and 2 mL of trace elements solution were added to the culture. The resulting culture was incubated for 30 mins at 18 °C and 90 RPM and ~30 μM IPTG (isopropyl β-D-1-thiogalactopyranoside) was added to induce protein expression. After incubating the culture for ~24 h at 18 °C and 90 rpm, it was centrifuged (5000 *g*, 10 min, 4 °C) to collect the cell pellet, which was stored frozen at −20 °C.

The frozen cell pellet was thawed and resuspended in 100 mL of lysis buffer (100 mM KPi, pH 7.5, 300 mM KCl, 20 mM imidazole). The cells were lysed by sonication using an Autotune CV334 Ultrasonic Processor equipped with a standard probe (136 mm x 13 mm; Sonics and Materials, US) using 30×10 s pulses with 50 s intervals. Cell debris were removed by centrifugation (18000 *g*, 20 mins, 4 °C). The supernatant was then loaded on to a 5 mL His-trap column (GE Healthcare) equilibrated with lysis buffer. The column was then washed with lysis buffer (25 mL). The bound protein was then eluted with elution buffer (100 mM KPi, pH 7.5, 300 mM KCl, 300 mM imidazole). Samples and buffers were applied to the column with flowrate of 3 ml min^{-1}. Eluted protein was concentrated by ultrafiltration using a Vivacell 100 centrifugal concentrator with a 10 kDa molecular weight cut-off membrane (Sartorius). The concentrated protein was eluted down a PD-10 desalting column (GE Healthcare) to remove excess imidazole and concentrated again to a final volume of 2 mL and glycerol was added to a final concentration of 50% v/v. The purified protein was stored at −20 °C. Crystals of the T252E variant with 4-trifluoromethoxybenzoic acid were prepared and the structure determined using the same methods described previously for the 4-methoxybenzoic acid-bound form of this enzyme.[24]

Activity assays

In vitro NADH oxidation assays: Glycerol was removed from proteins using a 5 mL gel filtration column (PD-10, GE Healthcare) and the concentration of each protein was quantified using UV-Vis spectrophotometry. In a final volume of 1.5 mL, oxygenated Tris buffer (50 mM, pH 7.4), CYP199A4 (0.5 or 0.05 μM), ferredoxin (HaPux, 5 μM), ferredoxin-reductase (HaPuR, 0.5 μM), bovine liver catalase (100 ng μL^{-1}) were combined and equilibrated at 30 °C for 2 min. NADH was added to A340≈2.0 (≈320 μM). Substrate was then added to the desired final concentration (1 mM or 0.5 mM) and the absorbance at 340 nm was monitored. The rate of oxidation of NADH was determined from the gradient of the plot of

A340 versus time, using the extinction coefficient of NADH, ε340 = 6.22 mM^{-1} cm^{-1}.

Peroxygenase assays: The peroxygenase oxidation assays were run at 16 °C or 30 °C in a total volume of 600 μL consisting of Tris buffer (pH 7.4, 50 mM), 1–5 μM enzyme and 200–1000 μM substrate. The reaction was started by addition of H_2O_2 (1–64 mM) or UHP (16/32/64 mM) and incubated for 20 h at 70 rpm. UHP was added as a solid powder while H_2O_2 was added from a 500 mM stock solution.

Light-driven peroxygenase activity of the T252E-CYP199A4 enzyme was assayed in a reaction mixture containing enzyme (1–5 μM), substrate (200 μM), EDTA (1 mM), FMN (200 μM) in oxygen saturated Tris buffer, 50 mM, pH 7.4 with a total reaction volume of 1 mL. Samples were shaken at 70 rpm at room temperature and assays were initiated by illumination from an Arlec 5700 kW light source. Total assay time was 20 hr, after which the light was switched off. The reactions were terminated by the addition of 10 μL catalase (10 mg/mL stock) before being prepared for HPLC analysis. Dark reactions were carried out in the same conditions but within a N-Biotek NB-205 L tinted shaking incubator with a dark cloth covering the incubator.

Heme bleaching assay: A 600 μL aliquot of WT CYP199A4 or the T252E mutant (3 μM) in Tris buffer (50 mM, pH 7.4) was used to baseline the UV-vis spectrophotometer. Substrate (1 mM) and H_2O_2 (1–60 mM) were added, and the UV-Vis spectrum was recorded. Heme prosthetic group destruction was monitored by recording UV-Vis spectra at 2 min intervals.

Product analysis: For HPLC analysis, after reactions were completed, 132 μL of the reaction mixture was mixed with 2 μL of an internal standard solution (10 mM 9-hydroxyfluorene solution in EtOH) and 66 μL of CH_3CN. Samples were acidified with 0.2 μL of trifluoroacetic acid. Products were identified by co-elution with authentic product standards.[38,44] Products were calibrated against the internal standard. All reactions were performed in triplicate or duplicate.

For GC-MS analysis, the reaction mixture (1000 μL or 600 μL) was mixed with 10 μL of an internal standard (10 mM 9-hydroxyfluorene solution in EtOH) and extracted with EtOAc (2×400 μL). The extracts were dried with $MgSO_4$ and solvent was removed under N_2. The remaining residue was resuspended in anhydrous acetonitrile (150 μL) and derivatisation agent (15 μL, BSTFA + TMCS, 99:1). The mixtures were left for 2 h at 37 °C prior to analysis by GC-MS.

Synthesis experiments: All reactions were performed under an atmosphere of nitrogen unless otherwise specified. Chemicals and reagents of the highest grade were purchased from Sigma-Aldrich (Sydney, Australia) and were used without further purification. Solvents were purchased from Sigma-Aldrich and Merck. NMR solvents were purchased from Cambridge Isotope Laboratories Inc. (MA, USA) and Sigma-Aldrich and were used without further purification. D_2O (99.8%) was supplied by AECL, Canada. Analytical thin-layer chromatography (TLC) was performed using Merck aluminium backed silica gel 60 F_{254} (0.2 mm) plates, which were visualised with shortwave (254 nm) ultraviolet light or with potassium permanganate, vanillin, Hanessian's or bromocresol green stains. Flash column chromatography was performed using Merck Kieselgel 60 (230-400 mesh) silica gel, with the eluent mixture reported as the volume:volume ratio. Hydrothermal reactions were performed in D_2O at high temperatures by mixing the appropriate benzoic acid derivative with NaOH and Pd/C (10% w/w) in a Mini Benchtop 4560 Parr reactor (450 mL vessel capacity, 3000 psi maximum pressure, 350 °C maximum temperature) (Moline, USA). Nuclear magnetic resonance spectra were recorded at 300 K using either a Bruker AVANCE DRX400 (400 MHz) spectrometer. ^1H chemical shifts are expressed as parts per million (ppm) with residual methanol (δ 3.31) and dimethyl sulfoxide (δ 2.50) as reference and are reported as chemical shift (δ); relative integral; multiplicity; coupling constants (*J*) reported in Hz. ^{13}C chemical shifts are expressed as parts per million (ppm) with residual methanol (δ 49.0) and dimethyl sulfoxide (δ 39.52) as reference and reported as chemical shift (δ); multiplicity. ^2H chemical shifts are reported as parts per million (ppm) and are reported as chemical shift (δ); multiplicity. Low-resolution mass spectrometry (LRMS) was recorded using electrospray ionisation (ESI) recorded on a 4000 QTrap AB Sciex spectrometer. The overall percentage deuteration of the molecules were calculated by MS using the isotope distribution analysis of the different isotopologues. This was calculated taking into consideration the ^{13}C natural abundance, whose contribution was subtracted from the peak area of each M + 1 isotopologue to allow for accurate estimation of the percentage deuteration of each isotopologue.

Synthetic Procedures

4-Hydroxybenzoic-d_4 acid: (Scheme 4; step a) A mixture of 4-hydroxybenzoic acid (7 g, 50.7 mmol), sodium hydroxide (4.5 g, 111.5 mmol) and palladium on carbon (10% w/w, 1.58 g, 1.52 mmol) in D_2O (120 mL) was heated at 210 °C for 2 h in a 450 mL Parr reactor. After cooling to room temperature the mixture was passed through a pad of Celite and the filtrate concentrated under reduced pressure to a volume of about 100 mL. The aqueous solution was acidified (pH = 2) with aqueous hydrochloric acid (6 M) and extracted with ethyl acetate (5×75 mL). The combined organic extracts were dried over magnesium sulfate and concentrated under reduced pressure to obtain a crude mixture of the desired benzoic acid derivative and phenol. The desired product was isolated by flash column chromatography using ethyl acetate, hexane (3:7 to 1:0) as an eluent to obtain 4-hydroxybenzoic-d_4 acid (0.26 g, 3.6%) as a white solid, R_f = 0.1 (2:3 EtOAc, hexane); ^1H NMR (400 MHz, MeOD) δ 7.88 (residual), 6.82 (residual) ppm; ^2H NMR (6e1.4 MHz, MeOD) δ 7.91 (2D, bs), 6.86 (2D, bs) ppm; ^{13}C[44] NMR (101 MHz, MeOD) δ 170.1, 163.3, 122.5 ppm; $^{13}C\{^1H, ^2H\}$ NMR (101 MHz, MeOD) δ 170.1, 163.3, 132.6, 122.5, 115.7 ppm; MS (ESI−) $[M-H]^-$: 141.2 (major isotopologue), 89.6%D.

4-(Methoxy-d_3)benzoic-d_4 acid: (Scheme 4; step b) To a suspension of 4-hydroxybenzoic-d_4 acid (0.26 g, 1.83 mmol) and potassium carbonate (0.76 g, 5.49 mmol) in acetone (5 mL) was added methyl iodide-d_3 (0.34 mL, 5.49 mmol), dropwise. The mixture was warmed to reflux and stirred for 6 h. Mass spectrometry analysis of an aliquot of the reaction mixture revealed a mixture of methylated products. Additional methyl iodide-d_3 (0.34 mL, 5.49 mmol) was added and heating was continued for a further 4 h. Volatiles were removed under reduced pressure and the residue taken up in a mixture of CD_3OD (5 mL) and tetrahydrofuran (2 mL). To this was added aqueous lithium hydroxide (2 M, in D_2O, 2.7 mL) and the mixture stirred for 16 h at room temperature. The volatiles were

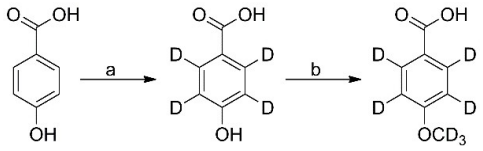

Scheme 4. Synthesis of 4-(methoxy-d_3)benzoic-d_4 acid. *Reagents and conditions*: (a) Pd/C, NaOH, D_2O, 210 °C, 2 h, 4%, 89.6%D; (b) i) CD_3I, K_2CO_3, reflux, 10 h, ii) LiOH (aq.), MeOD, THF, rt, 16 h, 62%, 93.3%D.

removed under reduced pressure and the residual aqueous solution washed with dichloromethane (5 mL), acidified (pH = 3) with aqueous hydrochloric acid (6 M) and extracted with ethyl acetate (4 × 50 mL). The combined organic extracts were dried over anhydrous magnesium sulfate and concentrated under reduced pressure. The resulting crude solid was purified by flash column chromatography using ethyl acetate, hexane (0 : 1 to 7 : 13) as an eluent to obtain 4-(methoxy-d_3)benzoic-d_4 acid (0.18 g, 62 %) as a white solid, R_f = 0.4 (1 : 1 EtOAc, hexane); ^{1}H NMR (400 MHz, DMSO-d_6) δ 7.89 (residual), 7.01 (residual) ppm; ^{2}H NMR (61.4 MHz, DMSO-d_6) δ 7.92 (2D, bs), 7.04 (2D, bs), 3.77 (3D, s) ppm; ^{13}C{^{1}H}NMR (101 MHz, DMSO-d_6) δ 167.0, 162.8, 122.8 ppm; ^{13}C{^{1}H, ^{2}H} NMR (101 MHz, DMSO-d_6) δ 167.0, 162.8, 131.0, 122.8, 113.5, 54.6 ppm; MS (ESI−) $[M-H]^-$: 158.1 (major isotopologue), 70.9 % d_7, 17.4 % d_6, 2.4 % d_5, 1.2 % d_4, 1.5 % d_3, 93.3 %D.

Acknowledgements

The authors acknowledge the award of Australian Government Research Training Program Scholarships to J.H.Z.L (PhD, University of Adelaide Constance Fraser Scholarship) and M.N.P. (M. Phil). J.H.Z.L thanks the CSIRO Synthetic Biology Future Science Platform for a PhD top-up Scholarship. The work was funded in part through Australian Research Council grant DP200102411 (to S.G.B. and others). The research was supported by a National Deuteration Facility grant (Proposal 9152). The National Deuteration Facility in Australia is partly funded by The National Collaborative Research Infrastructure Strategy (NCRIS), an Australian Government initiative. This research was undertaken in part using the MX1 beamline at the Australian Synchrotron, part of ANSTO. We thank Dr Charlotte Williams (CSIRO) for helpful suggestions on the work and the manuscript. Open access publishing facilitated by The University of Adelaide, as part of the Wiley - The University of Adelaide agreement via the Council of Australian University Librarians.

Conflict of Interest

The authors declare no conflict of interest.

Data Availability Statement

The data that support the findings of this study are available in the supplementary material of this article.

Keywords: biocatalysis · heme enzymes · monooxygenases · peroxygenases · protein engineering

[1] P. R. Ortiz de Montellano, in *Cytochrome P450: Structure, Mechanism, and Biochemistry* 4th ed., Springer International Publishing, Switzerland, **2015**.
[2] G. D. Roiban, M. T. Reetz, *Chem. Commun.* **2015**, *51*, 2208–2224.
[3] J. Rittle, M. T. Green, *Science* **2010**, *330*, 933–937.
[4] J. T. Groves, G. A. McClusky, *J. Am. Chem. Soc.* **1976**, *98*, 859–861.
[5] F. Hannemann, A. Bichet, K. M. Ewen, R. Bernhardt, *Biochim. Biophys. Acta* **2007**, *1770*, 330–344.
[6] T. Coleman, J. E. Stok, M. N. Podgorski, J. B. Bruning, J. J. De Voss, S. G. Bell, *J. Biol. Inorg. Chem.* **2020**.
[7] M. J. Cryle, J. J. De Voss, *ChemBioChem* **2008**, *9*, 261–266.
[8] T. Hishiki, H. Shimada, S. Nagano, T. Egawa, Y. Kanamori, R. Makino, S. Y. Park, S. Adachi, Y. Shiro, Y. Ishimura, *J. Biochem.* **2000**, *128*, 965–974.
[9] M. Ishigooka, T. Shimizu, K. Hiroya, M. Hatano, *Biochemistry* **1992**, *31*, 1528–1531.
[10] R. Raag, S. A. Martinis, S. G. Sligar, T. L. Poulos, *Biochemistry* **1991**, *30*, 11420–11429.
[11] E. O'Reilly, V. Kohler, S. L. Flitsch, N. J. Turner, *Chem. Commun.* **2011**, *47*, 2490–2501.
[12] P. C. Cirino, F. H. Arnold, *Angew. Chem. Int. Ed. Engl.* **2003**, *42*, 3299–3301.
[13] I. Zachos, C. Nowak, V. Sieber, *Curr. Opin. Chem. Biol.* **2019**, *49*, 59–66.
[14] F. E. Zilly, A. Taglieber, F. Schulz, F. Hollmann, M. T. Reetz, *Chem. Commun.* **2009**, 7152–7154.
[15] K. Jensen, P. E. Jensen, B. L. Møller, *ACS Chem. Biol.* **2011**, *6*, 533–539.
[16] S. Krishnan, D. Wasalathanthri, L. Zhao, J. B. Schenkman, J. F. Rusling, *J. Am. Chem. Soc.* **2011**, *133*, 1459–1465.
[17] A. K. Udit, F. H. Arnold, H. B. Gray, *J. Inorg. Biochem.* **2004**, *98*, 1547–1550.
[18] N. H. Tran, D. Nguyen, S. Dwaraknath, S. Mahadevan, G. Chavez, A. Nguyen, T. Dao, S. Mullen, T. A. Nguyen, L. E. Cheruzel, *J. Am. Chem. Soc.* **2013**, *135*, 14484–14487.
[19] I. Matsunaga, A. Ueda, T. Sumimoto, K. Ichihara, M. Ayata, H. Ogura, *Arch. Biochem. Biophys.* **2001**, *394*, 45–53.
[20] M. Girhard, S. Schuster, M. Dietrich, P. Durre, V. B. Urlacher, *Biochem. Biophys. Res. Commun.* **2007**, *362*, 114–119.
[21] I. Matsunaga, T. Sumimoto, A. Ueda, E. Kusunose, K. Ichihara, *Lipids* **2000**, *35*, 365–371.
[22] M. A. Rude, T. S. Baron, S. Brubaker, M. Alibhai, S. B. Del Cardayre, A. Schirmer, *Appl. Environ. Microbiol.* **2011**, *77*, 1718–1727.
[23] K. E. Slessor, A. J. Farlow, S. M. Cavaignac, J. E. Stok, J. J. De Voss, *Arch. Biochem. Biophys.* **2011**, *507*, 154–162.
[24] M. N. Podgorski, J. S. Harbort, J. H. Z. Lee, G. T. H. Nguyen, J. B. Bruning, W. A. Donald, P. V. Bernhardt, J. R. Harmer, S. G. Bell, *ACS Catal.* **2022**, *12*, 1614–1625.
[25] O. Shoji, T. Fujishiro, K. Nishio, Y. Kano, H. Kimoto, S.-C. Chien, H. Onoda, A. Muramatsu, S. Tanaka, A. Hori, H. Sugimoto, Y. Shiro, Y. Watanabe, *Catal. Sci. Technol.* **2016**, *6*, 5806–5811.
[26] N. Ma, Z. Chen, J. Chen, J. Chen, C. Wang, H. Zhou, L. Yao, O. Shoji, Y. Watanabe, Z. Cong, *Angew. Chem. Int. Ed.* **2018**, *57*, 7628–7633; *Angew. Chem.* **2018**, *130*, 7754–7759.
[27] T. Coleman, S. H. Wong, M. N. Podgorski, J. B. Bruning, J. J. De Voss, S. G. Bell, *ACS Catal.* **2018**, *8*, 5915–5927.
[28] H. Onoda, S. Tanaka, Y. Watanabe, O. Shoji, *Faraday Discuss.* **2022**, *234*, 304–314.
[29] J. Hernández-Ruiz, M. B. Arnao, A. N. P. Hiner, F. García-Cánovas, M. Acosta, *Biochem. J.* **2001**, *354*, 107–114.
[30] N. Kawakami, O. Shoji, Y. Watanabe, *Angew. Chem. Int. Ed.* **2011**, *50*, 5315–5318; *Angew. Chem.* **2011**, *123*, 5427–5430.
[31] E. G. Ankudey, H. F. Olivo, T. L. Peeples, *Green Chem.* **2006**, *8*, 923–926.
[32] K. N. Ingenbosch, S. Quint, M. Dyllick-Brenzinger, D. S. Wunschik, J. Kiebist, P. Suss, U. Liebelt, R. Zuhse, U. Menyes, K. Scheibner, C. Mayer, K. Opwis, J. S. Gutmann, K. Hoffmann-Jacobsen, *ChemBioChem* **2021**, *22*, 398–407.
[33] R. Ramanan, K. D. Dubey, B. Wang, D. Mandal, S. Shaik, *J. Am. Chem. Soc.* **2016**, *138*, 6786–6797.
[34] B. Wang, C. Li, K. D. Dubey, S. Shaik, *J. Am. Chem. Soc.* **2015**, *137*, 7379–7390.
[35] C. B. Brewer, J. A. Peterson, *J. Biol. Chem.* **1988**, *263*, 791–798.
[36] M. R. Sarkar, S. D. Houston, G. P. Savage, C. M. Williams, E. H. Krenske, S. G. Bell, J. J. De Voss, *J. Am. Chem. Soc.* **2019**, *141*, 19688–19699.
[37] Y. Watanabe, S. Oae, T. Iyanagi, *Bull. Chem. Soc. Jpn.* **1982**, *55*, 188–195.
[38] T. Coleman, A. M. Kirk, R. R. Chao, M. N. Podgorski, J. S. Harbort, L. R. Churchman, J. B. Bruning, P. V. Bernhardt, J. R. Harmer, E. H. Krenske, J. J. De Voss, S. G. Bell, *ACS Catal.* **2021**, *11*, 1995–2010.
[39] M. Girhard, E. Kunigk, S. Tihovsky, V. V. Shumyantseva, V. B. Urlacher, *Biotechnol. Appl. Biochem.* **2013**, *60*, 111–118.
[40] H. Xu, L. Ning, W. Yang, B. Fang, C. Wang, Y. Wang, J. Xu, S. Collin, F. Laeuffer, L. Fourage, S. Li, *Biotechnol. Biofuels* **2017**, *10*, 208.

[41] H. Onoda, O. Shoji, K. Suzuki, H. Sugimoto, Y. Shiro, Y. Watanabe, *Catal. Sci. Technol.* **2018**, *8*, 434–442.
[42] C. J. Hartley, C. C. Williams, J. A. Scoble, Q. I. Churches, A. North, N. G. French, T. Nebl, G. Coia, A. C. Warden, G. Simpson, A. R. Frazer, C. N. Jensen, N. J. Turner, C. Scott, *Nat. Catal.* **2019**, *2*, 1006–1015.
[43] M. A. A. Abdelhamid, K. Motomura, T. Ikeda, T. Ishida, R. Hirota, A. Kuroda, *Appl. Microbiol. Biotechnol.* **2014**, *98*, 5677–5684.
[44] M. N. Podgorski, T. Coleman, R. R. Chao, J. J. De Voss, J. B. Bruning, S. G. Bell, *J. Inorg. Biochem.* **2020**, *203*, 110913.

Manuscript received: May 3, 2022
Accepted manuscript online: June 16, 2022
Version of record online: ■■, ■■■

RESEARCH ARTICLE

A single amino acid mutation can convert cytochrome P450 monooxygenases into peroxygenase. These do not require the addition of nicotinamide cofactors or electron transfer proteins greatly simplifying their application. For example, urea-hydrogen peroxide and light can be used to drive the selective oxidations catalysed by these enzymes.

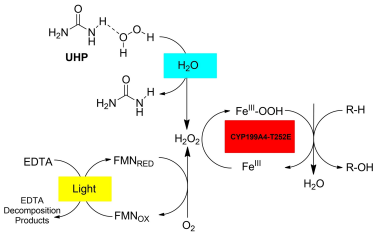

*J. H. Z. Lee, M. N. Podgorski, Dr. M. Moir, A. R. Gee, Dr. S. G. Bell**

3 Biocatalytic Cascade Reactions of P450 Peroxygenases and Oxidases

3.1 Introduction

P450 peroxygenases are P450s that are able to use H_2O_2 to generate the active oxidant in P450 reactions, Cpd I. However, H_2O_2 can degrade the heme centre of P450 peroxygenases (Chapter 2).[181] We have reported the use of chemical oxygen surrogates such as urea-hydrogen peroxide and light-driven flavin systems to form H_2O_2 *in situ* to drive peroxygenase activty with both natural ($P450_{BS\beta}$) and engineered (T252E-CYP199A4) P450 peroxygenases (Chapter 2).[181] The *in situ* generation of H_2O_2 would minimise the degradation of the peroxygenase through a slow formation of H_2O_2 at a constant level in solution with the peroxygenase.[160,161,165,168,181]

An alternative approach to generate H_2O_2 is the use of oxidase enzymes.[178,182] Oxidases are a family of enzymes that possess a domain that binds the flavin adenine dinucleotide (FAD) cofactor and catalyses oxidation-reduction reactions with dioxygen (O_2) as an electron acceptor.[182] Substrate oxidation by oxidase enzymes generates H_2O_2 as a by-product from O_2 and this characteristic could be exploited to develop a method of generating H_2O_2 for P450 peroxygenase activity. Oxidase enzymes that were targeted for study in this chapter include Alditol Oxidase (AldOx) from *Streptomyces coelicolor* A3(2), Formate Oxidase (AoFOx) from *Aspergillus oryzae* and an engineered choline oxidase (AcC06-AcChOx) from *Arthrobacter cholorphenolicus* (Figure 3.1) which has been altered to oxidise 1-hexanol as a substrate.[178–180]

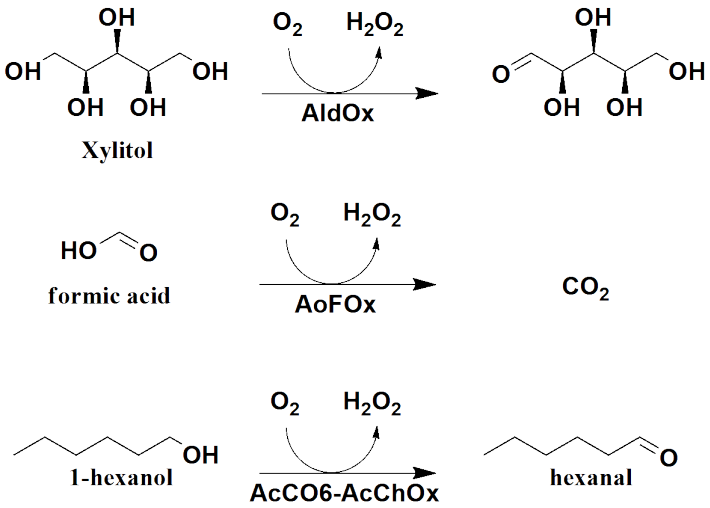

Figure 3.1: Reactions carried out by oxidases enzymes AldOx, AoFOx and mutant F357R-M359R (AcCO6) of AcChOx.

AldOx is an oxidase enzyme that has been reported to be produced in high yield in *E.coli*.[178] AldOx can oxidise substrates with primary alcohol groups such as glycerol, sorbitol and xylitol (Figure 3.1), and also diols such as 1,2-pentanediol and 1,2-hexanediol.[183] AoFOx is an oxidase enzyme of a fungal origin that possesses an unusual 8-formyl FAD cofactor that is not present in other oxidase enzymes. This enzyme is able to oxidise formic acid instead of alcohols (Figure 3.1).[184] The 8-formyl FAD cofactor is formed spontaneously *in situ* through self-oxidation of the FAD cofactor by AoFOx.[185] AcChOx is another bacterial oxidase enzyme that has shown oxidation activity towards primary alcohols.[179] Structure guided directed evolution was carried out with AcChOx to generate mutant variant F357R-M359R (AcCO6). Mutant AcCO6 showed improved oxidation activity towards hexanol alongside an increased thermostability of the enzyme (Figure 3.1).[179] The heterologous production of all three oxidases has been previously reported using *E.coli*.[178,179,184]

The three oxidases mentioned above all generate H_2O_2 while oxidising their respective substrates (Figure 3.1) and will be tested as an approach to supply H_2O_2 *in situ* for P450 peroxygenase reactions as a biocatalytic cascade (Figure 3.2).[178,179,184]

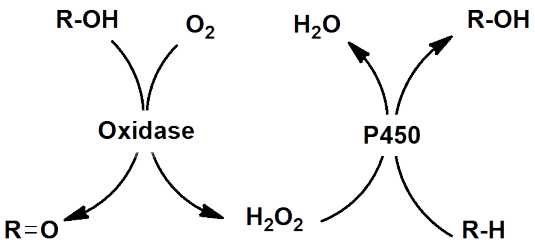

Figure 3.2: Biocatalytic cascade of oxidase that generates H_2O_2. The P450 peroxygenase will then use the H_2O_2 generated to carry out P450-catalysed reactions.

A previous study utilising oxidase enzymes to drive P450 peroxygenase activity was carried out by Munro *et. al.*[131] AldOx was fused to CYP152L1 ($P450_{Olet}$) through a short chain of amino acids generating a two-domain multifunctional protein (Figure 3.3).

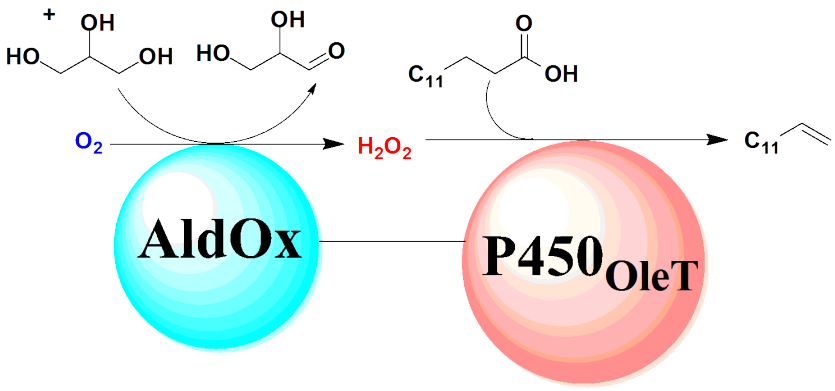

Figure 3.3: Reaction scheme of the two-domain AldOx fused to $P450_{OleT}$ designed by Munro *et.al.*[131]

The rationale for using this multifunctional enzyme is that H_2O_2 will be generated *in situ* in a controlled manner through measured addition of the AldOx substrate. The controlled release of H_2O_2 in close proximity to the P450 would both drive peroxygenase reactions and also mitigate damage to the P450 heme centre.[131] We envision applying similar principles with an engineered peroxygenase variant of CYP199A4, the T252E mutant. Mutant T252E of CYP199A4 will be fused to the three oxidases (AldOx, AoFOx and AcChOx) to produce multidomain oxidase + P450 enzymes. Plasmids with an insert containing the DNA sequence of the fused protein will be constructed with Gibson (isothermal) DNA assembly.[186] Expression of these sequences will then be carried out with these plasmids in *E.coli*.

P450 peroxygenases only require H_2O_2 for catalytic activity and does not require additional partner proteins or co-factors.[33] P450 peroxygenases are therefore a suitable candidate to attempt flow biocatalysis reactions, where the peroxygenase is immobilised to a solid surface. H_2O_2 and substrate could be eluted through the immobilised peroxygenase and drive enzymatic activity. Commercially available ion-exchange resins have been used to immobilise various enzymes for biocatalytic applications.[187] One example is the immobilisation of lipase on to D152H cation exchange resin has led to enhanced catalytic activity and thermal stability.[188] T252E-CYP199A4 has been immobilised previously to SOURCE15Q anion exchange media for protein purification and would serve as a suitable platform for enzyme immobilisation studies with this P450. Enzyme immobilisation of T252E-CYP199A4 will therefore be carried out with SOURCE15Q media and the enzymatic activity of the immobilised enzyme will be tested.

3.2 Materials and Methods

3.2.1 General

General reagents and organics were purchased from Sigma-Aldrich. Isopropyl-β-D-thiogalactopyranoside (IPTG) and buffer components were obtained from Astral Scientific (Australia). UV/Vis spectra and spectroscopic activity assays were performed on an Agilent Cary 60 spectrophotometer at 30 ± 5 °C.

3.2.2 Expression and Purification of T252E-CYP199A4

The T252E mutant of CYP199A4 was expressed and purified using previously established methods (Chapter 2).[156] The purified protein was stored in 50 % v/v glycerol and stored at -20 °C.

3.2.3 Expression and Purification Alditol Oxidase (AldOx), AcC06-Choline Oxidase (AcC06-AcChOx) and Formate Oxidase (AoFOx)

For all three oxidases, a pET28 plasmid containing the codon-optimised gene of AldOx, AcCo6-AcChOx and AoFOx with 6 × Histag residues at N-terminus were purchased commercially from Twist Biosciences. These plasmids were individually transformed into *E. coli* BL21 (DE3) competent cells (Sigma-Aldrich) and the bacteria were incubated overnight at 37 °C on an LB agar plate containing kanamycin (30 mg L^{-1}). Single colonies of the bacteria were used to inoculate 2 × 750 mL of LB broth with kanamycin (30 mg L^{-1}) and the cultures were allowed to incubate for 7 h at 37 °C and 120 rpm. The incubation conditions were changed to 18 °C and 90 rpm, and 2 % w/v EtOH and 0.02 % w/v of benzyl alcohol were added[189] to the culture. This was incubated for 30 mins before 30 µM IPTG was added to induce protein expression. After incubating the culture for a further 24 hours at 18 °C and 90 rpm, it was centrifuged (5000 *g*, 10 min, 4 °C) to collect the cell pellet, which was stored frozen at -20 °C. The frozen cell pellet was thawed and re-suspended in 100 mL of lysis buffer (50 mM potassium phosphate/KPi buffer, pH 7.5, 300 mM KCl, 20 mM imidazole). The cells were lysed by sonication using an Autotune CV334 Ultrasonic Processor equipped with a standard probe (136 mm × 13 mm; Sonics and Materials, US) using 30 × 10 s pulses with 50 s intervals. Cell debris were removed by centrifugation (18000 *g*, 20 mins, 4 °C) and the supernatant was then loaded on to a 5 mL His-trap column (GE Healthcare) equilibrated with the lysis buffer. Samples and buffers were applied to

the column with a flow-rate of 3 mL min^{-1}. After loading the protein, the column was washed with lysis buffer (25 mL). The bound protein was eluted with elution buffer (50 mM KPi, pH 7.5, 300 mM KCl, 200 mM imidazole) and yellow coloured fractions were collected. The eluted protein was concentrated by ultrafiltration using a Vivacell 100 centrifugal concentrator with a 10 kDa molecular weight cut-off membrane (Sartorius). For AldOx and AcC06-AcChOx, these proteins were purified further through elution down a HiPrep Sephacryl S-200 HR size-exclusion column (1 ml min^{-1}), 60 cm × 16 mm; GE Healthcare) with 50 mM KPi at pH 7.5. The purified protein was concentrated further to a final volume of 5 - 10 mL and flash-frozen in liquid N_2 in 200 µL aliquots to be stored at -80 °C.

The oxidases were quantified using the extinction coefficient of Alditol Oxidase: 12.5 mM^{-1} cm^{-1} at 452 nm.[178]

3.2.4 Oxidase and P450 Turnover Assays

Glycerol was removed from P450 enzymes using a 5 mL gel filtration column (PD-10, GE Healthcare), while oxidase enzymes were thawed slowly on ice. The concentration of each protein was quantified using UV-visible spectrometry. For AoFOx reactions, a 100 µL aliquot of AoFOx was added to the reactions due to the dilute protein obtained from nickel affinity chromatography. In a volume of 600 µL, P450 (1 µM), oxidase (0.25 µM to 1 µM), P450 substrate (200 µM), and Tris buffer (50 mM, pH 7.4) were combined. The substrate for the relevant oxidase (glycerol, hexan-1-ol or sodium formate) was added last to start the reaction. Reactions were left for 4 h or 20 h. A 132 µL aliquot of each reaction was taken at 4 h and 20 h. All reactions were performed in at least duplicate.

3.2.5 Metabolite Analysis

For HPLC analysis, after reactions were completed, 132 µL of the reaction mixture was mixed with 2 µL of an internal standard solution (10 mM of 9-hydroxyfluorene solution in EtOH) and 66 µL of acetonitrile. Samples were acidified with 0.2 µL of trifluoroacetic acid.

For GC-MS analysis, the reaction mixture (600 µL) was mixed with 6 µL of an internal standard (10 mM 9-hydroxyfluorene solution in EtOH) and extracted with EtOAc (2 × 400 µL). The extracts were dried with $MgSO_4$ and solvent was removed under N_2. The remaining residue was re-suspended in anhydrous acetonitrile (150 µL) and

derivatisation agent (15 µL, BSTFA + TMCS, 99:1). The mixtures were left for 2 h at 37 °C prior to analysis by GC-MS.

Analytical High Performance Liquid Chromatography (HPLC) was performed on a Shimadzu LC-20AD equipped with a Phenomenex Kinetex 5u XB-C18 100A column (250 mm × 4.6 mm, 5 µM), SIL-20A autosampler, CTO-20A column oven, SPD-20A UV detector and CBM-20Alite communications module. A gradient of 20 - 95 % acetonitrile in water (both containing trifluoroacetic acid, TFA, 0.1 %) was performed at a flow rate of 1 mL min^{-1} over 30 minutes and detector wavelength was set at 254 nm.

GC-MS analysis was performed using a Shimadzu GC-2010 gas chromatograph equipped with an autoinjector and a GCMS-QP2010S detector; the column used was a DB-5MS UI column. The interface and injection port temperatures were held at 280 and 250 °C. The column was held at 120 °C for 3 min, and the temperature was then increased to 240 °C at a rate of 7.5 °C min^{-1} and held at 240 °C for 6 min.

To quantify enzyme metabolites, calibration curves were constructed from authentic product standards. Standard solutions of 10, 20, 50, 100, 200, 500 and 1000 µM were prepared for HPLC analysis as per reaction samples. The area of the product and the internal standard peaks were measured using Shimadzu LabSolutions software. A plot of product peak/internal standard area vs concentration of standard was made and the calibration factor was calculated to quantify the amount of product in the reaction sample. Once the concentration of the product is known, the total turnover number for each reaction was calculated.

3.2.6 Agarose Gel Electrophoresis

A 0.8 % w/v agarose gel was prepared by dissolving 0.4 g of agarose in 50 mL of TAE buffer (40 mM Tris, 1 mM EDTA). This was dissolved by heating in a microwave at 10 - 30 sec intervals. The solution was then cooled to 50 °C and 0.5 µL of ethidium bromide solution (10 mg mL^{-1}) was added. The gel was then cast and left to set for 2 h before being immersed in TAE buffer (250 mL) containing 1.5 µL of ethidium bromide (10 mg mL^{-1}).

DNA from restriction digests (15 µL) was mixed with 80 % glycerol (4 µL) and loaded into separate lanes of the gel alongside a molecular weight DNA ladder (1 kB, Geneworks). The gels were run at 60 V for 1.5 h. The DNA bands were then viewed under UV light and the desired fragments were excised and purified.

Analytical gel electrophoresis was also carried out using the gels that were prepared as above. Gel loading buffer (4 µL of 6 × buffer, New England Biolabs) was added to the DNA samples before loading into the gels. Gels were run at 100 V for 0.5 h and visualised with a ChemiDoc MP Imaging system (BioRad).

3.2.7 Construction of Plasmids for Oxidase + P450 Fusion Enzymes

The plasmids containing the DNA sequence of T252E-CYP199A4 fused to an oxidase enzyme (AldOx, AcCo6-AcChOx or AoFOx) were constructed using Gibson (isothermal) assembly.[186] A pET28 plasmid (500 ng) was first digested at the *NcoI* and *HindIII* restriction sites with 0.5 µL of each restriction enzyme (New England Biolabs) and 10x CutSmart buffer (2 µL, New England Biolabs) in a total reaction volume of 20 µL. The digested plasmid was purified using agarose gel electrophoresis (Section 3.2.6) and the EZ-10 Spin Column Plasmid DNA Minipreps Kit from Bio Basic Inc.

Isothermal assembly was carried out with the P450 gBlock (25 ng, IDT, Appendix B.1), oxidase gBlock (25 ng, IDT, Appendix B.1) and the digested pET28 plasmid (50 ng) added to the NEBuilder HiFi DNA Assembly Master Mix (5 µL, New England Biolabs) to a total volume of 10 µL with the remaining volume made up with MilliQ water. The isothermal assembly reactions were incubated in a thermocycler at 50 °C for 1 h. An aliquot of the reaction mixture (2 µL) was transformed into competent DH5α *E.coli* cells (35 µL, Geneworks) and incubated at 0 °C for 60 min. This was followed by heat shock at 42 °C for 50 s. After 2 min incubation at 0 °C, SOC media (150 µL) was added to the cells and the resulting culture shaken at 37 °C and 120 rpm for 1 h. The cells were then grown on Luria-Bertani Medium (LB) selection plates containing 30 µg mL^{-1} kanamycin.

Single colonies were harvested from the selection plates and used to inoculate a culture of LB broth (16 mL) with the appropriate antibiotic. The newly assembled plasmid vectors were purified from the cell pellet of these cultures using the Promega Wizard Plus SV Minipreps DNA Purification System as per manufacturer's protocol. To confirm if the oxidase and P450 gBlocks were successfully cloned into the pET28 plasmid as one continuous insert (oxidase + P450), the purified plasmids were digested with *XbaI* (0.5 µL) and *HindIII* (0.5 µL) restriction enzymes in 10x CutSmart buffer (2 µL, New England Biolabs) to a total volume of 20 µL. Analytical agarose gel electrophoresis was then carried out to confirm if the insert is of the correct size (Section 3.2.6).

The sequence of the oxidase + P450 insert was then confirmed by sequencing the plasmids (900 - 1000 ng in 9 µL) at the Adelaide Genome Research Facility using the

T7 promoter and T7 terminator primers which recognises sequences on the pET28 plasmid. Due to the size of the cloned insert (2600 - 3100 bp), the T7 primers were not sufficient to fully sequence the insert. Additional primers were thus designed to bind to the DNA sequences of each oxidase and the HRV3C linker to allow the insert to be fully sequenced. These primers can be seen in Appendix B.2 and the binding sites of the primers for the AldOx + T252E-CYP199A4 insert is shown in Figure 3.4. Maps of primers pairs for sequencing reactions is seen in Appendix B.2.

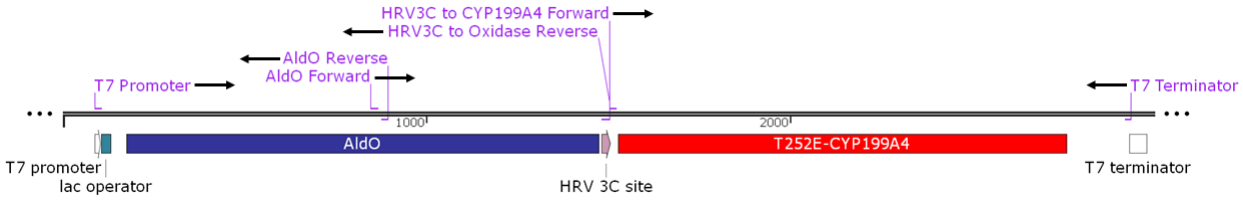

Figure 3.4: Map showing the binding sites of sequencing primers for the cloned insert of the AldOx + T252E-CYP199A4 fusion enzyme. Primer binding sites are seen in purple. The direction of PCR amplification of each primer is shown in black arrows.

3.2.8 Expression of Oxidase + P450 Fusion Enzymes

Plasmids containing the oxidase + P450 fusion protein from Section 3.2.7 were transformed into E. coli BL21 (DE3) competent cells (Sigma-Aldrich) and the bacteria were incubated overnight at 37 °C on an LB agar plate containing kanamycin (30 mg L^{-1}). Colonies of the bacteria were used to inoculate 2 × 750 mL of LB broth with kanamycin (30 mg L^{-1}). Protein expression carried out as per Section 3.2.3. The color of the cell pellet was assessed for protein expression.

3.2.9 Expression and Purification of CYP152A1 ($P450_{BS\beta}$)

A pET28 plasmid containing the gene for CYP152A1 ($P450_{BS\beta}$) with 6 × Histag residues at the N-terminus and a silica binding amino acid sequence (MP-GRARAQRQSSRGR)[190] at the C-terminus was purchased commercially from Twist Biosciences (Appendix B17).

This plasmid was transformed into *E. coli* BL21 (DE3) competent cells (New England Biolabs) and the bacteria were incubated overnight at 37 °C on an LB agar plate containing kanamycin (30 mg L^{-1}). Protein expression and purification were carried out as per Section 3.2.3. The purified protein was stored in 50 % v/v glycerol and stored at -20 °C.

3.2.10 Immobilisation and Reactions of T252E-CYP199A4 to Source 15Q Media

Glycerol was removed from T252E-CYP199A4 with a 5 mL gel filtration column (PD-10, GE Healthcare) using Buffer T (50 mM Tris, pH 7.5). The concentration of T252E-CYP199A4 (ε_{419} = 119 $mM^{-1}cm^{-1}$) was determined by UV-visible spectroscopy. In a 1.5 mL Eppendorf tube, $\sim$ 50 mg of SOURCE 15Q ion exchange media was measured and washed twice with Buffer T. T252E-CYP199A4 (1 or 5 µM) was added to the washed SOURCE 15Q media and gently re-suspended until homogenised. The homogenised P450 and SOURCE 15Q media was centrifuged at 5000 *g* for 5 mins at 4 °C. The UV-visible spectrum (600 nm to 300 nm) of the supernatant was measured to determine the extent of protein binding to the immobilisation media. The SOURCE15Q media bound with P450 was washed with buffer T (500 µL) and centrifuged again to remove the supernatant. The UV-visible spectrum of supernatant from the washing step was also measured to determine if any P450 has been stripped from the immobilisation media.

Reactions of P450-bound SOURCE15Q media was carried out in a total volume of 1200 µL by addition of 4-methoxybenzoic acid as substrate (500 µM) and H_2O_2 (10 mM) to the media while the remaining volume was made up with Buffer T. Control reactions were carried out that omitted either the P450 enzyme or H_2O_2. All reactions were carried out in duplicate. These reactions were left at room temperature and gently mixed with a BioSan TS-100C Thermo Shaker (250 rpm) to ensure homogeneity. An aliquot (132 µL) of the reactions were taken at 20 min, 60 min, 120 min, 240 min and 22 h.

After 22 h, the P450-bound SOURCE15Q media was washed again in Buffer T while the same substrate (500 µM) and H_2O_2 (10 mM) was added and left for a further 72 h to determine the extent T252E-CYP199A4 can maintain enzymatic activity while bound to SOURCE15Q. After 72 h, an aliquot of the reaction was taken. The preceding step was repeated for the final time with additional substrate and H_2O_2 added and left for an additional 24 h.

3.2.11 Continuous Flow Reaction with T252E-CYP199A4

A chromatography column (6.6 mm × 150 mm, Cole-Parmer) was packed with SOURCE15Q media to a bed height of 0.5 cm. The packed media was washed with Buffer T (10 mL) and T252E-CYP199A4 (5 µM) was loaded on to the column at a flow

rate of 1 mL min^{-1}. A reservoir (50 mL) containing 4-methoxybenzoic acid (1 mM) and H_2O_2 (10 mM) in solution with Buffer T was eluted in a continuous loop through the packed column as seen in Figure 3.5. The continuous flow reaction was left for 27 h and an aliquot of the reservoir was taken at 0 min, 4 min, 60 min, 20 h and 27 h.

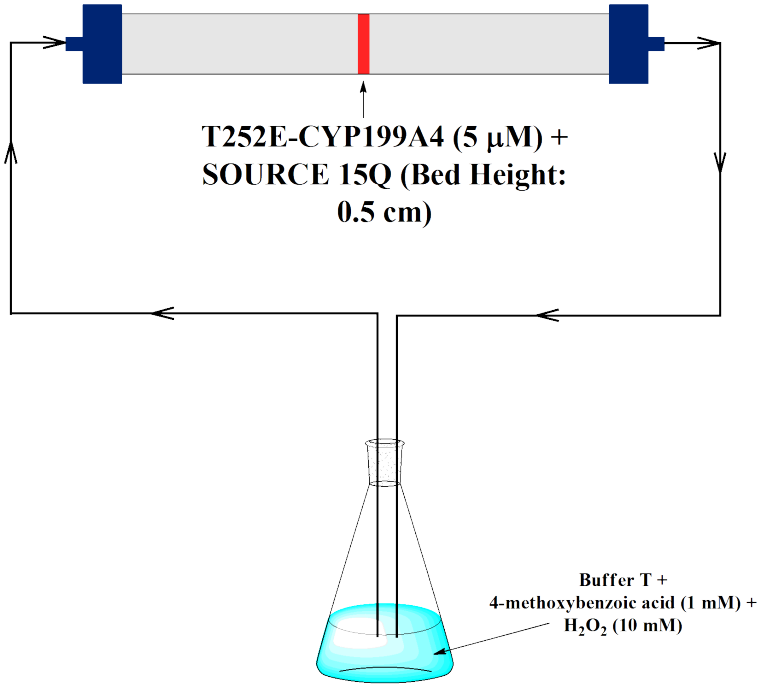

Figure 3.5: Scheme for continuous flow reactions with T252E-CYP199A4.

3.3 Results

3.3.1 Expression and Purification of Oxidase Enzymes

The heterologous production of AldOx, AcCo6-AcChOx and AoFOx was done in *E.coli* using 1.5 L LB broth. The initial purification was carried out using nickel affinity chromatography. Of the three oxidases purified, AldOx gave the highest yield ($\sim$ 20 mg) from 1.5 L of LB broth. The absorbance spectrum of AldOx measured showed a λ_{max} at 452 nm (Figure 3.6) that is characteristic of a flavin co-factor and a separate smaller absorbance peak at 350 nm.[178] This spectrum observed with AldOx matches with spectra reported previously for this enzyme.[178]

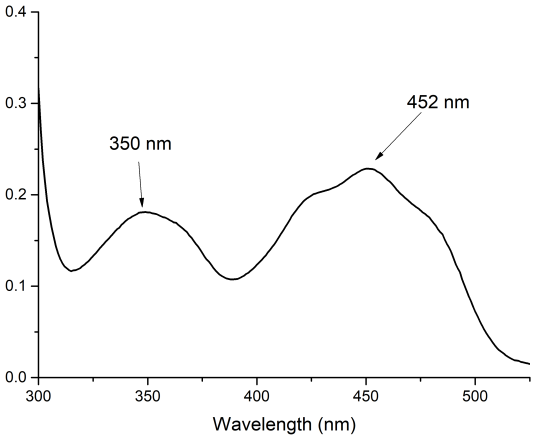

Figure 3.6: UV-visible spectrum of purified AldOx. Two absorbance peaks for this enzyme was observed with λ_{max} at 452 and 350 nm.

SDS-PAGE analysis of the protein after size exclusion chromatography showed a single band at $\approx$ 45 kDa (Figure 3.7) showing a protein with high purity. The size of the band observed was consistent with the reported size of AldOx (45.1 kDa).[178]

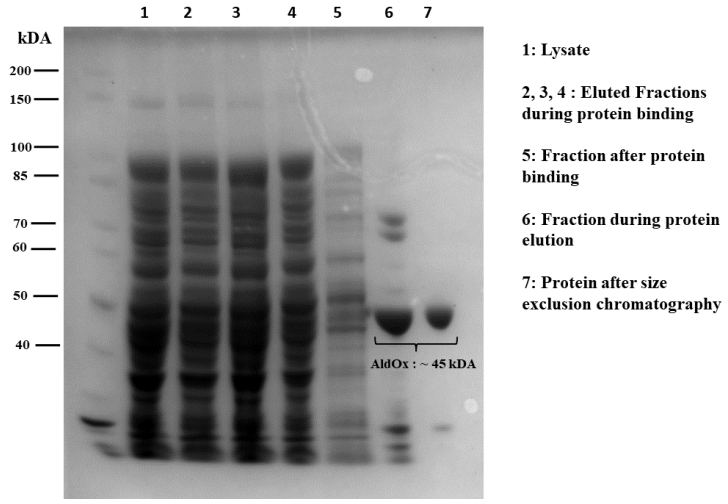

Figure 3.7: SDS-PAGE analysis of the purification of AldOx. SDS-PAGE was performed with SurePAGE 4 - 12 % Bis-Tris Precast gel (GenScript). A broad range protein ladder (10 - 200 kDa, NEB) was used.

Expression and purification of AcCo6-AcChOx was successful as confirmed by SDS-PAGE (Figure B18). The band observed for this enzyme was approximately 60 kDa and was consistent with the calculated mass (60 kDa). The absorbance spectrum of AcCo6-AcChOx was measured and showed a λ_{max} at 447 nm with smaller absorbance peaks at 350 and 375 nm (Figure 3.8). The extinction coefficient of AcCo6-AcChOx was not reported previously. However, the UV-visible spectrum for AcCo6-AcChOx shown in Figure 3.8 was similar to the spectrum measured for AldOx (Figure 3.6) as both contain a flavin cofactor. Therefore, the extinction coefficient for AldOx (ε_{452nm} = 12.5 mM^{-1} cm^{-1}) was used to estimate the yield and concentration of AcChOx purified. The approximate yield for AcChOx expressed was calculated to be 5.8 mg from 1.5 L of LB broth.

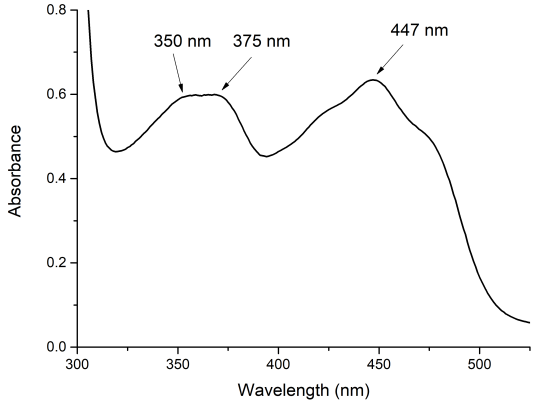

Figure 3.8: UV-visible spectrum of purified AcC06-AcChOx. A λ_{max} peak for this enzyme was measured at 447 nm. Additional absorbance peaks were observed at 450 and 475 nm.

The levels of production of AoFOx were significantly lower than the other two oxidases. The UV-visible spectrum for the concentrated fractions from nickel affinity purification did show small absorbance peaks at 375, 425 and 475 nm. These peaks were not entirely consistent with previously reported absorbance spectra of AoFOx.[180] The low absorbance observed was suggestive of low levels of soluble protein using *E.coli*. The yield of this protein prevented further purification and presented difficulties in accurate quantification. SDS-PAGE analysis of the dilute protein showed a band at 60 kDa consistent with the expected mass of this protein (64.3 kDa, Figure B18).

In summary, of the three oxidase enzymes tested for expression, AldOx from *Streptomyces coelicolor* A3(2) gave the highest yield of expression in *E.coli*. This was followed by mutant AcC06 of AcChOx from *Arthrobacter cholorphenolicus* and AoFOx from *Aspergillus oryzae* was poorly expressed in low yield.

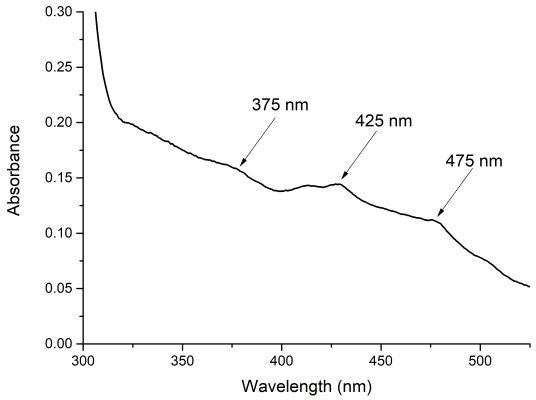

Figure 3.9: UV-visible spectrum of the concentrated fractions of AoFOx from Histag purification. Low absorbance peaks were observed at 375, 425 and 475 nm.

3.3.2 P450 Peroxygenase Reactions with Oxidase Enzymes

The oxidase enzymes from Section 3.3.1 were used to generate H_2O_2 *in situ* with P450 peroxygenases. AldOx, AcCo6-AcChOx and AoFOx use glycerol, hexan-1-ol and formate respectively as substrates which generates product and H_2O_2.[131,179,180] These substrates were tested with their respective oxidase enzymes in order to drive P450 peroxygenase activity.

We tested the *O*-demethylation of 4-methoxybenzoic acid by T252E-CYP199A4 (1 µM) in the presence of AldOx (0.5 µM) and AcCo6-AcChOx (0.5 µM). A 100 µL aliquot of extracted AoFOx was used due to the low yield and purity observed alongside the inability to determine the enzyme concentration accurately. HPLC analysis of the initial screening (Figure 3.10) showed 4-hydroxybenzoic acid was detected as the P450 reaction product for all three oxidase enzymes.

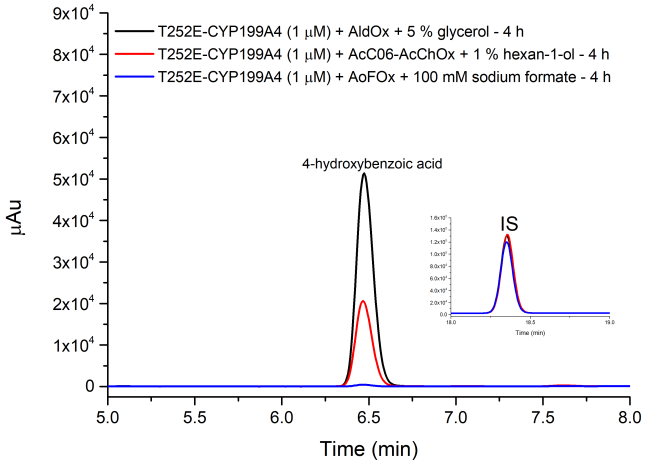

Figure 3.10: HPLC analysis of initial screening reactions of T252E-CYP199A4 (1 µM) with oxidase enzymes. Reactions with 4-methoxybenzoic and T252E-CYP199A4 were carried out in the presence of AldOx (0.5 µM, black), AcC06-AcChOx (0.5 µM, red) and AoFOx (100 µL aliqout, blue) to drive P450 peroxygenase activity. The P450 product detected was 4-hydroxybenzoic acid (t_r = 6.5 min) from the *O*-demethylation of 4-methoxybenzoic acid (t_r = 12.4 min) by T252E-CYP199A4. The reaction with AldOx showed the highest product formation.

The reaction with AldOx showed the highest level of 4-hydroxybenzoic acid production, followed by AcCo6-AcChOx (Figure 3.10). Low levels of 4-hydroxybenzoic were formed in the reactions with AoFOx. Due to the low product levels observed with AoFOx alongside poor expression of this enzyme, only AldOx and AcCo6-AcChOx was used for further experiments.

Negative control experiments were carried out that omitted either T252E-CYP199A4 or the oxidase enzymes (AldOx and AcCo6-AcChOX) to determine if the presence of the oxidase enzymes were important for P450 peroxygenase activity. The negative controls showed that omitting the P450 or oxidase enzymes resulted in no product formation, showing that the oxidase enzymes were needed to form P450-dependent enzymatic activity (Figure 3.11). This is confirmation the oxidase enzymes are generating H_2O_2 *in situ* that is subsequently used by T252E-CYP199A4 for P450 peroxygenase activity.

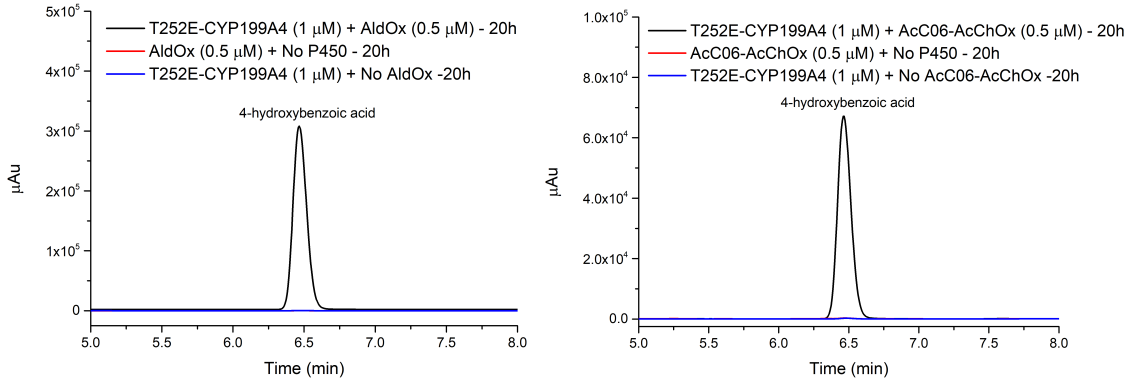

(a) (b)

Figure 3.11: HPLC analysis of the reaction with T252E-CYP199A4 and 4-methoxybenzoic acid (t_r = 12.4 min) in the presence of oxidase enzymes (black). Controls include no P450 (red) and no oxidase (blue). In (a), AldOx was tested and (b) AcC06-AcChOx was tested instead. Oxidase substrates tested was glycerol for (a) and hexan-1-ol for (b). Product detected was 4-hydroxybenzoic acid (t_r = 6.5 min).

The capability of AldOx and AcC06-AcChOx to drive product formation with T252E-CYP199A4 were then compared against each other. The effect of altering the concentration of oxidase relative to the P450 was investigated. The concentration of T252E-CYP199A4 was maintained at 1 µM while the concentration of oxidase was varied. The levels of product formed was found to be higher with AldOx when compared to AcC06-AcChOx for all the conditions tested (Figure 3.10). When the ratio of AldOx to the P450 is either halved (1:2) or equal (1:1), the levels of product formation remained similar ($\sim$ 120 µM, Figure 3.12). For AcC06-AcChOx, when the ratio of oxidase to P450 was 1:2, product formation levels was only slightly less compared to when the oxidase and P450 concentrations were equal (1:1, Figure 3.12).

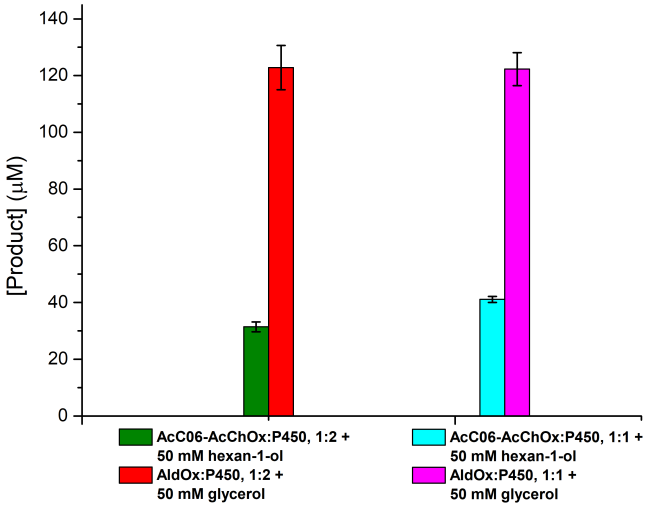

Figure 3.12: Product formation analysis comparing reactions of T252E-CYP199A4 (1 µM) with either AldOx and AcC06-AcChOx. Columns on the left were when the oxidase concentration was half of the P450 (1:2) while columns on the right were when oxidase and P450 concentrations were equal (1:1). In all conditions tested, AldOx (red and magenta) had higher levels of product compared to AcC06-AcChOx (green and cyan). The concentration of oxidase substrate was 50 mM for all conditions.

Further experiments where the concentration of AldOx was five times lower than the P450 enzyme (1:5), demonstrated product formation that was only moderately lower compared to when the ratio of oxidase to P450 were 1:1 or 1:2. (Figure 3.13).

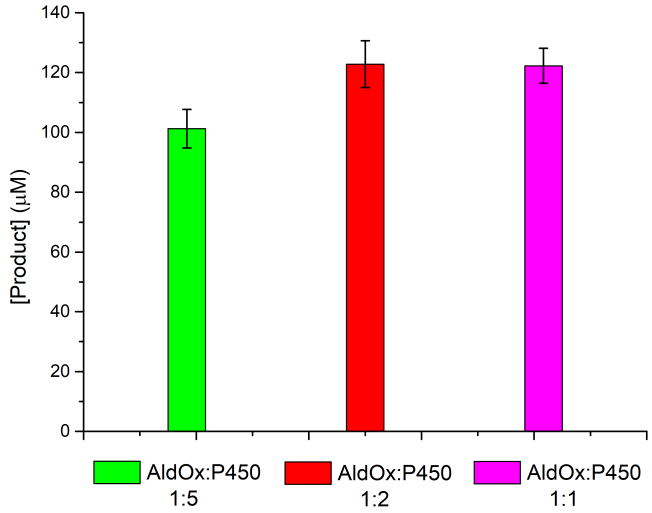

Figure 3.13: Product formation analysis comparing different concentrations of AldOx relative to T252E-CYP199A4. Concentration of T252E-CYP199A4 was 1 µM for all conditions. Conditions of AldOx:P450 shown include 1:5 (green), 1:2 (red) and 1:1 (magenta).

AldOx was also tested with CYP152A1 ($P450_{BS\beta}$) to assess if this oxidase is able to drive reactions with a natural P450 peroxygenase. Previous experiments with light-driven flavins systems to generate H_2O_2 for the oxidation of tetradecanoic acid by $P450_{BS\beta}$ showed the occurrence of fatty acid hydroxylation and chain shortening (Chapter 2).[181] GC-MS analysis of the reaction between $P450_{BS\beta}$ and tetradecanoic acid in the presence of AldOx showed hydroxylation products of tetradecanoic acid as

the major product. There was no detectable shorter chain fatty acids observed but low levels of hydroxylated tridecanoic and dodecanoic acid products were observed that is indicative fatty acid chain shortening.

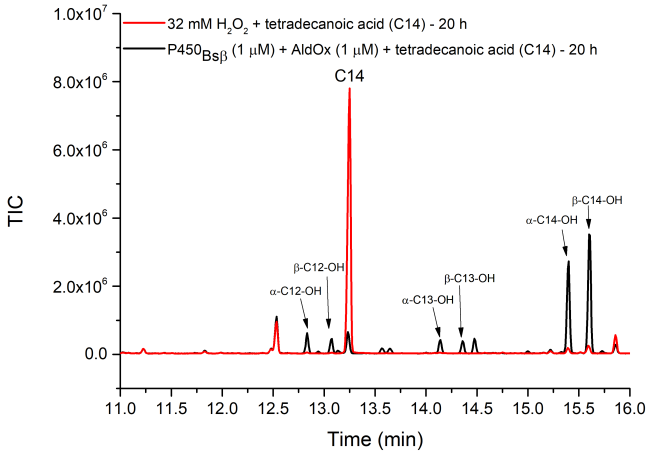

Figure 3.14: GC-MS analysis of the reaction of $P450_{BS\beta}$ oxidation of tetradecanoic acid (C14) in the presence of glycerol (50 mM) and AldOx (1 µM, black). The hydroxylated products of shorter chain fatty acids such as α/β-hydroxy-tridecanoic acid (α/β-C13-OH) and α/β-hydroxy-dodecanoic acid (α/β-C12-OH) was also observed. Control reaction shown was tetradecanoic acid with 32 mM H_2O_2 only.

Overall, AldOx showed the highest level of P450 product formation with T252E-CYP199A4 compared to AcC06-AcChOx and AoFOx. AldOx was also capable of driving P450 peroxygenase activity with $P450_{BS\beta}$.

3.3.3 Plasmid Construction and Expression of Oxidase + P450 Fusion Enzymes

Gibson (isothermal) DNA assembly was used to construct plasmids to express oxidase + P450 fusion enzymes using gBlocks containing the DNA sequences of the oxidase enzymes (AldOx, AcCo6-AcChOx and AoFOx) and T252E-CYP199A4. Individual gBlocks (Integrated DNA Technologies) containing the DNA sequence of T252E-CYP199A4 and each of the three oxidase enzymes were cloned into the digested pET28 plasmid backbone using isothermal assembly (Figure 3.15). Full sequences of each gBlock used is shown in Appendix B.1. The gBlocks for the P450 and individual oxidase were designed to have overlapping regions of homology with each other and also with the pET28 plasmid digested *NcoI* and *HindIII* (Figure 3.15). The overlapping region between the P450 and oxidase gBlocks contains a DNA sequence that encodes for the HRV3C cleavage site.

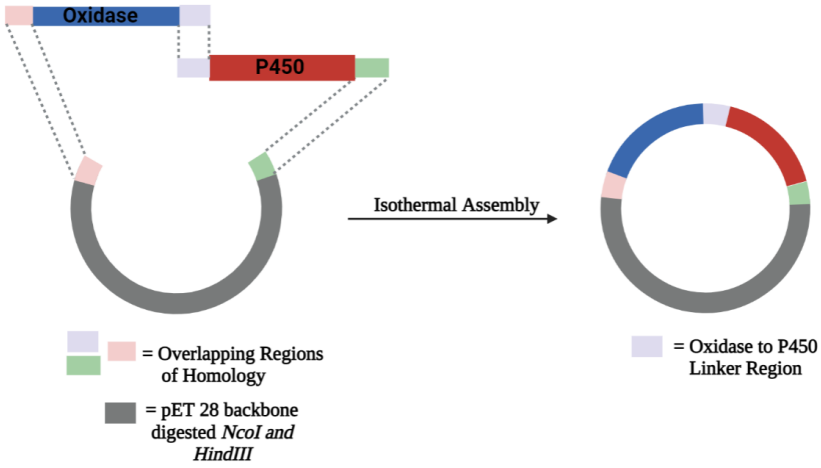

Figure 3.15: Isothermal assembly of plasmids containing an insert of the oxidase-P450 fusion enzymes.

The isothermal DNA assembly experiment was successful in generating colonies of all three oxidase + P450 combinations and the plasmid DNA from these colonies were extracted and purified. The purified plasmid DNA was digested with *XbaI* and *HindIII* to confirm if the desired insert was successfully cloned into the pET28 plasmid. Agarose gel electrophoresis analysis of plasmids containing fusion enzymes of AldOx + T252E-CYP199A4, AcCo6-AcChOx + T252E-CYP199A4 and AoFOx + T252E-CYP199A4 showed bands that correspond to the expected size of inserts containing both oxidase and P450 DNA sequences (Figure 3.16 and Figure B19).

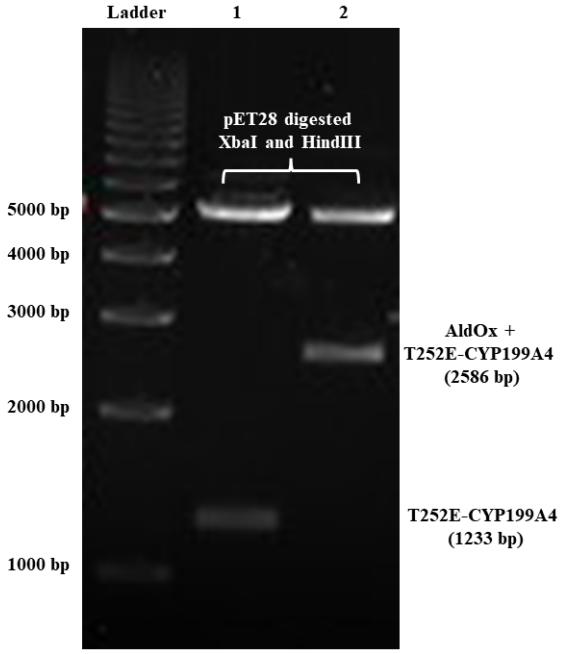

Figure 3.16: Agarose gel electrophoresis analysis (0.8 % gel) of AldOx + T252E-CYP199A4 cloned into pET28 via isothermal DNA assembly. This plasmid was digested at *XbaI* and *HindIII* restriction sites (Lane 2). The same digest was carried out with a pET28 plasmid containing an insert of only T252E-CYP199A4 as a control (Lane 1). It can be seen that a band corresponding to the expected size of an insert with both AldOx and T252E-CYP199A4 DNA sequences were observed (Lane 2, 2586 bp). A 1 kb DNA ladder from Geneworks was used.

Sequencing of the inserts were also carried out using primers shown in Appendix B.2. The inserts containing AldOx + T252E-CYP199A4 and AcCo6-AcChOx + T252E-CYP199A4 were fully sequenced successfully. The insert containing AoFOx + T252E-CYP199A4 was fully sequenced and no errors were found, but given the low levels of production and product formation with AoFOX observed previously (Section 3.3.1), we decided to test for protein production before proceeding further.

The three plasmids (pET28 vector) containing the inserts of oxidase + T252E-CYP199A4 were then transformed into *E.coli* BL21 (DE3) competent cells and protein production was attempted (Section 3.2.8). The cell pellets and their respective lysates were not coloured. Oxidase and P450 enzymes usually produce yellow and red coloured lysates respectively. Attempts at protein purification with nickel affinity chromatography showed no observable binding of protein to the nickel affinity column suggestive of poor production of soluble protein for these oxidase + T252E-CYP199A4 fusions. We did not pursue this avenue further as the yield of the biocatalyst is an important consideration and decided to focus on the immobilisation of T252E-CYP199A4.

3.3.4 Reactions of T252E-CYP199A4 Immobilised to SOURCE15Q Ion Exchange Media

Initial immobilisation of T252E-CYP199A4 (1 µM) to SOURCE15Q anion-exchange media ($\sim$ 50 mg) was carried out. CYP199A4 and its mutants are negatively charged proteins that have shown successful binding to the positively charged SOURCE15Q media for protein purification.[48,148] The UV-visible spectrum of the P450 enzyme before binding was measured and compared to the supernatant after binding showed a observable decrease in absorbance at the λ_{max} of T252E-CYP199A4 (419 nm, Figure 3.17). This shows the binding of T252E-CYP199A4 to the SOURCE15Q media was successful. The P450-bound SOURCE15Q media was washed with Buffer T and the supernatant of the wash indicated the P450 remained immobilised (Figure 3.17).

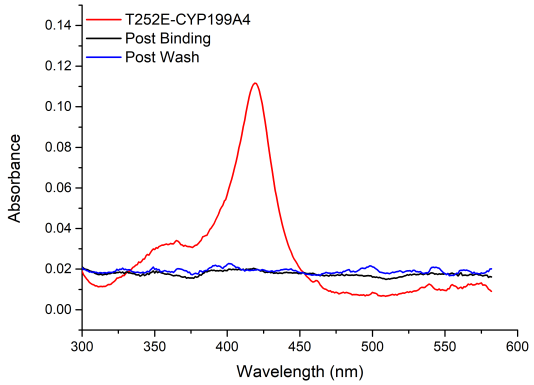

Figure 3.17: UV-visible spectra of a solution of T252E-CYP199A4 before (red) and after immobilising to SOURCE15Q media (black). The media was washed with buffer T after P450 immobilisation and the absorbance spectrum of the supernatant from the washing step is shown also (blue).

The peroxygenase activity of immobilised T252E-CYP199A4 was tested by adding Buffer T containing H_2O_2 and 4-methoxybenzoic acid to the immobilised enzyme (Figure 3.18a). A negative control reaction of adding Buffer T containing only substrate to the immobilised P450 was also carried out. The final negative control reaction tested was a suspension of SOURCE15Q media in Buffer T and H_2O_2. The peroxygenase activity of immobilised T252E-CYP199A4 (1 µM) was also compared to the same concentration of enzyme as a free solution. All reactions were monitored over a period of 22 h using 500 µM of 4-methoxybenzoic acid and 10 mM of H_2O_2 (Figure 3.18b).

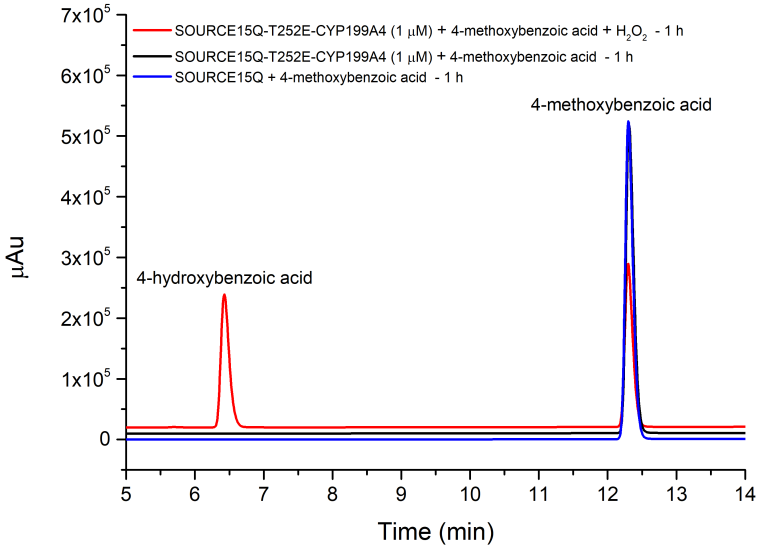

(a)

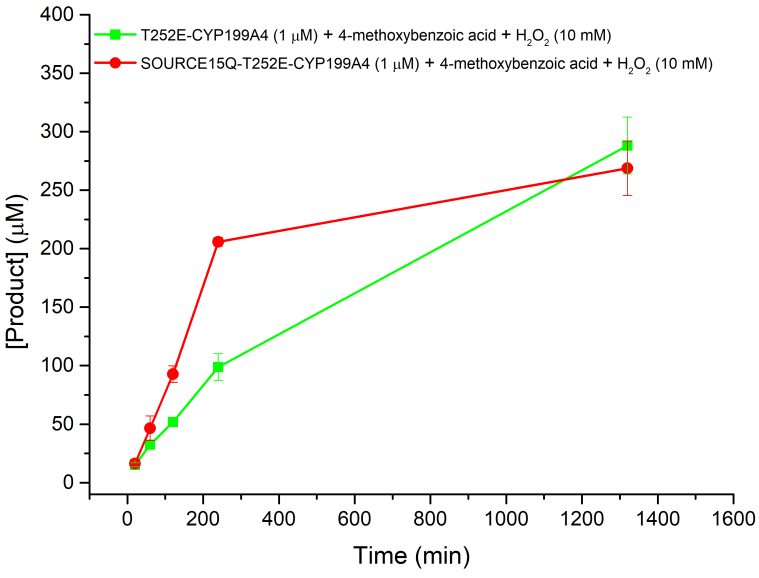

(b)

Figure 3.18: (a) HPLC analysis of the peroxygenase reaction of T252E-CYP199A4 immobilised to SOURCE15Q media with 4-methoxybenzoic acid (500 µM) as substrate and H_2O_2 (10 mM) (black). Controls reactions include a no H_2O_2 control (red) and a no immobilised P450 control (blue). (b) Time-course analysis of the peroxygenase reaction of T252E-CYP199A4 immobilised to SOURCE15Q media (red) in comparison to T252E-CYP199A4 in solution (green).

The reaction of immobilised T252E-CYP199A4 with 4-methoxybenzoic acid and H_2O_2

demonstrated the formation of 4-hydroxybenzoic acid from an enzymatic reaction (Figure 3.18a). The negative controls showed no product formation and indicates that peroxygenase activity with immobilised T252E-CYP199A4 was possible in the presence of H_2O_2 (Figure 3.18a). When comparing the product formation between immobilised versus free enzyme, the former was initially higher compared to the latter. At 22 h, the levels of product formed from peroxygenase activity was similar between the two enzyme states (Figure 3.18b).

Immobilised T252E-CYP199A4 was then tested for stability and activity with successive reactions in the presence of H_2O_2. P450 enzyme (5 µM) was immobilised and the reaction was carried out with 4-methoxybenzoic acid (500 µM) and H_2O_2 (10 mM). After 22 h, the immobilised enzyme was washed with Buffer T (500 µL), and a new stock of substrate and H_2O_2 was added for a second successive reaction. After a 72 h reaction period, a third reaction was performed. The supernatant of the successive reactions and subsequent washes do not show the presence of free P450 enzyme in solution (Figure B20), suggesting that the enzyme remains bound to the SOURCE15Q media after successive washes and reactions. The first and second successive reactions generated a similar level of product (Figure 3.19) but the third reaction however showed a significant decrease in product formation. With all three successive reactions, T252E-CYP199A4 was immobilised and maintained activity for over 100 h.

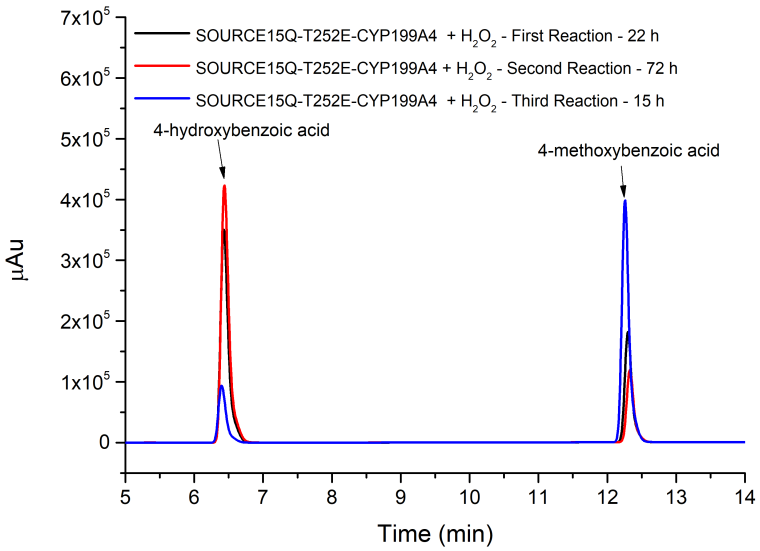

Figure 3.19: HPLC analysis of successive peroxygenase reactions of immobilised T252E-CYP199A4. Three successive reactions were carried out with the immobilised P450 enzyme (red, black, blue). The immobilised enzyme was washed before each subsequent reaction. A new stock of 4-methoxybenzoic acid (500 µM) and H_2O_2 (10 mM) was added for each reaction. The first (black) and second (red) reactions formed similar levels of product. The third reaction (blue) showed a decrease in product formation.

T252E-CYP199A4 (5 µM) was then immobilised onto SOURCE15Q media (bed height = 0.5 cm) within a chromatography column. A reservoir of buffer T with dissolved

4-methoxybenzoic acid (1 mM) and H_2O_2 (10 mM) was then eluted through the column containing immobilised T252E-CYP199A4 in a continuous flow reaction (Section 3.2.11). HPLC analysis of the flow reaction over 27 h showed low levels of product formation.

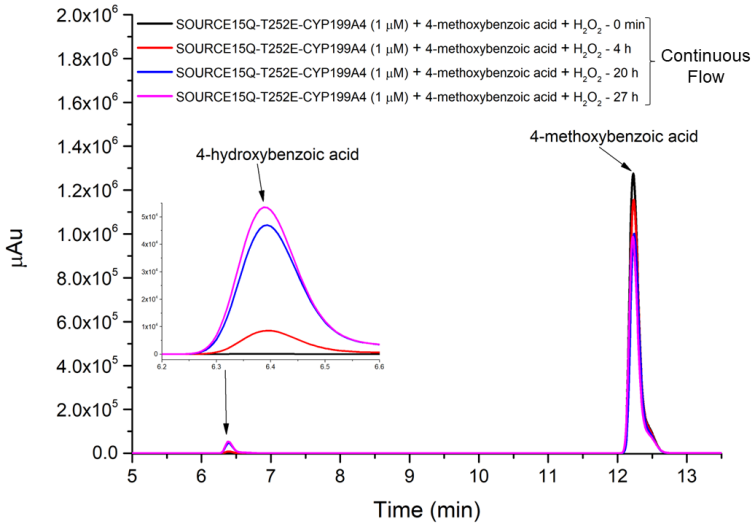

Figure 3.20: HPLC analysis of continuous flow peroxygenase reactions with immobilised T252E-CYP199A4 (5 µM). A reservoir of 4-methoxybenzoic acid (1 mM) and H_2O_2 (10 mM) was eluted over the immobilised enzyme for 27 h. The formation of 4-hydroxybenzoic acid (t_r = 6.5 min) by peroxygenase activity by the P450 enzyme at 0 min, 4 h, 20 h and 27 h was assessed.

3.4 Discussion

In this study, the expression and purification of two H_2O_2-generating oxidase enzymes, AldOx and mutant AcC06 of AcChOx were successful in sufficient yield and purity for study. A third enzyme, AoFOx was detected by SDS-PAGE analysis after production using *E.coli* but did not yield enough protein for further analysis. Of the two enzymes purified in workable yield, AldOx was purified in the highest amount ($\sim$ 20 mg) compared to AcC06-AcChOx ($\sim$ 6 mg). The first reported purification of AldOx was able to produce 350 mg of protein from only 1 L of culture broth but the expression yield of AcC06-AcChOx has not been reported.[178,179] The extremely high yield of AldOx reported was attributed to fusing AldOx to a maltose-binding protein (MBP).[178] MBP is a secretion enhancing tag that has been reported to increase protein expression in eukaryotic systems.[191] Future studies that would fuse AldOx, AcC06-AcChOx and AoFOx to MBP may be a viable approach to improve the yields of all these enzymes and the fusion proteins in *E.coli*. The yield for AoFOx using LB broth in this study was quite low and it has been previously reported that yields of 17 mg/mL can be achieved using Terrific Broth.[178] Terrific broth is a richer growth media with greater buffering capacity compared to LB broth and could be a contributing factor in improving the yields of AoFOx production in *E.coli*.[192] Higher yields of the three oxidase enzymes would provide facile and detailed characterisation of their capability to generate H_2O_2 for P450 peroxygenase reactions.

Product formation by T252E-CYP199A4 was observed in the presence of oxidase enzymes indicating that H_2O_2 was being generated and subsequently used by the P450 for peroxygenase activity. T252E-CYP199A4 (1 µM) formed the highest amount of product ($\sim$120 µM from 200 µM substrate) using AldOx (0.5 or 1 µM) with 50 mM glycerol as the oxidase substrate. When the ratio of AldOx to P450 was decreased, product formation levels did not change dramatically (ranged from 100 to 120 µM). This suggests that the oxidase enzyme generates H_2O_2 at a fast enough rate at all concentrations tested that it does not significantly alter product formation by the P450 peroxygenase. We also tested this method of supplying H_2O_2 to a natural P450 peroxygenase, $P450_{BS\beta}$ using AldOx. Fatty acid hydroxylation and low levels of fatty acid chain shortening was observed. The levels of fatty acid chain shortening occurred at significantly lower levels compared to when a light-flavin system was used to supply H_2O_2 *in situ* (Chapter 2).[181] Previous applications of supplying H_2O_2 to $P450_{OleT}$, using AldOx and 0.1 % glycerol achieved not only hydroxylation but also alkene formation with fatty acids.[131] Alkenes are an important class of biofuels[193] and the use of oxidase enzymes could be more advantageous as a way to tune for a specific P450

activity such as P450 hydroxylation or alkene formation. The amount and the rate that H_2O_2 is generated by the oxidase enzymes studied here could be assessed in the future to allow for more precise design and optimisation of P450 peroxygenase reactions involving these oxidase enzymes.

Glycerol and hexan-1-ol were chosen as the substrates tested for AldOx and AcC06-AcChOx as they are easily accessible compounds that have been reported to have high activity with the enzymes tested.[131,179] AcC06-AcChOx converts hexan-1-ol to hexanal, whereby hexanal is a useful flavouring additive and a biocatalytic cascade reaction of this enzyme alongside a P450 enzyme could potentially provide two useful metabolites from one-pot. The lower P450 product formation when AcC06-AcChOx was used compared to AldOx could be a result of the higher volatility of hexan-1-ol compared to glycerol, resulting in lower amounts of oxidase substrate available to generate H_2O_2. Choline was identified as the natural substrate of AcC06-AcChOx and could be an alternative substrate to test for H_2O_2 generation. Steady-state kinetic experiments with AldOx have shown that sorbitol and xylitol has greater affinity towards this enzyme compared to glycerol.[183] Future experiments with P450 peroxygenases and oxidase enzymes could utilise these alternate substrates to potentially improve P450 product formation levels.

Plasmids containing the DNA sequence of AldOx, AcC06-AcChOx and AoFOx fused to T252E-CYP199A4 were successfully constructed using isothermal DNA assembly. However, expression of these plasmids in *E.coli* was not successful. Previously reported fusions of P450 enzymes include $P450_{cam}$ that has been successfully fused to its physiological electron transfer partners and expressed for whole-cell reactions in *E.coli.*[194] AldOx has been fused to $P450_{OleT}$ by Munro *et al.* using a cleavable HRV3C amino acid linker and was expressed successfully in *E.coli.*[131] The HRV3C amino acid linker was chosen in our study to exploit its cleavable nature and linked the P450 and oxidase domains by flexible Ser and Gly residues. It is possible that the flexibility of the linker region allowed the P450 or oxidase domains to maintain mobility. The mobility could allow interference in the folding of the adjacent protein domains and eventually causes insoluble protein to form.[195] It has been reported that the insertion of a flexible Ser and Gly based linker in transferrin-based fusion proteins caused poor expression yields.[196] A possible alternative is the use of more rigid linkers with the sequence of $(EAAAK)_n$ that are able to form α-helices which maintain a fixed distance between two domains of a fusion protein and improve protein expression.[197]

Peroxygenase reactions with T252E-CYP199A4 were successfully undertaken after immobilisation to SOURCE15Q ion exchange media. The immobilisation of the T252E

mutant to SOURCE15Q was facile. SOURCE15Q media is an anion exchanger that is used in the purification of CYP199A4 and its mutants due to the negative charge of this P450.[30,155,156] Immobilised T252E-CYP199A4 was able to generate product comparable to the free enzyme. The immobilised P450 was stable and able to maintain enzymatic activity even after being immobilised for over 100 h. There was no evidence of enzyme leaching from the immobilisation media. In contrast, the continuous flow reaction of T252E-CYP199A4 with H_2O_2 showed low levels of product formation but serves as a suitable indication that flow biocatalysis was possible with this engineered P450 peroxygenase.

The design of flow biocatalytic reactions requires the consideration of both residence time and enzyme reaction rates.[198] Residence time is length of time the desired substrate is in contact with the enzyme and in this study would depend on the bed height of the immobilisation media. The small bed height chosen for this study was 0.5 cm as to ensure full saturation of the media with enzyme but this bed height could potentially limit the surface area of exposure for the enzyme to react with the continuously flowing substrate. Flow biocatalytic reactions can also be hampered by slow enzymatic reactions and the low levels of product formation could be due to how P450 peroxygenase activity with the T252E mutant occurs at slow rates.[156] Future optimisation could involve increasing the bed height of media saturated with the P450 enzyme and allowing substrate to elute at a slower rate to increase residence time and mitigate the slow reaction rates of the P450 peroxygenase. Studies into steady-state kinetics of T252E-CYP199A4 alongside future mutagenesis studies to improve the peroxygenase activity of this enzyme could provide insights into improving its product formation in flow biocatalytic reactions.

In summary, oxidase enzymes were expressed and purified. These oxidase enzymes were successfully used to generate H_2O_2 for P450 peroxygenase activity, whereby AldOx showed the highest levels of P450 product formation. Isothermal DNA assembly was used to successfully construct plasmids encoding oxidase + P450 fusions but were unable to be expressed in *E.coli*. Peroxygenase reactions of T252E-CYP199A4 were present even when immobilised but continuous flow reactions with T252E-CYP199A4 would need to be optimised further to become a viable method for synthetic applications.

4 *In crystallo* reactions of T252E-CYP199A4

4.1 Introduction

Cytochrome P450 enzymes are heme-thiolate monooxygenases that catalyse the insertion of one atom of O_2 into C-H bonds. This enables them to catalyse a wide variety of complex transformations including epoxidation, sulfoxidation, C-C bond cleavage and formation.[199,200] P450 enzymes are involved in the biosynthesis of physiologically important compounds and xenobiotic metabolism.[200] The sequence identity between P450s of different families can vary widely but their structural and spectroscopic properties are easily identifiable due to the highly conserved P450 structure and heme catalytic centre.[201,202] One of the most well characterised P450 enzyme is CYP101A1 ($P450_{cam}$),[16,203] where the three-dimensional structure of a P450 was first reported with this enzyme.[204–206] Since the structure of $P450_{cam}$ was first determined, many new structures have been solved with P450s from various domains of life.[207]

With the structure of different P450 enzymes accessible through X-ray crystallography, reactive intermediates of the P450 catalytic cycle can be explored in detail. The use of cryogenic temperatures and rapid-data collection techniques have allowed for the trapping and direct structural characterisation of intermediates in enzyme-catalysed reactions *in crystallo*.[208] A major challenge in trapping such reaction intermediate in P450 enzymes is initiating the reaction in protein crystals. This is hampered by the need for external electron transfer partners and NADH to initiate reactions.[209] Sligar *et al.* was able to overcome this by reducing a crystal of substrate-bound $P450_{cam}$ with electrons from the X-ray beam to generate an oxyferryl intermediate consistent with Cpd I, the main oxidant of the P450 catalytic cycle.[210] However, the reduction strategy required irradiating the crystal for 3 hours with X-rays that could potentially damage the enzyme structure.[211]

An alternate strategy to initiating enzymatic reactions in protein crystals of P450 enzymes is the use of the peroxide shunt pathway.[33] The peroxide shunt pathway is able to generate Cpd I (Figure 4.1) directly using hydrogen peroxide (H_2O_2) and some P450s are able to use this pathway for catalysis to act as a peroxygenase.[33] As the shunt only requires H_2O_2 to initiate the reactions, diffusion triggered *in crystallo* reactions is a possible approach to trap and study reactive intermediates in P450 enzyme reactions.

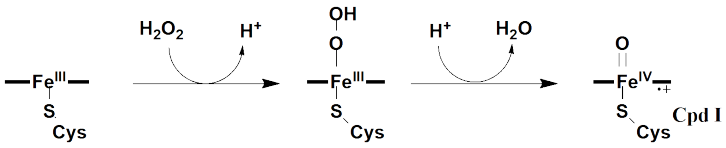

Figure 4.1: Peroxide Shunt Pathway of P450 Enzymes.

Crystals of proteins display large pore sizes that are mostly filled with water molecules.[212] These pores are wide enough to allow diffusion of chemical compounds through the crystal lattice. The diffusion of proteins such as cytochrome *c* into crystals have been observed.[212] In addition, the diffusion of smaller compounds such as molecular oxygen and H_2O_2 have also been reported.[213,214] A well-established example is the soaking of protein crystals with heavy atom containing compounds (i.e mercury compounds) to solve the phase problem in protein crystallography.[215,216]

Since P450 peroxygenases do not require NADH or electron transfer partners, they could be co-crystallised with substrate and then soaked with H_2O_2, which would diffuse through the pores of the crystal. The diffused H_2O_2 can then interact with the heme centre to trigger the peroxide shunt pathway *in crystallo*. This diffusion triggered *in crystallo* reaction could potentially be stopped at various time points to capture reaction intermediates and elucidate the reaction pathway of the enzyme.[214]

A reaction carried out *in crystallo* with a P450 enzyme and the peroxide shunt pathway has been described by Liu *et. al.*[217] They identified a hydroxylated intermediate in the active site after substrate-bound crystals of CYP121 were soaked with H_2O_2 and its X-ray structure solved.[217] A separate study by Karplus *et al.* also exploited the peroxide shunt pathway to initiate *in crystallo* enzymatic reactions with sulfur-containing peroxiredoxin. Crystals of peroxiredoxin were soaked with H_2O_2 and structures were solved.[214] Atomic resolution snapshots of the peroxiredoxin proceeding through thiolate, sulfenate, and sulfinate species were obtained.[214]

CYP199A4 is a bacterial P450 from *Rhodospeudomonas palustris* HaA2 that has high catalytic activity towards the oxidation of *para*-substituted benzoic acids.[23,30,155] The structure of CYP199A4 has been studied extensively by crystallography to elucidate the binding modes of various ligands and rationalise it's activity.[153,218] CYP199A4 and its mutants have been used as a model system to the investigate mechanistic details of P450 reactions.[134,153,219,220] An engineered variant of CYP199A4, the T252E mutant, was found to have enhanced peroxygenase activity and is able use H_2O_2 for catalytic activity.[156]

A crystal structure of T252E-CYP199A4 complexed with 4-methoxybenzoic acid has been solved (Figure 4.2).[156] We aim to use this T252E variant to carry out *in crystallo*

enzymatic reactions using the peroxide shunt pathway. By soaking various crystals of T252E-CYP199A4 bound to substrates with H_2O_2, we aim to assess if peroxygenase activity could occur in the crystals.

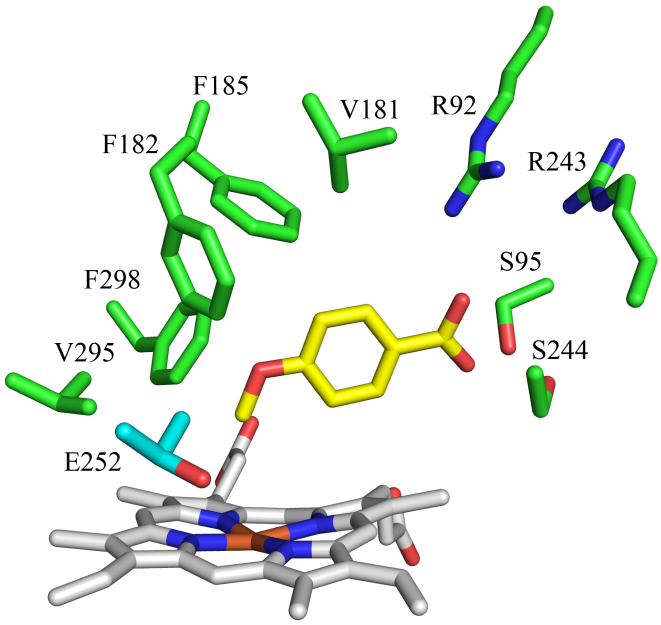

Figure 4.2: Active site structure of T252E-CYP199A4 (PDB: 7REH). The E252 residue is in cyan.

4.2 Materials and Methods

4.2.1 General

General reagents and organics were purchased from Sigma-Aldrich. Isopropyl-β-D-thiogalactopyranoside (IPTG) and buffer components were obtained from Astral Scientific (Australia). UV/Vis spectra and spectroscopic activity assays were performed on an Agilent Cary 60 spectrophotometer at 30 ± 5 °C.

4.2.2 Production and Purification of T252E-CYP199A4

Mutant T252E of CYP199A4 was expressed as previously described but with the addition of 4-methoxybenzoic acid to a concentration of 1 mM to the expression media before induction.[156] The expressed protein was then purified using previously established methods.[156] Proteins were stored in 50 % v/v glycerol at -20 °C.

4.2.3 Protein Crystallography and *In Crystallo* Enzymatic Reactions

Crystallisation experiments were performed with T252E-CYP199A4. Immediately prior to preparation of crystal trays, the protein was purified via elution through a HiPrep Sephacryl S-200 HR size-exclusion column (60 cm × 16 mm; GE Healthcare) with Buffer T at a flow rate of 1 mL min^{-1}. The purity of the protein was assessed based on the Reinheitszahl value, RZ = A_{420}/A_{280}, whereby fractions with RZ = 2 were collected and combined.

Substrate (4-methoxy- or 4-hydroxybenzoic acid) was then added to the combined fractions to a final concentration of 1 mM from a 100 mM stock of EtOH/DMSO to the concentrated protein. The combined fractions with substrate were incubated at 4 °C and then concentrated via ultrafiltration using a Microsep Advance centrifugal device (10 kDa MWCO, Pall Corporation) to a concentration of approximately 30 – 35 mg mL^{-1}. Crystallisation trays were prepared using the following optimised buffer conditions previously reported:[157] 0.2 M magnesium acetate, 100 mM Bis-Tris buffer (adjusted with acetic acid to pH 5.0 - 5.75) and 20 - 32 % w/v polyethylene glycol (PEG) 3350.

Protein crystallisation was achieved using the hanging-drop vapour diffusion method in 24-well trays. An equal volume of crystallisation buffer was mixed with hanging drops of 1.2 - 2 µL of protein and was equilibrated with a reservoir of the same buffer

(500 µL) at 16 °C. Red plate-like crystals were obtained after half a day to one week.

In crystallo reactions were carried out with T252E-CYP199A4 co-crystallised with 4-methoxybenzoic acid. Single crystals were picked from individual wells and soaked in their respective crystallisation buffer containing H_2O_2. The crystals were soaked at different concentrations of H_2O_2 (0.5 to 10 mM) with variable soaking times (0, 5 and 10 min). After soaking, single crystals were mounted onto Micromounts or Microloops (MiTeGen LLC, New York, USA). Mounted crystals were immersed in Parabar 10312 Oil (Paratone-N, Hampton Research, California, USA) before flash-cooled in liquid N_2.

X-ray diffraction data were obtained (360 images per crystal) at the Australian Synchrotron using the MX1 beamline[221] with an exposure time of 1 s, oscillation angle of 1 °, wavelength of 0.9537 Å and temperature of 100 K. Diffraction images were indexed and integrated using iMosfilm.[222] Aimless[223] from the CCP_4 suite of programs[224] was used to carry out scaling, merging and R_{free} labelling (5 % of reflections, randomly selected). The phase problem was solved using Molecular Replacement in Phaser[225] using a high-resolution structure of WT CYP199A4 (1.54 Å, PDB: 5UVB) as the search model. The ligands and solvent molecules were removed from the search model prior to phasing to eliminate model bias. Weighted $2mF_o$-DF_c maps and F_o-F_c difference maps were obtained and used to rebuild the model in WinCoot and determine the substrate binding mode.[226] Structural refinements were carried out over multiple cycles using Phenix Refine, available in the Phenix suite of programs.[227]

Composite-omit or feature enhanced maps that reduce model bias were generated in Phenix to allow inspection of the ligand binding site and reveal the location of all substrate atoms.[228,229] Detailed data collection and structural refinement statistics are provided in Appendix C.

To model the location of the Cpd I oxygen atom, the CreateAtomAlongBond script was employed. Computational studies of Cpd I have calculated that the Fe-O bond length is very consistent at 1.62 Å. This was determined both in the absence and in the presence of substrate for CYPs 2C9, 2D6, 3A4 and $P450_{cam}$.[230,231] The oxygen atom was thus positioned 1.62 Å from the heme iron of the CYP199A4 structures.

4.3 Results

4.3.1 *In crystallo* *O*-demethylation of 4-methoxybenzoic acid by T252E-CYP199A4

For *in crystallo* enzymatic reactions with T252E-CYP199A4, 4-methoxybenzoic acid was chosen as the substrate as it binds tightly to WT CYP199A4 (K_d = 0.3 µM)[48] and mutant T252E (K_d = 1.1 µM).[156,181,219] Protein crystals of T252E-CYP199A4 complexed with 4-methoxybenzoic acid were soaked with different concentrations of H_2O_2 to trigger the *in crystallo* reaction.

A total of 24 crystals of the T252E mutant were soaked in varying concentrations of H_2O_2 for different lengths of time and then flash-frozen in liquid N_2. X-ray diffraction data were collected. Only three of these crystals showed high quality diffraction patterns. T252E-CYP199A4 is reported to catalytically demethylate 4-methoxybenzoic acid to form 4-hydroxybenzoic acid (Figure 4.3).[48,156]

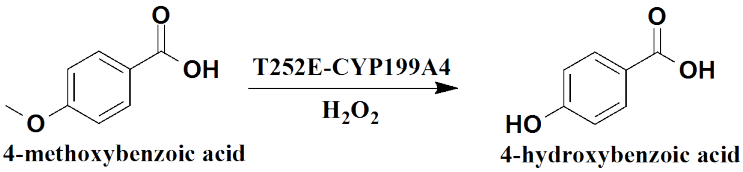

Figure 4.3: *O*-demethylation reaction of T252E-CYP199A4 with 4-methoxybenzoic acid.

Diffraction data of T252E-CYP199A4 co-crystallised with 4-hydroxybenzoic acid were collected as a control for comparison to the H_2O_2-soaked crystals. The structures of these crystals were determined and refined. F_o-F_c difference maps were generated to assess negative and positive electron density around the bound molecule and confirm if *in crystallo* demethylation to generate 4-hydroxybenzoic acid occurred. Negative density (red) show areas where atoms have been incorrectly placed and no experimental electron density is present. Positive density (green) shows where the model is missing atoms and does not account for the electron density.

The structure of T252E-CYP199A4 co-crystallised with 4-hydroxybenzoic acid was solved and refined to a resolution of 2.03 Å (PDB: 8GLY). Structural refinement and data collection statistics were shown in Table C1. The overall protein fold was similar to a structure of T252E-CYP199A4 (PDB: 7REH)[156] solved previously (RMSD = 0.157 Å. Figure C1). There was electron density present within the active site consistent with a bound ligand as previously observed with other substrate-bound structures of CYP199A4.[156,218] This electron density was modelled as 4-hydroxybenzoic acid and also 4-methoxybenzoic acid as control (Figure 4.4). The difference in the F_o-F_c maps

between these two modelled ligands would assist in determining if the H_2O_2-soaked crystals of T252E-CYP199A4 underwent demethylation.

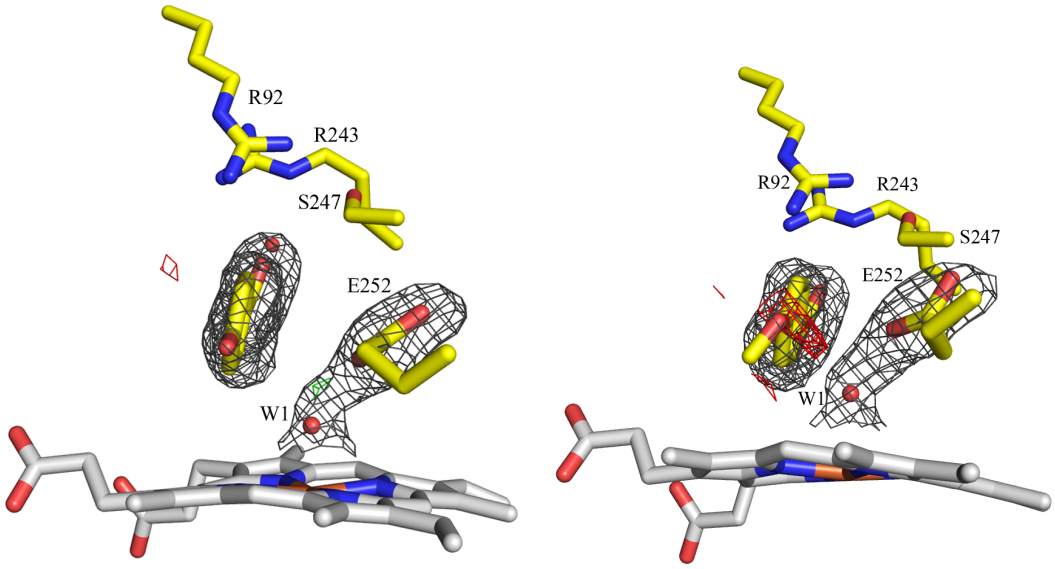

(a) (b)

Figure 4.4: Crystal structure of T252E-CYP199A4 co-crystallised with 4-hydroxybenzoic acid (yellow sticks, PDB: 8GLY). In (a), the electron density of the bound substrate was modelled as 4-hydroxybenzoic acid and in (b) it was modelled as 4-methoxybenzoic acid. Composite-omit maps ($2mF_o$-F_c) are shown as a grey mesh contoured to 1.0 σ (1.5 Å carve) around the substrate, residue E252 and heme-bound water in (a) and (b). F_o-F_c maps contoured to 2.5 σ are also shown as a green or red mesh. In (b), there is a region of negative density (red mesh) around the methoxy functional group of the bound ligand.

When the ligand was modelled as 4-hydroxybenzoic acid (Figure 4.4a), F_o-F_c maps showed no positive or negative density around the ligand. This was in contrast to when 4-methoxybenzoic acid was modelled (Figure 4.4b), showing a distinct region of negative density at the methoxy functional group. As this structure was co-crystallised with 4-hydroxybenzoic acid only, the negative density was expected with the model of 4-methoxybenzoic acid as the additional atoms in the methoxy group would be a poor fit.

The electron density of the bound ligand in the H_2O_2-soaked crystals will therefore be modelled with either 4-hydroxybenzoic acid and 4-methoxybenzoic acid. Positive densities observed around the 4-hydroxybenzoic acid model would indicate excess electron density that has not been accounted for and demethylation may not have occurred. If negative densities were observed around the 4-methoxybenzoic acid model, it would indicate demethylation has occurred with the H_2O_2-soaked crystals. These H_2O_2-soaked structures were solved and their overall protein fold (RMSD: 0.250 - 0.268, Figure C2, C3 and C3) was similar to the structure of T252E-CYP199A4 solved previously (PDB: 7REH).[156] Refinement and data collection statistics can be seen in Table C1.

The first structure solved for the *in crystallo* reactions was a crystal soaked with 1 mM H_2O_2 for a brief period (< 10s) and flash-frozen immediately (denoted as 0 min). This structure was solved and refined to a resolution of 1.85 Å (PDB: 8GM1). The electron density of the bound ligand was again modelled with both 4-hydroxybenzoic acid and 4-methoxybenzoic acid with F_o-F_c maps generated (Figure 4.5).

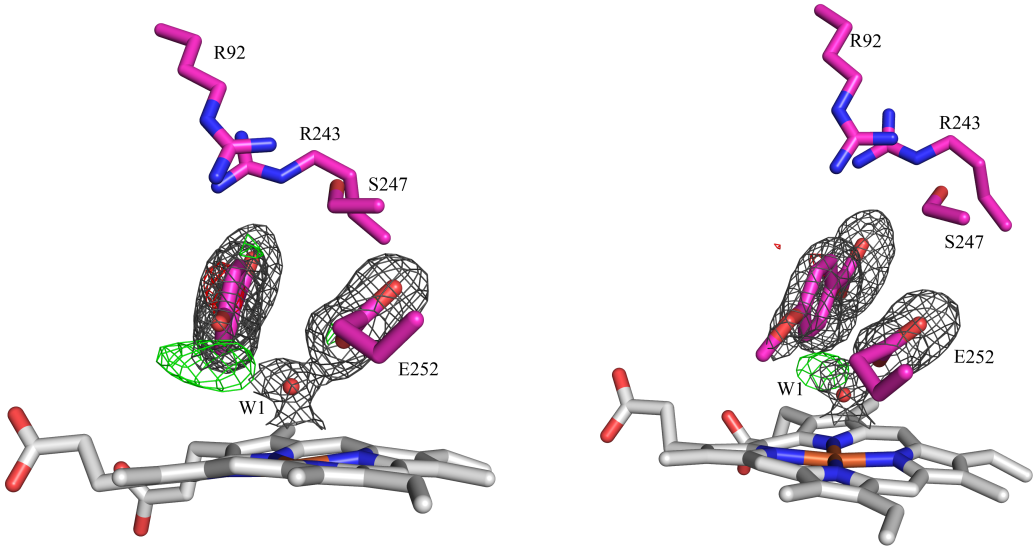

(a) (b)

Figure 4.5: Crystal structure of T252E-CYP199A4 co-crystallised with 4-methoxybenzoic acid and soaked with 1 mM H_2O_2 for 0 min (magenta sticks, PDB: 8GM1). This structure was solved to a resolution of 1.85 Å. In (a), the electron density of the bound substrate was modelled as 4-hydroxybenzoic acid and in (b) it was modelled as 4-methoxybenzoic acid. Composite-omit maps ($2mF_o$-F_c) are shown as a grey mesh contoured to 1.0 σ (1.5 Å carve) around the substrate, residue E252 and heme-bound water in (a) and (b). F_o-F_c maps contoured to 2.5 σ are also shown as a green or red mesh. In (a), there is a region of positive density (green mesh) around the hydroxy functional group of the bound ligand. In (b), the region of positive density has shrunk when 4-methoxybenzoic acid was modelled.

When comparing the F_o-F_c maps between the two models, the 4-hydroxybenzoic acid model (Figure 4.5a) showed a large region of positive density surrounding the *para*-hydroxy moiety indicating the model used is missing atoms in this region. In contrast to the 4-methoxybenzoic acid model (Figure 4.5b), no positive or negative density was observed near the *para* position of the bound ligand. This demonstrates that little or no demethylation of 4-methoxybenzoic acid occurred within the crystal. It is noted that there is still a region of positive density above the heme and the aqua ligand in Figure 4.5b. An attempt to model a H_2O_2 molecule above the heme resulted in negative density in the F_o-F_c map (Figure C5), suggesting that H_2O_2 is not above the heme centre.

For the two remaining crystals soaked in H_2O_2, the ligand in each crystal was modelled with 4-methoxybenzoic acid and 4-hydroxybenzoic acid. F_o-F_c maps for each substrate was generated as before (Figure 4.6 and Figure 4.7).

In Figure 4.6, the crystal of T252E-CYP199A4 with 4-methoxybenzoic acid was soaked with 4 mM of H_2O_2 for 5 min and was solved at a resolution of 2.02 Å (PDB: 8GLZ). The F_o-F_c maps of this crystal showed only a small region of positive density near the *para*-moiety when 4-hydroxybenzoic acid is the modelled ligand (Figure 4.6a). In contrast, the 4-methoxybenzoic acid model showed negative density around the *para*-methoxy moiety that is indicative of poor agreement between this model and the electron density observed (Figure 4.6b). For this structure, the F_o-F_c and composite-omit maps were similar to that of T252E-CYP199A4 bound to 4-hydroxybenzoic acid (Figure 4.4). This was therefore evidence of 4-hydroxybenzoic acid bound to the active site. The positive density surrounding the 4-hydroxybenzoic acid model (Figure 4.6a) is also significantly smaller in comparison to the crystal where little or no demethylation of the substrate occurred (Figure 4.5a). This strongly suggests that an *in crystallo* demethylation reaction occurred within this crystal after soaking with 4 mM H_2O_2.

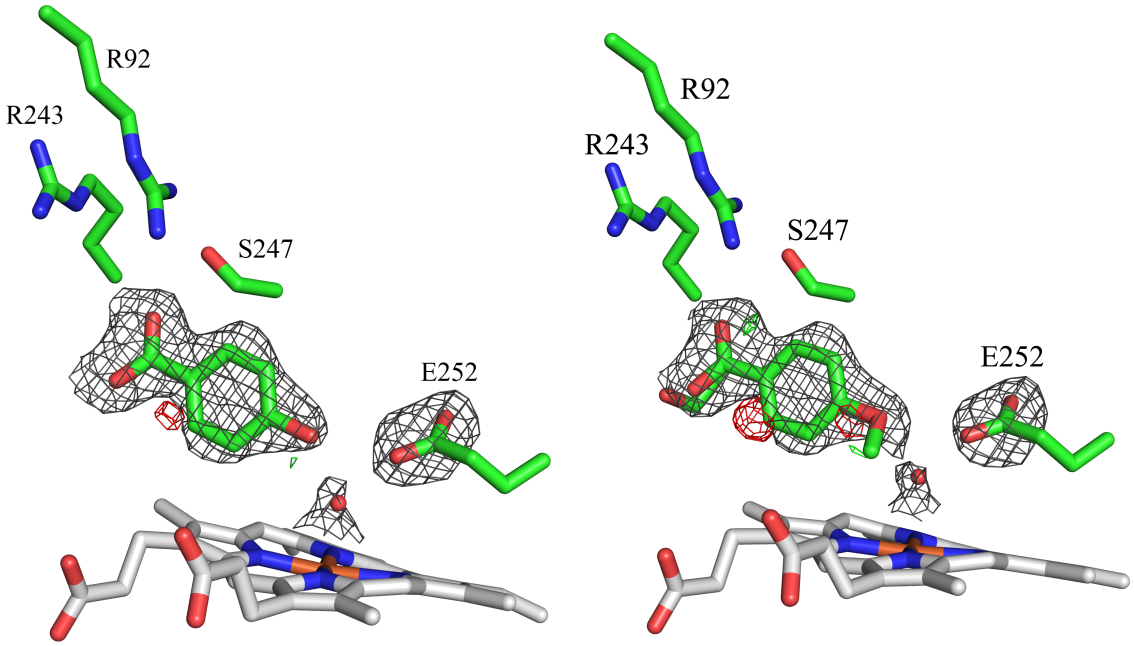

(a) (b)

Figure 4.6: Crystal structure of T252E-CYP199A4 co-crystallised with 4-methoxybenzoic acid and soaked with 4 mM H_2O_2 for 5 min (green sticks, PDB: 8GLZ). This structure was solved to a resolution of 2.02 Å. In (a), the electron density of the bound substrate was modelled as 4-hydroxybenzoic acid and in (b) it was modelled as 4-methoxybenzoic acid. Composite-omit maps ($2mF_o$-F_c) are shown as a grey mesh contoured to 1.0 σ (1.5 Å carve) around the substrate, residue E252 and heme-bound water in (a) and (b). F_o-F_c maps contoured to 2.5 σ are also shown as a green or red mesh. In (a), there is a small region of positive density (green mesh) around the hydroxy functional group of the bound ligand. In (b), there are regions of negative density around the substrate.

The last crystal structure was of T252E-CYP199A4 bound to 4-methoxybenzoic acid that was soaked in 2 mM H_2O_2 for 10 min (Figure 4.7). The resolution of this structure was at 2.33 Å (PDB: 8GM2). The model of both 4-hydroxybenzoic acid and 4-methoxybenzoic acid showed no regions of negative density around either model.

However, a small region of positive density was observed with the 4-hydroxybenzoic acid model (Figure 4.7a). This could be indicative that only a portion of the 4-methoxybenzoic acid bound has undergone demethylation within this crystal.

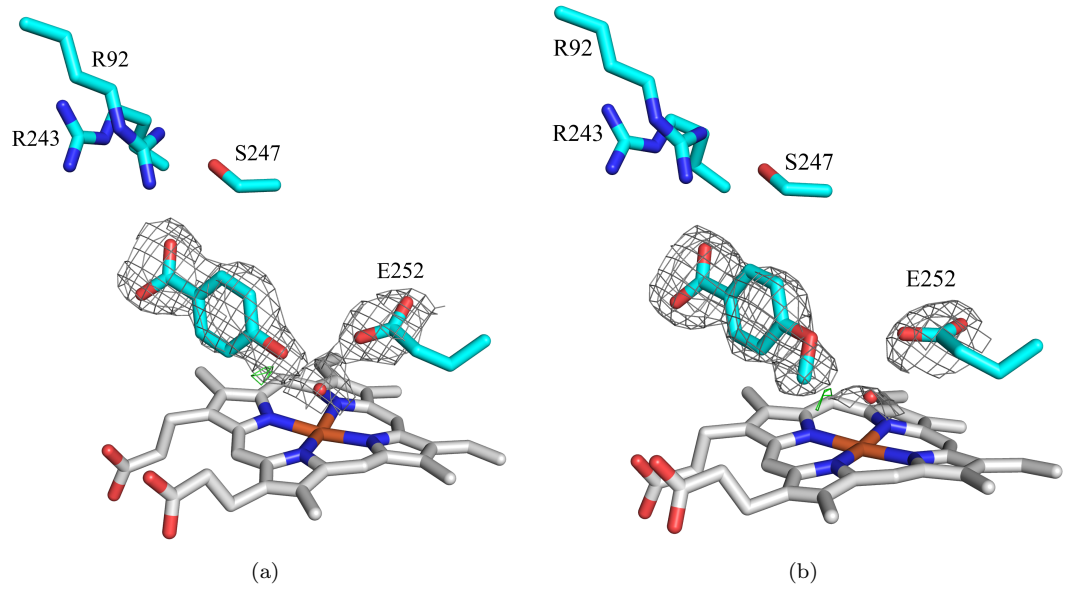

(a) (b)

Figure 4.7: Crystal structure of T252E-CYP199A4 co-crystallised with 4-methoxybenzoic acid and soaked with 2 mM H_2O_2 for 10 min (cyan sticks, PDB: 8GM2). This structure was solved to a resolution of 2.33 Å. In (a), the electron density of the bound substrate was modelled as 4-hydroxybenzoic acid and in (b) it was modelled as 4-methoxybenzoic acid. Composite-omit maps ($2mF_o$-F_c) are shown as a grey mesh contoured to 1.0 σ (1.5 Å carve) around the substrate, residue E252 and heme-bound water in (a) and (b). F_o-F_c maps contoured to 2.5 σ are also shown as a green or red mesh.

Modelling the electron density of the ligands bound to the different H_2O_2-soaked crystals with either 4-methoxybenzoic acid and 4-hydroxybenzoic acid suggests that different proportions of the initial substrate and demethylated metabolite were present in the T252E-CYP199A4 crystals. To further investigate the extent of the *in crystallo* enzymatic reaction, both 4-methoxybenzoic acid and 4-hydroxybenzoic acid were modelled in same location using different altloc identifiers and the occupancies of both ligands refined (Table 4.1). The average B-factors between atoms of the heme centre and the two ligands were found to be similar which suggests refining the occupancy of the ligands concurrently was justified (Table 4.1).

Table 4.1: Occupancies of 4-methoxybenzoic acid and 4-hydroxybenzoic acid co-refined at the same location in H_2O_2-soaked crystals of T252E-CYP199A4. The average B-factor of the atoms for both ligands is also compared against the average B-factor of the atoms for the heme.

Condition	**Ligand Occupancy** (%)		**Average B**	
	4-hydroxybenzoic acid	4-methoxybenzoic acid	Heme	Ligands
4 mM H_2O_2 for 5 min	70	30	21.5	21.7
2 mM H_2O_2 for 10 min	35	62	35.7	35.6
1 mM H_2O_2 for 0 min	47	50	15.1	14.9

The refined occupancies of the bound ligand to the soaked crystals were largely consistent with what was observed with the F_o-F_c maps (Figures 4.5, 4.6 and 4.7). The 4 mM H_2O_2-soaked crystal showed the highest proportion of 4-hydroxybenzoic acid (70 %, Table 4.1) which agrees with demethylation being observed with its respective F_o-F_c maps (Figure 4.6). Crystals soaked with 1 mM and 2 mM H_2O_2 showed less or no *in crystallo* demethylation occurring based on the F_o-F_c maps (Figure 4.5 and 4.7). The occupancy of 4-methoxybenzoic acid for these two crystals was indeed higher compared to the demethylated product (Table 4.1), whereby 4-methoxybenzoic acid had the highest occupancy in the crystal soaked in 2 mM H_2O_2 (62 %) suggesting that *in crystallo* demethylation occurred to a lesser extent compared to the other conditions.

Overall, three crystal structures of T252E-CYP199A4 soaked with H_2O_2 for different lengths of time were solved and refined (Figure 4.8). The crystal soaked for 4 mM H_2O_2 for 5 mins strongly suggests that an *in crystallo* peroxygenase reaction has occurred.

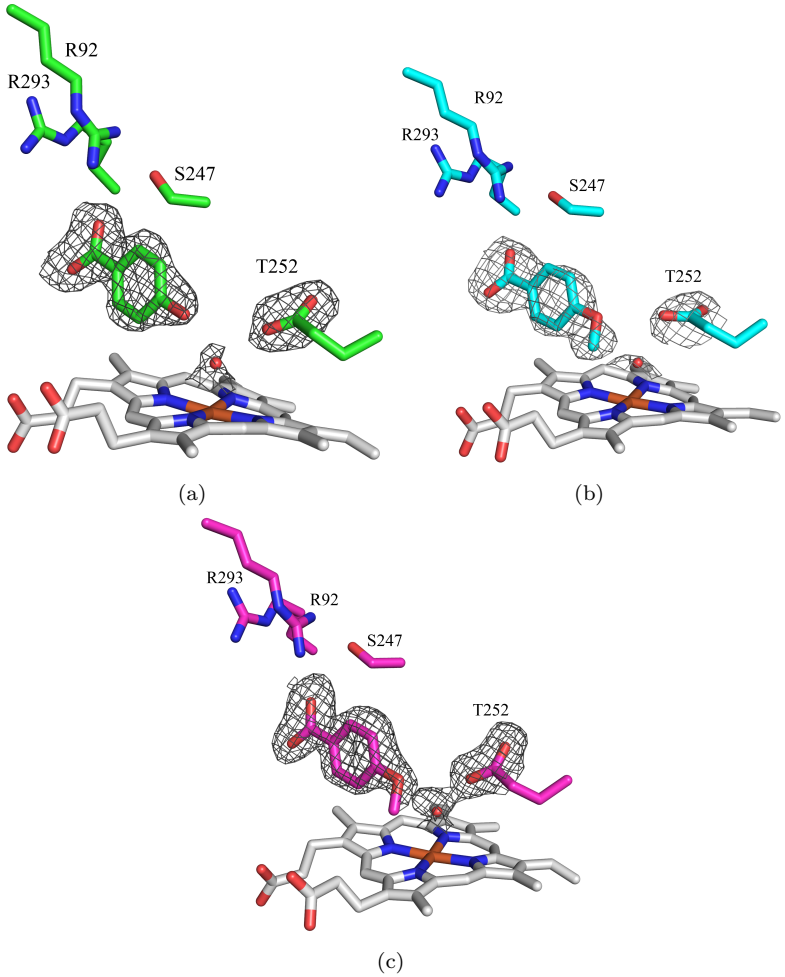

Figure 4.8: Crystal structures of T252E-CYP199A4 soaked with H_2O_2. In (a), crystal was soaked with 4 mM H_2O_2 for 5 mins and 4-hydroxybenzoic acid was the highest occupancy ligand observed. In (b) and (c), crystals were soaked with 2 mM and 1 mM H_2O_2 respectively while 4-methoxybenzoic acid was the highest occupancy ligand observed for both (b) and (c).

Structures of CYP199A4 bound to enzymatic products have not been reported. As 4-hydroxybenzoic acid is a product of oxidative demethylation by T252E-CYP199A4

with 4-methoxybenzoic acid, a more detailed study into the active site structure when the T252E mutant is bound to product would be of interest. In addition to this, the exposure of peroxide to P450s such as T252E-CYP199A4 and other P450 peroxygenases has been shown to damage the heme centre.[156,181,232] We wish to assess if this peroxide-driven damage causes any changes with the H_2O_2-soaked crystals that can be observed with crystallography. Crystals that were soaked with 4 mM H_2O_2 and 2 mM H_2O_2 for 5 mins and 10 mins respectively were chosen. These crystal structures were modelled with their respective ligand with the highest refined occupancy in Table 4.1. Distances and angles of key active site features for all crystal structures were measured and shown in Table C2. The active site structure of each crystal was compared a structure of T252E-CYP199A4 bound to 4-methoxybenzoic acid (PDB: 7REH).

The full active site structure of T252E-CYP199A4 with 4-hydroxybenzoic acid (PDB: 8GLY) is shown in Figure 4.9. The chloride capping anion is present alongside water molecules that interact with the heme and benzoic acid moiety of the ligand as per previously solved structures of T252E-CYP199A4.[156,157] The occupancies of heme-bound water (W1) was 83 % and 4-hydroxybenzoic was 86 %. The 4-hydroxybenzoic acid complex structure was superimposed to T252E-CYP199A4 complexed with 4-methoxybenzoic acid (PDB: 7REH, Figure 4.9b). It is seen the active site structure between two complexes were similar with little or no differences observed between the positioning of key active site residues. The heme-bound water ligand (W1, Figure 4.9a) is still present when 4-hydroxybenzoic acid is complexed to the T252E mutant as previously observed with other ligands bound to this mutant.[156]

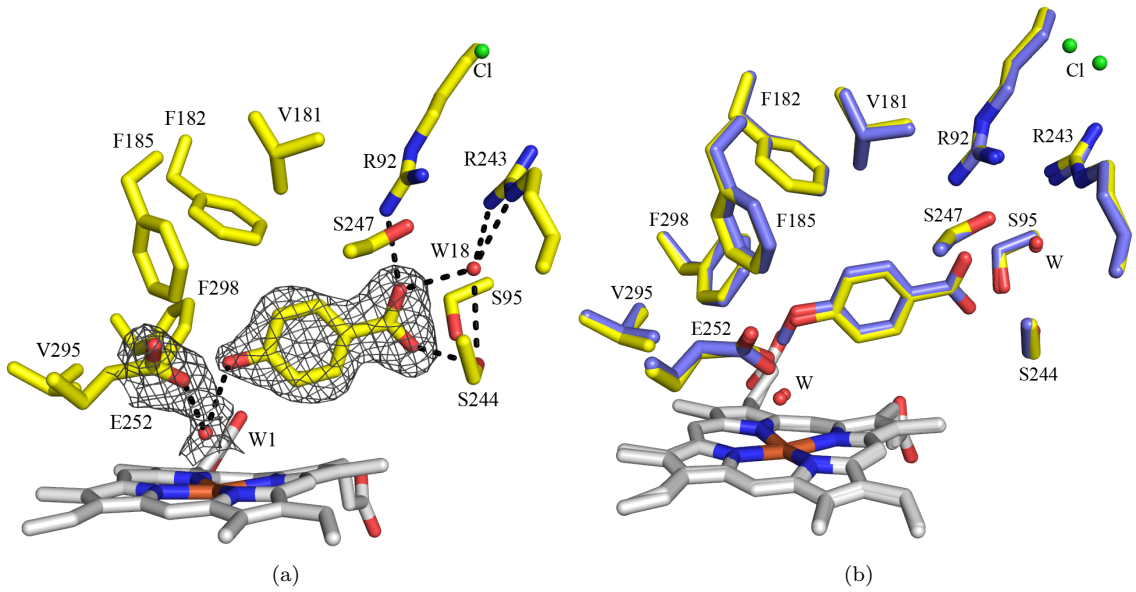

Figure 4.9: (a) A structure of T252E-CYP199A4 complexed with 4-hydroxybenzoic acid (yellow sticks, PDB: 8GLY) solved to a resolution of 2.03 Å. A composite-omit map ($2mF_o$-F_c) is shown around the bound ligand, residue E252 and heme-bound water (W1) as a grey mesh (1.0 σ, 1.5 Å carve) (b) Superimposed structures of T252E-CYP199A4 complexed with 4-hydroxybenzoic acid (yellow sticks) and compared to the same enzyme complexed with 4-methoxybenzoic acid (navy sticks, PDB: 7REH).

The structure of crystallised T252E-CYP199A4 soaked with 4 mM H_2O_2 for 5 mins was modelled and refined with 4-hydroxybenzoic acid as the bound ligand (Figure 4.10, PDB: 8GLZ). The occupancy of the heme-bound water ligand was at 88 %. The active site structure of this H_2O_2-soaked crystal T252E-CYP199A4 also showed no significant differences with the previously reported structure of this enzyme (Figure 4.10b, PDB: 7REH).

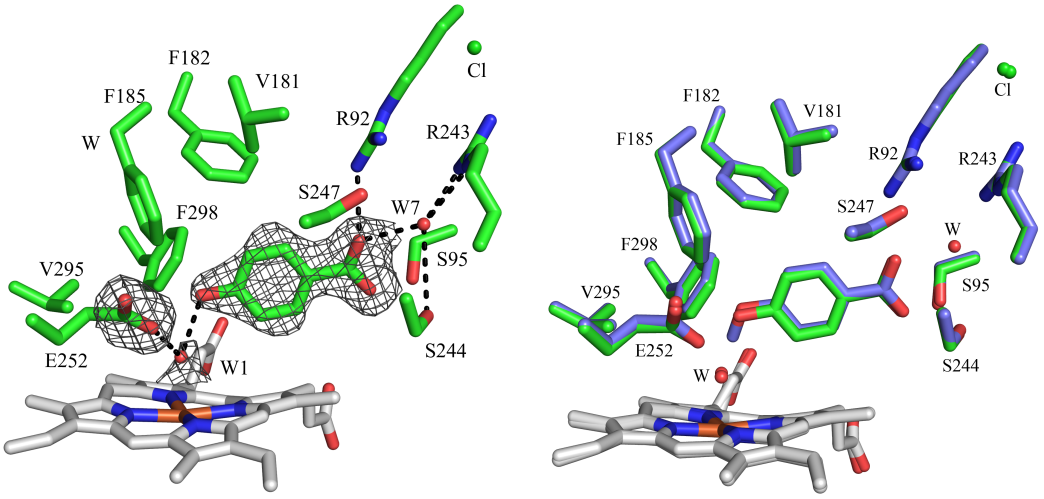

Figure 4.10: (a) A structure of T252E-CYP199A4 crystallised with 4-methoxybenzoic acid solved to 2.02 Å that underwent *in crystallo* demethylation after soaking with 4 mM H_2O_2 for 5 mins (green sticks, PDB: 8GLZ). The ligand bound was modelled as 4-hydroxybenzoic acid. A composite-omit map ($2mF_o$-F_c) is shown around the bound ligand, residue E252 and heme-bound water (W1) as a grey mesh (1.0 σ, 1.5 Å carve) (b) Structure of T252E-CYP199A4 soaked with 4 mM H_2O_2 (green sticks) superimposed with the same enzyme complexed with 4-methoxybenzoic acid (navy sticks, PDB: 7REH).

The crystal structure of T252E-CYP199A4 soaked with 2 mM H_2O_2 for 10 min (2.33 Å, PDB: 8GM2, Figure 4.11) was also compared to the structure of the same mutant complexed with 4-methoxybenzoic acid (Figure 4.11b, PDB: 7REH) or 4-hydroxybenzoic acid (Figure 4.11c, PDB: 8GLY). The ligand of the H_2O_2-soaked structure was modelled as 4-methoxybenzoic acid and the heme-bound water had 100 % occupancy. The active site conformation between the compared structures were largely similar. But interestingly, an altered conformation for residue E252 was observed after soaking with H_2O_2 for 10 minutes (Figure 4.11b). The carboxylate of the E252 residue was oriented upwards by $\sim$ 18 ° after soaking with H_2O_2 and becomes more in parallel with the plane of the heme (Figure 4.11d).

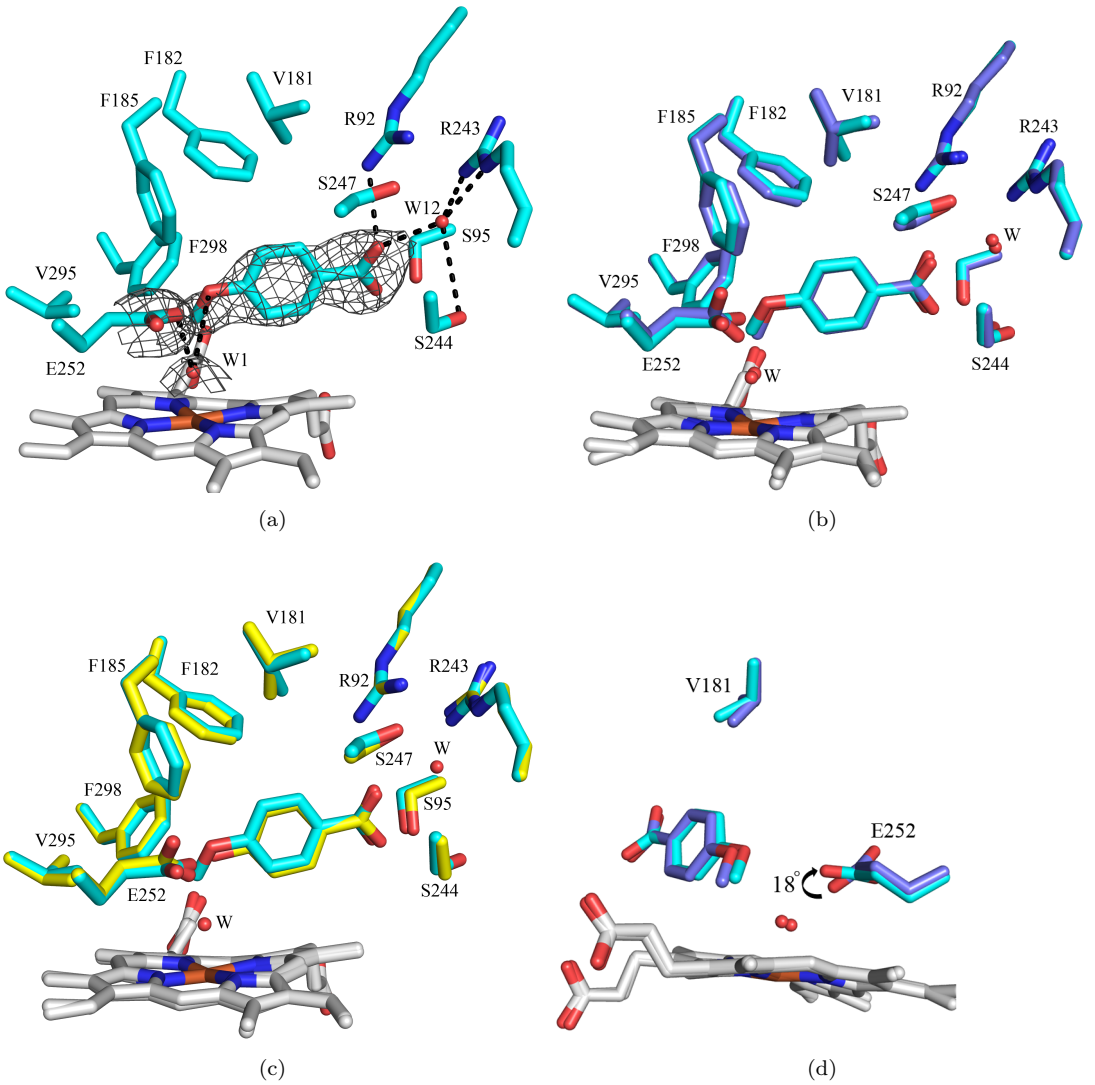

Figure 4.11: (a) A structure of T252E-CYP199A4 crystallised with 4-methoxybenzoic acid solved to 2.33 Å that was soaked with 2 mM H_2O_2 for 10 min (cyan sticks, PDB: 8GM2). The ligand bound was modelled as 4-methoxybenzoic acid. A composite-omit map is shown around the bound ligand, residue E252 and heme-bound water (W1) as a grey mesh (1.0 σ, 1.5 Å carve) (b) Structure of T252E-CYP199A4 soaked with 2 mM H_2O_2 (cyan sticks, PDB: 8GM2) superimposed with the same enzyme complexed with 4-methoxybenzoic acid (navy sticks, PDB: 7REH). (c) Structure of T252E-CYP199A4 soaked with 2 mM H_2O_2 (cyan sticks, PDB: 8GM2) superimposed with the same enzyme complexed with 4-hydroxybenzoic acid (yellow sticks, PDB: 8GLY). (d) The E252 residue of H_2O_2-soaked structure (cyan sticks) has orientated to be in parallel with the plane of the heme. The black arrow shows the direction the E252 residue moved.

The distances and angles of key active site features for T252E-CYP199A4 bound to 4-hydroxybenzoic acid (PDB: 8GLY) and with the H_2O_2-soaked crystals of this enzyme (PDB: 8GLZ and 8GM2) were measured. It was found that these measurements did not differ significantly from each other or with the previously reported structure of this CYP199A4 mutant (Table C2, PDB: 7REH).

4.4 Discussion

The structure of T252E-CYP199A4 in complex with 4-hydroxybenzoic acid has been solved for the first time. This ligand is a product of *O*-demethylation by CYP199A4 using 4-methoxybenzoic acid as a substrate. 4-Methoxybenzoic acid binds tightly to WT CYP199A4 (K_d = 0.3 µM)[137] and the T252E mutant (K_d = 1.11 µM).[156] No dissociation constants have been measured with 4-hydroxybenzoic acid but it would be expected to bind less tightly. The dissociation constants for $P450_{cam}$ with its physiological substrate, camphor (K_d = 0.25 µM)[233] showed it was bound nearly 40-fold tighter compared to the product, 5-*exo*-hydroxycamphor (K_d = ∼10 µM).[234] From this, we can infer CYP199A4 and its mutant would behave similarly, whereby 4-hydroxybenzoic acid will bind less tightly to CYP199A4 compared to 4-methoxybenzoic acid. The refined occupancy of 4-hydroxybenzoic acid bound to T252E-CYP199A4 was found to be 86 %. The ligand binding mode and active site geometry of T252E-CYP199A4 was not altered significantly with 4-hydroxybenzoic acid compared to 4-methoxybenzoic acid. A structure of $P450_{cam}$ bound to the hydroxylation product, 5-*exo*-hydroxycamphor found the product and substrate are held in exactly the same position.[235]

The structure of $P450_{cam}$ with 5-*exo*-hydroxycamphor also revealed an interaction between the product OH group and the heme-iron centre (Fe-O, ≈ 2.7 Å). This maintained the enzyme in a low-spin state and slows reduction by electron transfer proteins.[235] The equivalent interaction in T252E-CYP199A4 and 4-hydroxybenzoic acid was much further apart in distance (Fe-O_7, 4.8 Å) and it is unlikely the bound ligand would have any effect on the heme-iron centre. However, a heme-bound distal water ligand (83 % occupancy) was also present when 4-hydroxybenzoic acid is complexed to this mutant. This was to be expected as bulkier benzoic acid substrates were also unable to displace this heme-bound water.[236] This is due to the distal water interacting with the carboxylate of E252 (2.6 Å) and allows it to remain bound to the heme-iron.[156] Matthew Podgorski of the University of Adelaide solved a structure of WT CYP199A4 complexed to 4-hydroxybenzoic acid (Unpublished, Figure 4.12a). This structure was compared to the structure of T252E-CYP199A4 complexed to the same ligand. The WT enzyme has additional waters in the active site. This cluster of waters is hydrogen-bonded to the *para* OH group of the ligand and more importantly a heme-bound water is also present. The polarity in the active site of T252E afforded by the E252 residue likely mimics the hydrogen bonding network seen in the WT enzyme and prevents additional waters from entering the active site. Further studies into the binding of enzymatic metabolites of CYP199A4 to the enzyme and its mutants would be of interest

to assess if similar interactions of active site waters with the heme are present.

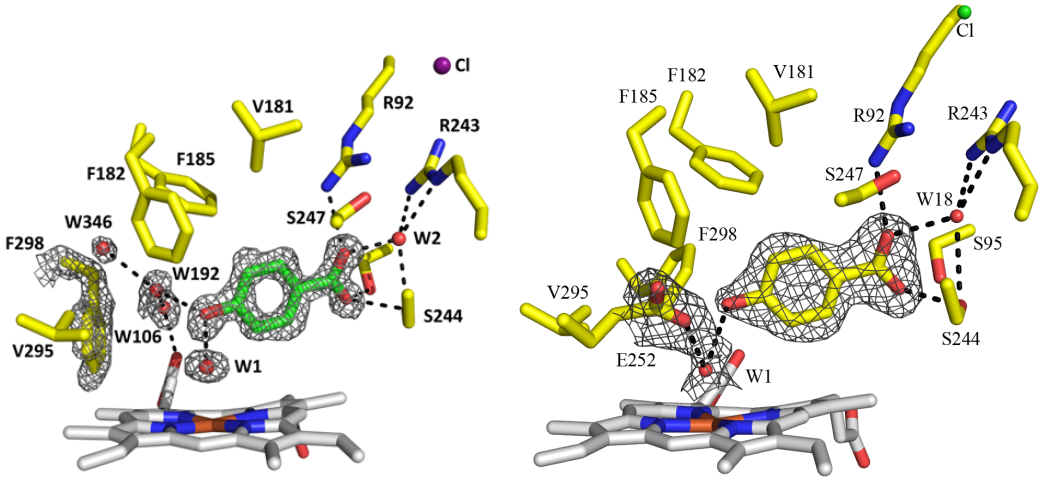

Figure 4.12: (a) Crystal structure of WT CYP199A4 in complex with 4-hydroxybenzoic acid, solved at 1.54-Å resolution provided by Matthew Podgorski. A feature-enhanced map of the substrate, F298 residue, heme-bound aqua ligand (W1) and active-site waters (W192, W346, W106) is shown as grey mesh contoured at 1.5 σ. The side chain of F298 is displaced to accommodate these additional active-site waters (W192 and W106). (b) Crystal structure of T252E-CYP199A4 in complex with 4-hydroxybenzoic acid as seen in Figure 4.9.

In crystallo *O*-demethylation reactions were demonstrated with crystallised T252E-CYP199A4 bound to 4-methoxybenzoic acid and soaked with H_2O_2. The soaking condition that drove demethylation to the greatest degree being 4 mM H_2O_2 for 5 min and this was the highest concentration of H_2O_2 tested. Analysis revealed 4-hydroxybenzoic acid with an occupancy of 70 %. The alternate soaking conditions of 2 mM H_2O_2 for 10 mins drove *in crystallo* demethylation the least (35 % occupancy of 4-hydroxybenzoic acid) compared to soaking in 1 mM H_2O_2 for 0 min (47 % occupancy of 4-hydroxybenzoic acid). This discrepancy with the higher concentration of H_2O_2 forming less 4-hydroxybenzoic acid could be due to poorer diffusion of H_2O_2 into the crystal lattice. The rate of diffusion of molecules into the crystal lattice does not only depend on a high concentration of the soaked molecule during the soaking step but also the crystals need to be small with large diffusion coefficients.[212] Crystal sizes chosen for this study were random. Crystals with edge lengths in single digit µm or smaller is recommended for diffusion triggered *in crystallo* reactions.[212]

During dataset collection, it is possible that the X-rays used can cause damage to the heme centre and perturbations in the active site.[211,237] Heme centres in proteins are known to undergo photoreduction to change its redox state alongside the formation of free radical species when irradiated by ionising X-ray radiation.[237] It has been reported that $P450_{cam}$ was able to be reduced to form Cpd I as the active oxidant through exposure to an X-ray source for 3 h.[210] This study only irradiated the single crystals

for 6 min during data collection and was carried out 100 K, which should alleviate any damaging effects arising from X-ray exposure. The T252E mutant of CYP199A4 also demonstrated poor capability to undergo reduction by sodium dithionite.[156]

Further investigations could involve large-scale batch crystallisation to form microcrystals of T252E-CYP199A4. Facile crystallisation of microcrystals in batch have been achieved with different enzymes by incorporating ammonium sulfate precipitation to the vapour diffusion crystallisation conditions of these enzymes.[238] Microcrystals are susceptible to damage to X-ray radiation,[212] but large batches of microcrystals can be used for serial crystallography. This involves thousands of microcrystals being exposed to X-ray free electron lasers (XFEL) that damages the microcrystals but diffraction occurs at a femtosecond scale.[212,239] As diffraction is essentially instantaneous, large batches of crystals could be used in serial crystallography to obtain diffraction data for structure determination. Microcrystals of T252E-CYP199A4 used for H_2O_2 triggered *in crystallo* reactions could be investigated with serial crystallography to explore femtosecond resolved structures along the catalytic pathway of this enzyme.

Crystals with large diffusion coefficients would allow fast diffusion of the target molecule into the crystal lattice and is influenced by large, water-filled channels within the crystallised protein.[212] The size of the solvent pores within crystals of CYP199A4 has not been assessed. A possible approach to improve the diffusion of H_2O_2 into the crystals of this P450 enzyme would be analysing the solvent channels of the enzyme using CAVER 3.0.[240] This analysis tool was used to identify and estimate the importance of the solvent channels in haloalkane dehalogenase DhaA for catalytic activity.[240]

In crystallo P450 reactions driven by the peroxide shunt has only been demonstrated with CYP121 with a synthetic probe designed to mimic its native substrate, cyclo(l-Tyr-l-Tyr) (cYY).[217] Soaking of CYP121 co-crystallised with the synthetic probe in H_2O_2 formed a hydroxylated intermediate that was potentially captured by X-ray crystallography (Figure 4.13).[217] This hydroxylated intermediate was reported to share 50 % occupancy with the substrate precursor.[217] In our current study, the highest occupancy observed for an *in crystallo* demethylation product with T252E-CYP199A4 was 70 %. Future work could include testing other substrates with crystallised T252E-CYP199A4 that could undergo different *in crystallo* P450 reactions such as hydroxylation and sulfoxidation. It is envisioned that trapping H_2O_2 within the crystallised enzyme could be achieved to assess how the peroxide molecule interacts with the active site residues. Trapping of a peroxide molecule with other iron containing enzymes has been shown to be possible.[241]

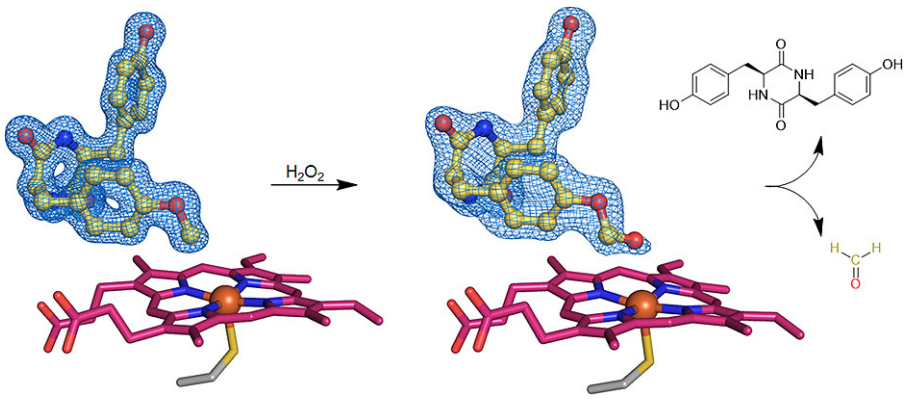

Figure 4.13: *In crystallo* reaction of CYP121 with a synthetic mimic of its natural substrate, cyclo(l-Tyr-l-Tyr) (cYY). The crystal was soaked with H_2O_2 and a small tail of excess electron density was observed with the F_o-F_c map (blue mesh, 2.5 σ) consistent with a hydroxylated intermediate.[217]

In summary, a crystal structure of T252E-CYP199A4 complexed with 4-hydroxybenzoic acid was solved for the first time. Active site geometry and ligand binding modes of enzyme complex did not differ significantly from when the enzyme was bound to 4-methoxybenzoic acid. *In crystallo* demethylation of 4-methoxybenzoic acid was demonstrated for the first time within crystallised T252E-CYP199A4.

5 Investigation of C-C Bond Cleavage by CYP199A4

5.1 Introduction

P450 enzymes are involved in the biosynthetic pathways of different steroidal compounds and can catalyse multistep oxidative reactions that involve the scission of carbon-carbon (C-C) bonds in complex molecules.[90] CYP17A1 is one such P450 involved in the synthesis of androgenic steroids such as androstenedione and dehydroepiandrosterone (DHEA) from progesterone and pregnenolone respectively.[90] CYP17A1 is a membrane bound protein and is expressed in most steroidogenic tissue.[242] This P450 first carries out 17α-hydroxylase activity to generate an α-hydroxyketone at the C17 position of pregnenolone. Subsequently, it will catalyse C17-lyase activity to cleave the C-C bond of the α-hydroxyketone to form a new carbonyl moiety and acetic acid in a Baeyer-Villiger type-reaction (Figure 5.1). CYP17A1 is theorised to use the ferric-peroxo intermediate as the nucleophilic oxidant in C17-lyase activity and forms a hemiketal intermediate. Evidence for this includes ^{18}O isotopic labelling studies that incorporated the ^{18}O atom in the acetic acid cleavage product rather than the the androgen product (Figure 5.1b).[60,100] CYP17A1 is also a target for drug inhibition in the treatment of prostate cancer.[87,243]

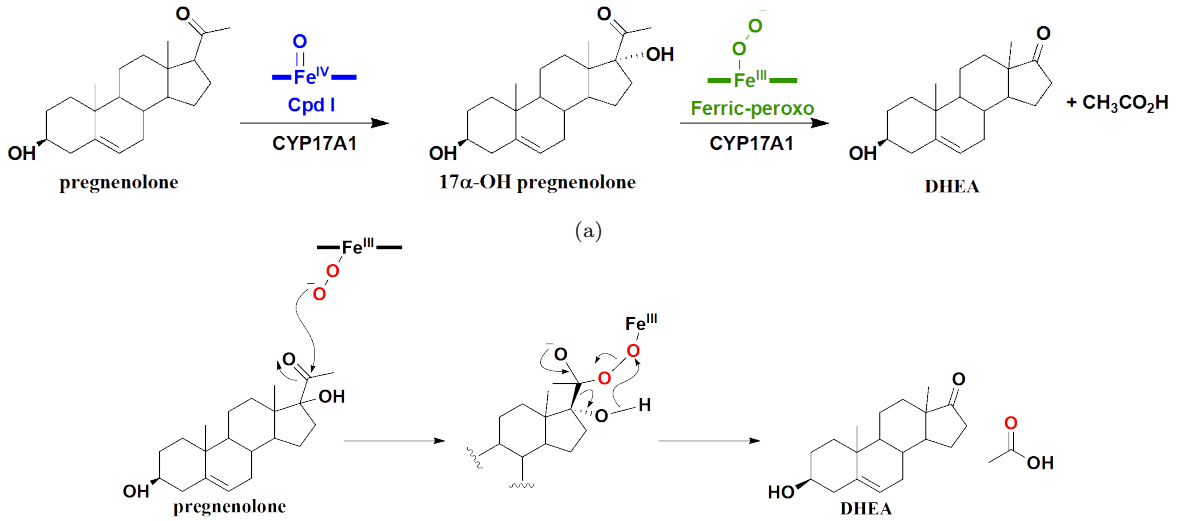

Figure 5.1: (a) CY17A1 reaction pathway for DHEA synthesis. (b) Proposed mechanism for the C-C cleavage reaction with CYP17A1. Studies with ^{18}O (red oxygen atom) postulates that the ferric-peroxo intermediate is involved in a nucleophilic attack of the α-hydroxyketone and a subsequent Baeyer-Villiger reaction incorporates the ^{18}O atom into the acetic acid cleavage product. The Baeyer-Villiger reaction could occur through different rearrangements as seen in Figure 1.14.

Investigations into the oxidant involved in P450 catalysed C-C bond cleavage activity using deuterated solvent have shown an inverse kinetic solvent isotope effect (KSIE) in the reaction between 17α-hydroxypregnenolone and CYP17A1, which supports a role for the ferric-peroxo intermediate.[244] This is further supported by the trapping of the ferric-peroxo complex of substrate-bound CYP17A1 at low temperatures.[245] This complex then further converts to a hemiketal transition state at higher temperatures that was characterised by optical and Raman spectroscopy.[245,246] Some indirect evidence has also been presented that the ferryl-oxo oxidative intermediate, Cpd I is responsible for C-C bond cleavage in CYP17A1.[94] The role of Cpd I in C-C cleavage reactions was supported through the use of an oxygen surrogate, iodosylbenzene that allowed C-C cleavage metabolites to form with CYP17A1.[94] Iodosylbenzene is a single oxygen donor that forms Cpd I directly (Figure 5.2) and is unable to form the ferric-peroxo species as the latter requires two peroxo-oxygen atoms to exist.[247] Further studies of CYP17A1 and other membrane-bound mammalian steroid metabolising P450 enzymes often encounter challenges such as low levels of heterologous protein production, protein purification and associated redox partners, ease of crystallisation and low *in vitro* turnover with poorly coupled redox activity.

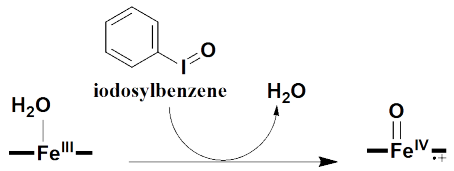

Figure 5.2: Formation of Cpd I by iodosylbenzene.[247]

CYP199A4 from *Rhodopseudomonas palustris* HaA2 is a bacterial P450 that exclusively oxidises *para*-substituted benzoic acids. The high selectivity of CYP199A4 provides opportunities to use it as a model system to investigate the mechanism of P450 catalysed C-C bond cleavage with benzoic acids that resemble physiological substrates of CYP17A1.[30,48,134,153] The availability of crystal structures for CYP199A4 allows structural binding modes to be elucidated and activities rationalised.[157,218]

WT CYP199A4 can generate α-hydroxyketone compounds using benzoic acids such as 4-propionyl- and 4-(2′-oxopropyl)-benzoic acid (Figure 5.3).[248] In preliminary studies, no further C-C cleavage activity with WT CYP199A4 was observed *in vitro* or *in vivo* with these two substrates.[248] It is possible that with excess NADH, WT CYP199A4 could catalyse C-C cleavage activity with the α-hydroxyketone products of 4-propionyl- and 4-(2′-oxopropyl)-benzoic acid.

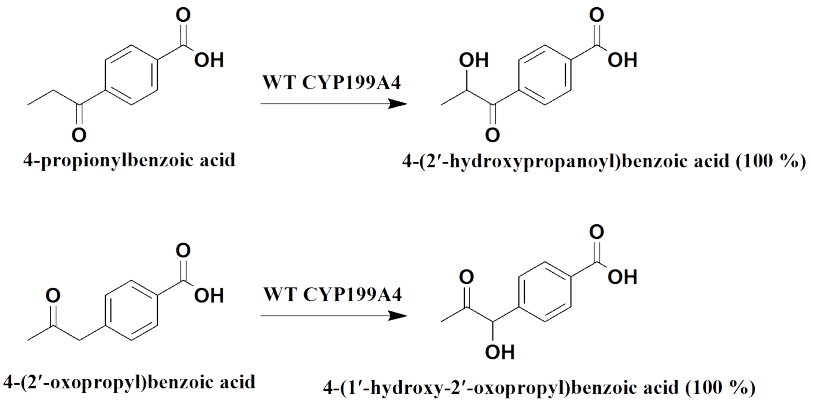

Figure 5.3: Reaction of 4-propionylbenzoic acid and 4-(2′-oxopropyl)-benzoic acid with WT CYP199A4.[248]

Benzoic acid substrates with α-hydroxyketone moieties at the *para*-position (Figure 5.4) were synthesised by Dr Justin Miller of the University of Illinois to probe the mechanisms of P450-catalysed hydroxylation and C-C cleavage.[249] We hypothesise that α-hydroxyketone compounds designed to resemble the 17-hydroxy steroid substrates of CYP17A1 will allow CYP199A4 to serve as a model system for C-C cleavage activity.

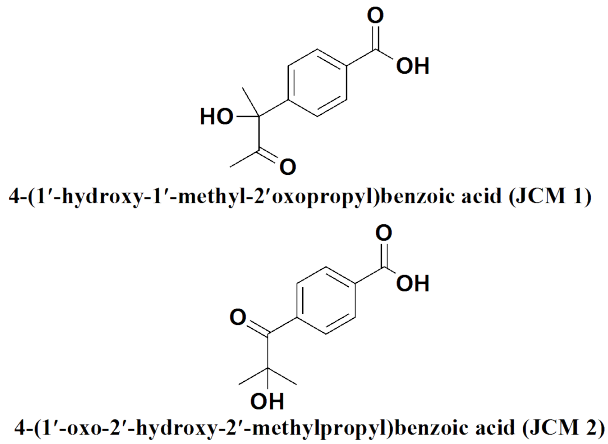

Figure 5.4: α-Hydroxyketone substrates to be tested with CYP199A4 in the study of C-C cleavage reactions.

CYP199A4 could therefore be used to study P450 catalysed C-C cleavage reactions with various substrates. X-ray crystal structures of the P450 with target substrates bound will be presented where possible to rationalise binding modes. Site-directed mutagenesis using X-ray structural information will also be carried out with CYP199A4 to improve activity of the enzyme towards target substrates.

5.2 Materials and Methods

5.2.1 General

General reagents and organics were purchased from Sigma-Aldrich. Isopropyl-β-D-thiogalactopyranoside (IPTG) and buffer components were obtained from Astral Scientific (Australia). UV/Vis spectra and spectroscopic activity assays were performed on an Agilent Cary 60 spectrophotometer at 30 ± 5 °C.

The syntheses of α-hydroxyketone substrates, JCM 1 and JCM 2 (Figure 5.4) were carried out by Dr Justin Miller of the University of Illinois at Urbana-Champaign.

Analytical High Performance Liquid Chromatography (HPLC) was performed on a Shimadzu LC-20AD equipped with a Phenomenex Kinetex 5u XB-C18 100A column (250 mm × 4.6 mm, 5 µM), SIL-20A auto-sampler, CTO-20A column oven, SPD-20A UV detector and CBM-20Alite communications module. A gradient of 20 - 95 % acetonitrile in water (both containing trifluoroacetic acid, TFA, 0.1 %) was run at a flow rate of 1 mL min^{-1} over 30 minutes and detector wavelength was set at 254 nm.

GC-MS analysis was performed using a Shimadzu GC-2010 gas chromatograph equipped with an autoinjector and a GCMS-QP2010S detector; the column used was a DB-5MS column. The interface and injection port temperatures were held at 280 and 250 °C. The column was held at 120 °C for 3 min, and the temperature was then increased to 240 °C at a rate of 7.5 °C min^{-1} and held at 240 °C for 6 min.

5.2.2 Production and purification of enzymes

HaPux, HaPuR and WT CYP199A4 were all expressed and purified as described previously.[156] Variants T252E, F298V and F182L of CYP199A4 were expressed as previously described for WT CYP199A4 but with the addition of 4-methoxybenzoic acid to a concentration of 1 mM to the expression media before induction. Proteins were stored in 50 % glycerol at -20 °C.

5.2.3 *In vitro* NADH Oxidation Assays

Glycerol was removed from proteins through elution with a 5 mL gel filtration column (PD-10, GE Healthcare) and 50 mM Tris buffer (Buffer T, pH 7.4). The concentration of each protein was quantified using UV-Vis spectrophotometry with extinction

coefficients given in Table 5.1.

Table 5.1: Extinction Coefficients for CYP199A4, HaPux and HaPuR.

Protein	**Wavelength (nm)**	**Extinction Coefficient ($mM^{-1}cm^{-1}$)**
CYP199A4	419	119
HaPux	416	11.2
HaPuR	454	10

In vitro NADH turnovers were performed at 30 °C and contained P450 (1 µM), HaPux (5 µM), HaPuR (0.5 µM) and 100 ng μL^{-1} bovine liver catalase in oxygenated Buffer T with a total volume of 1200 µL or 600 µL. The absorbance at 340 nm was set to zero and the mixture was incubated at 30 °C for 2 min before NADH was added to a concentration of ≈ 320 µM, (an absorbance of ≈ 2.0). The rate of NADH background oxidation (the 'leak' rate) was measured before initiating the reaction. To start the reaction, substrate was added from a 100 mM stock in EtOH/DMSO to the desired concentration (1 mM, 0.5 mM, 0.2 mM or 0.15 mM) and NADH depletion was monitored at 340 nm. The rate of NADH consumption (N) by the P450 enzyme in units of (µM-NADH)$(\mu M\text{-P450})^{-1}$ min^{-1} was calculated from the slope of the graph of A_{340nm} versus time using an extinction coefficient of ε_{340nm} = 6.22 mM^{-1} cm^{-1} and reported as min^{-1}.

All experiments were performed in triplicate with the mean and standard deviation reported. Control reactions were also performed in which either the P450 or NADH was omitted from the turnover mixture (replaced with the same volume of buffer).

5.2.3.1 Assays with 4-propionylbenzoic acid and 4-(2′-oxopropyl)-benzoic acids

To generate an excess of the α-hydroxyketone products of 4-propionylbenzoic acid and 4-(2′-oxopropyl)-benzoic acids (Figure 5.3), *in vitro* turnovers were carried out with WT CYP199A4 (5 µM), HaPux (5 µM), HaPuR (1 µM), 100 ng μL^{-1} of bovine liver catalase, substrate (200 µM) and NADH (2 mM) in oxygenated buffer T to a total volume of 2 × 1500 µL in 2 × 1.5 mL Eppendorf Tubes for each substrate. Reactions were left shaking at 100 rpm and 18 °C. After 2 h, a 132 µL aliquot was taken for HPLC analysis and the reactions were incubated at 60 °C for 30 min to denature the remaining enzymes. These reactions were subsequently centrifuged (20000 *g*) to remove the precipitated protein. The remaining supernatant containing the α-hydroxyketone product was cooled to 4 °C and 500 µL aliquots were taken for further experiments.

For NADH-driven assays, the reaction mixture containing the α-hydroxyketone (200

µM in 500 µL) was added to WT/F182L-CYP199A4 (1 µM), HaPux (5 µM), HaPuR (1 µM), 100 ng μL^{-1} of bovine liver catalase and NADH (320 µM).

For H_2O_2-driven assays, the reaction mixture containing the α-hydroxyketone (200 µM in 500 µL) was added to WT/T252E-CYP199A4 (1 µM) and 5 mM H_2O_2 (from 1 M stock). A control experiment only omitting the P450 enzyme was also carried out to determine if the α-hydroxyketone products were susceptible to oxidation by H_2O_2. Any remaining volume was made up with Buffer T. All reactions were incubated at 25 °C. At 2 h and 24 h, 132 µL aliquot of the reaction was taken.

5.2.4 Regenerating NADH Oxidation Assays

In a total volume of 600 µL of Buffer T in 1.5 mL Eppendorf tubes, the reactions contained the following components: P450 (1 µM), HaPuR (0.5 µM), HaPux (5 µM), alcohol dehydrogenase (ADH, 4.5 µL of 0.029 g mL^{-1} suspension, Roche), bovine liver catalase (100 ng μL^{-1}, Sigma-Aldrich), EtOH (12 µL) and substrate (0.2 mM – 0.05 mM). NADH (320 µM) was added last to start the reaction. Reactions were carried out at 25 °C and 250 rpm for 24 h.

5.2.5 H_2O_2-driven Oxidation Assays

In a total volume of 600 µL in Buffer T in 1.5 mL Eppendorf tubes, the reactions contained the following components: P450 (1 µM) and substrate (50 or 250 µM). Hydrogen peroxide (16 - 32 mM H_2O_2 from 1 M stock) was added to start the reaction. A control experiment only omitting the P450 enzyme was also carried out. Any remaining volume was made up with Buffer T. All reactions were incubated at 25 °C. At 2 h and 24 h, a 132 µL aliquot of the reaction was taken.

5.2.6 Kinetic Solvent Isotope Assays

For protonated solvent, *in vitro* NADH oxidation assays were carried out as per Section 5.2.3. For deuterated solvent, Buffer T (50 mM Tris, pH 7.4) was instead made using deuterated water (D_2O). Glycerol was removed from proteins through elution using a 5 mL gel filtration column (PD-10, GE Healthcare) equilibrated with deuterated Buffer T. *In vitro* NADH oxidation assays as per Section 5.2.3 were then carried out with the eluted proteins using NADH and bovine liver catalase stock solutions made using deuterated buffer. All reactions were monitored at 340 nm. NADH consumption rate

(N), coupling efficiency and product formation rate were calculated as in Section 5.2.3 and 5.2.8.

5.2.7 Substrate Binding Assays

WT CYP199A4 and/or its mutant were diluted to a concentration of 1-2 µM with Buffer T. To 0.5 mL of protein, 0.1 - 5 µL aliquots of 100 mM substrate stock in EtOH or DMSO were added, recording the UV-visible spectrum after each addition, until no further shift is observed.

5.2.8 Metabolite Analysis

Turnover reactions were prepared for HPLC analysis by taking a 132 µL aliquot of the reaction and this was mixed with 66 µL of acetonitrile and 2 µL of internal standard (10 mM of 9-hydroxyfluorene in EtOH). The HPLC sample was centrifuged (20000 *g*) to remove particulate matter. Metabolite products from *in vitro* activity assays were identified via co-elution using HPLC and/or GC-MS with authentic samples of potential oxidation products. HPLC analysis methods were described in Section 5.2.1.

To quantify enzyme metabolites, calibration curves were constructed from authentic product standards or if the standards are not available, the substrate was used. Standard solutions of 10, 20, 50, 100, 200, 500 and 1000 µM were prepared for HPLC analysis as per reaction samples. The area of the product and the internal standard peaks were measured using Shimadzu LabSolutions. A plot of product/internal standard area vs concentration of standard was made and the calibration factor was calculated to quantify the amount of product in the reaction sample.

Once the concentration of the product is known, the coupling efficiency (C) was calculated. The coupling efficiency is defined as the percentage of NADH that was used to oxidise the substrate and is given by the following equation:

$$\mathrm{C} = \frac{[\mathrm{Product}]}{[\mathrm{NADH}]} \times 100\% \tag{5.1}$$

The coupling efficiency can be used to calculate the product formation rate (PFR) from the NADH consumption rate (N, Section 5.2.3) using the following equation:

$$\mathrm{PFR} = \frac{\mathrm{C}}{100} \times \mathrm{N} \tag{5.2}$$

5.2.9 Protein X-ray Crystallography

Crystallisation experiments were performed with the F182L mutant of CYP199A4. Immediately prior to preparation of crystal trays, the protein was purified via elution through a HiPrep Sephacryl S-200 HR size-exclusion column (60 cm × 16 mm; GE Healthcare) with Buffer T at a flow rate of 1 mL min^{-1}. The purity of the protein was assessed based on the Reinheitszahl value, RZ = A_{420}/A_{280}, whereby fractions with RZ $\geq$ 2 were collected and combined.

The combined fractions were then concentrated via ultrafiltration using a Microsep Advance centrifugal device (10 kDa MWCO, Pall Corporation) to a concentration of approximately 30 – 35 mg mL^{-1}. Substrate was then added to a final concentration of 1 mM from a 100 mM stock of EtOH and DMSO to the concentrated protein. Crystallisation trays were prepared using the following optimised buffer conditions previously reported: 0.2 M magnesium acetate, 100 mM Bis-Tris buffer (adjusted with acetic acid to pH 5.0 - 5.75) and 20 - 32 % w/v polyethylene glycol (PEG) 3350.[157]

Protein crystallisation was achieved using the hanging-drop vapour diffusion method in 24-well trays. An equal volume of crystallisation buffer was mixed with hanging drops of 1.2 - 2 µL of protein and was equilibrated with a reservoir of the same buffer (500 µL) at 16 °C. Red plate-like crystals were obtained after half a day to one week. Single crystals were mounted onto Micromounts or Microloops (MiTeGen LLC, New York, USA). Mounted crystals were soaked and dragged in Parabar 10312 Oil (Paratone-N, Hampton Research, California, USA) before flash-frozen in liquid N_2.

X-ray diffraction data were obtained (360 images per crystal) at the Australian Synchrotron using beamlines MX1 or MX2[221,250] with exposure time of 1 s, oscillation angle of 1°, wavelength of 0.9537 Å and temperature of 100 K. Diffraction images were indexed and integrated using iMosfilm.[222] Aimless[223] from the CCP4 suite of programs[224] was used to carry out scaling, merging and R_{free} labelling (5 % of reflections, randomly selected). The phase was solved using Molecular Replacement in Phaser[225] using a high-resolution structure of WT CYP199A4 (1.54 Å, PDB: 5UVB) as the search model. The ligands and solvent molecules were removed from the search model prior to phasing to eliminate model bias. Weighted $2mF_o$-DF_c map and F_o-F_c difference map were obtained and used to rebuild the model in WinCoot and determine the substrate bound.[226] Structural refinements were carried out over multiple cycles using Phenix Refine, available in the Phenix suite of programs.[227] If the bound substrate was a racemic mixture, both enantiomers were modelled within the substrate binding site separately and underwent several cycles of refinement to determine the identity

of the bound enantiomer. If the conformation of the enantiomer was still unclear, the occupancies of both enantiomers were refined in the same location using different alternative conformation labels (altLoc identifiers) in the same PDB coordinates file.

Composite-omit or feature enhanced maps that reduce model bias were generated in Phenix to allow inspection of the ligand binding site and reveal the location of all substrate atoms.[228,229] Detailed data collection and structural refinement statistics are provided in Supplementary Data. The coordinates for the crystal structures were deposited in to the wwPDB (Worldwide Protein Data Bank).[251,252] PDB accession codes were presented where reported (Table D1).

5.3 Results

5.3.1 Reactions of WT CYP199A4 with 4-propionylbenzoic acid and 4-(2′-oxopropyl)-benzoic acids

The binding affinity (K_d) of 4-propionylbenzoic acid (9.1 µM) with WT CYP199A4 was tighter compared to 4-(2′-oxopropyl)-benzoic acid (80 µM).[248] However, the product formation rate was faster for the reaction of the latter with WT CYP199A4 (123 min^{-1} vs 29 min^{-1}, Table 5.2). This is largely a result of the higher coupling efficiency of NADH usage to product formation (83 %, Table 5.2). Both substrates bound less tightly and formed products significantly slower compared 4-*n*-propyl benzoic acid (K_d = 0.54 µM, PFR = 594 min^{-1}), which lacks the carbonyl ketone present in 4-propionylbenzoic acid and 4-(2′-oxopropyl)-benzoic acid (Table 5.2).

Table 5.2: Substrate binding and *in vitro* turnover data for WT CYP199A4 with 4-*n*-propyl benzoic acid and related carbonyl containing substrates. Rates are given as µmol.µmol$_{P450}^{-1}$.min^{-1}.

Substrate	% HS (%)	K_d (µM)[a]	N[b]	PFR[c]	Coupling[d]
4-*n*-propylbenzoic acid[220]	≥ 95	0.54 ± 0.02	688 ± 24	594 ± 72	86 ± 8
4-propionylbenzoic acid[e]	(420 nm)[f]	9.1 ± 0.4	282 ± 23	29 ± 7	20 ± 2
4-(2′-oxopropyl)-benzoic acid[e]	≥ 50	80 ± 3	151 ± 3	123 ± 10	83 ± 3

[a]Dissociation constant [b]NADH oxidation rate. [c]Product formation rate. [d]% of NADH consumed that led to metabolite formation. [e]Data for substrate binding and activity studies carried out previously by Dr Tom Coleman using WT CYP199A4 with 4-propionylbenzoic acid and 4-(2′-oxopropyl)-benzoic acid.[248] [f]A red-shift to 420 nm was observed.

WT CYP199A4 hydroxylates 4-propionyl- and 4-(2′-oxopropyl)-benzoic acid at the *para* position to form 4-(2′-hydroxypropanoyl)benzoic acid and 4-(1′-hydroxy-2′-oxopropyl)benzoic acid, respectively (Figure 5.3). These two products possess an α-hydroxyketone moiety at the *para*-position that should serve as a centre for C-C cleavage activity. We therefore assessed whether CYP199A4 is able to react further with these α-hydroxyketone compounds using different conditions. Firstly, excess NADH was used in oxidation reactions of WT CYP199A4 to fully convert both carbonyl containing substrates to the α-hydroxyketone metabolites (Figure 5.5).

WT CYP199A4 was successful in fully converting both carbonyl-containing substrates to the corresponding α-hydroxyketone metabolite when excess NADH was used (Figure 5.5). There were also low levels of possible further oxidation metabolites with both substrates. If WT CYP199A4 was capable of further catalysing a C-C cleavage re-

action on the α-hydroxyketone metabolites, terephthalic acid or 4-formylbenzoic acid would be generated as the final cleavage products (Figure 5.6).[94,99] The oxidation of 4-propionylbenzoic acid by WT CYP199A4 formed minor products (Figure 5.5a) that were not identified as either 4-formylbenzoic acid or terephthalic acid through co-elution experiments. The reaction with 4-(2′-oxopropyl)benzoic acid did show low amounts of a metabolite with the same retention time as terephthalic acid (Figure 5.5b).

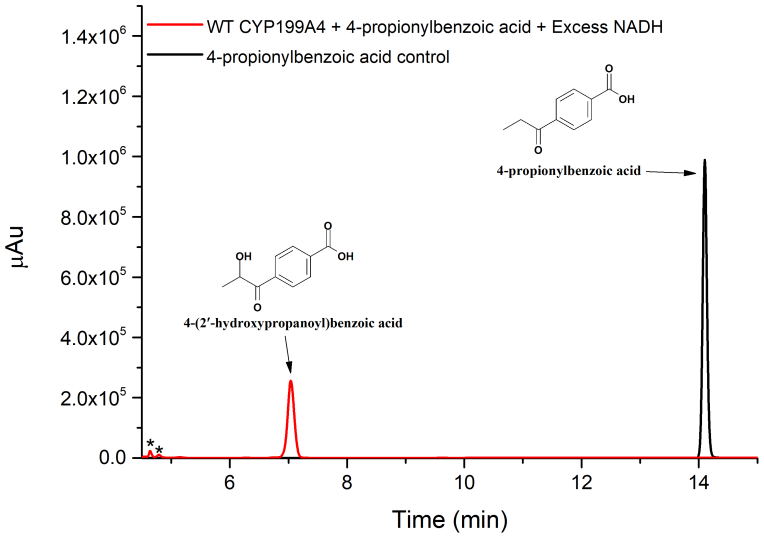

(a)

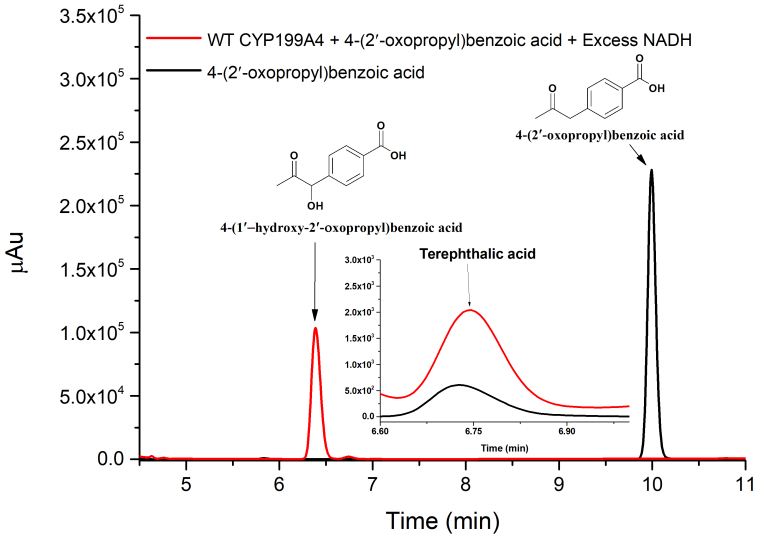

(b)

Figure 5.5: HPLC analysis of the *in vitro* oxidation reactions (red) of WT CYP199A4 with (a) 4-propionylbenzoic acid and (b) 4-(2′-oxopropyl)-benzoic acid with excess NADH (in red). Substrate controls are shown in black. The 4-propionylbenzoic acid reaction also had potential further oxidation products marked with " * ". The metabolites formed are 4-(2′-hydroxypropanoyl)benzoic acid (t_R = 7.1 min), 4-(1′-hydroxy-2′-oxopropyl)benzoic acid (t_R = 6.4 min) and terephthalic acid (t_R = 9.54 min).

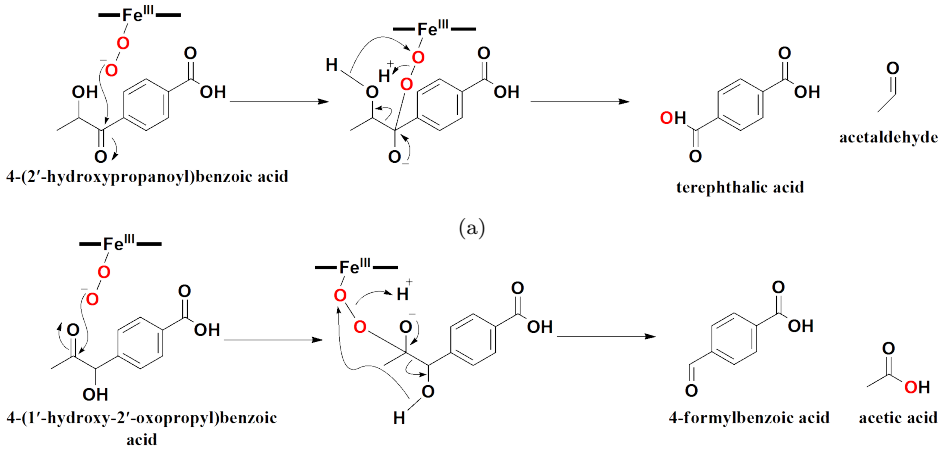

Figure 5.6: Proposed mechanism for P450 catalysed C-C bond cleavage of 4-(2′-hydroxypropanoyl)benzoic acid (a) and 4-(1′-hydroxy-2′-oxopropyl)benzoic acid (b). The reactions proceed via nucleophilic attack of the α-hydroxy carbonyl by the ferrix-peroxo intermediate of the P450. The proton (H^+) for this reaction is provided by surrounding water molecules.

5.3.2 Reactions of CYP199A4 with 4-(2′-hydroxypropanoyl)benzoic acid and 4-(1′-hydroxy-2′-oxopropyl)benzoic acid

The α-hydroxyketone compounds, 4-(2′-hydroxypropanoyl)benzoic acid and 4-(1′-hydroxy-2′-oxopropyl)benzoic acid were successfully generated through oxidation of the respective precursors by WT CYP199A4. Monooxygenase reactions with WT CYP199A4 driven by NADH were then carried out with these α-hydroxyketone metabolites to assess if P450 catalysed C-C cleavage activity can occur with these compounds. CYP199A4 has also been reported to function as a peroxygenase that uses H_2O_2 to catalyse enzymatic reactions.[156] Mutant T252E of CYP199A4 is an engineered variant with enhanced peroxygenase activity.[156] Reactions with the WT and T252E variants of CYP199A4 driven by H_2O_2 were performed with the α-hydroxyketone metabolites to determine if C-C cleavage reactions can arise from P450 peroxygenase activity. The peroxygenase and monooxygenase reactions were also carried out in the same pot as Section 5.3.1 with the original carbonyl starting material fully converted into the α-hydroxyketone metabolites. Control reactions of the α-hydroxyketone metabolites in H_2O_2 alone were also carried out.

The H_2O_2-driven peroxygenase reaction of WT CYP199A4 with 4-(2′-hydroxypropanoyl)benzoic acid showed a low level formation of terephthalic acid that is accompanied by a decrease in substrate levels (Figure 5.7). There was also the formation of other metabolites (indicated by " * ") that eluted at an early retention time (t_R = 4.6 min, 4.75 min and 5.25 min, Figure 5.7). The formation of terephthalic acid is consistent with C-C cleavage activity occurring with this α-hydroxyketone. The same reaction but with NADH generated a lower amount of terephthalic acid. This

NADH-driven reaction formed higher levels of the unknown metabolites (" * ", Figure 5.7). These unknown metabolites could be further oxidation products arising from P450-catalysed single or double hydroxylation events of the initial α-hydroxyketone.

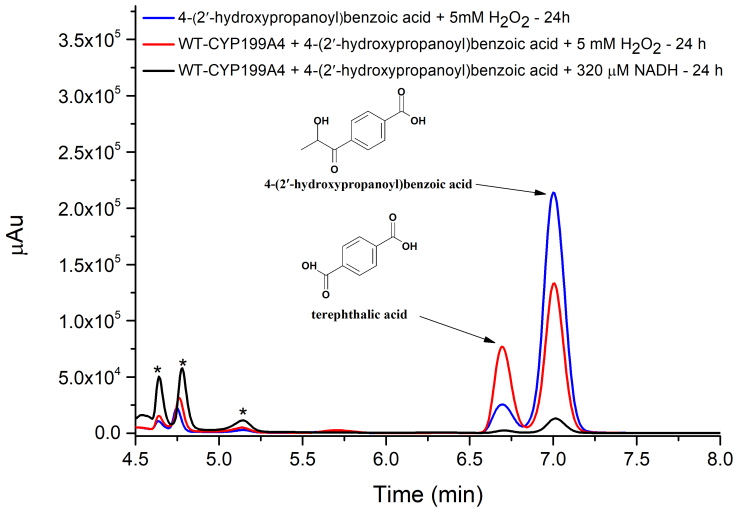

Figure 5.7: HPLC analysis of the *in vitro* oxidation reactions of WT CYP199A4 with 4-(2′-hydroxypropanoyl)benzoic acid (t_R = 7.1 min) using H_2O_2 (red) or NADH (black). Terephthalic acid (t_R = 6.76 min) was detected and confirmed with co-elution. Further oxidation metabolites (t_R = 4.6 min, 4.75 min and 5.25 min) is indicated by " * ". A control reaction of 4-(2′-hydroxypropanoyl)benzoic acid with H_2O_2 was shown (blue).

The H_2O_2-driven reaction of T252E-CYP199A4 with 4-(2′-hydroxypropanoyl)benzoic acid also formed terephthalic acid but at lower levels compared to WT CYP199A4 (Figure 5.8). A control reaction of 4-(2′-hydroxypropanoyl)benzoic acid with H_2O_2 also formed terephthalic acid but the amount formed was lower than what was observed with the WT and T252E variant (Figure 5.8). Overall, WT CYP199A4 generated the highest level of the C-C cleavage metabolite with the peroxygenase pathway.

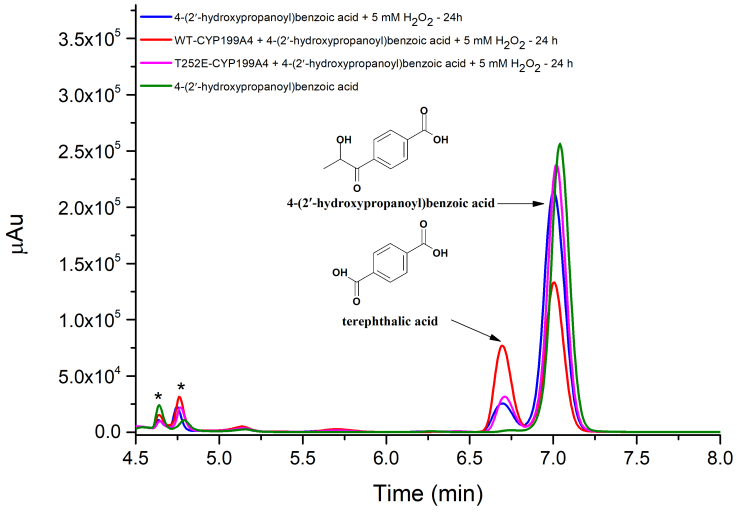

Figure 5.8: HPLC analysis of the *in vitro* oxidation reactions of WT (red) or T252E (magenta) CYP199A4 with 4-(2′-hydroxypropanoyl)benzoic acid (t_R = 7.1 min) with H_2O_2. A control reaction of 4-(2′-hydroxypropanoyl)benzoic acid with 5 mM H_2O_2 (blue) and the α-hydroxyketone control (green) is also shown. Terephthalic acid (t_R = 6.76 min) is present. Further oxidation metabolites is indicated by " * " (t_R = 4.6 min and 4.75 min).

The cleavage of 4-(1′-hydroxy-2′-oxopropyl)benzoic acid by a P450 should form 4-formylbenzoic acid (Figure 5.6b) as the initial product but the reactivity of the aldehyde moiety should make it susceptible to further oxidation to terephthalic acid. The peroxygenase reaction of 4-(1′-hydroxy-2′-oxopropyl)benzoic acid with WT CYP199A4 showed an increase in both terephthalic acid and 4-formylbenzoic acid while coupled with a decrease in substrate levels (Figure 5.9). A control reaction of 4-(1′-hydroxy-2′-oxopropyl)benzoic acid with H_2O_2 alone also formed terephthalic acid. The NADH-driven monooxygenase reaction of WT CYP199A4 with 4-(1′-hydroxy-2′-oxopropyl)benzoic acid formed lower levels of terephthalic acid compared to the H_2O_2 only control. Peroxygenase reactions of T252E-CYP199A4 with the same substrate also did not form higher levels of metabolites over the H_2O_2 only control (Figure D3). Low levels of further oxidation metabolites (" * ") were also observed with this substrate with both peroxygenase and monooxygenase reactions in the presence of WT CYP199A4.

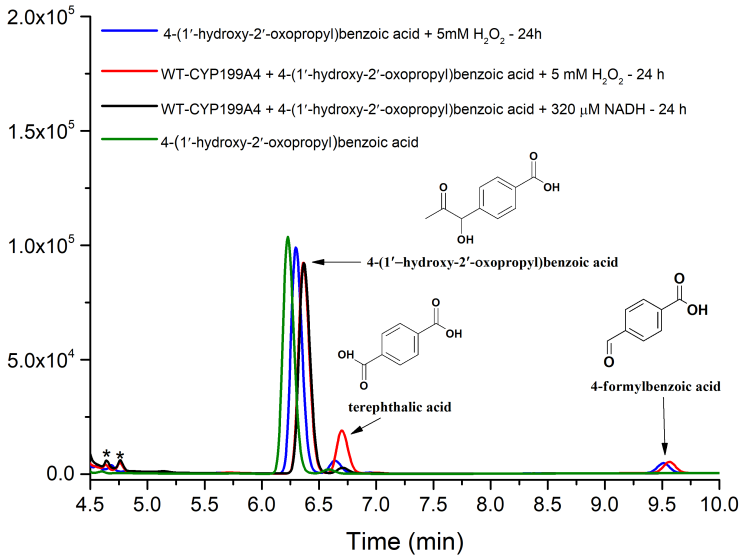

Figure 5.9: HPLC analysis of the *in vitro* oxidation reactions of WT CYP199A4 with 4-(1′-hydroxy-2′-oxopropyl)benzoic acid (t_R = 6.4 min). Reactions of WT CYP199A4 using H_2O_2 (red) or NADH (black). A control of 4-(1′-hydroxy-2′-oxopropyl)benzoic acid alone (green, offset in x-axis) and with 5 mM H_2O_2 (blue, offset in x-axis). Further oxidation metabolites is indicated by " * " (t_R = 4.6 min and 4.75 min). Terephthalic acid (t_R = 6.76 min) and 4-formylbenzoic acid (t_R = 9.54 min) were confirmed by co-elution experiments (Figure D2).

Overall, WT CYP199A4 seems to show higher activity towards C-C cleavage activity with α-hydroxyketones with reactions in the peroxygenase pathway. However, control reactions of both α-hydroxyketones with H_2O_2 generates the expected C-C cleavage metabolites that could arise from P450-catalysed activity. The decrease in substrate levels alongside the formation of other oxidation metabolites with reactions involving CYP199A4 does suggest that this P450 enzyme is able to oxidise these substrates but more conclusive evidence is desirable.

5.3.3 Substrate-Binding and Turnovers of WT/T252E CYP199A4 with JCM 1 and JCM 2

JCM 1 and JCM 2 are α-hydroxyketone compounds synthesised by Dr Justin Miller of the University of Illinois.[249] These two compounds are designed to resemble the 17-hydroxy steroids favoured by CYP17A1 in C-C cleavage reactions. In the position *para* to the benzoic acid moiety, JCM 1 has the hydroxy group α to the aromatic ring forming a chiral centre and the carbonyl group attached to the adjacent β carbon (Figure 5.10). JCM 2 has the positions of the carbonyl and hydroxy group switched in comparison. In comparison to the α-hydroxyketone compounds in Section 5.3.2, JCM 1 and JCM 2 contains an additional methyl group adjacent to the ketone moiety. It is expected that both JCM 1 and JCM 2 would be able to bind the active site of CYP199A4 and the *para* substituent would be oxidised. We predict that either C-C cleavage or hydroxylation would occur upon binding of JCM 1 and JCM 2 to CYP199A4. Reactions were carried out with both WT CYP199A4 and the T252E mutant.

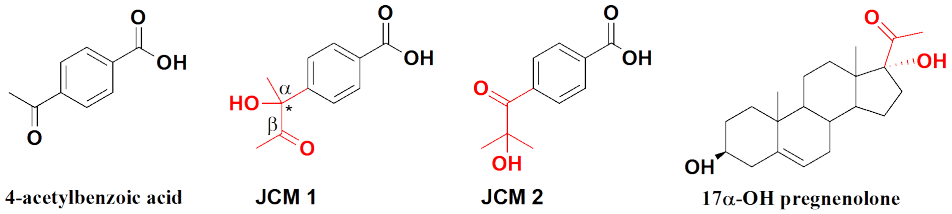

Figure 5.10: Structures of 4-acetylbenzoic acid, JCM 1, JCM 2 and 17α-OH pregnenolone. The α-hydroxyketone moieties for each substrate is highlighted in red. The chiral centre for JCM 1 is marked with " * ".

In addition, 4-acetylbenzoic acid was investigated as a control substrate, as it only has the ketone moiety but lacks the hydroxyl group. This could be used to further investigate the effects of polar groups at the *para* position on the binding and activity with CYP199A4 in comparison to other substrates such as 4-methoxybenzoic acid and the other α-hydroxyketone compounds in Section 5.3.2. Substrate binding and turnover data for 4-acetylbenzoic acid with WT CYP199A4 was collected by Rebecca Chao and is shown in Table 5.3.[253]

The addition of JCM 1 and JCM 2 to WT CYP199A4 induced a change in the UV-visible spectrum of the enzyme that corresponds to a ≤ 10 % high spin state (Table 5.3). The minimal spin-state shift observed with JCM 1 and JCM 2 could indicate that both substrates likely did not favour binding within the active site of WT CYP199A4 or, if binding did occur, it does not displace the distal heme-bound water. WT CYP199A4 upon addition of 4-acetylbenzoic acid only showed a small spectral red shift of ~ 1 nm from 418 nm but when difference spectra was measured it showed a typical Type I spectrum with a peak at ~ 390 nm and trough at ~ 420 nm (Figure D5).

Table 5.3: Binding and activity parameters determined for the carbonyl substrates investigated with CYP199A4. Shown are spin state shift analyses (% HS), Rates are µmol (µmolCYP)$^{-1}$ min^{-1} which is abbreviated to min^{-1} in the text. The data for 4-*n*-propylbenzoic acid with WT CYP199A4 are shown for comparison.[220]

Substrate	% HS[a]	N[b]	PFR[c]	Coupling[d]
JCM 1 - WT	< 5 %	185 ± 5	-[f]	-[f]
JCM 2 - WT	< 10 %	33 ± 4	-[f]	-[f]
4-acetylbenzoic acid[253]	~ 10[e]	407 ± 4	220 ± 12	49 ± 3
4-*n*-propylbenzoic acid[220]	≥ 95	688 ± 24	594 ± 72	86 ± 8

[a]% High-Spin state induced. [b]NADH oxidation rate. [c]Product formation rate. [d] % of NADH consumed that led to metabolite formation. [e] Red-shift of ~ 1 nm observed but Type I difference spectrum of 10 % was measured. [f] No product formation observed.

JCM 1 and JCM 2 were used as substrates for NADH-driven oxidation reactions with WT CYP199A4. Kinetic data for the oxidation of 4-*n*-propylbenzoic acid with WT CYP199A4 was used as a comparison as it possesses a carbon chain of the same length at the *para* position as JCM 1 and JCM 2 but lacks the polar functional groups. When JCM 1 was used as a substrate, it induced a NADH oxidation rate of 185 µmol (µmolCYP)$^{-1}$ min^{-1} (henceforth abbreviated as min^{-1}). With JCM 2, the rate was 33 min^{-1}. These NADH oxidation rates were slower than that of 4-acetylbenzoic acid[253] (407 min^{-1}, Table 5.3) and 4-*n*-propylbenzoic acid[220] (688 min^{-1}, Table 5.3).

It is expected that terephthalic acid would be formed from P450 catalysed C-C cleavage activity with JCM 2 (Figure 5.11). The NADH-driven reaction of WT CYP199A4 with JCM 2 formed low levels of terephthalic acid (Figure 5.12). This was confirmed via co-elution experiments with an authentic standard. However, 4-formylbenzoic acid was also detected as an impurity of the synthesised JCM 2 (Figure 5.12). This impurity could be oxidised to terephthalic acid. Further experiments were carried out to determine if terephthalic acid formation was enzyme catalysed (Figure 5.13). It was observed that terephthalic acid was formed when H_2O_2 alone was added to JCM 2 (Figure 5.13) and therefore its formation could not be conclusively be attributed to enzymatic activity.

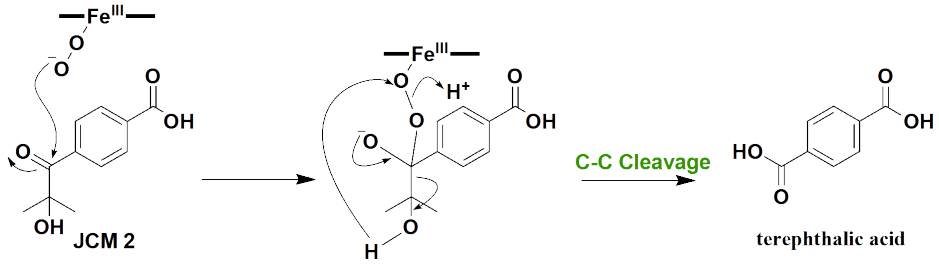

Figure 5.11: Possible reaction pathway of WT CYP199A4 with JCM 2 to form terephthalic acid through the ferric-peroxo intermediate and a Baeyer-Villiger rearrangement.

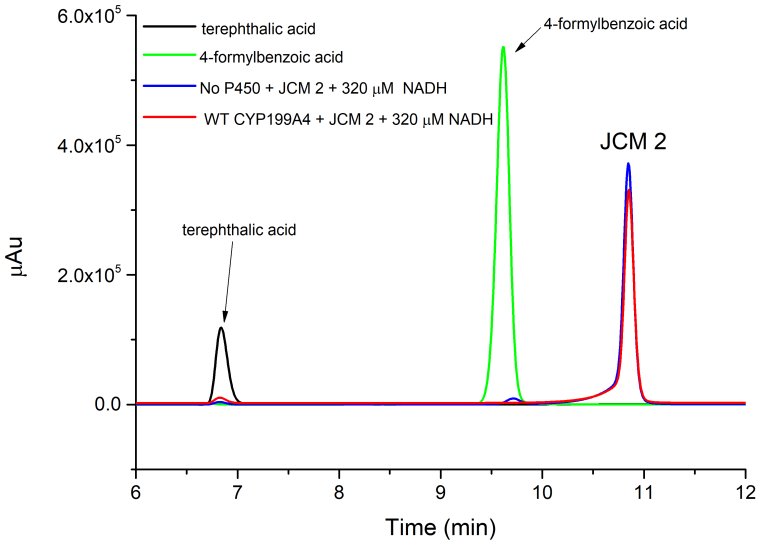

Figure 5.12: HPLC analysis of the reaction of WT CYP199A4 with JCM 2 (t_R = 10.9 min). The experimental turnover is shown in red and a no P450 control is shown in blue. Standards of 4-formylbenzoic acid (green, t_R = 9.5 min) and terephthalic acid (black, t_R= 6.8 min) are shown also. Terephthalic acid was detected in low amounts in the reaction with the P450.

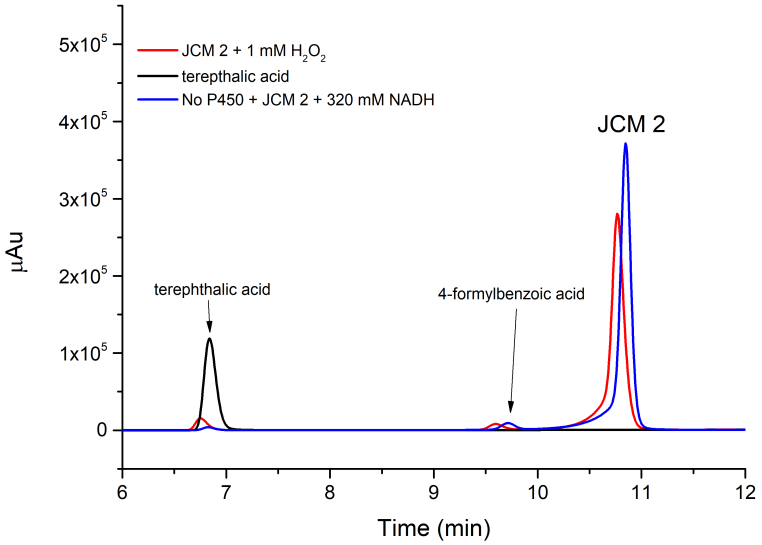

Figure 5.13: HPLC analysis of the reaction of JCM 2 (t_R = 10.9 min) in the presence of H_2O_2 (red) and a no P450 with NADH only control (blue). Terephthalic acid (t_R= 6.8 min) standard is shown in black. Other peaks detected include 4-formylbenzoic acid (t_R = 9.5 min). The reaction JCM 2 with H_2O_2 alone formed low levels of terephthalic acid.

The NADH oxidation reaction of WT CYP199A4 with the addition of JCM 1 showed the formation of one major metabolite (Figure 5.14a). This metabolite co-eluted with 4-(2′-hydroxyacetyl)benzoic acid which is the product generated from the hydroxylation of 4-acetylbenzoic acid by CYP199A4.[253] 4-Acetylbenzoic acid is the expected metabolite of C-C bond cleavage of JCM 1 (Figure 5.14b). Therefore, the formation of 4-(2′-hydroxyacetyl)benzoic acid may indicate C-C bond cleavage activity occurring first to form 4-acetylbenzoic acid, which was followed by a hydroxylation reaction. However, the as synthesised JCM 1 substrate contained low levels of 4-acetylbenzoic

acid as an impurity (Figure 5.14a). The presence of this impurity could give rise to the observed 4-(2′-hydroxyacetyl)benzoic acid.

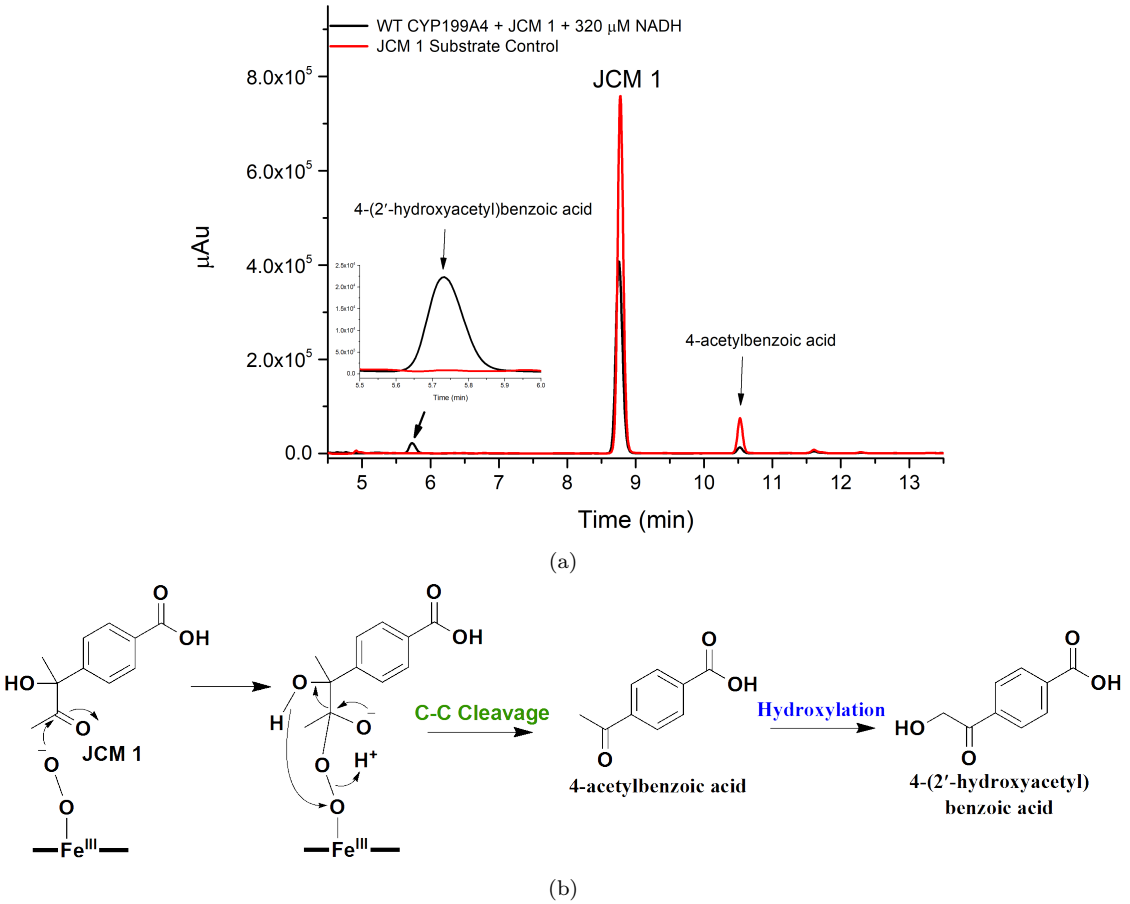

Figure 5.14: (a) HPLC analysis of the in vitro turnover of WT CYP199A4 (black) with JCM 1 (t_R = 8.8 min). A JCM 1 standard control is shown in red. (b) Possible reaction pathway for JCM 1 with CYP199A4. A P450 catalysed C-C cleavage reaction would generate 4-acetylbenzoic acid (t_R = 10.5 min) via a Baeyer-Villiger rearrangement and subsequent P450 hydroxylation would generate 4-(2′-hydroxyacetyl)benzoic acid (t_R = 5.8 min).

We next used a NADH regenerating system containing alcohol dehydrogenase (ADH) to oxidise JCM 1 using WT CYP199A4 (Figure 5.15).[254] This system was used to completely oxidise the 4-acetylbenzoic acid impurity after which JCM 1 could then be oxidised by the P450 using continuously regenerated NADH. A control reaction of with the same regenerating system was used to oxidise 4-acetylbenzoic acid with CYP199A4. HPLC analysis of the reaction between WT CYP199A4 and JCM 1 showed no decrease in the amount of this substrate (Figure 5.15a). The 4-acetylbenzoic acid impurity was fully oxidised to form 4-(2′-hydroxyacetyl)benzoic acid and other additional metabolites (Figure 5.15a). In the control reaction, 4-acetylbenzoic acid was also fully consumed by WT CYP199A4 to form the same hydroxylated product (Figure 5.15b).

HPLC analysis also identified terephthalic acid and two potential other/further oxidation products (“ $ ” and “ * ”, Figure 5.15b) were present in the oxidation of 4-acetylbenzoic by WT CYP199A4. Terephthalic acid could be a product of C-C cleavage

activity of 4-(2′-hydroxyacetyl)benzoic acid, as the latter contains an α-hydroxyketone moiety. Overall, there was no conclusive evidence of the oxidation JCM 1 by WT CYP199A4.

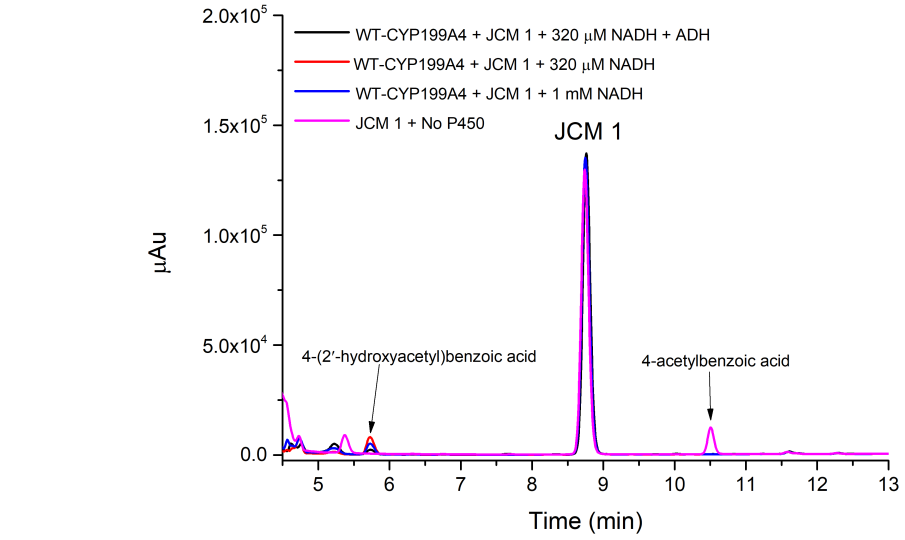

(a)

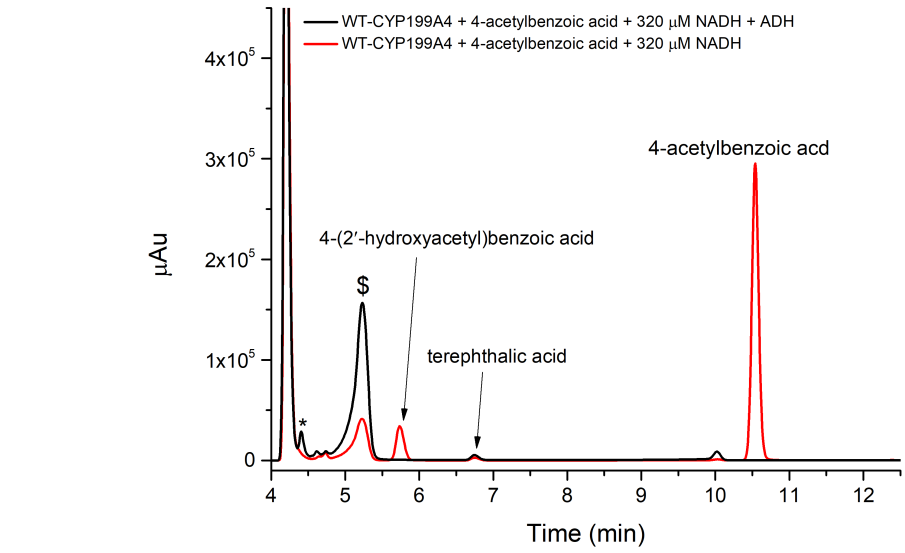

(b)

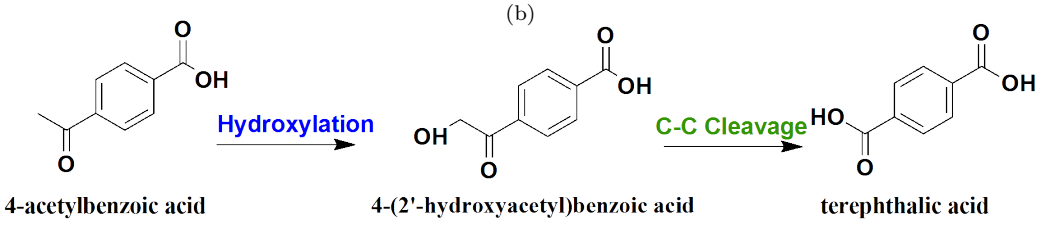

(c)

Figure 5.15: HPLC analysis of reactions using a NADH regenerating system with alcohol dehydrogenase (ADH) with WT CYP199A4 and JCM 1. In (a), JCM 1 (t_R = 9.8 min) is used as substrate and (b) 4-acetylbenzoic acid (t_R = 10.5 min) is used. The NADH regenerating system reaction is shown in black, no ADH control in red, excess NADH control in blue and no P450 control is shown in magenta. (c) Possible reaction pathway of WT CYP199A4 with 4-acetylbenzoic acid. Metabolites detected include terephthalic acid (t_R = 6.8 min) and 4-(2′-hydroxyacetyl)benzoic acid (t_R = 5.8 min).

To investigate if CYP199A4 could utilise peroxygenase activity to oxidise JCM 1, WT

CYP199A4 and it's engineered peroxygenase variant, T252E, was used in H_2O_2-driven reactions with JCM 1 as substrate. JCM 2 was not tested due to to its susceptibility to oxidation by H_2O_2 (Figure 5.13). Neither WT or T252E variant showed any apparent product formation with JCM 1 via the peroxygenase pathway (Figure 5.16a and Figure D6).

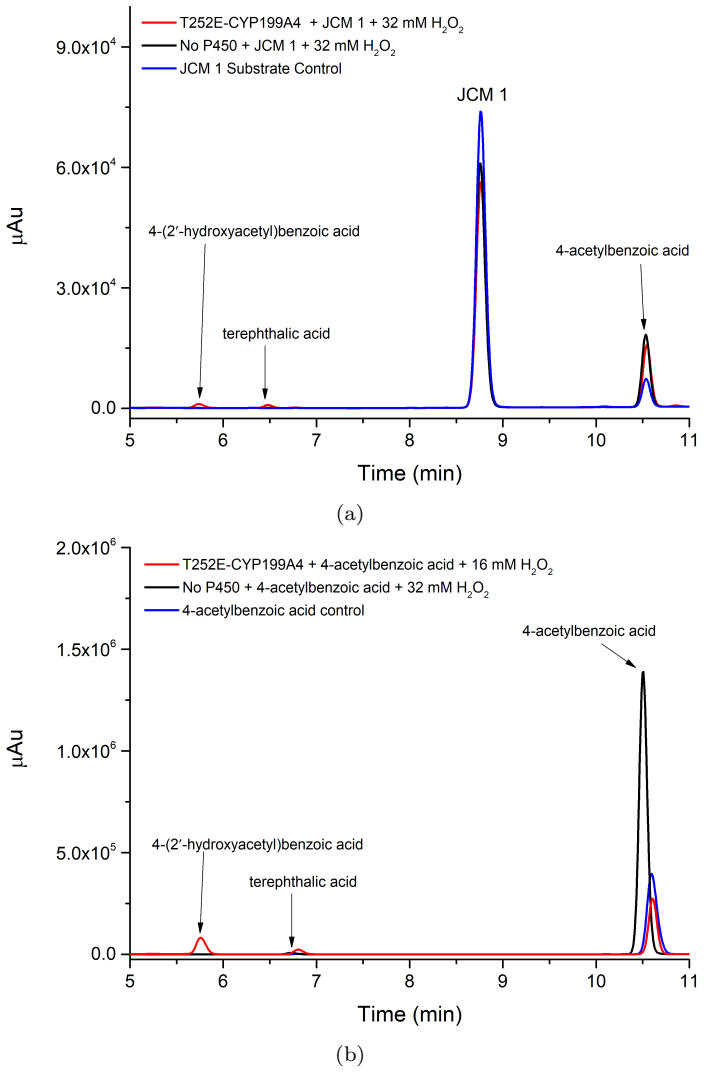

Figure 5.16: HPLC analysis of H_2O_2-driven reactions with T252E-CYP199A4 (red) with (a) JCM 1 (t_R = 9.8 min) and (b) 4-acetylbenzoic acid (t_R = 10.5 min). No P450 controls are shown in black and the substrate only controls in blue.

The T252E variant did show product formation with 4-acetylbenzoic acid in the presence of H_2O_2 (Figure 5.16). The metabolites formed from this reaction were 4-(2′-hydroxyacetyl)benzoic acid and terephthalic acid. The same impurity within the JCM 1 reaction was also consumed by the T252E variant (Figure 5.16a) to form the same metabolites. This was consistent with the reaction of WT CYP199A4 and 4-acetylbenzoic acid with the NADH regenerating system (Figure 5.15b). There was little or no formation of further oxidation products with these H_2O_2-driven reactions. It is important to note that JCM 1 is also stable in the presence of H_2O_2, showing no

apparent degradation products or decrease in JCM 1 levels (Figure 5.16a).

Further attempts to oxidise JCM 1 with WT CYP199A4 at a lower substrate concentration (50 µM) in the NADH regenerating system to mitigate the presence of 4-acetylbenzoic acid as an impurity were unsuccessful (Figure D7). The lack of a spin-state shift and a product formed for the reaction of JCM 1 with WT CYP199A4 infers the substrate does not bind in a suitable position for oxidation or C-C cleavage to occur.

5.3.4 F182L and F298V CYP199A4: Expression, Purification and Substrate Binding

WT CYP199A4 and various mutants of this P450 enzyme have been crystallised and their X-ray crystal structures determined. This provides a platform by which rational mutagenesis and protein engineering approaches could alter the binding orientation of JCM 1 and JCM 2 to enable their oxidation. The structures of the active sites of WT CYP199A4 and T252E-CYP199A4 are shown in Figure 5.17.

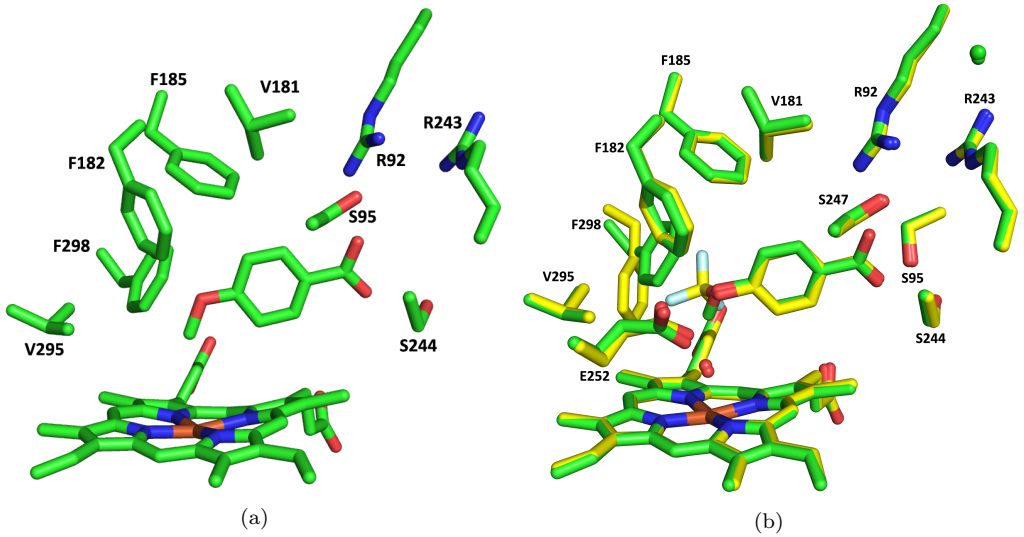

Figure 5.17: a) The crystal structure of the heme and the active site of WT CYP199A4 with 4-methoxybenzoic acid bound to the active site (PDB: 4DO1).[137] (b) Crystal structures of T252E-CYP199A4 bound to 4-trifluoromethoxybenzoic acid (8D1C, yellow sticks) and 4-methoxybenzoic acid (7REH, green sticks).[181]

The active site structures of the CYP199A4 enzymes, shows that the substrate is in close proximity to residues F182 and F298. The presence of a *para* substituent with greater steric bulk such as trifluoromethoxy causes the F298 residue to rotate away from the active site to accommodate the extra bulk (Figure 5.17b). It is therefore hypothesised that mutations at F182 and F298 that introduce a smaller amino acid (Val or Leu) at these positions could enhance the binding of substrates with greater steric bulk at the *para* position.

Two mutants of CYP199A4, F182L and F298V, were thus produced and purified in *E.coli* using previously established methods.[155,156] Substrate-binding studies were conducted with these two mutants with JCM 1 and JCM 2. The addition of JCM 1 to F182L-CYP199A4 caused a shift from 419 nm to ∼400 nm consistent with a 60 % conversion from low spin to high spin of a ferric species (Figure 5.18a). The UV-visible difference spectrum with the same conditions confirmed a Type I spectrum for F182L-CYP199A4 after the addition of JCM 1 (Figure 5.18b). A Type I spectrum shows that the heme-bound water ligand is displaced on binding of JCM 1 into the active site of F182L-CYP199A4. This demonstrates that the substrate is binding in the active site close to the heme.

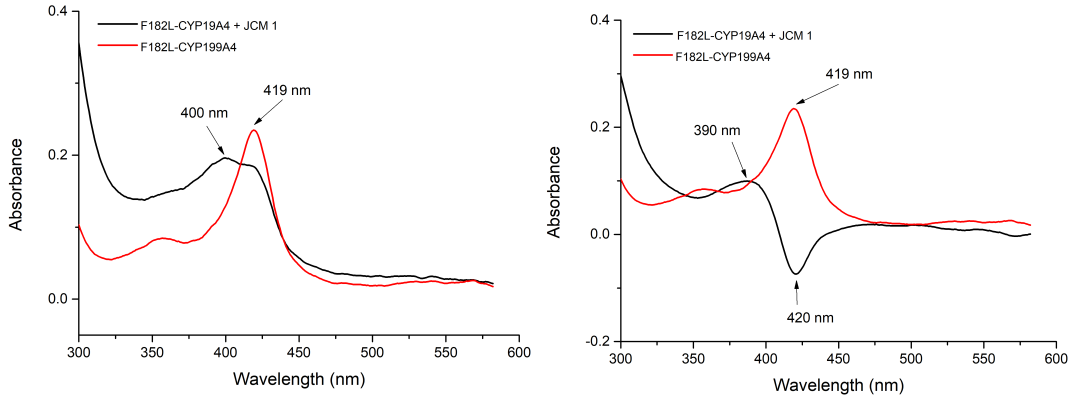

Figure 5.18: (a) Spin-state shift analysis of F182L-CYP199A4 with JCM 1. (b) Difference spectra of F182L-CYP199A4 with JCM 1. A shift to high spin (≈ 60 %) was observed upon addition of JCM 1. The substrate-free form is shown in red and the substrate-bound form in black.

The addition of JCM 2 to F182L-CYP199A4 also induced a Type I shift but this was smaller (≈ 25 %) than that of JCM 1 (Figure 5.19). This indicates that JCM 2 displaces a smaller proportion of the heme-bound water compared to JCM 1.

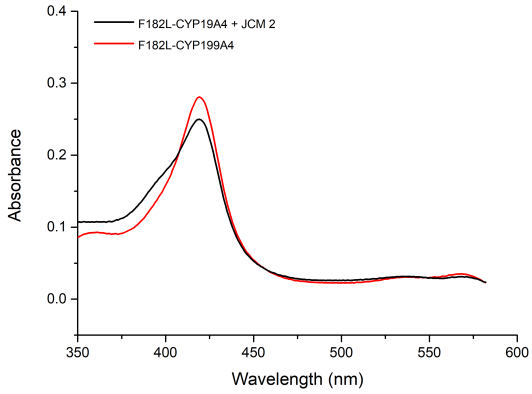

Figure 5.19: Spin-state shift analysis of F182L-CYP199A4 and JCM 2. The substrate-free form is shown in red and the substrate-bound form in black.

UV-visible analysis of F298V-CYP199A4 after the addition of JCM 1 displayed a small red-shift of the Soret band from 419 nm to 420 nm (Figure 5.20a). The difference spec-

trum for the F298V mutant and JCM 1 showed that a Type II spectrum was induced by JCM 1 (Figure 5.20b). Type II spectra are often a characteristic of compounds containing a stronger field donor atom, such as an oxygen atom. JCM 2 has a terminal oxygen atom that could interact with heme-bound water and stabilise the low spin complex.[49] The addition of JCM 2 to F298V-CYP199A4 induced only a small change in spin-state (< 5 %, Figure D8).

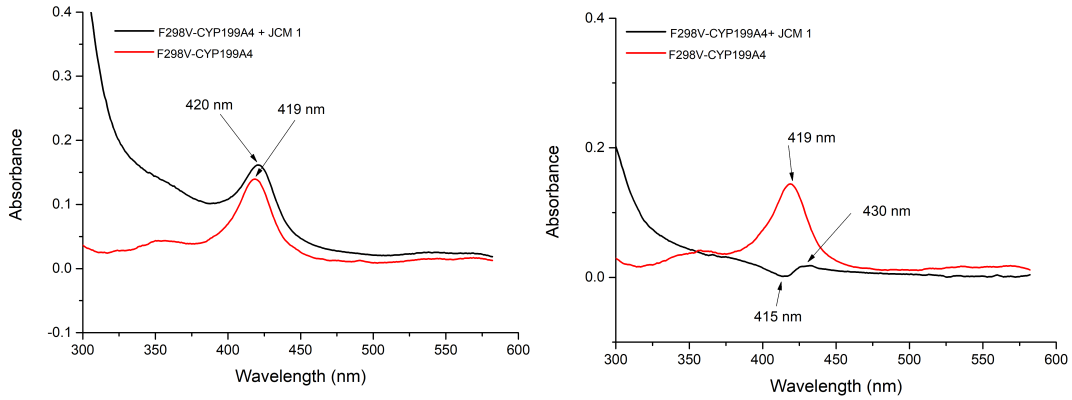

(a) (b)

Figure 5.20: (a) UV-visible analysis of F298V-CYP199A4 before and after addition of JCM 1. (b) Difference spectrum of F298V-CYP199A4 with JCM 1. It is observed that a small type II shift occurred upon addition of JCM 1. The substrate-free form is shown in red and the substrate-bound form in black.

UV-visible spectroscopy showed 4-acetylbenzoic acid induced a high-spin state of 80 % (Figure 5.21) with the F182L mutant. This is in contrast with WT CYP199A4 (Figure D5) that undergoes a small red-shift after addition of this substrate.[253] Both the F182L variant and WT enzyme show a Type I difference spectrum with 4-acetylbenzoic acid but the greater spin-state shift for the F182L variant shows that it can better displace the heme-bound water (Figure 5.21 and D5). Variant F298V-CYP199A4 showed a change in spin-state of < 5 % with 4-acetylbenzoic acid (Figure D8).

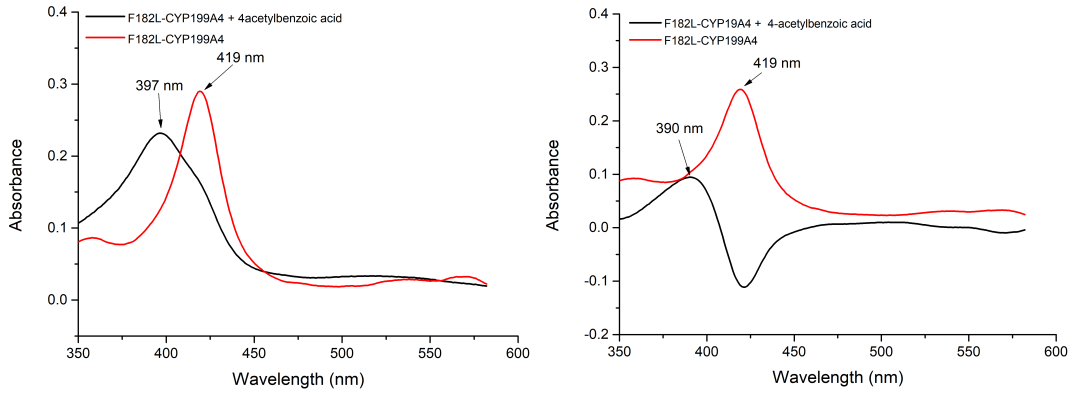

(a) (b)

Figure 5.21: (a) UV-visible analysis of F182L-CYP199A4 with 4-acetylbenzoic acid. (b) Difference spectra of F182L-CYP199A4 with 4-acetylbenzoic acid. The substrate-free form is shown in black, and the substrate-bound form in red.

Overall, JCM 2 seems to bind to the F182L and F298V mutant in a manner which is less likely to yield a productive turnover of the catalytic cycle compared to JCM 1. The F182L mutant seems more likely to show greater enzyme activity with JCM 1 over F298V given the higher spin-state shift (Table 5.4).

Table 5.4: Spin-state shift data (HS) for F182L and F298V mutants of CYP199A4 with various carbonyl containing substrates.

CYP199A4 Mutant	Substrate	% HS
F182L	JCM 1	60
	JCM 2	25
	4-acetylbenzoic acid	≈ 80
F298V	JCM 1	red-shift
	JCM 2	< 5

5.3.5 Reactions of JCM 1 and JCM 2 with F182L and F298V CYP199A4

NADH-driven oxidation reactions were carried out with the F182L and F298V mutants using JCM 1 and JCM 2 as substrates. The NADH oxidation rate measured for the reaction of JCM 2 with the F182L mutant was fast at a rate of 1423 min^{-1} (Figure D9). HPLC analysis of this reaction showed that two possible metabolites were formed (Figure 5.22). One metabolite was an unknown (" # " , $t_R = 6.3$ min) and the other co-eluted with terephthalic acid ($t_R = 6.8$ min) as was observed with the WT reactions (Figure 5.12). However, terephthalic acid was also present in a control reaction with no P450 enzyme (Figure 5.22).

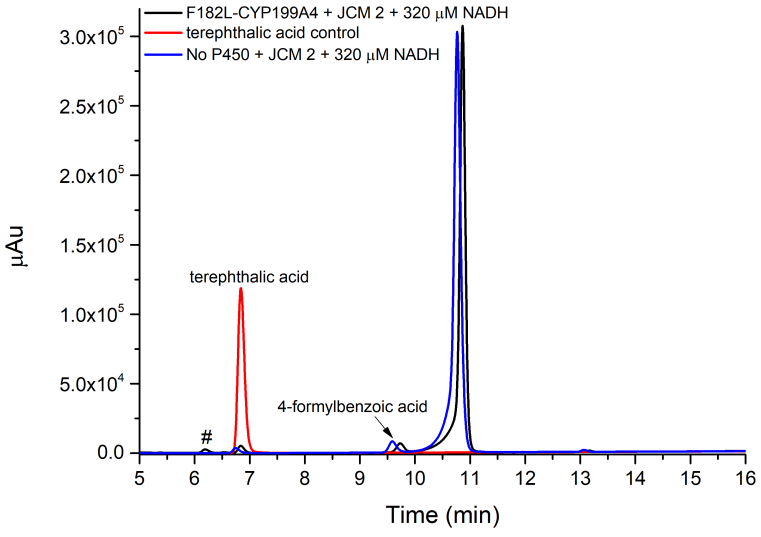

Figure 5.22: HPLC analysis of the NADH oxidation reaction of F182L-CYP199A4 with JCM 2 (black, $t_R = 10.9$ min). Terephthalic acid control (red, $t_R = 6.8$ min) and a control containing no P450 (blue) is shown also. There is an additional metabolite peak as indicated by " # " ($t_R = 6.3$ min).

Experiments were carried out to further investigate if the terephthalic acid formed arose from enzymatic activity using NADH and H_2O_2-driven reactions (Figure 5.23 and D10) with F182L-CYP199A4. Formation of terephthalic acid occurred when H_2O_2 was added to JCM 2 with or without P450 enzyme (Figure D10). The unknown metabolite, " # " was however confirmed to be arising from P450 enzymatic activity (Figure 5.23). This metabolite does not co-elute with any likely C-C bond cleavage metabolite of JCM 2 and likely arises from hydroxylation. Given the susceptibility of JCM 2 towards reacting with H_2O_2, further experiments were focused on JCM 1 as the model substrate for P450 C-C cleavage reactions.

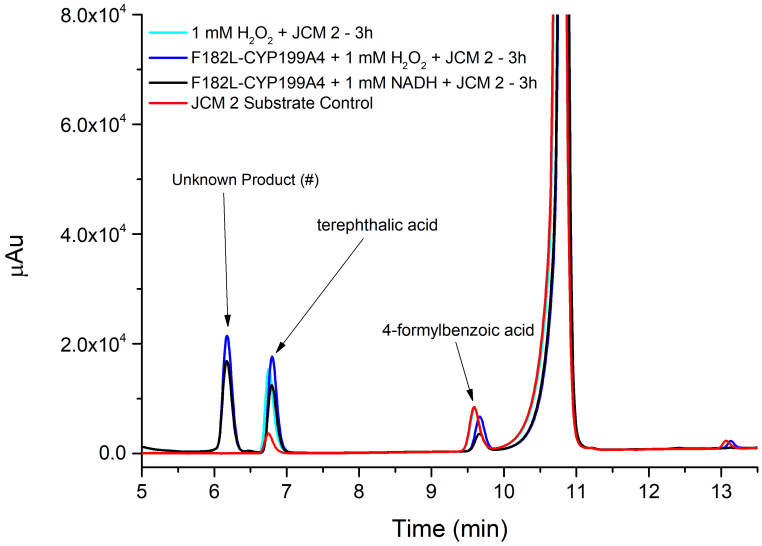

Figure 5.23: HPLC analysis of the reactions F182L-CYP199A4 with JCM 2 (t_R = 10.9 min) with NADH (black) or H_2O_2 (blue). A control reaction of JCM 2 with H_2O_2 only is shown (cyan). JCM 2 standard control is shown in red. Other peaks detected include terephthalic acid (t_R = 6.8 min), unknown product " # " (t_R = 6.3 min) and 4-formylbenzoic acid (t_R = 10.5 min).

The NADH oxidation rate measured for F182L-CYP199A4 catalysed oxidation of JCM 1 was only 68 min^{-1} (Figure D11) which was slower than the rate measured for WT CYP199A4 and JCM 1 (185 min^{-1}, Table 5.3), despite the higher spin-state shift induced by JCM 1 with the F182L mutant (60 %, Table 5.4).

Reactions carried out with the NADH regenerating system using the F182L mutant and JCM 1 as a substrate showed increased formation of 4-(2′-hydroxyacetyl)benzoic acid over WT CYP199A4 (Figure 5.15a) and more importantly this was coupled with an observable decrease in JCM 1 substrate levels (Figure 5.24). This was accompanied by the formation of unknown metabolites denoted by " * " (t_R = 4.4 min), " # " (t_R = 4.6 min), " $ " (t_R = 5.3 min) and " & " (t_R = 6.1 min) alongside terephthalic acid (t_R = 6.8 min). Mutant F298V of CYP199A4 was also tested using the NADH regenerating system with JCM 1. The F298V mutant also showed a decrease in JCM 1 substrate levels and formation of 4-(2′-hydroxyacetyl)benzoic acid but the level of

product formation for this mutant was significantly lower than the F182L mutant (Figure 5.24).

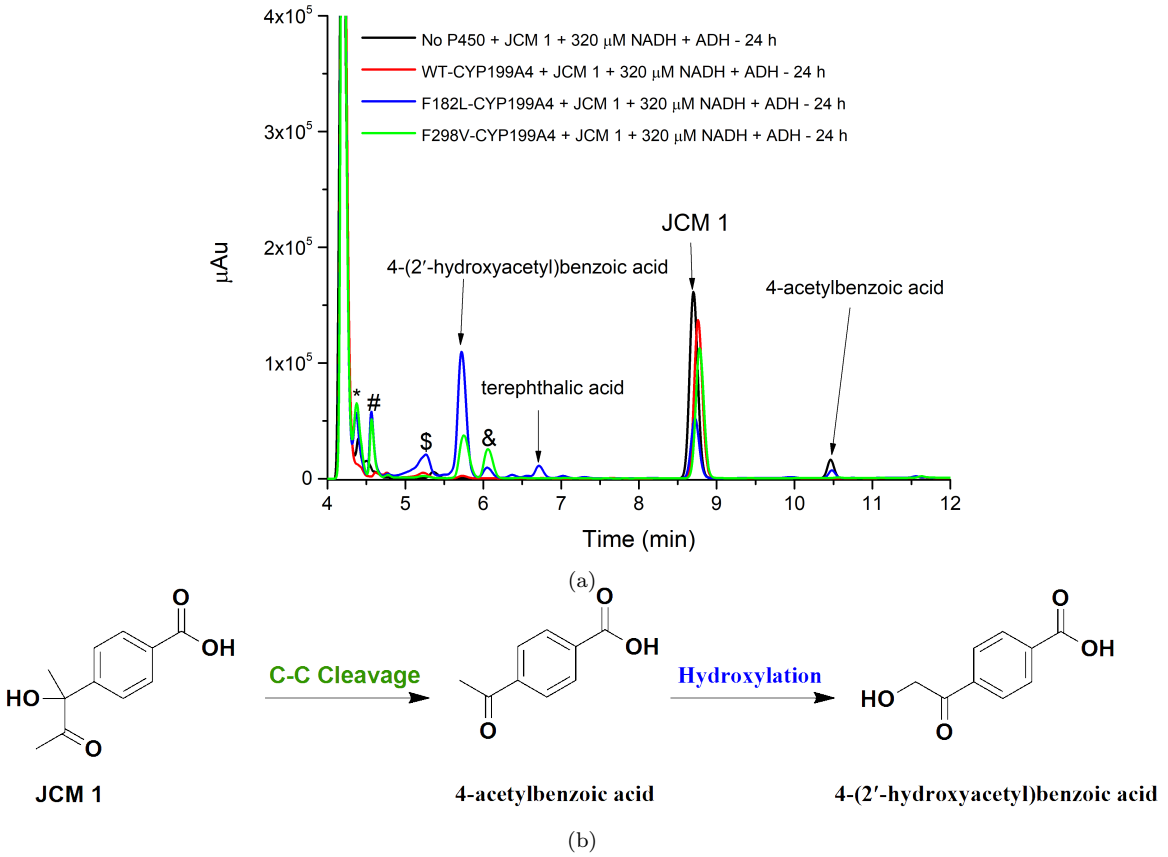

Figure 5.24: (a) HPLC analysis of the oxidation reaction of F182L (blue) and F298V (green) mutants of CYP199A4 with JCM 1 (t_R = 8.9 min) using the NADH regenerating system (ADH). The same reaction with WT CYP199A4 is also shown (red). A no P450 enzyme control is shown in black. Peaks detected include 4-(2′-hydroxyacetyl)benzoic acid (t_R = 5.8 min), terephthalic acid (t_R = 6.8 min), 4-acetylbenzoic acid (t_R = 10.5 min) and unknown metabolites: " $ " (t_R = 5.3 min), " # " (t_R = 4.6 min), " * " (t_R = 4.4 min) and " & " (t_R = 6.1 min). (b) Reaction pathway for JCM 1 with F182L-CYP199A4. JCM 1 first undergoes C-C cleavage to form 4-acetylbenzoic acid and subsequent P450 hydroxylation forms 4-(2′-hydroxyacetyl)benzoic acid.

To eliminate the possibility of the 4-acetylbenzoic acid impurity in JCM 1 is giving rise to the metabolites observed, a further synthesis and purification of JCM 1 was carried out by Dr Justin Miller to yield JCM1 in 99+ % purity. This purified JCM 1 was used in NADH oxidation reactions with mutant F182L (Figure D12). The metabolite profile of purified JCM 1 with F182L-CYP199A4 was similar to what was observed previously in Figure 5.24.

Based on these results, it is likely JCM 1 is undergoing P450 catalysed C-C bond cleavage to form 4-acetylbenzoic acid. 4-Acetylbenzoic acid is then hydroxylated further to form 4-(2′-hydroxyacetyl)benzoic acid (Figure 5.24b). The source of the further oxidation products and terephthalic acid could arise from a separate oxidation pathway of either JCM 1 or 4-(2′-hydroxyacetyl)benzoic acid. To assess this, oxidation reactions

were carried out with the F182L and F298V mutants using 4-acetylbenzoic acid as substrate with the NADH regenerating system (Figure 5.25).

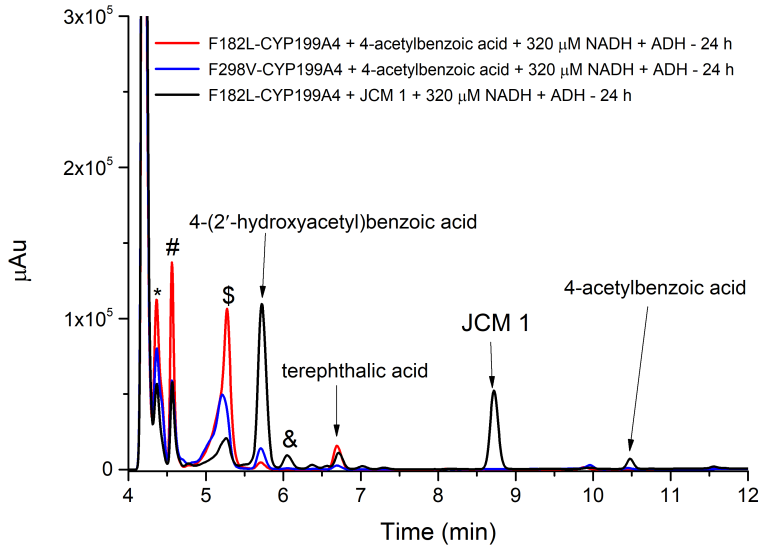

Figure 5.25: HPLC analysis of the oxidation reaction of F182L (red) and F298V (blue) mutants of CYP199A4 with 4-acetylbenzoic acid (t_R = 10.5 min) using the NADH regenerating system (ADH). For comparison, the same reaction of F182L-CYP199A4 with JCM 1 (t_R = 8.9 min) is shown also (black). Peaks detected include 4-(2′-hydroxyacetyl)benzoic acid (t_R = 5.8 min), terephthalic acid (6.8 min), and unknown metabolites: " $ " (t_R = 5.3 min), " # " (t_R = 4.6 min), " * " (t_R = 4.4 min) and " & " (t_R = 6.1 min).

In comparison to JCM 1, 4-acetylbenzoic acid is fully oxidised as a substrate with both F182L and F298V variants forming 4-(2′-hydroxyacetyl)benzoic acid (Figure 5.25). However, the levels of this metabolite were low and the formation of unknown oxidation metabolites (" *, # and $ ") and terephthalic acid was notably higher with 4-acetylbenzoic acid as substrate compared to JCM 1 (Figure 5.25). These metabolites and terephthalic acid are likely arising from the oxidation of 4-(2′-hydroxyacetyl)benzoic acid rather than the direct oxidation of JCM 1. Terephthalic acid could be formed from C-C bond cleavage of 4-(2′-hydroxyacetyl)benzoic acid. One unknown metabolite denoted by " & " (t_R = 6.1 min) in the reaction between the F182L mutant with JCM 1 (Figure 5.24) was not present in the reaction of 4-acetylbenzoic acid with the same mutant (Figure 5.25).

The NADH oxidation rate of F182L-CYP199A4 with 4-acetylbenzoic acid was 488 min^{-1} with product formation occurring at a rate of 414 min^{-1} and a coupling efficiency of 85 %. The product formation rate for JCM 1 with the F182L mutant was 1.3 min^{-1} with a coupling efficiency of 1.9 % that is, significantly lower than that of the 4-acetylbenzoic acid reaction.

GC-MS analysis of the JCM 1 reaction (Figure D13) with the F182L mutant allowed one of the metabolites (" & ") to be assigned as a potential hydroxylation product

of JCM 1 (Figure D14). Peaks matching the mass of the substrate and the major product, 4-(2′-hydroxyacetyl)benzoic acid were also identified (Figure D14). One further oxidation metabolite (“ $ ”) was successfully identified as a glyoxal compound, 4-(2′-oxoacetyl)benzoic acid (Figure 5.26) through HPLC co-elution experiments with a synthesised standard from Dr Isobella Stone, University of Adelaide (Figure D15).[255] This glyoxal compound could potentially be a precursor to terephthalic acid also (Figure 5.26).

Overall, F182L/F298V-CYP199A4 seem to be catalysing C-C bond cleavage of JCM 1 to form 4-acetylbenzoic acid (Figure 5.26). The P450 has higher affinity and oxidation activity for 4-acetylbenzoic acid over JCM 1 and it is preferentially oxidised when formed. Thus, the accumulation of 4-acetylbenzoic acid is not observed in downstream analysis. 4-Acetylbenzoic acid is hydroxylated to form 4-(2′-hydroxyacetyl)benzoic acid (Figure 5.26). The hydroxy product could undergo further oxidation to form a glyoxal product, 4-(2′-oxoacetyl)benzoic acid (“ $ ”). This glyoxal and the hydroxy precursor could then undergo further C-C cleavage activity to form terephthalic acid (Figure 5.26).

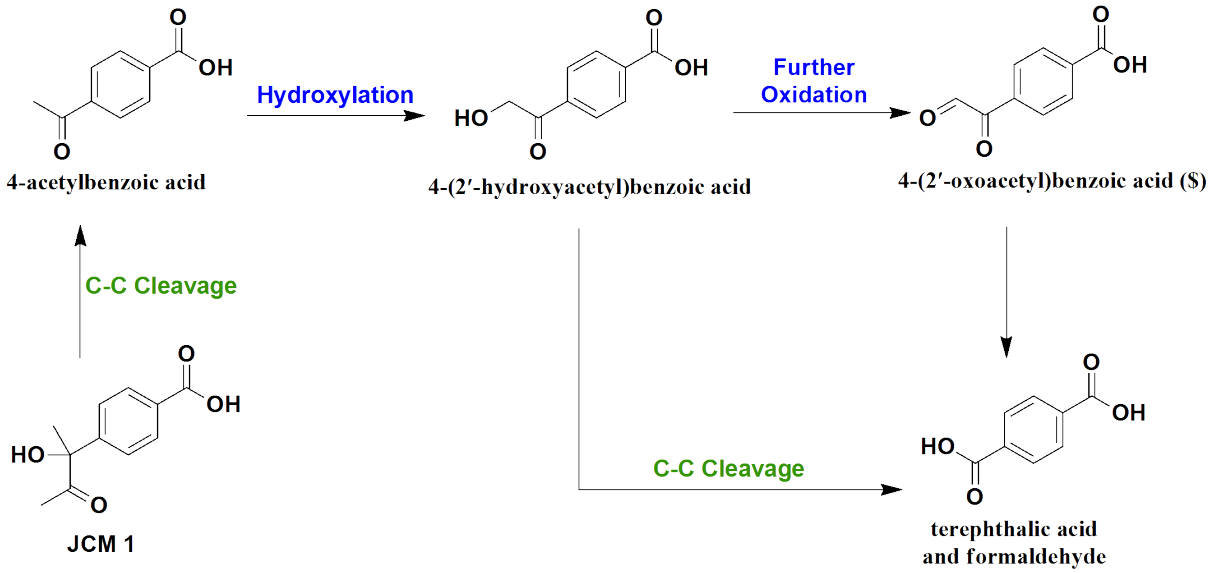

Figure 5.26: Possible reaction pathways of JCM 1 with F182L-CYP199A4.

5.3.6 Further Studies of C-C Cleavage Reactions with F182L-CYP199A4

Encouraged by the activity of F182L-CYP199A4 in the oxidation of JCM 1 using the NADH regenerating system, we decided to use this mutant to study C-C cleavage reactions with the α-hydroxycarbonyl substrates oxidised from 4-propionylbenzoic acid and 4-(2′-oxopropyl)-benzoic acid (Section 5.3.1). WT CYP199A4 was used again to convert 4-propionylbenzoic acid and 4-(2′-oxopropyl)-benzoic acid to their respective α-

hydroxyketone compounds (Section 5.3.2). Reactions were then carried out in the same pot with the α-hydroxyketone compounds using F182L-CYP199A4 and the NADH regenerating system (Figure 5.27 and 5.28).

The reaction of F182L-CYP199A4 with 4-(2′-hydroxypropanoyl)benzoic acid and 4-(1′-hydroxy-2′-oxopropyl)benzoic acid with the NADH regenerating system showed both α-hydroxyketones were fully consumed (Figure 5.27 and 5.28). With the reaction between 4-(2′-hydroxypropanoyl)benzoic acid and the F182L mutant, terephthalic acid was the major product formed and is the predicted product for the C-C cleavage reaction with this α-hydroxyketone (Figure 5.27b). This reaction also showed the presence of further oxidation metabolites (" * ", Figure 5.27a).

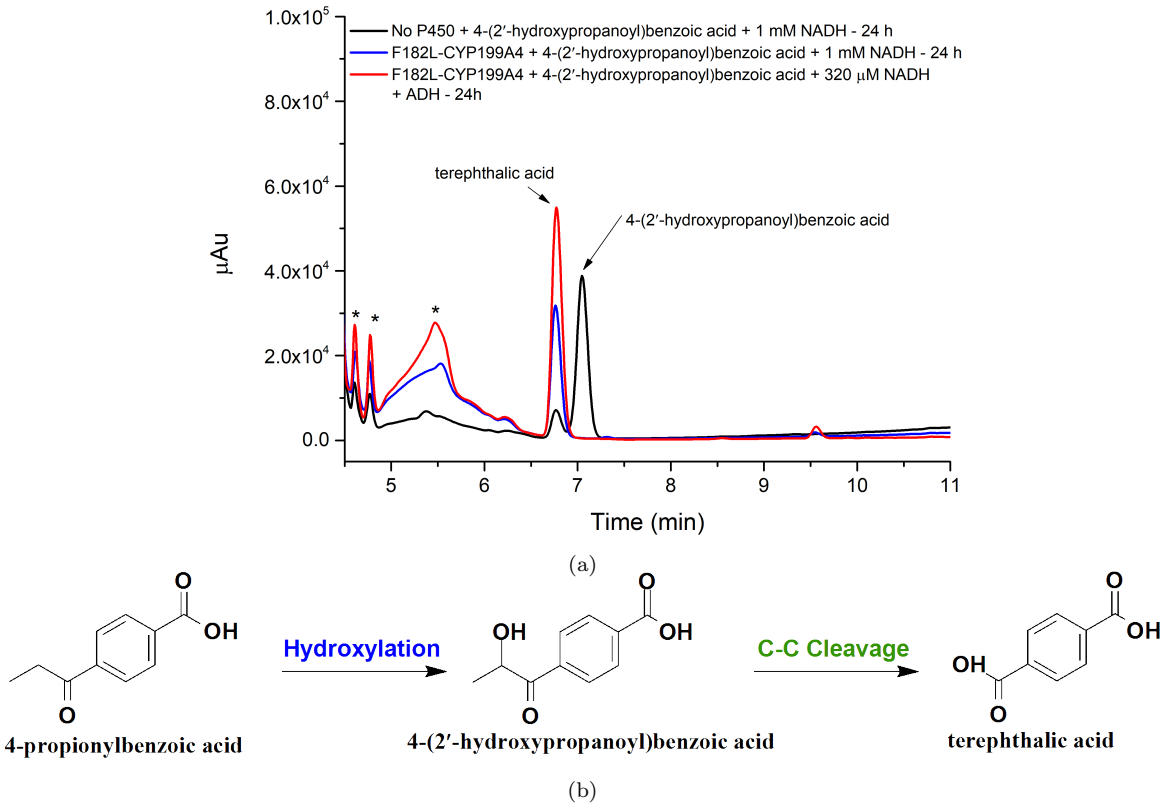

Figure 5.27: (a) HPLC analysis of the oxidation reaction of F182L-CYP199A4 with 4-(2′-hydroxypropanoyl)benzoic acid (t_r = 7.1 min) using the NADH regenerating system (ADH, red). Controls shown include the same reaction with no NADH regenerating system (blue) and a no P450 control (black). Possible further oxidation products are shown as " * ". Terephthalic acid was detected (t_r = 6.8 min) (b) Reaction pathway for P450-catalysed hydroxylation of 4-propionylbenzoic acid to form 4-(2′-hydroxypropanoyl)benzoic acid and followed by C-C cleavage to form terephthalic acid.

The expected C-C cleavage product for 4-(1′-hydroxy-2′-oxopropyl)benzoic acid is 4-formylbenzoic acid (Figure 5.28b). However, in the reaction between the F182L mutant and 4-(1′-hydroxy-2′-oxopropyl)benzoic acid, the detected levels 4-formylbenzoic acid were low (Figure 5.28a). It is likely the F182L mutant can oxidise any 4-formylbenzoic acid formed to terephthalic acid. The oxidation reaction of WT CYP199A4 with 4-formylbenzoic acid was previously reported by Rebecca Chao to form terephthalic

acid (Figure D16).[253] Further oxidation metabolites (" * ") were also present for this reaction.

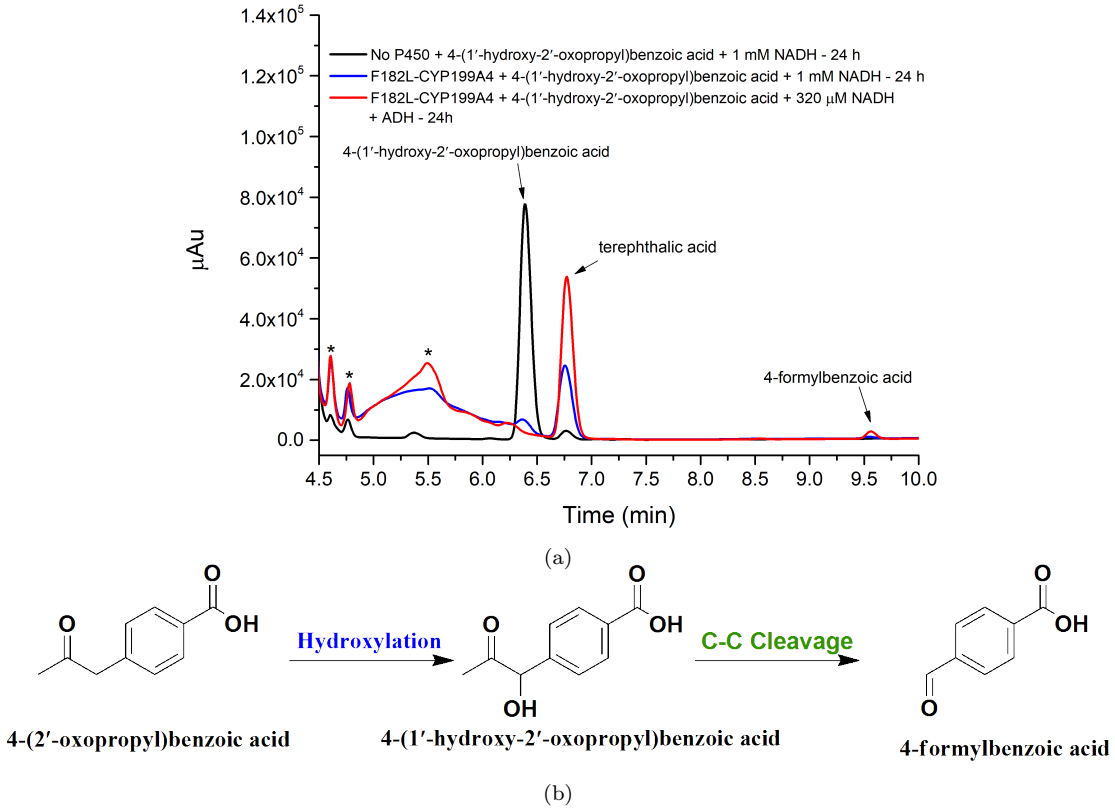

Figure 5.28: (a) HPLC analysis of the oxidation reaction between F182L-CYP199A4 and 4-(1′-hydroxy-2′-oxopropyl)benzoic acid (t_r = 6.8 min) with the NADH regenerating system. Possible further oxidation products are indicated by " * ". Metabolites detected include 4-formylbenzoic acid (t_r = 9.54 min) and terephthalic acid (t_r = 6.76 min). (b) Reaction pathway for P450 catalysed hydroxylation of 4-(2′-oxopropyl)-benzoic acid to form 4-(1′-hydroxy-2′-oxopropyl)benzoic acid and followed by C-C cleavage to form 4-formylbenzoic acid. 4-Formylbenzoic acid is susceptible to oxidation to terephthalic acid by the P450 (Figure D16).

We wish to also investigate whether the F182L mutant of CYP199A4 was capable of acting as a peroxygenase to catalyse C-C cleavage of JCM 1 using H_2O_2. JCM 1 has demonstrated high stability towards H_2O_2 but JCM 2 was not tested due to its instability towards the oxidant. Reactions of F182L-CYP199A4 with JCM 1 in the presence of H_2O_2 were carried out. A NADH-driven reaction also performed as a control (Figure 5.29).

In the presence of H_2O_2, the F182L mutant was able to generate 4-(2′-hydroxyacetyl)benzoic acid as per the NADH-driven control (Figure 5.29). This hydroxy metabolite arises from the hydroxylation of 4-acetylbenzoic acid which was established previously as a product of C-C cleavage with JCM 1. This is strong evidence that the F182L mutant is also able to use the peroxygenase pathway to catalyse C-C cleavage reactions with α-hydroxyketone substrates. The H_2O_2-driven reactions also showed some formation of 4-acetylbenzoic acid which was not observed in the NADH-

driven reactions (Figure 5.29).

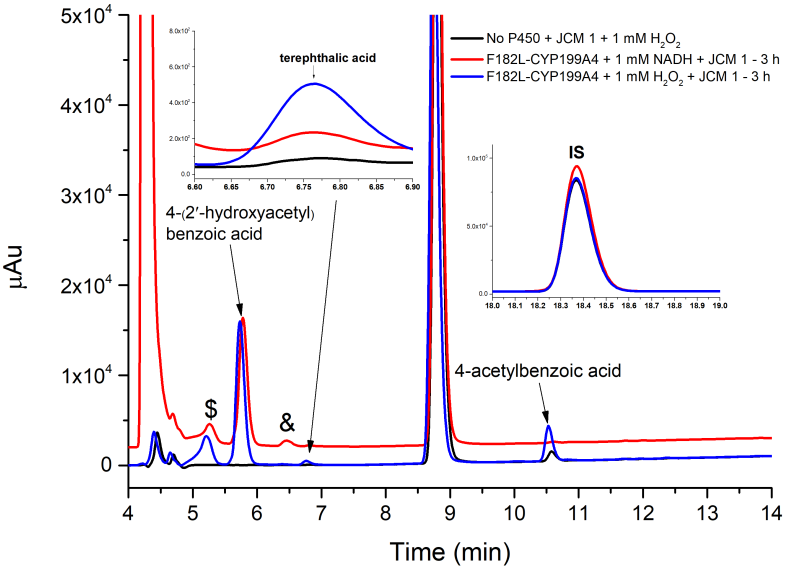

Figure 5.29: HPLC analysis of the oxidation reaction of F182L-CYP199A4 with JCM 1 using with H_2O_2 (blue) or NADH (red). A no P450 control is shown in black.

Overall, the F182L mutant is capable of efficiently catalysing C-C cleavage of α-hydroxyketone subtrates other than JCM 1 using the NADH regenerating system. It can also act as a peroxygenase to catalyse C-C cleavage reactions.

5.3.7 Kinetic Solvent Isotope Experiments with F182L-CYP199A4

C-C cleavage activity of P450 enzymes with α-hydroxyketone compounds has been theorised to proceed through nucleophilic attack of the C=O centre by a ferric-peroxo intermediate (Figure 5.30). The ferric-peroxo intermediate can be protonated and undergoes O-O bond cleavage to form Cpd I that is responsible for P450 hydroxylation reactions (Figure 5.30).

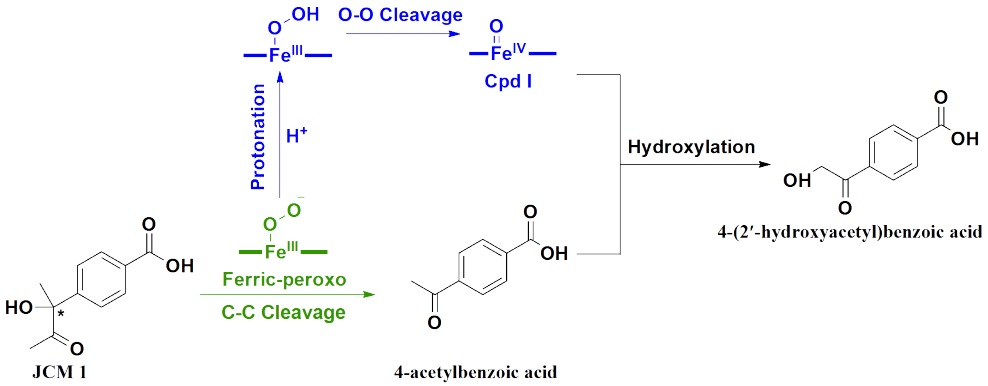

Figure 5.30: Reaction pathway of P450 C-C cleavage reaction (green) that involves the ferric-peroxo intermediate and the hydroxylation pathway that involves the Cpd I intermediate (blue). Protonation occurs using H^+ from surrounding water molecules.

To investigate the intermediate involved in P450 catalysed C-C cleavage activity, NADH oxidation experiments were carried out with JCM 1 and 4-acetylbenzoic acid as substrates in the presence of deuterated (D_2O) or protonated (H_2O) solvent using WT CYP199A4 and the F182L mutant. The hydroxylation of 4-acetylbenzoic acid by the F182L and WT enzymes in D_2O is investigated as this reaction should be sensitive to a kinetic solvent isotope effect (KSIE). This is because in D_2O, the protonation of the P450 ferric-peroxo species is slowed and consequently Cpd I formation would be hindered to generate less product (Figure 5.30). In contrast, reactions with JCM 1 which first involve a C-C cleavage reaction that does not require protonation of the ferric-peroxo species (Figure 5.30) should have an inverse kinetic isotope effect with greater product formation in D_2O. This phenomenon has been observed in human CYP17A1 with steroidal substrates.[244,246]

All CYP199A4 reactions were carried out with electron transfer partners and NADH. Product formation was analysed by HPLC and the concentration of products were quantified using a calibration curve made with standard solutions of 4-acetylbenzoic acid (Figure D18). Coupling efficiencies and product formation rates were then calculated (Table 5.5).

Table 5.5: Kinetic and substrate binding data for CYP199A4 variants with JCM 1 and 4-acetylbenzoic acid in different solvents. Rates are given as µmol.µmol$_{P450}^{-1}$.min^{-1} (min^{-1}).

Substrate	Enzyme	Buffer	N[a]	PFR[b]	Coupling[c]
JCM 1	F182L	D_2O	74 ± 9	1.8 ± 0.4	2.4 ± 0.2
		H_2O	68 ± 1	1.3 ± 0.2	1.9 ± 0.3
4-acetylbenzoic acid	F182L	D_2O	317 ± 11	308 ± 18	97 ± 2
		H_2O	488 ± 9	414 ± 0.1	85 ± 2
	WT	D_2O	291 ± 16	210 ± 7.3	74 ± 1.5
		H_2O	265 ± 20	213 ± 21	80 ± 1.6

[a]NADH oxidation rate. [b]Product formation rate. [c] % of NADH consumed that led to metabolite formation.

The oxidation of JCM 1 by the F182L mutant (Table 5.5, Figure 5.31a) occurred with higher coupling efficiency (2.4 ± 0.2 %) and faster product formation (1.8 ± 0.4 min^{-1}) in D_2O compared to that of the same reaction in H_2O (1.9 ± 0.3 %, 1.3 ± 0.2 min^{-1}). The faster product formation and higher coupling efficiency in D_2O is indicative of

an inverse kinetic solvent isotope effect (KSIE). When the levels of metabolites were considered, the ratio between the H_2O and D_2O reactions were 0.77 ± 0.1 for C-C cleavage activity (4-(2′-hydroxyacetyl)benzoic acid) and 1.56 ± 0.2 (" & ", Figure 5.31a) for hydroxylation activity. The higher levels of the C-C cleavage metabolite in D_2O is further evidence of an inverse KSIE and normal KSIE for the C-C cleavage and hydroxylation pathways respectively. The reaction of JCM 1 would first involve P450-catalysed C-C bond cleavage followed by C-H bond hydroxylation, the presence of an inverse KSIE shows that hindering protonation has an affect on the reactive intermediate involved in C-C cleavage activity.

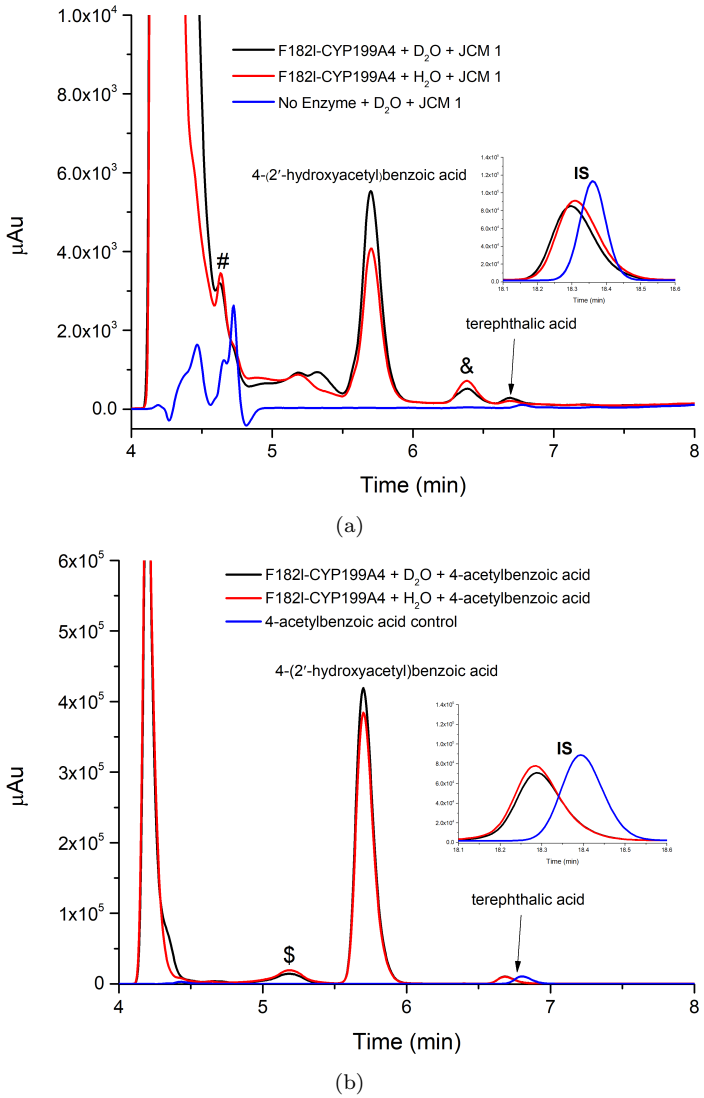

Figure 5.31: HPLC analysis of the metabolites formed from the oxidation of (a) JCM 1 and (b) 4-acetylbenzoic acid in H_2O (red) and D_2O (black). No enzyme controls are shown also (blue).

Analysis of the oxidation of 4-acetylbenzoic acid by the F182L mutant (Figure 5.31b) showed a slower product formation in D_2O (308 ± 18 min^{-1}) compared to when in H_2O (414 ± 0.1 min^{-1}) that is evidence of a standard KSIE (Table 5.5). The coupling efficiency in D_2O (97 ± 2 %) is marginally higher than in H_2O (85 ± 2 %). The

control reaction of WT CYP199A4 with 4-acetylbenzoic in D_2O showed slower product formation (210 ± 7.3 min^{-1}) and lower coupling efficiency (74 ± 1.5 %) than in H_2O (213 $\pm$ 21 %, 80 ± 1.6 min^{-1}). The slower product formation in D_2O with the hydroxylation reaction of F182L and WT enzymes is an indication of a standard KSIE occurring during the formation of Cpd I.

The contrasting kinetic solvent isotope effects between the oxidation of JCM 1 and 4-acetylbenzoic acid suggests that F182L-CYP199A4 uses a different intermediate to Cpd I in C-C bond cleavage reactions.

5.3.8 Crystal Structure of F182L-CYP199A4 with JCM 1

The F182L variant of CYP199A4 has not been crystallised or had its X-ray crystal structure determined. The rationale behind the mutagenesis of residue F182 in the active site of CYP199A4 was to introduce a smaller amino acid (Leu) near the heme centre to allow for the binding and oxidation of bulkier *para*-substituted benzoic acids by CYP199A4. F182L-CYP199A4 was successful in not only binding JCM 1 but also demonstrated strong evidence of P450 catalysed C-C cleavage activity. Crystallisation of this CYP199A4 variant and determining its structure would allow us to elucidate the binding modes of substrates such as JCM 1 or JCM 2 and rationalise any oxidation activity observed. It could also enable the design of new P450 variants with enhanced C-C cleavage activity.

F182L-CYP199A4 was successfully crystallised in the presence of both JCM 1 and JCM 2 as substrates using conditions previously used for CYP199A4 and its mutants.[134,157,218] These crystals were then used to determine X-ray crystal structures of this variant. A crystal structure of F182L-CYP199A4 complexed with JCM 1 (PDB: 8G35) was determined to a resolution of 2.05 Å and the crystal structure with JCM 2 (PDB: 8G36) was solved at 2.16 Å. The overall structural fold for the F182L mutant is similar to that of WT CYP199A4 (Figure D19 and D20, RMSD = 0.492 Å or 0.597 Å). The electron density within the active site revealed the location of the bound substrate. The location of the substrate's benzoic acid moiety was in a similar position to that observed for other substrates bound to CYP199A4 and its mutants.[23,30,158,220,256]

In the structure of F182L-CYP199A4 crystallised with JCM 2 (Figure 5.32), the electron density of the bound molecule did not match that of the added ligand. The electron density of the bound molecule was instead modelled as terephthalic acid. There was also additional electron density in the active site that was modelled as water molecules. Terephthalic acid has been observed to be formed when JCM 2 reacts with hydrogen

peroxide (Figure 5.13). The sensitivity of JCM 2 could cause it to react with the ferric-heme or heme-bound water ligand over the course of crystal growth, storage or during data collection. The refinement statistics for F182L-CYP199A4 modelled with terephthalic acid are provided in Table D1.

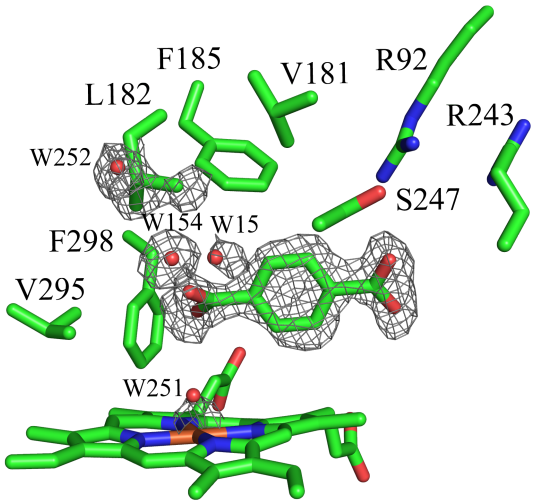

Figure 5.32: Crystal structure of F182L-CYP199A4 that was co-crystallised with JCM 2 (PDB: 8G36). A feature-enhanced map as a grey mesh contoured to 1.0 σ (1.5 Å carve) is shown around the substrate, residue L182 and active site waters. This crystal structure was solved to a resolution of 2.16 Å. The active site substrate appears to be terephthalic acid instead of JCM 2 and the electron density of the bound substrate was modelled as such.

As JCM 1 was synthesised as a racemic mixture, the crystal structure F182L-CYP199A4 bound to JCM 1 required the electron density of the substrate to be modelled separately as either the (*S*) or (*R*) enantiomer of JCM 1 (Figure 5.33).

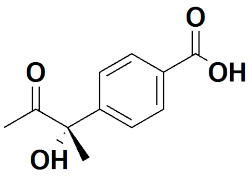

(*S*)-4-(2-hydroxy-3-oxobutan-2-yl)benzoic acid

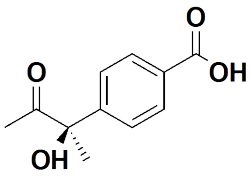

(*R*)-4-(2-hydroxy-3-oxobutan-2-yl)benzoic acid

Figure 5.33: The (*S*)- and (*R*)- enantiomers of JCM 1. Both enantiomers were modelled into the active site of F182L-CYP199A4.

The active site of F182L-CYP199A4 also contained additional electron density that could be modelled as water molecules. In addition to composite-omit maps to show electron density around important features in the active site, F_o-F_c difference maps were also generated to assess negative and positive electron density around the bound molecule. These difference maps show where the experimental data differs from the atomic model.[257] Negative density (red) show areas where atoms have been incorrectly placed where no experimental electron density is present. Positive density (green) shows where the model is missing atoms and does not account for the electron density. The

(*R*)-enantiomer of JCM 1 was modelled first within the crystal structure of F182L-CYP199A4 (Figure 5.34).

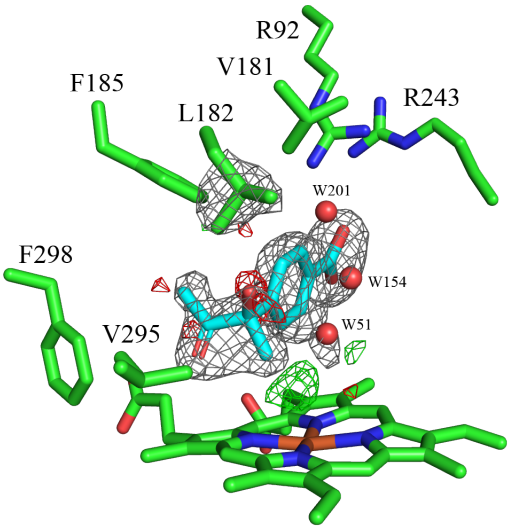

Figure 5.34: The active site for the crystal structure of F182L-CYP199A4 modelled with (*R*)-JCM 1 solved to a resolution of 2.05 Å, water molecules are present within the active site. A composite-omit map is shown (grey mesh, 1.0 σ at 1.5 carve) and a F_o-F_c map (red or green mesh, contoured at 2.5 σ). The F_o-F_c map showed positive density observed above the heme centre that would indicate a heme-bound water is present. Negative density is also observed where the α-hydroxy group is located.

When the (*R*)-enantiomer of JCM 1 was modelled into the structure of F182L-CYP199A4, the F_o-F_c map showed a distinct region of positive density above the heme (Figure 5.34). This positive density is likely to be a heme-bound water molecule. An attempt was made to model the heme-bound water but several refinement cycles using phenix.refine displaces the modelled water molecule away from the heme. If this water molecule was present, it would have steric clash with the heme-facing methyl group of the (*R*)-JCM 1. There is also negative density present at the α-hydroxy group of modelled (*R*)-JCM 1 (Figure 5.34), indicating the position of the modelled hydroxy group did not match the electron density present in that region.

Given the discrepancies observed with (*R*)-JCM 1, the (*S*)-enantiomer was then modelled. A similar region of positive density was observed above the heme (Figure 5.35a) and modelling this electron density as a water molecule was successful (Figure 5.35b, PDB: 8G35). The active site of the F182L mutant has additional waters (W255, W107, W267 and W289) not seen in the structure of the WT enzyme complexed with 4-methoxybenzoic acid (Figure 5.17a, PDB: 4DO1). Distances between the four water molecules and (*S*)-JCM 1 showed no steric clash (Figure 5.36a). The α-hydroxy group of the substrate did possess hydrogen bonding interactions to W291 (heme-bound) and W267 (water above W291) (Figure 5.36b). The occupancies of all active site waters are shown in Table 5.6. B-factors between the water molecules and their closest residues were found to be similar (Table D.1). This structure of F182L-CYP199A4 with the

(*S*)-enantiomer was deposited into the PDB (PDB: 8G35).

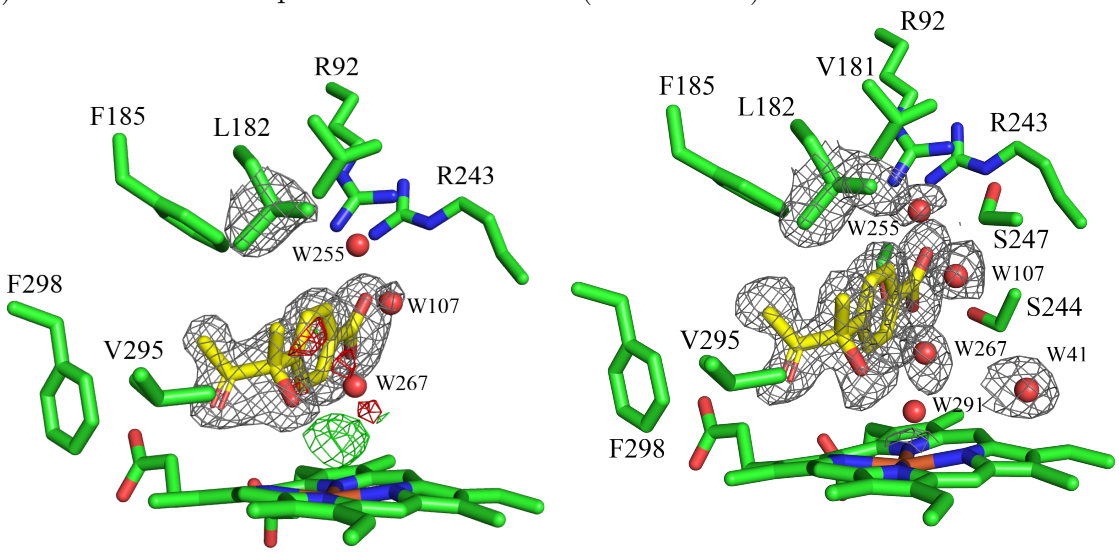

(a) (b)

Figure 5.35: Active site for the crystal structures of F182L-CYP199A4 modelled with (*S*)-JCM 1 and solved to a resolution of 2.05 Å. In (a), a composite-omit map is shown around the substrate while in (b) a feature-enhanced map is shown around the substrate and active site waters. Both maps are shown as a grey mesh (1.0 σ at 1.5 Å carve). The F_o-F_c (red or green mesh, contoured at 2.5 σ) is also shown in (a) and (b). In (a), there is a region of positive density above the heme centre. In (b), a water molecule was modelled above the heme.

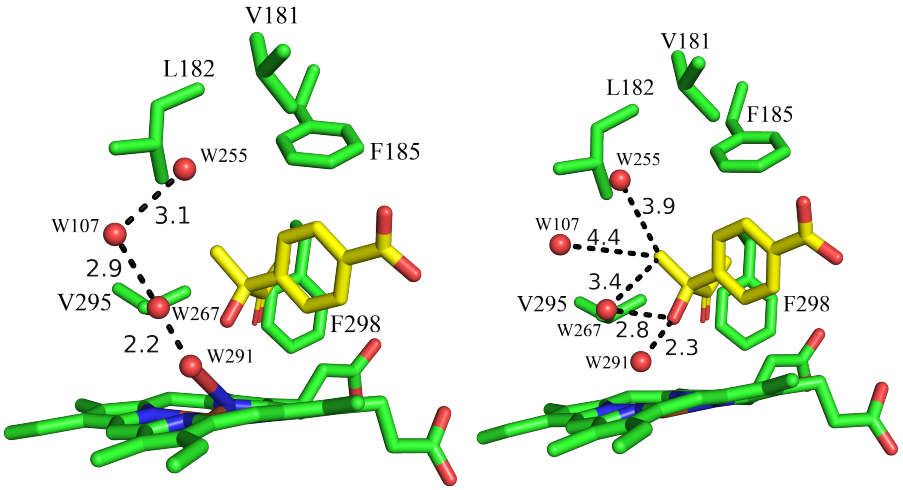

(a) (b)

Figure 5.36: Active site of F182L-CYP199A4 complexed with (*S*)-JCM 1 (PDB: 8G35) showing the distances (in Å) of active site water molecules with each other (a) and with the α-hydroxy and methyl groups of the substrate (b).

Table 5.6: Occupancies of water molecules modelled within the active site of F182L-CYP199A4 complexed with (*S*)-JCM 1.

Water Molecule	Refined Occupancy (%)
W291	63
W267	74
W107	86
W255	52

When comparing the I-helix of the F182L mutant to that of the WT enzyme (PDB: 4DO1), we observed that the oxygen binding groove of the mutant also had an additional water molecule (W41, Figure 5.37) that has a hydrogen bonding interaction with T253 and positions this residue closer to the heme (Figure 5.37b). Residues T253, A248, L250 and T252 also showed a change in conformation when compared to the WT enzyme. Residue T252 (alcohol group of the acid-alcohol pair involved in O_2 activation) in the F182L mutant has also been displaced away from the heme-centre to accommodate the additional water molecules (Figure 5.37b). The movement of the T252 residue also caused a widening of the oxygen-binding groove in the F182L mutant (Figure 5.38).

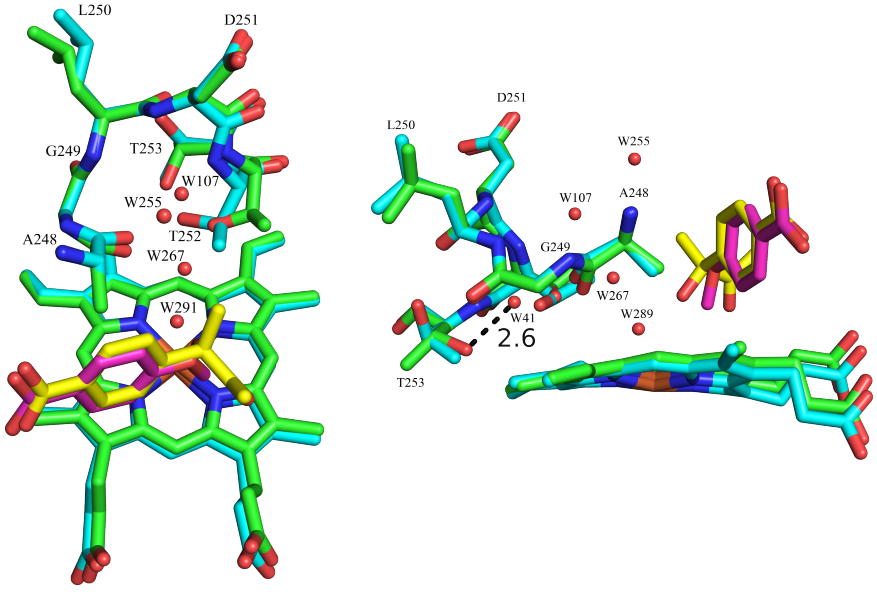

(a) (b)

Figure 5.37: (a) Oxygen binding groove of the I-helix of F182L-CYP199A4 (green sticks, PDB: 8G35) + (*S*)-JCM 1 (yellow sticks) overlaid with that of WT-CYP199A4 (cyan sticks, PDB: 4DO1) complexed with 4-methoxybenzoic acid (magenta sticks). (b) Alternate view of the T253 and L250 residues that have altered conformations in the F182L mutant. The T253 residue in the F182L mutant forms a hydrogen bonding interaction (dashed line) with W41.

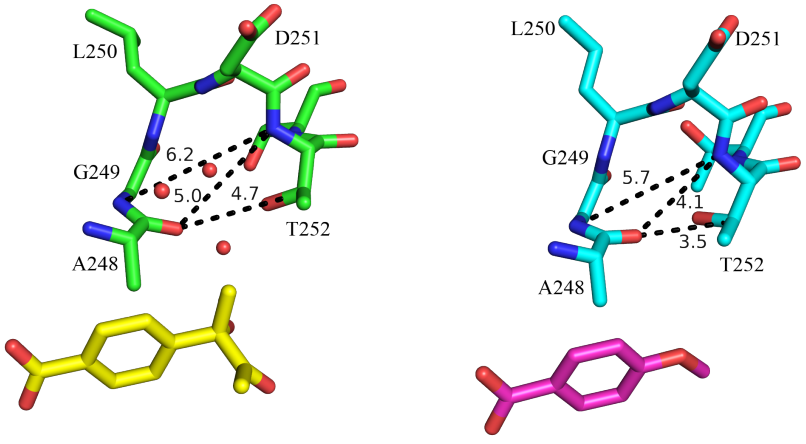

(a) (b)

Figure 5.38: Distances in Å between different residues of the oxygen binding groove of F182L (a) and WT (b) variants of CYP199A4. It can be seen in (a) that the F182L mutant showed a widening of the groove ($\sim$ 4.7 Å) compared to the groove (4.1 Å) shown in (b).

The conformation of the residues in the active site of the F182L mutant is similar to that of WT CYP199A4. It is observed the F298 residue of the F182L mutant rotates away from the heme-centre to accommodate the additional steric bulk from (*S*)-JCM 1 (Figure 5.39). A similar movement of the F298 residue is also present when CYP199A4 binds sterically demanding substrates such as 4-ethylthiobenzoic acid and 4-phenylbenzoic acid (Section 6.3.1).[220]

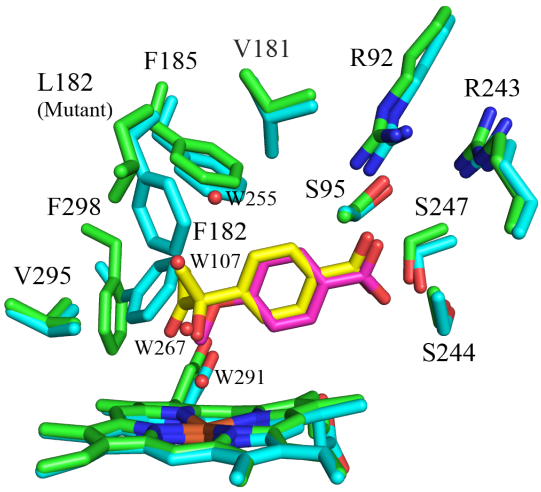

Figure 5.39: Active site complex of F182L-CYP199A4 (green sticks) + (*S*)-JCM 1 (yellow sticks) overlaid with that of WT-CYP199A4 (cyan sticks, PDB: 4DO1) + 4-methoxybenzoic acid (magenta sticks). The F298 residue has shifted to accommodate the additional steric bulk of (*S*)-JCM 1.

To elucidate why the F182L mutant is able to bind (*S*)-JCM 1, this substrate and the active site waters of the F182L mutant were superimposed into the substrate binding site of WT-CYP199A4 (PDB: 4DO1) (Figure 5.40). Distances between the substrate and the closest residues were measured. The distances of (*S*)-JCM 1 and active site waters to the closest residues of F182L-CYP199A4 was measured also (Figure 5.41).

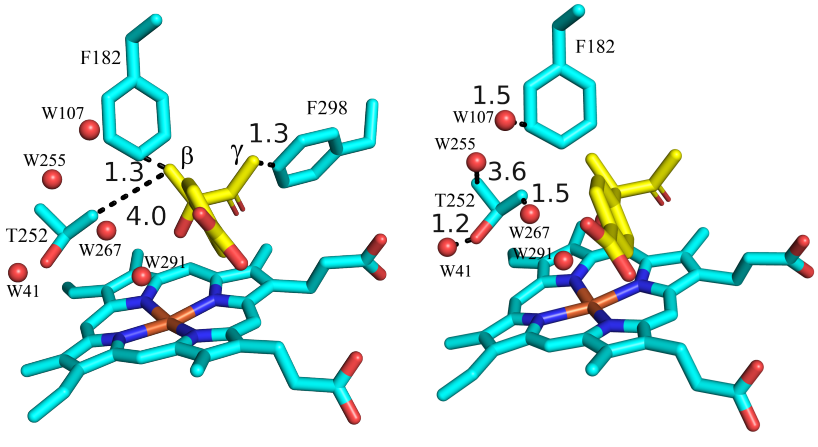

Figure 5.40: Substrate (*S*)-JCM 1 (yellow sticks) and active site waters (W291, W267, W255, W107) from the structure of F182L-CYP199A4 (Figure 5.36, PDB: 8G35) overlaid into the active site of the solved structure of WT-CYP199A4 complexed with 4-methoxybenzoic acid (cyan sticks, PDB: 4DO1). (a) The distances of atoms within residues F182, F298 and T252 closest to the (*S*)-JCM 1 are annotated. (b) Closest distances of the active site waters of F182L-CYP199A4 with residues F182 and T252 of the active site within WT-CYP199A4 (cyan sticks) are annotated.

In Figure 5.40a, the β and γ methyl groups of (*S*)-JCM 1 if present in the active site of WT CYP199A4 would have distances of ≈ 1.3 Å with residues F182 and F298 which would result in a steric clash. The F182L mutant orientates the F298 residue away from the heme which eliminates steric clash of this residue with (*S*)-JCM 1 (Figure 5.39). Active site waters that were present in F182L-CYP199A4 (W107, W41 and W267) would also have a clash of 1.2 - 1.5 Å with residues T252 and F182 (Figure 5.40b). In the F182L mutant (Figure 5.41), (*S*)-JCM 1 and the active site waters had no steric clashes with any of the active site residues in this mutant.

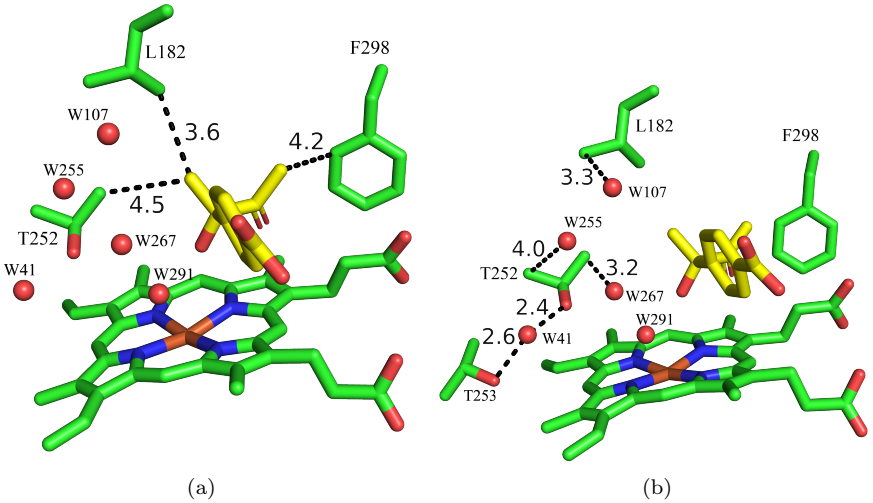

Figure 5.41: Active site structure of F182L-CYP199A4 (green sticks) + (*S*)-JCM 1 (yellow sticks). (a) Closest distances (in Å) of residues L182, F298 and T252 to the methyl carbons of the substrate. (b) Closest distances (in Å) between active site waters (W267, W107, W41 and W255). No steric clash is present between the substrate and active site waters with the surrounding residues.

Additionally, the distances of the β-carbonyl and the α-hydroxy carbon of (*S*)-JCM 1 with the heme centre of the F182L mutant were measured (Figure 5.42). These distances were compared to those measured for equivalent carbons of 17α-hydroxy-progesterone in the active site of A105L-CYP17A1 (PDB: 4NKY) and were found to be similar.[258]

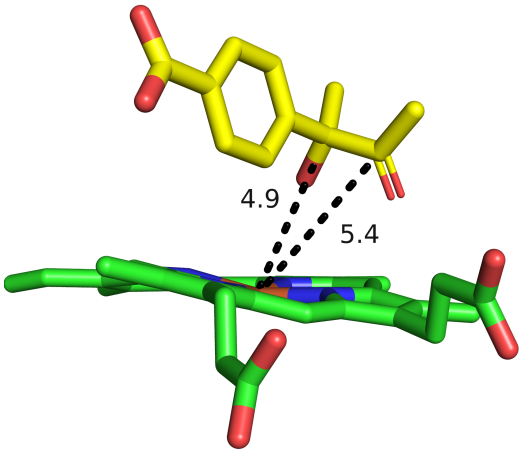

Figure 5.42: Distances measured (in Å) for the α-carbon and β-carbonyl of the (*S*)-JCM 1 substrate to the heme centre of F182L-CYP199A4.

Table 5.7: Distances measured (in Å) for the α-carbon and carbonyl of the (*S*)-JCM 1 substrate to the heme centre of F182L-CYP199A4 compared to equivalent carbons of 17α-hydroxy-progesterone in A105L-CYP17A1.[258] Atoms of interest are highlighted in bold.

Distance	(*S*)-JCM 1 + F182L-CYP199A4	17α-hydroxy-progesterone + A105L-CYP17A1
C$_\alpha$-OH (Å)	4.9	5.0
C$_\beta$=O (Å)	5.4	4.6

The occupancies of both (*R*)- and (*S*)-enantiomers of JCM 1 were refined within the same location in the active site using separate altloc (alternative location) identifiers for each enantiomer (Figure 5.43). The occupancy of the (*R*)-enantiomer was 11 % while the (*S*)-enantiomer was 89 %. The occupancy of the (*S*)-enantiomer shows that it occupies the substrate position at approximately 90 % of all asymmetric units in the crystal. The lower occupancy of the (*R*)-enantiomer could infer that it is the less preferred enantiomer for binding to the F182L mutant. However, it may still be present explaining the hydroxylation metabolite observed in the GC-MS analysis.

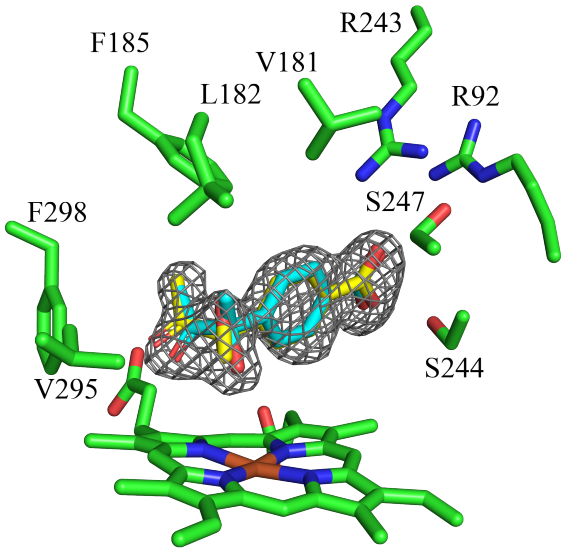

Figure 5.43: Active site structure of F182L-CYP199A4 with both (*S*) and (*R*)-JCM 1 modelled in the same location using different altloc identifiers. The occupancy of both enantiomers were refined. Occupancies for the (*S*)-enantiomer is 89 % and the (*R*)-enantiomer is 11 % .

5.4 Discussion

CYP199A4 could catalyse C-C cleavage bond reactions with the F298V and F182L mutants. The hydroxylation of WT CYP199A4 of 4-propionyl- and 4-(2′-oxopropyl)-benzoic acid proceeded with high efficiency enabling complete conversion to the α-hydroxyketone product but no and/or low levels of further oxidation and C-C cleavage products were observed.[248] One-pot reactions with these α-hydroxyketone products with WT, T252E and F182L variants of CYP199A4 showed C-C cleavage activity when none of the initial ketone substrates was available. It is likely that these α-hydroxyketone substrates are poorer substrates for CYP199A4 compared to the initial ketones. It was observed the F182L mutant showed the highest level of C-C cleavage metabolite formation with the NADH regenerating system. The high conversion of the initial ketone substrate to the α-hydroxyketone compounds provides a viable way to generate these compounds to further study C-C cleavage reactions. It has been noted that α-hydroxyketones are known to undergo rearrangement reactions to generate mixtures of tautomers and may not be well suited for isolation and long term storage.[259]

WT CYP199A4 was unable to show any oxidation activity with the synthesised benzoic acids functionalised with α-hydroxyketone moieties, JCM 1 and JCM 2. When compared to 4-methoxybenzoic acid, a substrate with tight binding and high oxidation activity with CYP199A4,[48,137] the *para* α-hydroxyketone moiety does impart higher steric bulk with JCM 1 and JCM 2. But, the lack of any activity was unexpected because WT CYP199A4 has been shown to bind and efficiently oxidise other bulky *para* substituents such as 4-*t*-butylbenzoic acid, 4-cyclohexylbenzoic acid and 4-*n*-propylbenzoic acid.[153,220,260]

Site-directed mutagenesis was used to generate mutants F182L and F298V that were able to bind and catalyse C-C cleavage reactions with JCM 1. Comparing crystal structures of WT CYP199A4 to that of the F182L mutant complexed with JCM 1 highlighted potential steric clashes between the *para* hydroxyketone moiety and the F182 residue in the WT enzyme. This could explain why WT CYP199A4 was unable oxidise JCM 1. Mutation of the F182 residue from the bulky phenylalanine residue to the less sterically demanding leucine afforded additional space in the active site to accommodate the binding of JCM 1. Mutation of an equivalent residue (F185) in the closely related enzyme, CYP199A2 enabled the P450 to hydroxylate bulky aromatic substrates such as cinnamic acid.[154] Recently, it has been reported that the F182L mutant of CYP199A4 also enabled the hydroxylation of an aromatic substrate, 4-phenylbenzoic acid (Chapter 6).[256]

The mechanism of CYP17A1 catalysed C-C bond cleavage is proposed to involve nucleophilic attack of the α-hydroxyketone carbonyl centre by the ferric-peroxo intermediate of the P450. Some indirect evidence has been reported that supports a Cpd I mechanism being involved in C-C cleavage activity with CYP17A1.[94] The distance between the C=O carbon of JCM 1 to the heme centre was 5.4 Å and was similar to the distance of the equivalent carbon (C20) for 17,20-lyase substrates of CYP17A1 (4.6 Å).[258] The similar distances of equivalent carbons to the heme centre between the two P450s further supports using F182L-CYP199A4 as a model system for CYP17A1 C-C cleavage activity.

JCM 2 induced a Type I shift of ≈ 25 % with F182L-CYP199A4 but showed a fast NADH oxidation rate (> 1423 min^{-1}) comparable to that of 4-methoxybenzoic acid with WT CYP199A4 (1200 min^{-1}).[30] However, only a small amount of any potential enzyme metabolite was detected. We also demonstrated that JCM 2 is susceptible to oxidation by H_2O_2 to generate terephthalic acid. Uncoupling reactions can occur in the P450 catalytic cycle where reducing equivalents are channelled unproductively to generate H_2O_2 (Figure 1.3).[261] The oxidation of JCM 2 by F182L-CYP199A4 could be uncoupled from the reducing equivalents and generates H_2O_2. The H_2O_2 generated would then react with JCM 2 to produce terephthalic acid. Uncoupling reactions have been attributed to mis-protonation of water molecules in the active site of the P450.[262] The crystal structure of F182L-CYP199A4 revealed that the active site contains additional water molecules over the WT enzyme. It is possible that interactions of JCM 2 within the active site residues and additional water molecules promotes poor proton transfer to the heme centre and causes uncoupling reactions to occur to generate H_2O_2. Detection and quantification of H_2O_2 generated by the oxidation of JCM 2 by the F182L mutant could reveal further insights towards the oxidation of this substrate.

The synthesis of JCM 1 generates a racemic mixture. CYP199A4 and its mutants should preferentially bind and oxidise one enantiomer over the other. The crystal structure of F182L-CYP199A4 revealed that the (*S*)-enantiomer of JCM 1 had an 89 % occupancy compared to the (*R*)-enantiomer (11 %). The lower occupancy of the (*R*)-enantiomer could allow the hydroxylation of (*R*)-JCM 1 at the β-methyl group and is consistent with the presence of singly hydroxylated JCM 1 in its doubly-derivatised form detected via GC-MS. The greater occupancy of (*S*)-JCM 1 indicates it is the preferred enantiomer and is likely the substrate involved in P450 catalysed C-C cleavage activity. Future crystallography studies of F182L-CYP199A4 with enantiopure samples of JCM 1 could involve performing an enzymatic turnover *in crystallo* (Chapter 4). A crystal of a substrate-bound oxy complex of F182L-CYP199A4 can be supplied with electrons from the X-ray beam to facilitate catalysis. It is envisioned that the

P450 can be captured whilst in the act of catalysis and allows for the identification of intermediates for P450 C-C cleavage reactions.[210]

The reaction of JCM 1 with F182L-CYP199A4 generates 4-(2′-hydroxyacetyl)benzoic acid as the major product (Figure 5.25). In contrast, the F182L mutant reacts with 4-acetylbenzoic acid to generate higher amounts of further oxidation products including terephthalic acid while 4-(2′-hydroxyacetyl)benzoic acid is present in smaller amounts compared to the reaction with JCM 1. It is important to observe that 4-acetylbenzoic acid is not detected in high levels in either reaction. This is to be expected as JCM 1 when undergoing C-C cleavage will first form 4-acetylbenzoic acid. 4-Acetylbenzoic acid is a better substrate than JCM 1 and would be hydroxylated if NADH is available. Therefore, the build-up of 4-acetylbenzoic acid is not observed. One of the further oxidation metabolites observed was terephthalic acid that could arise from C-C cleavage activity of 4-(2′-hydroxyacetyl)benzoic acid or the glyoxal intermediate detected.

The involvement of Cpd I and the ferric-peroxo anion species has both been implicated in C-C bond cleavage reactions.[90,94] Cpd I is generated from protonation of the ferric-peroxo anion and a second protonation of the distal oxygen causes homolytic cleavage of the O-O bond to form the high valent Cpd I complex. Uncoupling events can occur when mis-protonation events cause reducing equivalents to be channelled into generating H_2O_2 or a water molecule. Proton transfer in both Cpd I formation and uncoupling events can be slowed in deuterated solvent (D_2O).[246] If the ferric peroxo anion is the intermediate in C-C bond cleavage, then it should not require proton transfer to carry out catalysis. The slowing of proton transfer should allow the build-up of the ferric-peroxo anion but also hinder Cpd I formation and uncoupling reactions. The build-up of the peroxo anion will result in faster and higher product formation in D_2O: an inverse kinetic solvent isotope effect (KSIE). The reaction of JCM 1 and F182L-CYP199A4 was observed to have a higher coupling efficiency that resulted in a faster product formation in D_2O than H_2O that supports the presence of an inverse KSIE. This inverse KSIE was also observed with human CYP17A1 with 17,20-lyase substrates.[244,246] In contrast, reactions with 4-acetylbenzoic and F182L/WT CYP199A4 showed a slower product formation rate and/or lower coupling efficiency that could be consistent with D_2O inhibiting Cpd I formation with a standard KSIE.

The presence of multiple P450 metabolites arising from multiple and successive reaction pathways does complicate metabolite analysis. Future studies partitioning P450-catalysed C-C cleavage activity from hydroxylation would be of interest as to analyse product formation and kinetic solvent isotope effects with metabolites arising solely from C-C cleavage activity. For example, an approach to completely hinder protonation

events, Cpd I formation and subsequently hydroxylation by the P450 could be achieved through mutations of the highly conserved acid-alcohol pair in CYP199A4 (D251 and T252).[219] A similar approach to investigate the oxidants of P450-catalysed sulfoxidation and epoxidation was achieved using mutagenesis of this acid-alcohol pair.[158,219]

Peroxygenase activity was also tested for the first time with the F182L mutant with JCM 1 (Figure 5.29). The F182L mutant was able to catalyse both C-C cleavage and hydroxylation reactions in the presence of H_2O_2 with a similar product distribution compared to reactions driven by NADH. The peroxide-driven reactions with the F182L variant did show a build-up of 4-acetylbenzoic acid, which is the first metabolite arising from C-C cleavage activity and this was not observed with NADH-driven reactions. The peroxygenase pathway can be less efficient and this could contribute to the build-up of 4-acetylbenzoic acid.[145] The WT and T252E variants also showed evidence of catalysing C-C cleavage reactions using the peroxygenase pathway with α-hydroxyketone substrates. The WT enzyme appeared to have generated more C-C cleavage metabolites over the T252E mutant. This is despite previous reports that the T252E variant should have enhanced peroxygenase activity.[156] It is possible that the active site of the T252E variant binds to α-hydroxyketones less favourably compared to the WT. This could result in the lower peroxygenase activity observed with the T252E mutant but this requires further investigation.

It has been reported that CYP17A1 is able to catalyse C-C bond cleavage of α-hydroxyketones with iodosylbenzene but not with H_2O_2.[94] Iodosylbenzene is a single oxygen donor that forms Cpd I directly with P450s and precludes the ferric-peroxo anion species from forming.[247] Our work here reports that the F182L mutant of CYP199A4 can support C-C cleavage activity of α-hydroxyketones using H_2O_2 which provides evidence that the ferric-peroxo anion or a species other than Cpd I plays a role in C-C cleavage reactions modelled after CYP17A1.

In summary, C-C cleavage activity was demonstrated with different variants of CYP199A4. This work presented for the first time the design of an α-hydroxyketone substrate that mimics C-C cleavage substrates of CYP17A1. Using site-directed mutagenesis, mutant F182L of CYP199A4 was able to catalyse C-C bond cleavage with one substrate while the WT could not. Studies using deuterated solvent to probe reaction kinetics strongly suggest that the ferric peroxo anion intermediate is involved in C-C cleavage activity of α-hydroxyketones. This work provides confirmation that C-C cleavage reactions can be modelled outside the small subset of P450s that catalyse them and is a suitable foundation for future studies that explore these reactions in greater detail.

6 Engineering Aromatic Hydroxylation in CYP199A4

6.1 Introduction

Aliphatic C-H bond hydroxylation is the most well studied reaction catalysed by P450 enzymes.[34] In aliphatic hydroxylation, hydrogen atom abstraction of a C-H bond is carried out by Cpd I to form Cpd II and the substrate radical (Figure 6.1).[43,44] Cpd II then inserts the oxygen atom into the substrate radical at the abstracted centre via radical rebound (Section 1.5.1).[44,263]

In addition to aliphatic hydroxylation, aromatic hydroxylation can also be catalysed by P450 enzymes. However, as aromatic C-H bonds ($\sim$ 110 kcal mol^{-1})[264] are stronger than those in aliphatic systems ($\sim$ 100 kcal mol^{-1}),[54] hydrogen abstraction by Cpd I does not occur in aromatic systems.[265] It is theorised that P450 aromatic oxidation occurs through two potential mechanisms (Figure 6.1), namely arene oxide formation or *ipso*-substitution.

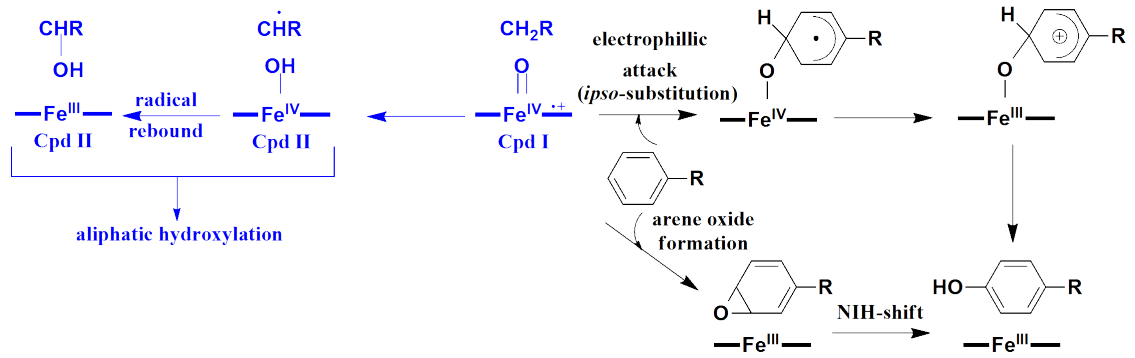

Figure 6.1: The different pathways of P450 hydroxylation (blue) and aromatic oxidation (black).[256]

If aromatic hydroxylation occurs through arene oxide formation, an NIH-shift reaction occurs (Figure 6.2) to move the hydrogen of the activated carbon to the adjacent position on the aromatic ring.[266–268]

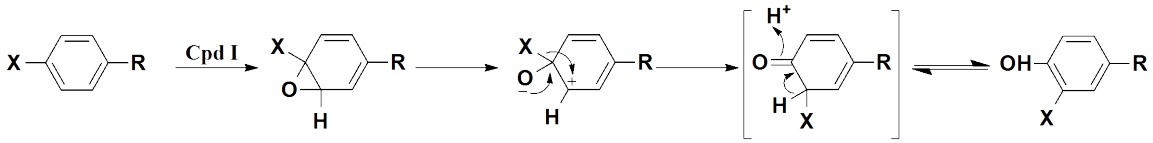

Figure 6.2: (a) Arene oxide pathway in aromatic hydroxylation. An NIH-shift step occurs to transfer the substituent (X) of the activated carbon to an adjacent position.

The second possible mechanism for P450-catalysed aromatic hydroxylation is through direct electrophilic attack by Cpd I on the aromatic π system and this is also referred to as *ipso*-substitution (Figure 6.3).[78,269,270]

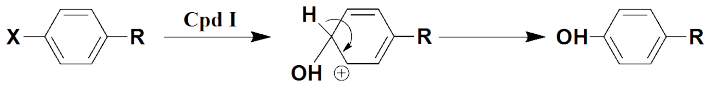

Figure 6.3: Direct electrophilic attack or *ipso*-substitution as an alternate pathway for aromatic hydroxylation by P450 enzymes.

Arene oxide is a possible intermediate of P450-catalysed aromatic oxidation involving the NIH-shift mechanism. The formation of arene oxide or products derived from it would therefore be direct evidence for an NIH-shift mechanism.[267] For example, De Voss *et al.* have successfully isolated an oxepin product from the oxidation of *t*-butylbenzene by $P450_{cam}$ and $P450_{cin}$.[266] This oxepin product is from the tautomerisation of the arene oxide intermediate of *t*-butylbenzene (Figure 6.4). The isolation of this oxepin from P450-catalysed aromatic oxidation is evidence for the NIH-shift mechanism.[266]

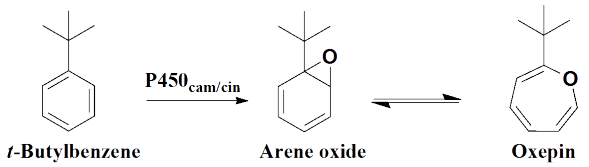

Figure 6.4: Epoxidation of *t*-butylbenzene by P450 enzymes. The oxepin product is formed by tautomerisation.

Aromatic hydroxylation that involves the NIH-shift and arene oxide formation will cause the hydrogen of the activated carbon to be transferred to an adjacent carbon.[267,271] It has been reported that the NIH-shift mechanism does not occur with all P450-catalysed aromatic hydroxylations. Deuterium labelling studies have shown for certain reactions, the hydrogen of the activated carbon is not transferred to the neighbouring carbon but is instead quantitatively lost.[270] The lack of NIH-shift activity was observed often for hydroxylations at positions *meta* to a halide substituent and is coupled with a normal isotope effect (k_H/k_D = 1.1 - 1.3).[270] This is in contrast to an inverse isotope effect ($k_H/k_D = \sim 0.95$) for hydroxylation at *para* and *ortho* positions.[272,273] From this, it is hypothesised that *meta* hydroxylation occurs through *ipso*-substitution. This alternate mechanism occurs with a carbon-oxygen bond forming between the ferryl oxygen and the activated carbon that undergoes proton loss directly to form the hydroxylated product (Figure 6.1).[78]

CYP199A4 from *Rhodopseudomonas palustris* HaA2 efficiently oxidises *para*-substituted benzoic acids and will be used in this study to explore P450-catalysed

aromatic hydroxylation. WT CYP199A4 did not display any oxidation activity with 4-phenylbenzoic acid (Figure 6.5) despite showing tight binding (~1.7 μM) and a fast NADH oxidation rate (~902 min^{-1}).[220] In contrast, WT CYP199A4 was able to hydroxylate 4-cyclohexylbenzoic acid where the *para* substituent is similar in size to a phenyl group but possesses aliphatic C-H bonds instead (Figure 6.5).[220]

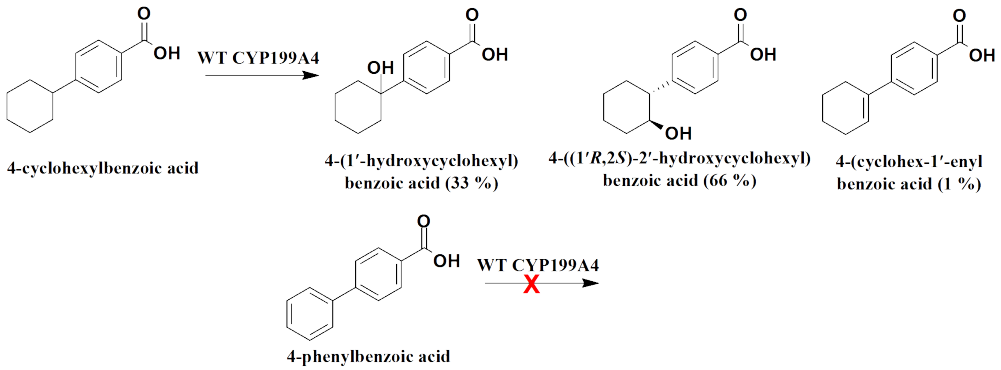

Figure 6.5: Oxidation activity of WT CYP199A4 with 4-phenylbenzoic acid and 4-cyclohexylbenzoic acid.

Screening of related substrates with aromatic functional groups at the *para* position also did not show any aromatic hydroxylation activity but *O*-demethylation and benzylic C-H hydroxylation has been observed (Figure 6.6).[256]

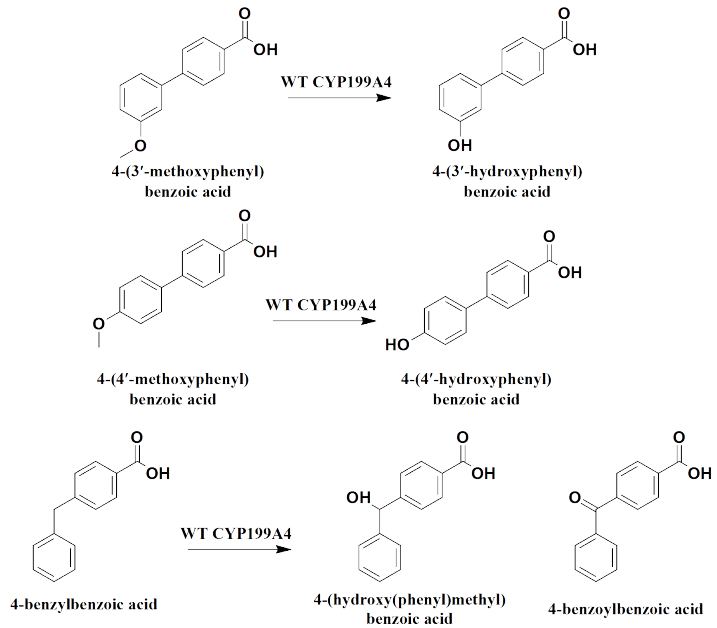

Figure 6.6: Oxidation activity of WT CYP199A4 with benzoic acid substrates containing aromatic groups.

In this study, crystallisation of WT CYP199A4 with 4-phenylbenzoic acid will be carried out to explore the binding mode of this substrate within the active site. Structural insights gleaned from the aforementioned crystal structure will be used to inform rational mutagenesis to enable aromatic hydroxylation in CYP199A4.

6.2 Materials and Methods

6.2.1 General

General reagents and organics were purchased from Sigma-Aldrich. Isopropyl-β-D-thiogalactopyranoside (IPTG) and buffer components were obtained from Astral Scientific (Australia). UV/Vis spectra and spectroscopic activity assays were performed on an Agilent Cary 60 spectrophotometer at 30 ± 5 °C.

Analytical High Performance Liquid Chromatography (HPLC) was performed on a Shimadzu LC-20AD equipped with a Phenomenex Kinetex 5u XB-C18 100A column (250 mm × 4.6 mm, 5 µM), SIL-20A autosampler, CTO-20A column oven, SPD-20A UV detector and CBM-20Alite communications module. A gradient of 20-95 % acetonitrile in water (both containing trifluoroacetic acid, TFA, 0.1 %) was run at a flow rate of 1 mL min^{-1} over 30 minutes and detector wavelength was set at 254 nm.

GC-MS analysis was performed using a Shimadzu GC-2010 gas chromatograph equipped with an autoinjector and a GCMS-QP2010S detector; the column used was a DB-5MS UI column. The interface and injection port temperatures were held at 280 and 250 °C. The column was held at 120 °C for 3 min, and the temperature was then increased to 240 °C at a rate of 7.5 °C min^{-1} and held at 240 °C for 6 min.

6.2.2 Production and purification of enzymes

HaPux, HaPuR and WT CYP199A4 were all expressed and purified as described previously.[156] Variants F298V and F182L-CYP199A4 were expressed as previously described for WT CYP199A4 but with the addition of 4-methoxybenzoic acid to a concentration of 1 mM to the expression media before induction. Proteins were stored in 50 % glycerol at -20 °C.

6.2.3 *In vitro* NADH Oxidation Assays

Glycerol was removed from proteins through elution with a 5 mL gel filtration column (PD-10, GE Healthcare) and 50 mM Tris buffer (Buffer T, pH 7.4). The concentration of each protein was quantified using UV-Vis spectrophotometry with extinction coefficients given in Table 5.1 in Chapter 5.

In vitro NADH turnovers were performed at 30 °C and contained P450 (1 µM), HaPux

(5 µM), HaPuR (0.5 µM) and 100 ng μL^{-1} bovine liver catalase in oxygenated Buffer T with a total volume of 1.2 mL. The absorbance at 340 nm was set to zero and the mixture was incubated at 30 °C for 2 min before NADH was added to a concentration of ≈ 320 µM, (an absorbance of ≈ 2.0). The rate of NADH background oxidation (the 'leak' rate) was measured before initiating the reaction. To start the reaction, substrate was added from a 100 mM stock in EtOH/DMSO to the desired concentration (1 mM, 0.5 mM, 0.2 mM or 0.15 mM) and NADH depletion was monitored at 340 nm. The rate of NADH consumption (N) by the P450 enzyme in units of (µM-NADH)(µM-P450)$^{-1}$ min^{-1} was calculated from the slope of the graph of A_{340nm} versus time using an extinction coefficient of $\varepsilon_{340nm} = 6.22$ mM^{-1} cm^{-1} and reported as min^{-1}.

All experiments were performed in triplicate with the mean and standard deviation reported. Control reactions were also performed in which either the P450 or NADH was omitted from the turnover mixture (replaced with the same volume of buffer).

6.2.4 Metabolite Analysis

For HPLC analysis, after reactions were completed, 132 µL of the reaction mixture was mixed with 2 µL of an internal standard solution (10 mM of 9-hydroxyfluorene solution in EtOH) and 66 µL of acetonitrile. Samples were acidified with 0.2 µL of trifluoroacetic acid.

For GC-MS analysis, the reaction mixture (1000 µL or 600 µL) was mixed with 10 µL of an internal standard (10 mM of 9-hydroxyfluorene solution in EtOH) and extracted with EtOAc (2 × 400 µL). The extracts were dried with $MgSO_4$ and solvent was removed under N_2. The remaining residue was re-suspended in anhydrous acetonitrile (150 µL) and derivatisation agent (15 µL, BSTFA + TMCS, 99:1). The mixtures were left for 2 h at 37 °C prior to analysis by GC-MS.

HPLC and GC-MS analysis methods were performed as described in Section 6.2.1. To quantify enzyme metabolites, calibration curves were constructed from authentic product standards or if the standards were not available, substrate was used. Standard solutions of 10, 20, 50, 100, 200, 500 and 1000 were prepared for HPLC analysis as per reaction samples. The area of the product and the internal standard peaks were measured using Shimadzu LabSolutions. A plot of product peak area/internal standard area peak versus concentration of standard was made and the calibration factor was calculated to quantify the amount of product in the reaction sample. Once the concentration of the product is known, the total turnover number for each reaction was calculated.

Once the concentration of the product is known, the coupling efficiency (C) was calculated. The coupling efficiency is defined as the percentage of NADH that was used to oxidise the substrate and is given by the following equation:

$$C = \frac{[\text{Product}]}{[\text{NADH}]} \times 100\% \tag{6.1}$$

The coupling efficiency can be used to calculate the product formation rate (PFR) from the NADH consumption rate (N, Section 6.2.3) using the following equation:

$$\text{PFR} = \frac{C}{100} \times N \tag{6.2}$$

6.2.5 X-Ray Protein Crystallography

Crystallisation experiments were performed with WT CYP199A4. Immediately prior to preparation of crystal trays, the protein was purified via elution through a HiPrep Sephacryl S-200 HR size-exclusion column (60 cm × 16 mm; GE Healthcare) with Buffer T at a flow rate of 1 mL min^{-1}. The purity of the protein was assessed based on the Reinheitszahl value, RZ = A_{420}/A_{280}, whereby fractions with RZ = 2 were collected and combined.

Substrate (4-phenylbenzoic acid) was then added to the combined fractions to a final concentration of 1 mM from a 100 mM stock of EtOH and DMSO to the concentrated protein. The combined fractions with substrate were incubated at 4 °C and then concentrated via ultrafiltration using a Microsep Advance centrifugal device (10 kDa MWCO, Pall Corporation) to a concentration of approximately 30 – 35 mg mL^{-1}. Crystallisation trays were prepared using the following optimised buffer conditions previously reported:[157] 0.2 M magnesium acetate, 100 mM Bis-Tris buffer (adjusted with acetic acid to pH 5.0 - 5.75) and 20 - 32 % w/v polyethylene glycol (PEG) 3350.

Protein crystallisation was achieved using the hanging-drop vapour diffusion method in 24-well trays. An equal volume of crystallisation buffer was mixed with hanging drops of 1.2 - 2 µL of protein and was equilibrated with a reservoir of the same buffer (500 µL) at 16 °C. Red plate-like crystals were obtained after half a day to one week.

X-ray diffraction data were obtained (360 images per crystal) at the Australian Synchrotron using the MX2 beamline[250] with exposure time of 1 s, oscillation angle of 1 °, wavelength of 0.9537 Å and temperature of 100 K. Diffraction images were indexed and integrated using iMosfilm.[222] Aimless[223] from the CCP_4 suite of programs[224] was

used to carry out scaling, merging and R_{free} labelling (5 % of reflections, randomly selected). The phase was solved using Molecular Replacement in Phaser[225] using a high-resolution structure of WT CYP199A4 (1.54 Å, PDB: 5UVB) as the search model. The ligands and solvent molecules were removed from the search model prior to phasing to eliminate model bias. Weighted $2mF_o$-DF_c map and F_o-F_c difference map were obtained and used to rebuild the model in WinCoot and determine the substrate bound.[226] Structural refinements were carried out over multiple cycles using Phenix Refine, available in the Phenix suite of programs.[227]

Composite-omit or feature-enhanced maps that reduce model bias were generated in Phenix to allow inspection of the ligand binding site and reveal the location of all substrate atoms.[228,229] Detailed data collection and structural refinement statistics are provided in Supplementary Data.

The coordinates for the crystal structures were deposited in to the wwPDB (Worldwide Protein Data Bank).[251,252] Individual PDB accession codes have been presented where needed. To model the location of the Cpd I oxygen, the CreateAtomAlongBond script was employed. Computational studies of Cpd I have calculated that the Fe-O bond length is very consistent at 1.62 Å. This was determined both in absence and in presence of substrate for CYPs 2C9, 2D6, 3A4 and $P450_{cam}$.[230,231] The oxygen atom was thus positioned 1.62 Å from the heme iron of the CYP199A4 structures.

6.3 Results

6.3.1 Crystal Structure of WT CYP199A4 with 4-Phenylbenzoic acid

WT CYP199A4 is able to bind tightly to both 4-phenylbenzoic acid (1.7 µM, Table 6.1) and 4-cyclohexylbenzoic acid (0.45 µM, Table 6.1) while the former shows a faster NADH oxidation rate (902 min^{-1}) compared to the latter (169 min^{-1}).[220] WT CYP199A4 was unable to generate any oxidation products with 4-phenylbenzoic acid while 4-cyclohexylbenzoic acid formed both hydroxylation and desaturation products (Figure 6.5).[220] The *para*-substituents on both substrates are of similar size but differ in that 4-cyclohexylbenzoic acid has aliphatic C-H bonds while 4-phenylbenzoic acid has aromatic C-H bonds. It is noted that the cyclohexyl moiety adopts a chair-like conformation.[260] To elucidate why WT CYP199A4 is unable to oxidise 4-phenylbenzoic acid, the crystal structure of this P450 in complex with the aforementioned substrate was crystallised and its X-ray crystal structure was determined.

Table 6.1: Kinetic and substrate data for WT CYP199A4 with 4-phenyl- and 4-cyclohexylbenzoic acid. Rates are given as $\mu mol.\mu mol_{P450}{}^{-1}.min^{-1}$ (min^{-1}). Data for both substrates provided by Dr Tom Coleman.[220]

Substrate	% HS	K_d (µM)[a]	N[b]	PFR[c]	Coupling[d] (%)
4-phenylbenzoic acid	90	1.7 ± 0.1	902 ± 34	-[e]	-[e]
4-cyclohexylbenzoic acid	≥ 95	0.45 ± 0.05	169 ± 11	52 ± 6	33 ± 2

[a]Dissociation constant. [b]NADH oxidation rate. [c]Product formation rate. [d] % of NADH consumed that led to metabolite formation. [e] No product formation observed.

A crystal structure of WT CYP199A4 complexed with 4-phenylbenzoic acid (PDB: 7JW5) was determined with a resolution of 1.53 Å. The overall structural fold for WT CYP199A4 in complex with 4-phenylbenzoic acid was similar to a previously reported structure of the same enzyme (PDB: 4EGM) complexed with 4-ethylbenzoic acid (RMSD = 0.518, Figure E1). Within the active site of the solved structure, a region of electron density was readily modelled as 4-phenylbenzoic acid (Figure 6.7a).

The crystal structure of WT CYP199A4 complexed to 4-phenylbenzoic acid was then compared to a structure of the same enzyme but in complex with 4-cyclohexylbenzoic acid (PDB: 6C2D).[260] The latter structure was provided by Dr Tom Coleman of the University of Adelaide.[220] The active site residues of WT CYP199A4 showed minimal differences in conformation when 4-phenyl- or 4-cyclohexylbenzoic was bound (Figure 6.7b). When either substrate is bound, the F298 residue adopts a conformation that orients the residue away from the heme. This altered conformation of the

F298 residue is not observed when WT CYP199A4 is bound to 4-methoxybenzoic acid (Figure 6.8a).[137] A similar movement in residue F298 is observed when CYP199A4 is bound to bulky substrates such as 4-ethylthiobenzoic acid[220] and also with mutant F182L bound to an α-hydroxyketone compound, JCM 1 (Section 5.3.8, Figure 6.8b).

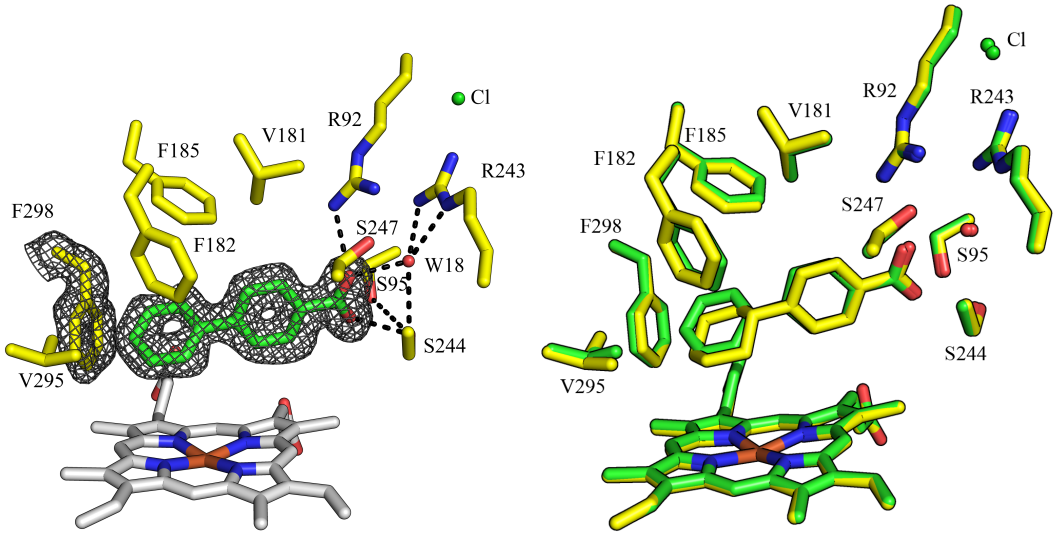

(a) (b)

Figure 6.7: (a) Crystal structure of WT CYP199A4 with co-crystallised with 4-phenylbenzoic acid (PDB 7JW5). A composite-omit map shown as a grey mesh contoured to 1.0 σ (1.5 Å carve) is shown around the substrate and residue F298. This crystal structure was solved to a resolution of 1.53 Å. (b) A comparison of the active site of WT CYP199A4 in complex with 4-phenylbenzoic acid (green sticks) against the same enzyme when bound to 4-cyclohexylbenzoic acid (yellow sticks, PDB: 6C2D).[220]

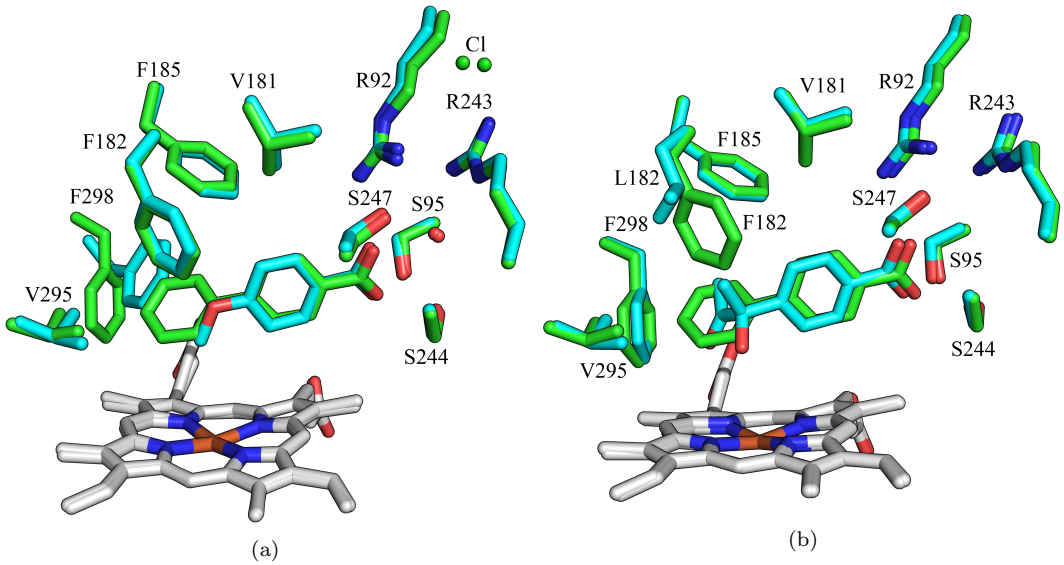

(a) (b)

Figure 6.8: (a) Active site structure of WT CYP199A4 with 4-methoxybenzoic acid (cyan sticks, PDB: 4DO1) compared to when 4-phenylbenzoic acid is bound (green sticks, PDB: 7JW5). (b) Active site structure of F182L-CYP199A4 bound to JCM 1 (cyan sticks, PDB: 8G35) compared to WT CYP199A4 bound to 4-phenylbenzoic acid (green sticks, PDB: 7JW5). In (b), the F298 residue orients away from the heme when either JCM 1 or 4-phenylbenzoic acid is bound, but not with 4-methoxybenzoic acid as seen in (a).

An oxygen atom was then modelled above the heme centre of WT CYP199A4 bound

to 4-phenylbenzoic acid. This oxygen atom was placed 1.62 Å away from the heme iron to approximate Cpd I.[230,231] Distances and angles between the substrate, Cpd I and other active site features were then measured and compared to the same measurements for the 4-cyclohexylbenzoic-bound structure (Table 6.2).[220] It was observed that the C_α, C_β and C_γ of 4-phenylbenzoic acid is positioned slightly further away (3.0 - 4.7 Å) from the modelled oxygen atom of Cpd I compared to equivalent atoms for 4-cyclohexylbenzoic acid (2.5 - 3.9 Å). But overall, the distances between carbons of the phenyl ring with active site residues was similar to equivalent measurements for the corresponding carbons in the cyclohexyl substituent (Table 6.2).

Overall, WT CYP199A4 binds both 4-phenylbenzoic acid and 4-cyclohexylbenzoic acid in a similar manner, which explains the high binding affinity of the P450 towards these substrates. However, no obvious explanation is revealed as to why 4-cyclohexylbenzoic acid is readily oxidised while 4-phenylbenzoic acid showed no activity was forthcoming.

Table 6.2: Distances and angles of the active site structure for WT CYP199A4 bound to 4-phenylbenzoic acid compared when 4-cyclohexylbenzoic acid is bound.

Distance (Å)	4-phenylbenzoic acid	4-cyclohexylbenzoic acid[b]
C_α - Fe	5.5	5.4
C_α - **O**=Fe	4.1	3.9
C_β - Fe	4.4	4.0
C_β - **O**=Fe	3.0	2.5
C_γ - Fe	4.7	4.2
C_γ - **O**=Fe	3.6	2.8
Angle (°)		
C_{04}-C_α-C_β	125.1	114.9
Dihedral[a]	59.1	45.3
C_α-C_β-C_γ	118.9	110.8
Fe=O-C_α	144.7	156.1
Fe=O-C_β	140.5	156.5
Fe=O-C_γ	126.6	137.8

[a]The atoms for the dihedral angle measured is shown below. [b]Data provided by Dr Tom Coleman.[220]

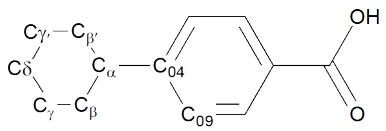

6.3.2 Reactions of F182L/F298V-CYP199A4 with 4-Phenylbenzoic acid

Based on the crystal structure of WT CYP199A4 bound to 4-phenylbenzoic acid, two different mutants of CYP199A4 were chosen in an attempt to enable aromatic hydroxylation in this P450 enzyme. Mutant F298V was chosen as introducing the less sterically demanding valine residue would allow for bulkier ligands to fill the space normally occupied by the side chain of residue F298. In the active site of WT CYP199A4, the C_α and C_β atoms of 4-phenylbenzoic acid is in close proximity to residue F182 (3.8 Å, Figure 6.10). Residue F182 was therefore mutated to a leucine to generate mutant F182L that should introduce additional space above the heme. An equivalent mutation in CYP199A2 enhanced aromatic hydroxylation with cinnamic acids.[154] This F182L mutant allowed the binding of α-hydroxyketones and enabled C-C cleavage activity with CYP199A4 (Chapter 5).

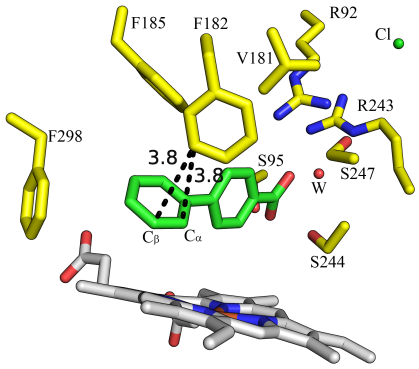

Figure 6.10: Distances measured (in Å) for the C_α and C_β atoms of 4-phenylbenzoic acid with residue F182 of WT CYP199A4 (PDB: 7JW5).

Mutants F182L and F298V were purified using the protocol in Section 6.2.2. NADH oxidation reactions with 4-phenylbenzoic acid were carried out with these two mutants. A negative control reaction was performed with WT CYP199A4 with the same substrate. The same mutants were tested with 4-cyclohexylbenzoic acid as a control for aliphatic hydroxylation. Kinetic data for both mutants is shown in Table 6.3.

Table 6.3: Kinetic data for F182L/F298V-CYP199A4 with 4-cyclohexylbenzoic acid and 4-phenylbenzoic acid. Rates are given as $\mu mol.\mu mol_{P450}{}^{-1}.min^{-1}$ (min^{-1}).

Mutant	Substrate	N[a]	PFR[b]	Coupling[c]
F182L	4-phenylbenzoic acid	75 ± 0.3	26 ± 3	30 ± 1.4
	4-cyclohexylbenzoic acid	115 ± 5	13 ± 1	11.3 ± 1.8
F298V	4-phenylbenzoic acid	1030 ± 90	-[d]	-[d]
	4-cyclohexylbenzoic acid	162 ± 55	52 ± 18	31 ± 9.3 %

[a]NADH oxidation rate. [b]Product formation rate. [c]% of NADH consumed that led to metabolite formation. [d]No product formation observed.

Reactions with 4-phenylbenzoic acid showed mutant F298V had a much faster NADH oxidation rate (1030 ± 90 min^{-1}) compared to mutant F182L (75 ± 0.3 min^{-1}, Table 6.3). However, HPLC analysis for the F298V mutant showed no product formation occurred with 4-phenylbenzoic acid (Figure 6.11). Product formation with the F182L mutant was more encouraging as three potential enzyme metabolites were detected with both HPLC (Figure 6.11) and GC-MS (Figure E2) analysis.

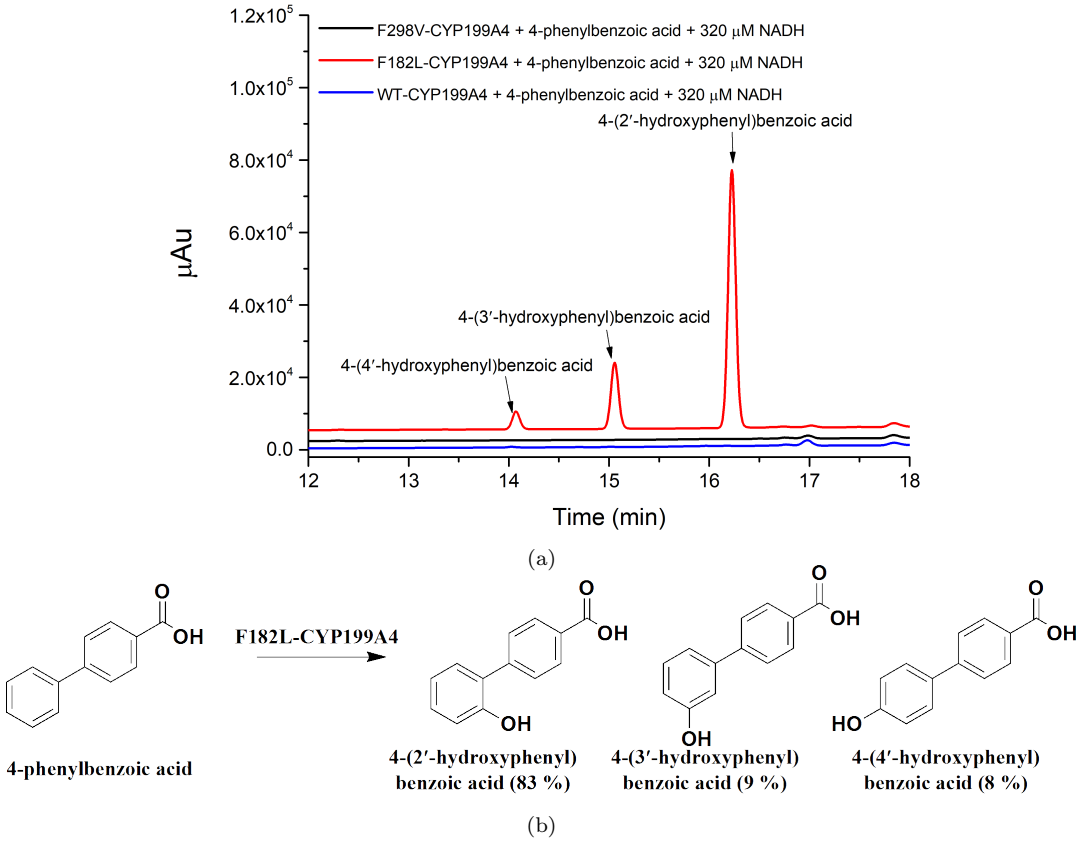

Figure 6.11: (a) HPLC analysis of the NADH oxidation reaction with WT CYP199A4 and 4-phenylbenzoic acid (blue). The same reactions with CYP199A4 mutants, F182L (red) and F298V (black) can be seen also. The chromatograms were offset in the y-axis for clarity Three different metabolites were detected in the reaction with the F182L mutant. These metabolites were identified as 4-(4′-hydroxyphenyl)benzoic acid (t_R = 14.1 min), 4-(3′-hydroxyphenyl)benzoic acid (t_R = 15.1 min) and 4-(2′-hydroxyphenyl)benzoic acid (t_R = 16.3 min). (b) Distribution of the products formed from the oxidation of 4-phenylbenzoic acid by F182L-CYP199A4.

Co-elution experiments (Figure 6.12 and E3) identified the metabolites detected as 4-(4′-hydroxyphenyl)benzoic acid, 4-(3′-hydroxyphenyl)benzoic acid and 4-(2′-hydroxyphenyl)benzoic acid which arise from *para*-, *meta*- and *ortho*-hydroxylation, respectively (Figure 6.11b). The MS spectra of the observed metabolites also matched those of the authentic product standards (Figure E4).

The major product formed from the oxidation of 4-phenylbenzoic acid by F182L-CYP199A4 was 4-(2′-hydroxyphenyl)benzoic acid (83 %). The remaining metabolites, 4-(4′-hydroxyphenyl)benzoic acid and 4-(3′-hydroxyphenyl)benzoic acid were formed at similar levels (8 - 9 %). The coupling efficiency for this reaction was 30 ± 1.4 %

that results in a product formation rate of 26 ± 3 min^{-1} (Table 6.3).

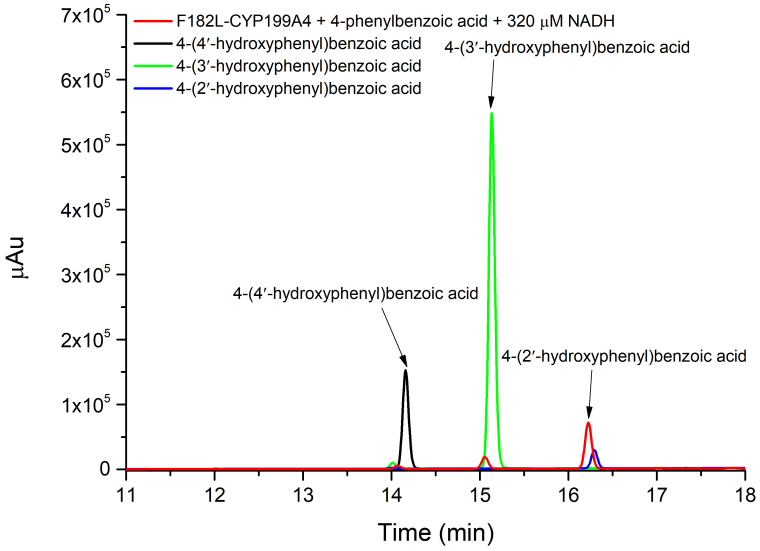

Figure 6.12: HPLC analysis of the reaction between F182L-CYP199A4 and 4-phenylbenzoic acid (red). Co-elution with standards of 4-(4′-hydroxyphenyl)benzoic acid (black, t_R = 14.1 min), 4-(3′-hydroxyphenyl)benzoic acid (green, t_R = 15.1 min) and 4-(2′-hydroxyphenyl)benzoic acid (blue, t_R = 16.3 min) can be seen also.

For the reaction of the F298V mutant with 4-cyclohexylbenzoic acid, the NADH oxidation rate was 162 ± 55 min^{-1} (Table 6.3) and comparable to that of the WT enzyme (169 min^{-1}, Table 6.1).[256] The F182L mutant showed a slower NADH oxidation rate of 115 ± 5 min^{-1}. HPLC analysis revealed both mutants formed metabolites with 4-cyclohexylbenzoic acid (Figure 6.13) and MS analysis (Figure E6) was used to identify the metabolites based on previously reported MS spectra of oxidation products arising from 4-cyclohexylbenzoic acid.[260]

For reactions carried out with 4-cyclohexylbenzoic acid, mutant F298V formed 4-(2′-hydroxycyclohexyl)benzoic acid as the major product (86 %) arising from the hydroxylation of the cyclohexy ring at the β position (Figure 6.13a). This product was also the major metabolite for WT CYP199A4 (76 %).[260] The F298V variant was able to generate a higher proportion of the hydroxylation product at the α-benzylic carbon (4-(1′-hydroxycyclohexyl)benzoic acid, 34 %) compared to the WT (24 %, Figure 6.13). For the F182L mutant, the hydroxylation product at this α carbon was instead the major metabolite formed while the levels of β-hydroxylation significantly decreased compared to the F298V mutant and WT CYP199A4 (Figure 6.13). The F182L mutant generated unknown metabolites (“ * ”) that eluted at t_R = 14.1 min and t_R = 13.4 min (Figure 6.13a). These unknown metabolites were observed at low levels with the WT and F298V variants. GC-MS analysis (Figure E6) for the F182L reaction showed the presence of singly and doubly hydroxylated metabolites. These hydroxylated metabolites could potentially be the unknown metabolites (“ * ”) detected in Figure 6.13a.

The unknown metabolites (t_R = 14.1 min, 13.4 min) eluted at an earlier retention time (Figure 6.13a) and could be double hydroxylation metabolites that are expected to be more polar.

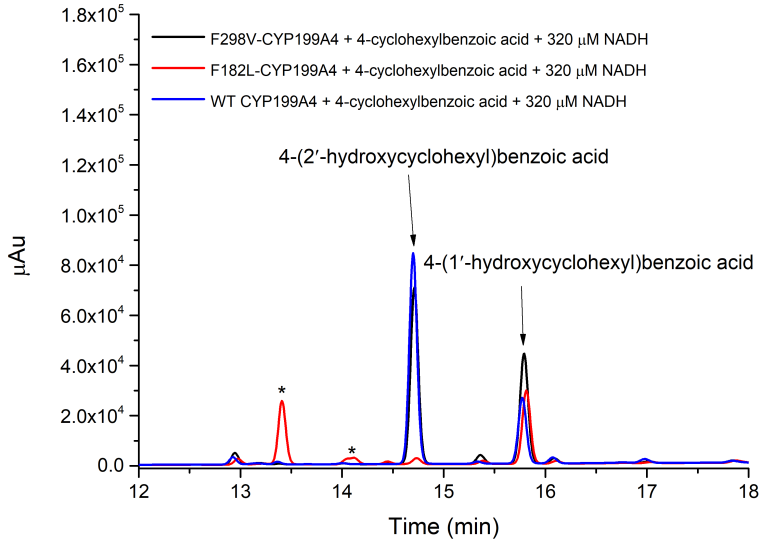

(a)

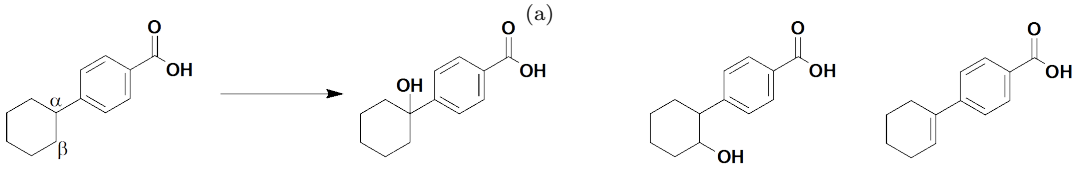

4-cyclohexylbenzoic acid	4-(1′-hydroxycyclohexyl) benzoic acid	4-(2′-hydroxycyclohexyl) benzoic acid	4-(cyclohex-1′-enyl) benzoic acid
WT	24 %	76 %	< 0.5 %
F298V	34 %	66 %	< 0.2 %
F182L[a]	50 %	5%	< 0.1 %

[a]Unknown Metabolites: " * " (45 %)

(b)

Figure 6.13: (a) HPLC analysis of the NADH oxidation reaction with WT CYP199A4 and 4-cyclohexylbenzoic acid (blue). The same reactions with CYP199A4 mutants, F182L (red) and F298V (black) can be seen also. Both 4-(2′-hydroxycyclohexyl)benzoic acid (t_R = 14.8 min) and 4-(1′-hydroxycyclohexyl)benzoic acid (t_R = 15.8 min) were detected in all three reactions and confirmed by GC-MS analysis. Early eluting metabolites (" * ") were detected for the F182L mutants at t_R = 14.1 min and t_R = 13.4 min. (b) Distribution of the products formed from the oxidation of 4-cyclohexylbenzoic acid by WT, F298V and F182L-CYP199A4. For the F182L mutant, metabolites at t_R = 14.1 min and t_R = 13.4 min form 45 % of the metabolites formed with this mutant.

The coupling efficiency calculated for the oxidation of 4-cyclohexylbenzoic acid by the F298V mutant was 31 ± 9.3 % with product forming at a rate of 52 ± 18 min^{-1}. The F182L mutant for the same reaction showed a coupling efficiency of 11.3 ± 1.8 % and a product forming at 13 ± 1 min^{-1}.

In summary, only the F182L mutant of CYP199A4 was able to carry out aromatic hydroxylation with 4-phenylbenzoic acid to give rise to hydroxylated metabolites with a preference for oxidation at the *ortho*-position. The F298V and F182L mutants were both able to oxidise 4-cyclohexylbenzoic acid with some changes in the product selectivity compared to WT CYP199A4.

6.4 Discussion

WT CYP199A4 was successfully crystallised with 4-phenylbenzoic acid and it's active site structure is largely similar to when 4-cyclohexylbenzoic acid is bound. This agrees with the tight binding observed for both substrates with WT CYP199A4. However, the crystal structures of WT CYP199A4 were unable to reveal why aromatic oxidation with 4-phenylbenzoic acid did not occur. Aromatic oxidation has been previously observed at low activity for CYP199A4 with 2-naphthoic acid and with high efficiency activity in other P450 systems.[48,274–276] When comparing the active site structures of CYP199A4 bound to 2-naphthoic acid and 4-phenylbenzoic acid, we can see the orientation of the aromatic ring differs significantly (Figure 6.14). One face of the π-aromatic ring of 2-naphthoic acid oriented towards the space above the oxygen binding site in CYP199A4 (Figure 6.14). When 4-phenylbenzoic acid is bound, neither face of the phenyl ring of the substrate faces the same plane as seen in 2-naphthoic acid and this orientation likely does not allow Cpd I of CYP199A4 to interact with the π-system of the substrate.

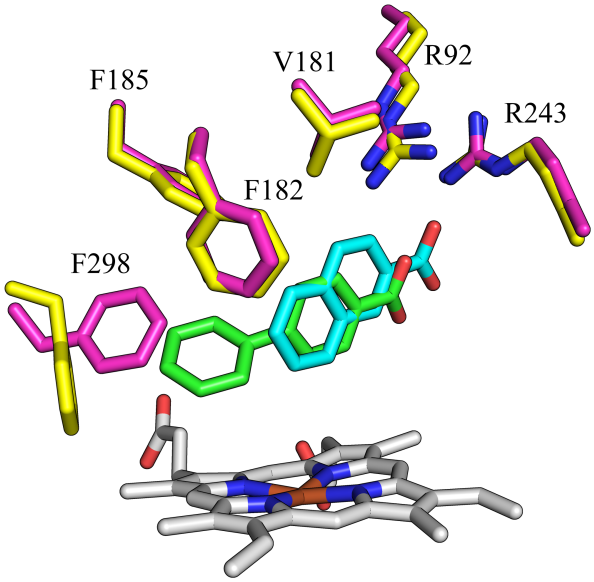

Figure 6.14: Comparing the active site structure of CYP199A4 bound to 2-napthoic acid (cyan sticks, PDB: 4EGP) against when the same enzyme is bound to 4-phenylbenzoic acid (green sticks, PDB: 7JW5). The binding orientation of the aromatic ring for the two substrates differ significantly.

Molecular dynamics (MD) simulations with WT CYP199A4 and 4-phenylbenzoic were carried out by Alicia Kirk at the University of Queensland. It was predicted that 4-phenylbenzoic acid was unable to attain a geometrical arrangement with Cpd I of CYP199A4 that was consistent with ideal geometries needed for aromatic oxidation to occur.[260] This lack of productive geometry prevents the Fe=O of Cpd I from interacting with the aromatic π-system of 4-phenylbenzoic acid.

Mutagenesis of the F182 residue of CYP199A4 to a leucine did successfully enable aromatic oxidation albeit with a slow product formation rate and low coupling efficiency. The F298V mutant was not successful in allowing aromatic oxidation. This agrees with previously reported studies of the closely related CYP199A2 enzyme where an equivalent mutation enhanced aromatic oxidation with cinnamic acid derivatives.[154] Mutant F182L was also studied in Chapter 5 to enable binding of α-hydroxyketone substrates and the mutant was able to demonstrate C-C cleavage activity with said substrates. The crystal structure of the F182L mutant (Figure 5.35) showed that additional space above the heme was afforded by the mutated active site residue. MD simulations of the F182L mutant bound to 4-phenylbenzoic acid was carried out by colleagues at the University of Queensland to elucidate why this mutant enabled aromatic oxidation.[256] It was demonstrated that additional space above the heme afforded by the L182 residue allowed the *para* phenyl ring of the substrate to rotate and achieve more productive conformations that enabled interactions between the phenyl π-system and Cpd I.[256] This productive conformation was likely not present with the F298V mutant.

The F182L mutant demonstrated a strong preference for hydroxylation at the *ortho* position of the phenyl ring. It is likely the binding orientation of the substrate possibly favours strong interactions between this position and the Fe=O of Cpd I. However, further MD simulations predict that *para* hydroxylation would be most preferred as this position showed the highest percentage of catalytically active poses during simulations.[256] It was also calculated that the *ortho* position has a lower energy barrier for oxidation and could explain why hydroxylation at this position was the major oxidation site observed experimentally.[256] Crystallisation of the F182L mutant with 4-phenylbenzoic would be needed to fully explain the product selectivity and enable further understanding on the geometric requirements for aromatic oxidation.

Mutants F298V and F182L was also able to catalyse the oxidation of 4-cyclohexylbenzoic acid with changes in product selectivity when compared to the WT enzyme. Mutant F182L strongly favoured oxidation at the α-benzylic position and the F298V mutant also showed higher selectivity for the same position compared to WT CYP199A4. WT CYP199A4 prefers oxidation at the β carbon and the crystal structure of the WT enzyme with 4-cyclohexylbenzoic acid reveals that the β carbon is positioned closest to the heme-iron.[260] The additional space in the active site afforded by both mutants likely allowed for a binding orientation that positioned the α-benzylic carbon closer to the heme to enhance the selectivity towards this position. The F182L mutant even showed formation of additional oxidation metabolites that were likely to arise from single or possibly even double hydroxylation events. The low coupling activity of the F182L mutant with 4-cyclohexylbenzoic acid would hinder its use with large-scale

whole-cell oxidation systems to generate these oxidation metabolites in larger yield for additional characterisation.[148] Further mutagenesis studies could be useful in attaining a CYP199A4 mutant that is able to generate higher levels of metabolites when oxidising 4-cyclohexylbenzoic acid.

Overall, aromatic oxidation was successfully enabled in CYP199A4 through rational mutagenesis. Further structural characterisation of this mutant would be useful to understand the requirements for aromatic oxidation by P450 enzymes.

7 Conclusions and Future Directions

In Chapter 2, the capability of different methods of supplying hydrogen peroxide (H_2O_2) *in situ* to P450 peroxygenases to drive enzymatic activity was explored. Mutant T252E is an engineered peroxygenase variant of CYP199A4 studied extensively in this work. *In situ* methods of supplying H_2O_2 include the use of the surrogate oxygen donor, urea-hydrogen peroxide (UHP) and a light-driven flavin system. Oxidative demethylation of 4-methoxybenzoic acid by T252E-CYP199A4 was achieved with UHP that yielded total turnover number (TTN) levels comparable when H_2O_2 was used at the same concentration. Optimisation of reactions conditions found 32 mM and 64 mM of either UHP or H_2O_2 gave the highest level of oxidised metabolite with 3 µM enzyme, 1 mM substrate at 30 °C. A flavin system that generates H_2O_2 from light and EDTA was also able to achieve total conversion of substrate to product for the reaction of T252E-CYP199A4 (2.5 % molar equivalents) with 4-methoxybenzoic acid (200 µM). This light-driven flavin system was also applied to the natural P450 peroxygenase, CYP151A1 ($P450_{BS\beta}$). Light-driven reactions with $P450_{BS\beta}$ and tetradecanoic acid showed metabolites consistent with oxidative decarboyxlation yielding shorter chain alkyl fatty acids alongside α/β-hydroxylation of said fatty acids.

This chapter also employed a deuterated substrate, 4-(methoxy-d_3)benzoic-d_4 acid in *O*-demethylation reactions with both T252E and WT variants of CYP199A4. It was found that no difference in product levels were observed between T252E (peroxygenase) or WT (monooxygenase) enzymes using the deuterated substrate, which suggests that no kinetic isotope effect was present. It is therefore concluded that C-H bond abstraction was not rate limiting in either peroxygenase and monooxygenase reaction mechanisms and consistent with Cpd I being the active intermediate with both mechanisms.

In Chapter 3, an enzymatic approach to generate H_2O_2 *in situ* for P450 peroxygenases was described. Three different oxidase enzymes, AldOx from *Streptomyces coelicolor* A3(2), AoFOx from *Aspergillus oryzae* and an engineered choline oxidase (AcC06-AcChOx) from *Arthrobacter cholorphenolicus* were investigated. AoFOx gave low expression of soluble protein but AldOx and AcC06-AcChOx was gave sufficiently high yield of purified protein. Both AldOx and AcC06-AcChOx was able to generate H_2O_2 in solution with T252E-CYP199A4 to allow the P450 enzyme to generate metabolites from the P450-catalysed demethylation of 4-methoxybenzoic acid through peroxygenase activity. When the concentration of either oxidase enzyme was lowered relative to the P450, the levels of product formation remained similar or only moderately lower

compared to when the oxidase and P450 enzymes were equal in concentration. This strongly suggests that the H_2O_2 production by the oxidase enzymes were not rate-limiting.

AldOx was also used to drive peroxygenase activity with the oxidation of tetradecanoic acid with $P450_{BS\beta}$. Product formation primarily from α/beta-hydroxylation was observed and evidence of fatty acid decarboyxlation was also present though to a lesser extent compared to the light-driven flavin system in Chapter 2. Future analysis into the amount and rate of H_2O_2 produced by the oxidase enzymes studied here could be useful to optimise reactions conditions involving oxidases and tune for selective oxidation reactions with P450 peroxygenases.

P450 peroxygenases provides an alternative biocatalytic pathway towards selective oxidation reactions that is both simpler and cost-effective compared to NADH-dependent reactions that require expensive co-factors and partner proteins. The optimisation of P450 peroxygenase reactions that were carried out here using T252E-CYP199A4 and different methods of supplying H_2O_2 *in situ* provides a platform to applying these methods to other P450 peroxygenases with useful synthetic applications (Figure 7.1).

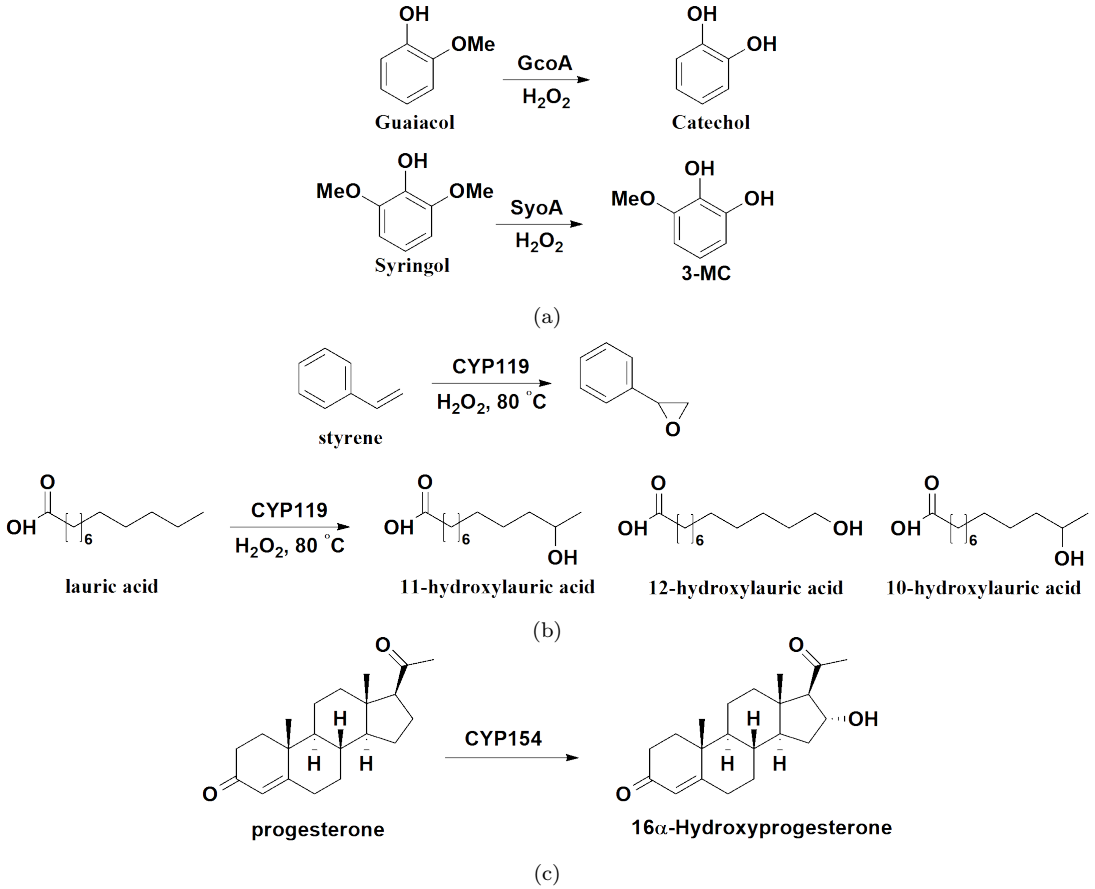

Figure 7.1: Reactions catalysed by P450 Peroxygenases. (a) CYP255 family of enzymes, GcoA and SyoA catalyses demethylation of lignin monoaromatics. (b) Thermophilic CYP119 catalyses epoxidation of styrene and ω-hydroxylation of fatty acids (c) CYP154 catalyses hydroxylation of progesterone.

P450 peroxygenases that are of interest for further study with *in situ* generation of H_2O_2 include the CYP255 family (GcoA and SyoA) that are *O*-demethylases of lignin monoaromatics (Figure 7.1a), whereby facile and cheap reactions with these P450 enzymes could provide new ways of supplying useful chemicals and materials derived from lignin waste.[277] A thermophilic P450 peroxygenase, CYP119 from *Sulfolobus solfataricus* is also a potential target to explore high temperature P450 reactions with faster reaction rates and product formation (Figure 7.1b).[278] P450 peroxygenases have also been reported to be involved in steroid metabolism, whereby CYP154 is able to catalyse the hydroxylation of progesterone using H_2O_2 (Figure 7.1c).[279,280] Peroxygenase reactions using CYP154 with the optimised methods presented here could provide an alternative pathway towards steroid metabolites derived from P450 oxidation activity that is cheaper and more accessible without resorting to highly challenging mammalian P450 systems.

Chapter 3 also explored constructing dual-function fusion enzymes that possesses both oxidase and P450 peroxygenase domains through isothermal DNA assembly. This approach would have allowed the P450 domain to utilise H_2O_2 generated by the oxidase in close proximity for peroxygenase reactions. The sequences of these fusion enzymes were successfully cloned into plasmid vectors, whereby an individual oxidase (AldOx, AoFOx and AcC06-AcChOx) was fused to T252E-CYP199A4. However, the expression of these fusion enzymes in *E.coli* were not successful. Optimising the expression of these fusion enzymes would be an important step to investigate the viability of this approach.

In addition, T252E-CYP199A4 was used in Chapter 3 for flow biocatalysis reactions driven by peroxygenase activity. The T252E mutant was successfully immobilised to SOURCE15Q ion exchange media. Subsequent experiments showed enzymatic metabolite formation with the immobilised enzyme in the presence of H_2O_2 and enzymatic activity was remained present even after immobilisation for 100 h. Flow biocatalysis reactions with immobilised T252E-CYP199A4 were performed and low levels of substrate conversion was observed. Flow biocatalysis reactions require fast enzymatic reaction rates. To improve the use of CYP199A4 for flow biocatalysis reactions, mutagenesis studies with this enzyme could be carried to enable faster peroxygenase reactions at lower concentrations of H_2O_2.

In Chapter 4, crystals of T252E-CYP199A4 in-complex with 4-methoxybenzoic acid showed evidence of *in crystallo* demethylation of the bound substrate after soaking with H_2O_2. This represents a significant step to investigate reaction intermediates for the P450 peroxygenase pathway of which the mechanism that forms Cpd I for this pathway is still unclear. The highest reported occupancy of the enzyme-bound

product relative to the initial substrate was 70 % with the conditions used in this chapter. Further testing and optimisation of crystal soaking conditions could be carried out with substrates of different P450 reactions such as hydroxylation, epoxidation and sulfoxidation to possibly trap and observe intermediates involved in these reactions. This study also provides a foundation for carrying out a larger breadth of *in crystallo* reactions with other P450 peroxygenases (Figure 7.1). Mutagenesis approaches could be applied to tune *in crystallo* peroxygenase activity and trap intermediates to better understand how H_2O_2 interacts with these enzymes.

Chapter 5 presents a successful attempt at modelling C-C bond cleavage/lyase activity of mammalian CYP17A1 with a bacterial P450. Substrates that mimic the α-hydroxyketone moiety of CY17A1 substrates were employed including a specifically designed substrate, JCM 1. Mutant F182L of CYP199A4 showed conclusively that C-C cleavage activity with an α-hydroxyketone substrate was introduced via rational mutagenesis of this P450 enzyme. A preliminary investigation exploring kinetic solvent isotope effects (KSIE) with the C-C cleavage reaction of F182L-CYP199A4 showed a small inverse KSIE present which would implicate the ferric peroxo anion intermediate involved in P450-catalysed C-C cleavage reactions. Conversely, the hydroxylation pathway showed a normal KSIE. The inverse KSIE observed during C-C cleavage activity was consistent with similar studies with CYP17A1 and shows that F182L-CYP199A4 is a suitable model for C-C cleavage reactions with α-hydroxyketones. The C-C cleavage reaction with JCM 1 generates metabolites that can be further hydroxylated by the F182L mutant and complicates downstream analysis. The partitioning of the C-C cleavage and hydroxylation reaction through mutagenesis of the F182L mutant would potentially generate more useful mutants to model CYP17A1 activity.

In addition, a crystal structure of F182L-CYP199A4 in complex with a bespoke α-hydroxyketone, JCM 1 was solved and reported in Chapter 5. The active site structure of this enzyme seems to preferentially bind the (*S*)-enantiomer of JCM 1. There was also a cluster of active site water molecules present in this mutant not seen with the WT enzyme. The F182L mutant was also able to show C-C cleavage activity with JCM 1 as a peroxygenase in the presence of H_2O_2. The crystals of this F182L mutant could then be used for *in crystallo* reactions using this mutant as seen in Chapter 4. An alternative *in crystallo* approach could involve reducing a crystal of this P450 with X-ray beams to generate Cpd I directly. These crystallographic approaches could potentially allow intermediates of P450-catalysed C-C cleavage reactions to be trapped and observed.

The work presented in Chapter 5 provides a basis for CYP199A4 to model not just C-C

cleavage reactions of CYP17A1 but also P450s such as mammalian derived CYP11A1[96] and CYP51[95] or CYP125 from *Mycobacterium tuberculosis*.[281] Substrates of these P450s that mimic the reaction centre of their physiological substrates (Figure 7.2) could be used concurrently with rational mutagenesis of CYP199A4 to model these reactions.

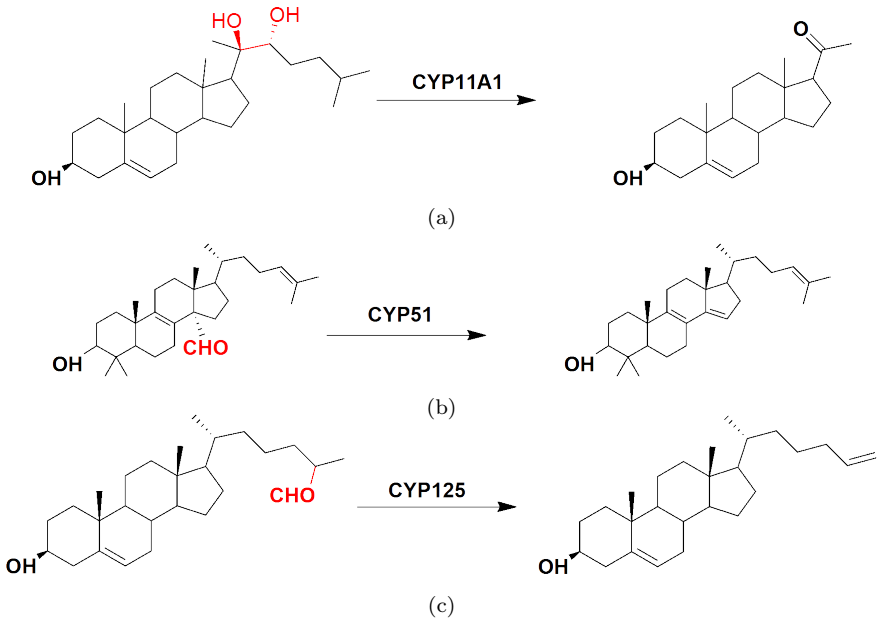

Figure 7.2: Different P450-catalysed C-C bond cleavage reactions that could potentially be modelled by CYP199A4. The reaction centres of each substrate is highlighted in red.

In Chapter 6, aromatic oxidation was successfully enabled in CYP199A4 through mutagenesis. The F182L mutant was able to catalyse the hydroxylation of the phenyl substituent of 4-phenylbenzoic acid with a preference for the *ortho* position. The hydroxylation metabolites at the *meta* and *para* positions were formed at lower levels. Solving a crystal structure of the F182L mutant in complex with 4-phenylbenzoic acid would be essential to rationalise the regioselectivity observed with this mutant. There is evidence that P450-catalysed hydroxylation at the *meta* position employs a different mechanism (*ipso*-substitution) than for *ortho* or *para* hydroxylation (NIH-shift).[270,273] The generation of new mutants of CYP199A4 that have exclusive regioselectivity at the *meta* or *ortho*/*para* positions could function as models for aromatic hydroxylation and probe the mechanistic underpinnings of this P450-catalysed reaction.

In summary, this thesis presents reaction and protein engineering studies with P450 enzymes to enable efficient and selective oxidations while also introducing new enzymatic activity in the enzymes studied. Chemical oxygen surrogates and light-driven flavin systems were able to allow T252E-CYP199A4 to carry out efficient oxidation reactions driven by peroxygenase activity. The application of oxidase enzymes to generate H_2O_2

for P450 peroxygenase enzymes was also explored. Protein engineering also enabled both C-C bond cleavage and aromatic oxidation with CYP199A4 which allows this enzyme to act as a suitable model for both reactions.

References

[1] Paul, P. E. V.; Sangeetha, V.; Deepika, R. G. *Recent Developments in Applied Microbiology and Biochemistry*; Elsevier, 2019; pp 107–125.

[2] Schmid, A.; Dordick, J. S.; Hauer, B.; Kiener, A.; Wubbolts, M.; Witholt, B. Industrial biocatalysis today and tomorrow. *Nature* **2001**, *409*, 258–268.

[3] Breuer, M.; Ditrich, K.; Habicher, T.; Hauer, B.; Keßeler, M.; Stürmer, R.; Zelinski, T. Industrial Methods for the Production of Optically Active Intermediates. *Angew. Chem. Int. Ed.* **2004**, *43*, 788–824.

[4] Menzel, A.; Werner, H.; Altenbuchner, J.; Gröger, H. From Enzymes to Designer Bugs in Reductive Amination: A New Process for the Synthesis of L-*tert*-Leucine Using a Whole Cell-Catalyst. *Eng. Life Sci.* **2004**, *4*, 573–576.

[5] Xu, Z. et al. Process Research and Development for an Efficient Synthesis of the HIV Protease Inhibitor BMS-232632. *Org. Process Res. Dev.* **2002**, *6*, 323–328.

[6] Solano, D. M.; Hoyos, P.; Hernáiz, M.; Alcántara, A.; Sánchez-Montero, J. Industrial biotransformations in the synthesis of building blocks leading to enantiopure drugs. *Bioresour. Technol.* **2012**, *115*, 196–207.

[7] Li, J.; Pan, J.; Zhang, J.; Xu, J.-H. Stereoselective synthesis of l-tert-leucine by a newly cloned leucine dehydrogenase from Exiguobacterium sibiricum. *J. Mol. Catal. B: Enzym.* **2014**, *105*, 11–17.

[8] Uppada, V.; Bhaduri, S.; Noronha, S. B. Cofactor regeneration – an important aspect of biocatalysis. *Curr. Sci.* **2014**, *106*, 946–957.

[9] Wang, L.; Zhu, W.; Gao, Z.; Zhou, H.; Cao, F.; Jiang, M.; Li, Y.; Jia, H.; Wei, P. Biosynthetic L-tert-leucine using *Escherichia coli* co-expressing a novel NADH-dependent leucine dehydrogenase and a formate dehydrogenase. *Electron. J. Biotechnol.* **2020**, *47*, 83–88.

[10] Wichmann, R.; Wandrey, C.; Bückmann, A. F.; regina Kula, M. Continuous enzymatic transformation in an enzyme membrane reactor with simultaneous NAD(H) regeneration. *Biotechnol. Bioeng.* **1981**, *23*, 2789–2802.

[11] Wu, S.; Snajdrova, R.; Moore, J. C.; Baldenius, K.; Bornscheuer, U. T. Biocatalysis: Enzymatic Synthesis for Industrial Applications. *Angew. Chem. Int. Ed.* **2021**, *60*, 88–119.

[12] Marshall, J. R.; Mangas-Sanchez, J.; Turner, N. J. Expanding the synthetic scope of biocatalysis by enzyme discovery and protein engineering. *Tetrahedron* **2021**, *82*, 131926.

[13] Dunham, N. P.; Arnold, F. H. Nature's Machinery, Repurposed: Expanding the Repertoire of Iron-Dependent Oxygenases. *ACS Catal.* **2020**, *10*, 12239–12255.

[14] Pau, M. Y. M.; Lipscomb, J. D.; Solomon, E. I. Substrate activation for O_2 reactions by oxidized metal centers in biology. *Proc. Natl. Acad. Sci. U.S.A.* **2007**, *104*, 18355–18362.

[15] Groves, J. T. The bioinorganic chemistry of iron in oxygenases and supramolecular assemblies. *Proc. Natl. Acad. Sci. U.S.A.* **2003**, *100*, 3569–3574.

[16] Mueller, E. J.; Loida, P. J.; Sligar, S. G. In *Cytochrome P450: Structure, Mechanism, and Biochemistry*; de Montellano, P. R. O., Ed.; Springer US: Boston, MA, 1995; pp 83–124.

[17] Sundaramoorthy, M.; Terner, J.; Poulos, T. L. The crystal structure of chloroperoxidase: a heme peroxidase–cytochrome P450 functional hybrid. *Structure* **1995**, *3*, 1367–1378.

[18] Nelson, D. R. Cytochrome P450 diversity in the tree of life. *Biochim. Biophys. Acta, Proteins Proteomics* **2017**,

[19] de Montellano, P. R. O. Hydrocarbon Hydroxylation by Cytochrome P450 Enzymes. *Chem. Rev.* **2010**, *110*, 932–948.

[20] Graham-Lorence, S.; Truan, G.; Peterson, J. A.; Falck, J. R.; Wei, S.; Helvig, C.; Capdevila, J. H. An Active Site Substitution, F87V, Converts Cytochrome P450 BM-3 into a Regio- and Stereoselective (14S,15R)-Arachidonic Acid Epoxygenase. *J. Biol. Chem.* **1997**, *272*, 1127–1135.

[21] Narhi, L. O.; Fulco, A. J. Characterization of a catalytically self-sufficient 119,000-dalton cytochrome P-450 monooxygenase induced by barbiturates in Bacillus megaterium. *J. Biol. Chem.* **1986**, *261*, 7160–7169.

[22] Ji, L.; Faponle, A. S.; Quesne, M. G.; Sainna, M. A.; Zhang, J.; Franke, A.; Kumar, D.; van Eldik, R.; Liu, W.; de Visser, S. P. Drug Metabolism by Cytochrome P450 Enzymes What Distinguishes the Pathways Leading to Substrate Hydroxylation Over Desaturation. *Chem. Eur. J* **2015**, *21*, 9083–9092.

[23] Bell, S. G.; Yang, W.; Dale, A.; Zhou, W.; Wong, L.-L. Improving the affinity and activity of CYP101D2 for hydrophobic substrates. *Appl. Microbiol. Biotechnol.* **2012**, *97*, 3979–3990.

[24] Bell, S. G.; Rouch, D. A.; Wong, L.-L. Selective aliphatic and aromatic carbon-hydrogen bond activation catalysed by mutants of cytochrome p450cam. *J. Mol. Catal. B: Enzym.* **1997**, *3*, 293 – 302.

[25] Shoji, O.; Wiese, C.; Fujishiro, T.; Shirataki, C.; Wünsch, B.; Watanabe, Y. Aromatic C–H bond hydroxylation by P450 peroxygenases: a facile colorimetric assay for monooxygenation activities of enzymes based on Russig's blue formation. *J. Biol. Inorg. Chem.* **2010**, *15*, 1109–1115.

[26] Cryle, M. J.; Voss, J. J. D. Carbon–carbon bond cleavage by cytochrome $P450_{Biol}$ (CYP107H1). *Chem. Commun.* **2004**, 86–87.

[27] Varfaj, F.; Zulkifli, S. N. A.; Park, H.-G.; Challinor, V. L.; Voss, J. J. D.; de Montellano, P. R. O. Carbon-Carbon Bond Cleavage in Activation of the Prodrug Nabumetone. *Drug Metab. Dispos.* **2014**, *42*, 828–838.

[28] Zhang, X.; Li, S. Expansion of chemical space for natural products by uncommon P450 reactions. *Nat. Prod. Rep.* **2017**, *34*, 1061–1089.

[29] Shiraga, T.; Kaneko, H.; Iwasaki, K.; Tozuka, Z.; Suzuki, A.; T., H. A. T. A. Identification of cytochrome P450 enzymes involved in the metabolism of zotepine, an antipsychotic drug, in human liver microsomes. *Xenobiotica* **1999**, *29*, 217–229.

[30] Coleman, T.; Wong, S. H.; Podgorski, M. N.; Bruning, J. B.; De Voss, J. J.; Bell, S. G. Cytochrome P450 CYP199A4 from Rhodopseudomonas palustris Catalyzes Heteroatom Dealkylations, Sulfoxidation, and Amide and Cyclic Hemiacetal Formation. *ACS Catal.* **2018**, *8*, 5915–5927.

[31] Nelson, D. R.; Kamataki, T.; Waxman, D. J.; Guengerich, F. P.; Estabrook, R. D.; Feyereisen, R.; Gonzalez, F. J.; Minor J., C.; Gunsalus, I. C.; Gotoh, O.; Okuda, K.; Nebert, D. W. The P450 Superfamily: Update on New Sequences, Gene Mapping, Accession Numbers, Early Trivial Names of Enzymes, and Nomenclature. *DNA Cell Biol.* **1993**, *12*, 1–51.

[32] Katagiri, M.; Ganguli, B. N.; Gunsalus, I. C. A Soluble Cytochrome P-450 Functional in Methylene Hydroxylation. *J. Biol. Chem.* **1968**, *243*, 3543–3546.

[33] Hrycay, E. G.; Bandiera, S. M. *Monooxygenase, Peroxidase and Peroxygenase Properties and Mechanisms of Cytochrome P450*; Springer International Publishing: Cham, 2015; pp 1–61.

[34] Ortiz de Montellano, P. R.; De Voss, J. J. In *Cytochrome P450: Structure, Mechanism, and Biochemistry*; Ortiz de Montellano, P. R., Ed.; Springer US: Boston, MA, 2005; pp 183–245.

[35] Dawson, J. H.; Sono, M. Cytochrome P-450 and chloroperoxidase: thiolate-ligated heme enzymes. Spectroscopic determination of their active-site structures and mechanistic implications of thiolate ligation. *Chem. Rev.* **1987**, *87*, 1255–1276.

[36] Omura, T.; Sato, R. The Carbon Monoxide-binding Pigment of Liver Microsomes. *J. Biol. Chem.* **1964**, *239*, 2370–2378.

[37] Estabrook, R. W.; Hildebrandt, A. G.; Baron, J.; Netter, K. J.; Leibman, K. A new spectral intermediate associated with cytochrome P-450 function in liver microsomes. *Biochem. Biophys. Res. Commun.* **1971**, *42*, 132–139.

[38] Holtmann, D.; Hollmann, F. The Oxygen Dilemma: A Severe Challenge for the Application of Monooxygenases? *ChemBioChem* **2016**, *17*, 1391–1398.

[39] Grinkova, Y. V.; Denisov, I. G.; McLean, M. A.; Sligar, S. G. Oxidase uncoupling in heme monooxygenases: Human cytochrome P450 CYP3A4 in Nanodiscs. *Biochem. Biophys. Res. Commun.* **2013**, *430*, 1223–1227.

[40] Wang, Y.; Li, Y.; Wang, B. Stochastic Simulations of the Cytochrome P450 Catalytic Cycle. *J. Phys. Chem. B* **2007**, *111*, 4251–4260.

[41] Bernhardt, R. Cytochromes P450 as versatile biocatalysts. *J. Biotechnol.* **2006**, *124*, 128 – 145, BioPerspectives—From basic research to industrial production-BioPerspectives Congress.

[42] Makris, T. M.; Denisov, I.; Schlichting, I.; Sligar, S. G. In *Cytochrome P450: Structure, Mechanism, and Biochemistry*; Ortiz de Montellano, P. R., Ed.; Springer US: Boston, MA, 2005; pp 149–182.

[43] Rittle, J.; Green, M. T. Cytochrome P450 Compound I: Capture, Characterization, and C-H Bond Activation Kinetics. *Science* **2010**, *330*, 933–937.

[44] Groves, J. T.; McClusky, G. A. Aliphatic hydroxylation via oxygen rebound. Oxygen transfer catalyzed by iron. *J. Am. Chem. Soc.* **1976**, *98*, 859–861.

[45] Denisov, I. G.; Sligar, S. G. In *Cytochrome P450: Structure, Mechanism, and Biochemistry*; Ortiz de Montellano, P. R., Ed.; Springer International Publishing: Cham, 2015; pp 69–109.

[46] Altun, A.; Shaik, S.; Thiel, W. What is the Active Species of Cytochrome P450 during Camphor Hydroxylation? QM/MM Studies of Different Electronic States of Compound I and of Reduced and Oxidized Iron-Oxo Intermediates. *J. Am. Chem. Soc.* **2007**, *129*, 8978–8987.

[47] Luthra, A.; Denisov, I. G.; Sligar, S. G. Spectroscopic features of cytochrome P450 reaction intermediates. *Arch. Biochem. Biophys.* **2011**, *507*, 26–35.

[48] Bell, S. G.; Zhou, R.; Yang, W.; Tan, A. B. H.; Gentleman, A. S.; Wong, L.-L.; Zhou, W. Investigation of the Substrate Range of CYP199A4: Modification of the Partition between Hydroxylation and Desaturation Activities by Substrate and Protein Engineering. *Chem. Eur. J.* **2012**, *18*, 16677–16688.

[49] Locuson, C. W.; Hutzler, J. M.; Tracy, T. S. Visible Spectra of Type II Cytochrome P450-Drug Complexes: Evidence that "Incomplete" Heme Coordination Is Common. *Drug Metab. Dispos.* **2007**, *35*, 614–622.

[50] Koppenol, W. H. Oxygen Activation by Cytochrome P450: A Thermodynamic Analysis. *J. Am. Chem. Soc.* **2007**, *129*, 9686–9690.

[51] Li, Y.; Ma, Y.; Li, P.; Zhang, X.; Ribitsch, D.; Alcalde, M.; Hollmann, F.; Wang, Y. Enantioselective Sulfoxidation of Thioanisole by Cascading a Choline Oxidase and a Peroxygenase in the Presence of Natural Deep Eutectic Solvents. *ChemPlusChem* **2020**, *85*, 254–257.

[52] Poulos, T. L. Heme Enzyme Structure and Function. *Chem. Rev.* **2014**, *114*, 3919–3962.

[53] Blanksby, S. J.; Ellison, G. B. Bond Dissociation Energies of Organic Molecules. *Acc. Chem. Res.* **2003**, *36*, 255–263.

[54] Tian, Z.; Fattahi, A.; Lis, L.; Kass, S. R. Cycloalkane and Cycloalkene C-H Bond Dissociation Energies. *J. Am. Chem. Soc.* **2006**, *128*, 17087–17092.

[55] Modi, A. R.; Dawson, J. H. *Advances in Experimental Medicine and Biology*; Springer International Publishing, 2015; pp 63–81.

[56] de Montellano, P. R. O.; Voss, J. J. D. Oxidizing species in the mechanism of cytochrome P450. *Nat. Prod. Rep.* **2002**, *19*, 477–493.

[57] Coon, M. J.; Vaz, A. D. N.; McGinnity, D. F.; Peng, H.-M. Multiple Activated Oxygen Species in P450 Catalysis. *Drug Metab. Dispos.* **1998**, *26*, 1190–1193.

[58] Akhtar, M.; Wright, J. N.; Lee-Robichaud, P. A review of mechanistic studies on aromatase (CYP19) and 17α-hydroxylase-17,20-lyase (CYP17). *J. Steroid Biochem. Mol. Biol.* **2011**, *125*, 2–12.

[59] Akhtar, M.; Njar, V. C.; Wright, J. N. Mechanistic studies on aromatase and related C-C bond cleaving P-450 enzymes. *J. Steroid Biochem. Mol. Biol.* **1993**, *44*, 375–387.

[60] Akhtar, M.; Corina, D.; Miller, S.; Shyadehi, A. Z.; Wright, J. N. Mechanism of the Acyl-Carbon Cleavage and Related Reactions Catalyzed by Multifunctional P-450s: Studies on Cytochrome P-45017.alpha. *Biochemistry (Mosc.)* **1994**, *33*, 4410–4418.

[61] Akhtar, M.; Wright, J. N. *Advances in Experimental Medicine and Biology*; Springer International Publishing, 2015; pp 107–130.

[62] de Montellano, P. R. O.; Stearns, R. A. Timing of the radical recombination step in cytochrome P-450 catalysis with ring-strained probes. *J. Am. Chem. Soc.* **1987**, *109*, 3415–3420.

[63] Auclair, K.; Hu, Z.; Little, D. M.; de Montellano, P. R. O.; Groves, J. T. Revisiting the Mechanism of P450 Enzymes with the Radical Clocks Norcarane and Spiro[2,5]octane. *J. Am. Chem. Soc.* **2002**, *124*, 6020–6027.

[64] Newcomb, M.; Tadic-Biadatti, M.-H. L.; Chestney, D. L.; Roberts, E. S.; Hollenberg, P. F. A nonsynchronous concerted mechanism for cytochrome P-450 catalyzed hydroxylation. *J. Am. Chem. Soc.* **1995**, *117*, 12085–12091.

[65] Newcomb, M.; Shen, R.; Choi, S.-Y.; Toy, P. H.; Hollenberg, P. F.; Vaz, A. D. N.; Coon, M. J. Cytochrome P450-Catalyzed Hydroxylation of Mechanistic Probes that Distinguish between Radicals and Cations. Evidence for Cationic but Not for Radical Intermediates. *J. Am. Chem. Soc.* **2000**, *122*, 2677–2686.

[66] Toy, P. H.; Dhanabalasingam, B.; Newcomb, M.; Hanna, I. H.; Hollenberg, P. F. A Substituted Hypersensitive Radical Probe for Enzyme-Catalyzed Hydroxylations: Synthesis of Racemic and Enantiomerically Enriched Forms and Application in a Cytochrome P450-Catalyzed Oxidation. *J. Org. Chem.* **1997**, *62*, 9114–9122.

[67] Toy, P. H.; Newcomb, M.; Hollenberg, P. F. Hypersensitive Mechanistic Probe Studies of Cytochrome P450-Catalyzed Hydroxylation Reactions. Implications for the Cationic Pathway. *J. Am. Chem. Soc.* **1998**, *120*, 7719–7729.

[68] Newcomb, M.; Lansakara-P., D. S. P.; Kim, H.-Y.; Chandrasena, R. E. P.; Lippard, S. J.; Beauvais, L. G.; Murray, L. J.; Izzo, V.; Hollenberg, P. F.; Coon, M. J. Products from Enzyme-Catalyzed Oxidations of Norcarenes. *J. Org. Chem.* **2007**, *72*, 1128–1133.

[69] Newcomb, M.; Aebisher, D.; Shen, R.; Chandrasena, R. E. P.; Hollenberg, P. F.; Coon, M. J. Kinetic Isotope Effects Implicate Two Electrophilic Oxidants in Cytochrome P450-Catalyzed Hydroxylations. *J. Am. Chem. Soc.* **2003**, *125*, 6064–6065.

[70] Sharma, P. K.; de Visser, S. P.; Shaik, S. Can a Single Oxidant with Two Spin States Masquerade as Two Different Oxidants? A Study of the Sulfoxidation Mechanism by Cytochrome P450. *J. Am. Chem. Soc.* **2003**, *125*, 8698–8699.

[71] Shaik, S.; Kumar, D.; de Visser, S. P.; Altun, A.; Thiel, W. Theoretical Perspective on the Structure and Mechanism of Cytochrome P450 Enzymes. *Chem. Rev.* **2005**, *105*, 2279–2328.

[72] Shaik, S.; Hirao, H.; Kumar, D. Reactivity patterns of cytochrome P450 enzymes: multifunctionality of the active species, and the two states–two oxidants conundrum. *Nat. Prod. Rep.* **2007**, *24*, 533–552.

[73] Shaik, S.; Cohen, S.; Wang, Y.; Chen, H.; Kumar, D.; Thiel, W. P450 Enzymes: Their Structure, Reactivity, and Selectivity—Modeled by QM/MM Calculations. *Chem. Rev.* **2009**, *110*, 949–1017.

[74] Visser, S.; Porro, C.; Quesne, M.; Sainna, M.; Munro, A. Overview on Theoretical Studies Discriminating the Two-Oxidant Versus Two-State-Reactivity Models for Substrate Monoxygenation by Cytochrome P450 Enzymes. *Curr. Top. Med. Chem.* **2013**, *13*, 2218–2232.

[75] Kamachi, T.; Yoshizawa, K. A Theoretical Study on the Mechanism of Camphor Hydroxylation by Compound I of Cytochrome P450. *J. Am. Chem. Soc.* **2003**, *125*, 4652–4661.

[76] Guallar, V.; Baik, M.-H.; Lippard, S. J.; Friesner, R. A. Peripheral heme substituents control the hydrogen-atom abstraction chemistry in cytochromes P450. *Proc. Natl. Acad. Sci. U.S.A.s* **2003**, *100*, 6998–7002.

[77] Shaik, S.; Cohen, S.; de Visser, S. P.; Sharma, P. K.; Kumar, D.; Kozuch, S.; Ogliaro, F.; Danovich, D. The "Rebound Controversy": An Overview and Theoretical Modeling of the Rebound Step in C-H Hydroxylation by Cytochrome P450. *Eur. J. Inorg. Chem.* **2004**, *2004*, 207–226.

[78] de Montellano, P. R. O. *Cytochrome P450*; Springer International Publishing, 2015; pp 111–176.

[79] Rydberg, P.; Ryde, U.; Olsen, L. Sulfoxide, Sulfur, and Nitrogen Oxidation and Dealkylation by Cytochrome P450. *J. Chem. Theory Comput.* **2008**, *4*, 1369–1377.

[80] Alvarez, J. C.; de Montellano, P. R. O. Thianthrene 5-oxide as a probe of the electrophilicity of hemoprotein oxidizing species. *Biochemistry (Mosc.)* **1992**, *31*, 8315–8322.

[81] Cryle, M. J.; Voss, J. J. D. Is the Ferric Hydroperoxy Species Responsible for Sulfur Oxidation in Cytochrome P450s? *Angew. Chem. Int. Ed.* **2006**, *45*, 8221–8223.

[82] Volz, T. J.; Rock, D. A.; Jones, J. P. Evidence for Two Different Active Oxygen Species in Cytochrome P450 BM3 Mediated Sulfoxidation and N-Dealkylation Reactions. *J. Am. Chem. Soc.* **2002**, *124*, 9724–9725.

[83] Wang, B.; Li, C.; Cho, K.-B.; Nam, W.; Shaik, S. The Fe^{III}-H_2O_2 Complex as a Highly Efficient Oxidant in Sulfoxidation Reactions: Revival of an Underrated Oxidant in Cytochrome P450. *J. Chem. Theory Comput.* **2013**, *9*, 2519–2525.

[84] Voss, J. J. D.; Cryle, M. J. *The Ubiquitous Roles of Cytochrome P450 Proteins*; John Wiley & Sons, Ltd, 2007; pp 397–435.

[85] Auchus, R. J.; Miller, W. L. *Cytochrome P450*; Springer International Publishing, 2015; pp 851–879.

[86] Guengerich, F. P. *Cytochrome P450*; Springer International Publishing, 2015; pp 523–785.

[87] Gomez, L.; Kovac, J. R.; Lamb, D. J. CYP17A1 inhibitors in castration-resistant prostate cancer. *Steroids* **2015**, *95*, 80–87.

[88] Haidar, S.; Ehmer, P. B.; Barassin, S.; Batzl-Hartmann, C.; Hartmann, R. W. Effects of novel 17α-hydroxylase/C17, 20-lyase (P450 17, CYP 17) inhibitors on androgen biosynthesis in vitro and in vivo. *J. Steroid Biochem. Mol. Biol.* **2003**, *84*, 555–562.

[89] Brodie, A. M. Aromatease, its inhibitors and their use in breast cancer treatment. *Pharmacol. Ther.* **1993**, *60*, 501–515.

[90] Guengerich, F. P.; Yoshimoto, F. K. Formation and Cleavage of C–C Bonds by Enzymatic Oxidation–Reduction Reactions. *Chem. Rev.* **2018**, *118*, 6573–6655.

[91] Simpson, E.; Boyd, G. The cholesterol side-chain cleavage system of the adrenal cortex: A mixed-function oxidase. *Biochem. Biophys. Res. Commun.* **1966**, *24*, 10–17.

[92] Shikita, M.; Hall, P. F. The Stoichiometry of the Conversion of Cholesterol and Hydroxycholesterols to Pregnenolone (3β-Hydroxypregn-5-en-20-one) Catalysed by Adrenal Cytochrome P-450. *Proc. Natl. Acad. Sci. U.S.A.* **1974**, *71*, 1441–1445.

[93] Yoshimoto, F. K.; Auchus, R. J. The diverse chemistry of cytochrome P450 17A1 (P450c17, CYP17A1). *J. Steroid Biochem. Mol. Biol.* **2015**, *151*, 52–65.

[94] Yoshimoto, F. K.; Gonzalez, E.; Auchus, R. J.; Guengerich, F. P. Mechanism of 17α,20-Lyase and New Hydroxylation Reactions of Human Cytochrome P450 17A1. *J. Biol. Chem.* **2016**, *291*, 17143–17164.

[95] Fischer, R. T.; Trzaskos, J. M.; Magolda, R. L.; Ko, S. S.; Brosz, C. S.; Larsen, B. Lanosterol 14 alpha-methyl demethylase. Isolation and characterization of the third metabolically generated oxidative demethylation intermediate. *J. Biol. Chem.* **1991**, *266*, 6124–6132.

[96] Davydov, R.; Strushkevich, N.; Smil, D.; Yantsevich, A.; Gilep, A.; Usanov, S.; Hoffman, B. M. Evidence That Compound I Is the Active Species in Both the Hydroxylase and Lyase Steps by Which P450scc Converts Cholesterol to Pregnenolone: EPR/ENDOR/Cryoreduction/Annealing Studies. *Biochemistry (Mosc.)* **2015**, *54*, 7089–7097.

[97] Yoshimoto, F. K.; Jung, I.-J.; Goyal, S.; Gonzalez, E.; Guengerich, F. P. Isotope-Labeling Studies Support the Electrophilic Compound I Iron Active Species, FeO^{3+}, Carbon Bond Cleavage Reaction of the Cholesterol Side-Chain Cleavage Enzyme, Cytochrome P450 11A1. *J. Am. Chem. Soc.* **2016**, *138*, 12124–12141.

[98] Larroque, C.; Rousseau, J.; Lier, J. E. V. Enzyme-bound sterols of bovine adrenocortical cytochrome P-450scc. *Biochemistry (Mosc.)* **1981**, *20*, 925–929.

[99] Miller, S. L.; Wright, J. N.; Corina, D. L.; Akhtar, M. Mechanistic studies on pregnene side-chain cleavage enzyme (17α-hydroxylase-17,20-lyase) using ^{18}O. *J. Chem. Soc., Chem. Commun.* **1991**, 157–159.

[100] Mak, A. Y.; Swinney, D. C. 17-O-Acetyltestosterone formation from progesterone in microsomes from pig testes: evidence for the Baeyer-Villiger rearrangement in androgen formation catalyzed by CYP17. *J. Am. Chem. Soc.* **1992**, *114*, 8309–8310.

[101] Shyadehi, A. Z.; Lamb, D. C.; Kelly, S. L.; Kelly, D. E.; Schunck, W.-H.; Wright, J. N.; Corina, D.; Akhtar, M. The Mechanism of the Acyl-Carbon Bond Cleavage Reaction Catalyzed by Recombinant Sterol 14α-Demethylase of Candida albicans (Other Names Are: Lanosterol 14α-Demethylase, P-45014DM, and CYP51). *J. Biol. Chem.* **1996**, *271*, 12445–12450.

[102] Hannemann, F.; Bichet, A.; Ewen, K. M.; Bernhardt, R. Cytochrome P450 systems—biological variations of electron transport chains. *Biochim Biophys Acta Gen Subj* **2007**, *1770*, 330–344.

[103] Kelly, S. L.; Lamb, D. C.; Jackson, C. J.; Warrilow, A. G.; Kelly, D. E. *Adv. Microb. Physiol.*; Elsevier, 2003; pp 131–186.

[104] Mot, R. D.; Parret, A. H. A novel class of self-sufficient cytochrome P450 monooxygenases in prokaryotes. *Trends Microbiol.* **2002**, *10*, 502–508.

[105] Daiber, A.; Shoun, H.; Ullrich, V. Nitric oxide reductase (P450nor) from Fusarium oxysporum. *J. Inorg. Biochem.* **2005**, *99*, 185–193, Heme-diatomic interactions, Part 1.

[106] Urlacher, V. B.; Bell, S. G.; Wong, L.-L. *Modern Biooxidation*; Wiley-VCH Verlag GmbH & Co. KGaA, 2007; pp 99–122.

[107] Lipscomb, J. D.; Sligar, S. G.; Namtvedt, M. J.; Gunsalus, I. C. Autooxidation and hydroxylation reactions of oxygenated cytochrome P-450cam. *J. Biol. Chem.* **1976**, *251*, 1116–1124.

[108] Hobisch, M.; Holtmann, D.; de Santos, P. G.; Alcalde, M.; Hollmann, F.; Kara, S. Recent developments in the use of peroxygenases – Exploring their high potential in selective oxyfunctionalisations. *Biotechnol. Adv.* **2021**, *51*, 107615.

[109] O'Reilly, E.; Kohler, V.; Flitsch, S. L.; Turner, N. J. Cytochromes P450 as useful biocatalysts: addressing the limitations. *Chem. Commun.* **2011**, *47*, 2490–2501.

[110] Zhao, H.; van der Donk, W. A. Regeneration of cofactors for use in biocatalysis. *Curr. Opin. Biotechnol.* **2003**, *14*, 583–589.

[111] Poznansky, B.; Thompson, L. A.; Warren, S. A.; Reeve, H. A.; Vincent, K. A. Carbon as a Simple Support for Redox Biocatalysis in Continuous Flow. *Org. Process Res. Dev.* **2020**, *24*, 2281–2287.

[112] Song, K.; Zhou, X.; Liu, Y.; Gong, Y.; Zhou, B.; Wang, D.; Wang, Q. Role of oxidants in enhancing dewaterability of anaerobically digested sludge through Fe (II) activated oxidation processes: hydrogen peroxide versus persulfate. *Sci. Rep.* **2016**, *6*.

[113] Carmona-Ribeiro, A. M.; Prieto, T.; Nantes, I. L. Nanostructures for peroxidases. *Front. Mol. Biosci.* **2015**, *2*.

[114] Alfonso-Prieto, M.; Biarnés, X.; Vidossich, P.; Rovira, C. The Molecular Mechanism of the Catalase Reaction. *J. Am. Chem. Soc.* **2009**, *131*, 11751–11761.

[115] Wang, Y.; Lan, D.; Durrani, R.; Hollmann, F. Peroxygenases *en route* to becoming dream catalysts. What are the opportunities and challenges? *Curr. Opin. Chem. Biol.* **2017**, *37*, 1–9.

[116] Munro, A. W.; McLean, K. J.; Grant, J. L.; Makris, T. M. Structure and function of the cytochrome P450 peroxygenase enzymes. *Biochem. Soc. Trans.* **2018**, *46*, 183–196.

[117] Strohmaier, S. J.; Voss, J. J. D.; Jurva, U.; Andersson, S.; Gillam, E. M. Oxygen Surrogate Systems for Supporting Human Drug-Metabolizing Cytochrome P450 Enzymes. *Drug Metab. Dispos.* **2020**, *48*, 432–437.

[118] Hanna, I. H.; Krauser, J. A.; Cai, H.; Kim, M.-S.; Guengerich, F. P. Diversity In Mechanisms Of Substrate Oxidation By Cytochrome P450 2d6: Lack Of An Allosteric Role Of NADPH-cytochrome P450 Reductase In Catalytic Regioselectivity. *J. Biol. Chem.* **2001**, *276*, 39553–39561.

[119] Nordblom, G. D.; White, R. E.; Coon, M. J. Studies on hydroperoxide-dependent substrate hydroxylation by purified liver microsomal cytochrome P-450. *Arch. Biochem. Biophys.* **1976**, *175*, 524–533.

[120] Hollenberg, P. F. Mechanisms of cytochrome P450 and peroxidase-catalyzed xenobiotic metabolism. *FASEB J.* **1992**, *6*, 686–694.

[121] Ullrich, R.; Nüske, J.; Scheibner, K.; Spantzel, J.; Hofrichter, M. Novel Haloperoxidase from the Agaric Basidiomycete *Agrocybe aegerita* Oxidizes Aryl Alcohols and Aldehydes. *Appl. Environ. Microbiol.* **2004**, *70*, 4575–4581.

[122] Hofrichter, M.; Ullrich, R. Oxidations catalyzed by fungal peroxygenases. *Curr. Opin. Chem. Biol.* **2014**, *19*, 116–125.

[123] Piontek, K.; Strittmatter, E.; Ullrich, R.; Gröbe, G.; Pecyna, M. J.; Kluge, M.; Scheibner, K.; Hofrichter, M.; Plattner, D. A. Structural Basis of Substrate Conversion in a New Aromatic Peroxygenase. *J. Biol. Chem.* **2013**, *288*, 34767–34776.

[124] Molina-Espeja, P.; Ma, S.; Mate, D. M.; Ludwig, R.; Alcalde, M. Tandem-yeast expression system for engineering and producing unspecific peroxygenase. *Enzyme Microb. Technol.* **2015**, *73-74*, 29–33.

[125] Molina-Espeja, P.; Garcia-Ruiz, E.; Gonzalez-Perez, D.; Ullrich, R.; Hofrichter, M.; Alcalde, M. Directed Evolution of Unspecific Peroxygenase from Agrocybe aegerita. *Appl. Environ. Microbiol.* **2014**, *80*, 3496–3507.

[126] Matsunaga, I.; Ueda, A.; Fujiwara, N.; Sumimoto, T.; Ichihara, K. Characterization of the ybdT gene product of Bacillus subtilis: Novel fatty acid β-hydroxylating cytochrome P450. *Lipids* **1999**, *34*, 841–846.

[127] Matsunaga, I.; Sumimoto, T.; Ueda, A.; Kusunose, E.; Ichihara, K. Fatty acid-specific, regiospecific, and stereospecific hydroxylation by cytochrome P450 (CYP152B1) from Sphingomonas paucimobilis: Substrate structure required for α-hydroxylation. *Lipids* **2000**, *35*, 365–371.

[128] Girvan, H. M.; Munro, A. W. Applications of microbial cytochrome P450 enzymes in biotechnology and synthetic biology. *Curr. Opin. Chem. Biol.* **2016**, *31*, 136–145.

[129] Girhard, M.; Schuster, S.; Dietrich, M.; Dürre, P.; Urlacher, V. B. Cytochrome P450 monooxygenase from Clostridium acetobutylicum: A new α-fatty acid hydroxylase. *Biochem. Biophys. Res. Commun.* **2007**, *362*, 114–119.

[130] Onoda, H.; Shoji, O.; Suzuki, K.; Sugimoto, H.; Shiro, Y.; Watanabe, Y. α-Oxidative decarboxylation of fatty acids catalysed by cytochrome P450 peroxygenases yielding shorter-alkyl-chain fatty acids. *Catal. Sci. Technol.* **2018**, *8*, 434–442.

[131] Matthews, S.; Tee, K. L.; Rattray, N. J.; McLean, K. J.; Leys, D.; Parker, D. A.; Blankley, R. T.; Munro, A. W. Production of alkenes and novel secondary products by $P450_{OleT_{JE}}$ using novel H_2O_2-generating fusion protein systems. *FEBS Lett.* **2017**, *591*, 737–750.

[132] Fujishiro, T.; Shoji, O.; Nagano, S.; Sugimoto, H.; Shiro, Y.; Watanabe, Y. Crystal Structure of H2O2-dependent Cytochrome P450SPα with Its Bound Fatty Acid Substrate. *J. Biol. Chem.* **2011**, *286*, 29941–29950.

[133] Shoji, O.; Watanabe, Y. Peroxygenase reactions catalyzed by cytochromes P450. *J. Biol. Inorg. Chem.* **2014**, *19*, 529–539.

[134] Coleman, T.; Stok, J. E.; Podgorski, M. N.; Bruning, J. B.; Voss, J. J. D.; Bell, S. G. Structural insights into the role of the acid-alcohol pair of residues required for dioxygen activation in cytochrome P450 enzymes. *J. Biol. Inorg. Chem.* **2020**, *25*, 583–596.

[135] Lee, D.-S.; Yamada, A.; Sugimoto, H.; Matsunaga, I.; Ogura, H.; Ichihara, K.; ichi Adachi, S.; Park, S.-Y.; Shiro, Y. Substrate Recognition and Molecular Mechanism of Fatty Acid Hydroxylation by Cytochrome P450 from Bacillus subtilis. *J. Biol. Chem.* **2003**, *278*, 9761–9767.

[136] Belcher, J.; McLean, K. J.; Matthews, S.; Woodward, L. S.; Fisher, K.; Rigby, S. E.; Nelson, D. R.; Potts, D.; Baynham, M. T.; Parker, D. A.; Leys, D.; Munro, A. W. Structure and Biochemical Properties of the Alkene Producing Cytochrome P450 OleTJE (CYP152L1) from the Jeotgalicoccus sp. 8456 Bacterium. *J. Biol. Chem.* **2014**, *289*, 6535–6550.

[137] Bell, S. G.; Yang, W.; Tan, A. B. H.; Zhou, R.; Johnson, E. O. D.; Zhang, A.; Zhou, W.; Rao, Z.; Wong, L.-L. The crystal structures of 4-methoxybenzoate bound CYP199A2 and CYP199A4: structural changes on substrate binding and the identification of an anion binding site. *Dalton Trans.* **2012**, *41*, 8703–8714.

[138] Sundaramoorthy, M.; Terner, J.; Poulos, T. L. Stereochemistry of the chloroperoxidase active site: crystallographic and molecular-modeling studies. *Chem. Biol.* **1998**, *5*, 461–473.

[139] Shoji, O.; Fujishiro, T.; Nagano, S.; Tanaka, S.; Hirose, T.; Shiro, Y.; Watanabe, Y. Understanding substrate misrecognition of hydrogen peroxide dependent cytochrome P450 from Bacillus subtilis. *J. Biol. Inorg. Chem.* **2010**, *15*, 1331–1339.

[140] Shoji, O.; Fujishiro, T.; Nishio, K.; Kano, Y.; Kimoto, H.; Chien, S.-C.; Onoda, H.; Muramatsu, A.; Tanaka, S.; Hori, A.; Sugimoto, H.; Shiro, Y.; Watanabe, Y. A substrate-binding-state mimic of H2O2-dependent cytochrome P450 produced by one-point mutagenesis and peroxygenation of non-native substrates. *Catal. Sci. Technol.* **2016**, *6*, 5806–5811.

[141] Huang, X.; Groves, J. T. Oxygen Activation and Radical Transformations in Heme Proteins and Metalloporphyrins. *Chem. Rev.* **2017**, *118*, 2491–2553.

[142] Wang, B.; Li, C.; Dubey, K. D.; Shaik, S. Quantum Mechanical/Molecular Mechanical Calculated Reactivity Networks Reveal How Cytochrome P450cam and Its T252A Mutant Select Their Oxidation Pathways. *J. Am. Chem. Soc.* **2015**, *137*, 7379–7390.

[143] Ramanan, R.; Dubey, K. D.; Wang, B.; Mandal, D.; Shaik, S. Emergence of Function in P450-Proteins: A Combined Quantum Mechanical/Molecular Mechanical and Molecular Dynamics Study of the Reactive Species in the H_2O_2-Dependent Cytochrome $P450_{SP\alpha}$ and Its Regio- and Enantioselective Hydroxylation of Fatty Acids. *J. Am. Chem. Soc.* **2016**, *138*, 6786–6797.

[144] Cirino, P.; Arnold, F. Regioselectivity and Activity of Cytochrome P450 BM-3 and Mutant F87A in Reactions Driven by Hydrogen Peroxide. *Adv. Synth. Catal.* **2002**, *344*, 932–937.

[145] Cirino, P. C.; Arnold, F. H. A Self-Sufficient Peroxide-Driven Hydroxylation Biocatalyst. *Angew. Chem. Int. Ed.* **2003**, *42*, 3299–3301.

[146] Li, Q.-S.; Ogawa, J.; Shimizu, S. Critical Role of the Residue Size at Position 87 in H2O2-Dependent Substrate Hydroxylation Activity and H2O2 Inactivation of Cytochrome P450BM-3. *Biochem. Biophys. Res. Commun.* **2001**, *280*, 1258–1261.

[147] Joo, H.; Lin, Z.; Arnold, F. H. Laboratory evolution of peroxide-mediated cytochrome P450 hydroxylation. *Nature* **1999**, *399*, 670–673.

[148] Bell, S. G.; Tan, A. B. H.; Johnson, E. O. D.; Wong, L.-L. Selective oxidative demethylation of veratric acid to vanillic acid by CYP199A4 from Rhodopseudomonas palustris HaA2. *Mol. BioSyst.* **2009**, *6*, 206–214.

[149] Larimer, F. W. et al. Complete genome sequence of the metabolically versatile photosynthetic bacterium Rhodopseudomonas palustris. *Nat. Biotechnol.* **2003**, *22*, 55–61.

[150] Bell, S. G.; Hoskins, N.; Xu, F.; Caprotti, D.; Rao, Z.; Wong, L.-L. Cytochrome P450 enzymes from the metabolically diverse bacterium Rhodopseudomonas palustris. *Biochem. Biophys. Res. Commun.* **2006**, *342*, 191–196.

[151] Oda, Y.; Larimer, F. W.; Chain, P. S. G.; Malfatti, S.; Shin, M. V.; Vergez, L. M.; Hauser, L.; Land, M. L.; Braatsch, S.; Beatty, J. T.; Pelletier, D. A.; Schaefer, A. L.; Harwood, C. S. Multiple genome sequences reveal adaptations of

a phototrophic bacterium to sediment microenvironments. *PNAS* **2008**, *105*, 18543–18548.

[152] Oda, Y.; Wanders, W.; Huisman, L. A.; Meijer, W. G.; Gottschal, J. C.; Forney, L. J. Genotypic and Phenotypic Diversity within Species of Purple Nonsulfur Bacteria Isolated from Aquatic Sediments. *Appl. Environ. Microbiol.* **2002**, *68*, 3467–3477.

[153] Podgorski, M. N.; Coleman, T.; Chao, R. R.; De Voss, J. J.; Bruning, J. B.; Bell, S. G. Investigation of the requirements for efficient and selective cytochrome P450 monooxygenase catalysis across different reactions. *J. Inorg. Biochem.* **2020**, *203*, 110913.

[154] Furuya, T.; Arai, Y.; Kino, K. Biotechnological Production of Caffeic Acid by Bacterial Cytochrome P450 CYP199A2. *Appl. Environ. Microbiol.* **2012**, *78*, 6087–6094.

[155] Coleman, T.; Chao, R. R.; Bruning, J. B.; De Voss, J. J.; Bell, S. G. CYP199A4 catalyses the efficient demethylation and demethenylation of para-substituted benzoic acid derivatives. *RSC Adv.* **2015**, *5*, 52007–52018.

[156] Podgorski, M. N.; Harbort, J. S.; Lee, J. H. Z.; Nguyen, G. T. H.; Bruning, J. B.; Donald, W. A.; Bernhardt, P. V.; Harmer, J. R.; Bell, S. G. An Altered Heme Environment in an Engineered Cytochrome P450 Enzyme Enables the Switch from Monooxygenase to Peroxygenase Activity. *ACS Catal.* **2022**, *12*, 1614–1625.

[157] Coleman, T.; Chao, R. R.; Voss, J. J. D.; Bell, S. G. The importance of the benzoic acid carboxylate moiety for substrate recognition by CYP199A4 from *Rhodopseudomonas palustris* HaA2. *Biochim. Biophys. Acta, Proteins Proteomics* **2016**, *1864*, 667–675.

[158] Podgorski, M. N.; Coleman, T.; Churchman, L. R.; Bruning, J. B.; Voss, J. J. D.; Bell, S. G. Investigating the active oxidants involved in cytochrome P450 catalyzed sulfoxidation reactions. *Chem. Eur. J.* **2022**, Accepted.

[159] Deurzen, M. P. V.; Seelbach, K.; van Rantwijk, F.; Kragl, U.; Sheldon, R. A. Chloroperoxidase: Use of a Hydrogen Peroxide-Stat for Controlling Reactions and Improving Enzyme Performance. *Biocatal. Biotransform.* **1997**, *15*, 1–16.

[160] Girhard, M.; Kunigk, E.; Tihovsky, S.; Shumyantseva, V. V.; Urlacher, V. B. Light-driven biocatalysis with cytochrome P450 peroxygenases. *Biotechnol. Appl. Biochem.* **2013**, *60*, 111–118.

[161] Paul, C. E.; Churakova, E.; Maurits, E.; Girhard, M.; Urlacher, V. B.; Hollmann, F. *In situ* formation of H_2O_2 for P450 peroxygenases. *Bioorg. Med. Chem.* **2014**, *22*, 5692–5696.

[162] Köninger, K.; Grote, M.; Zachos, I.; Hollmann, F.; Kourist, R. Light-driven Enzymatic Decarboxylation. *J. Vis. Exp.* **2016**,

[163] Churakova, E.; Kluge, M.; Ullrich, R.; Arends, I.; Hofrichter, M.; Hollmann, F. Specific Photobiocatalytic Oxyfunctionalization Reactions. *Angew. Chem. Int. Ed.* **2011**, *50*, 10716–10719.

[164] Perez, D. I.; Grau, M. M.; Arends, I. W. C. E.; Hollmann, F. Visible light-driven and chloroperoxidase-catalyzed oxygenation reactions. *Chem. Commun.* **2009**, 6848.

[165] Karmee, S. K.; Roosen, C.; Kohlmann, C.; Lütz, S.; Greiner, L.; Leitner, W. Chemo-enzymatic cascade oxidation in supercritical carbon dioxide/water biphasic media. *Green Chem.* **2009**, *11*, 1052.

[166] Krieg, T.; Hüttmann, S.; Mangold, K.-M.; Schrader, J.; Holtmann, D. Gas diffusion electrode as novel reaction system for an electro-enzymatic process with chloroperoxidase. *Green Chem.* **2011**, *13*, 2686.

[167] Lütz, S.; Vuorilehto, K.; Liese, A. Process development for the electroenzymatic synthesis of (R)-methylphenylsulfoxide by use of a 3-dimensional electrode. *Biotechnol. Bioeng.* **2007**, *98*, 525–534.

[168] Freakley, S. J.; Kochius, S.; van Marwijk, J.; Fenner, C.; Lewis, R. J.; Baldenius, K.; Marais, S. S.; Opperman, D. J.; Harrison, S. T. L.; Alcalde, M.; Smit, M. S.; Hutchings, G. J. A chemo-enzymatic oxidation cascade to activate C-H bonds with *in situ* generated H_2O_2. *Nat. Commun.* **2019**, *10*.

[169] Gandomkar, S.; Dennig, A.; Dordic, A.; Hammerer, L.; Pickl, M.; Haas, T.; Hall, M.; Faber, K. Biocatalytic Oxidative Cascade for the Conversion of Fatty Acids into α-Ketoacids via Internal H_2O_2 Recycling. *Angew. Chem. Int. Ed.* **2017**, *57*, 427–430.

[170] Sheldon, R. A.; van Pelt, S. Enzyme immobilisation in biocatalysis: why, what and how. *Chem. Soc. Rev.* **2013**, *42*, 6223–6235.

[171] Tran, D. N.; Balkus, K. J. Perspective of Recent Progress in Immobilization of Enzymes. *ACS Catal.* **2011**, *1*, 956–968.

[172] Sheldon, R. Enzyme Immobilization: The Quest for Optimum Performance. *Adv. Synth. Catal.* **2007**, *349*, 1289–1307.

[173] Cao, L. *Carrier-bound Immobilized Enzymes*; Wiley, 2005.

[174] Tosa, T.; Mori, T.; Fuse, N.; Chibata, I. Studies on continuous enzyme reactions. I. Screening of carriers for preparation of water-insoluble aminoacylase. *Enzymologia* **1966**, *31*, 214–24.

[175] Petri, A.; Gambicorti, T.; Salvadori, P. Covalent immobilization of chloroperoxidase on silica gel and properties of the immobilized biocatalyst. *J. Mol. Catal. B: Enzym.* **2004**, *27*, 103–106.

[176] Bertucci, C.; Petri, A.; Felix, G.; Perini, B.; Salvadori, P. Lipase-based HPLC stationary phase: enantioselective synthesis of 2-substituted 1,3-propanediol monoacetates. *Tetrahedron: Asymmetry* **1999**, *10*, 4455–4462.

[177] Kirk, O.; Christensen, M. W. Lipases from *Candida antarctica*: Unique Biocatalysts from a Unique Origin. *Org. Process Res. Dev.* **2002**, *6*, 446–451.

[178] Heuts, D. P. H. M.; van Hellemond, E. W.; Janssen, D. B.; Fraaije, M. W. Discovery, Characterization, and Kinetic Analysis of an Alditol Oxidase from *Streptomyces coelicolor*. *J. Biol. Chem.* **2007**, *282*, 20283–20291.

[179] Heath, R. S.; Birmingham, W. R.; Thompson, M. P.; Taglieber, A.; Daviet, L.; Turner, N. J. An Engineered Alcohol Oxidase for the Oxidation of Primary Alcohols. *Chembiochem* **2019**, *20*, 276–281.

[180] Tieves, F.; Willot, S. J.-P.; van Schie, M. M. C. H.; Rauch, M. C. R.; Younes, S. H. H.; Zhang, W.; Dong, J.; Gomez de Santos, P.; Robbins, J. M.; Bommarius, B.; Alcalde, M.; Bommarius, A. S.; Hollmann, F. Formate Oxidase (FOx) from *Aspergillus oryzae*: One Catalyst Enables Diverse H_2O_2-Dependent Biocatalytic Oxidation Reactions. *Angew. Chem. Int. Ed.* **2019**, *58*, 7873–7877.

[181] Lee, J. H. Z.; Podgorski, M. N.; Moir, M.; Gee, A. R.; Bell, S. G. Selective Oxidations Using a Cytochrome P450 Enzyme Variant Driven with Surrogate Oxygen Donors and Light. *Chem. Eur. J.* **2022**, *28*.

[182] Fraaije, M. W.; van Berkel, W. J.; Benen, J. A.; Visser, J.; Mattevi, A. A novel oxidoreductase family sharing a conserved FAD-binding domain. *Trends Biochem. Sci.* **1998**, *23*, 206–207.

[183] van Hellemond, E.; Vermote, L.; Koolen, W.; Sonke, T.; Zandvoort, E.; Heuts, D. P.; Janssen, D.; Fraaije, M. Exploring the Biocatalytic Scope of Alditol Oxidase from *Streptomyces coelicolor*. *Adv. Synth. Catal.* **2009**, *351*, 1523–1530.

[184] Doubayashi, D.; Ootake, T.; Maeda, Y.; Oki, M.; Tokunaga, Y.; Sakurai, A.; Nagaosa, Y.; Mikami, B.; Uchida, H. Formate Oxidase, an Enzyme of the Glucose-Methanol-Choline Oxidoreductase Family, Has a His-Arg Pair and 8-Formyl-FAD at the Catalytic Site. *Biosci. Biotechnol. Biochem.* **2011**, *75*, 1662–1667.

[185] Robbins, J. M.; Souffrant, M. G.; Hamelberg, D.; Gadda, G.; Bommarius, A. S. Enzyme-Mediated Conversion of Flavin Adenine Dinucleotide (FAD) to 8-Formyl FAD in Formate Oxidase Results in a Modified Cofactor with Enhanced Catalytic Properties. *Biochemistry* **2017**, *56*, 3800–3807.

[186] Gibson, D. G.; Young, L.; Chuang, R.-Y.; Venter, J. C.; Hutchison III, C. A.; Smith, H. O. Enzymatic assembly of DNA molecules up to several hundred kilobases. *Nat. Methods* **2009**, *6*, 343.

[187] Vaz, R. P.; Filho, E. X. F. *Applications of Ion Exchange Materials in Biomedical Industries*; Springer International Publishing, 2019; pp 13–27.

[188] Yan, Y.; Zhang, X.; Chen, D. Enhanced catalysis of Yarrowia lipolytica lipase LIP2 immobilized on macroporous resin and its application in enrichment of polyunsaturated fatty acids. *Bioresour. Technol.* **2013**, *131*, 179–187.

[189] de Marco, A.; Vigh, L.; Diamant, S.; Goloubinoff, P. Native folding of aggregation-prone recombinant proteins in Escherichia coli by osmolytes, plasmid- or benzyl alcohol–overexpressed molecular chaperones. *Cell Stress Chaperones* **2005**, *10*, 329.

[190] Abdelhamid, M. A. A.; Motomura, K.; Ikeda, T.; Ishida, T.; Hirota, R.; Kuroda, A. Affinity purification of recombinant proteins using a novel silica-binding peptide as a fusion tag. *Appl. Microbiol. Biotechnol.* **2014**, *98*, 5677–5684.

[191] Reuten, R.; Nikodemus, D.; Oliveira, M. B.; Patel, T. R.; Brachvogel, B.; Breloy, I.; Stetefeld, J.; Koch, M. Maltose-Binding Protein (MBP), a Secretion-Enhancing Tag for Mammalian Protein Expression Systems. *PLOS ONE* **2016**, *11*, e0152386.

[192] Lessard, J. C. *Methods in Enzymology*; Elsevier, 2013; pp 181–189.

[193] Wise, C. E.; Hsieh, C. H.; Poplin, N. L.; Makris, T. M. Dioxygen Activation by the Biofuel-Generating Cytochrome P450 OleT. *ACS Catal.* **2018**, *8*, 9342–9352.

[194] Sibbesen, O.; Voss, J. J. D.; de Montellano, P. R. O. Putidaredoxin Reductase-Putidaredoxin-Cytochrome P450cam Triple Fusion Protein. *J. Biol. Chem.* **1996**, *271*, 22462–22469.

[195] Chen, X.; Zaro, J. L.; Shen, W.-C. Fusion protein linkers: Property, design and functionality. *Adv. Drug Delivery Rev.* **2013**, *65*, 1357–1369.

[196] Amet, N.; Lee, H.-F.; Shen, W.-C. Insertion of the Designed Helical Linker Led to Increased Expression of Tf-Based Fusion Proteins. *Pharm. Res.* **2008**, *26*, 523–528.

[197] Huang, Z.; Zhang, C.; Xing, X.-H. *Linkers in Biomacromolecules*; Elsevier, 2021; pp 23–49.

[198] Lindeque, R.; Woodley, J. Reactor Selection for Effective Continuous Biocatalytic Production of Pharmaceuticals. *Catalysts* **2019**, *9*, 262.

[199] Guengerich, F. P.; Munro, A. W. Unusual Cytochrome P450 Enzymes and Reactions. *J. Biol. Chem.* **2013**, *288*, 17065–17073.

[200] Greule, A.; Stok, J. E.; Voss, J. J. D.; Cryle, M. J. Unrivalled diversity: the many roles and reactions of bacterial cytochromes P450 in secondary metabolism. *Nat. Prod. Rep.* **2018**, *35*, 757–791.

[201] Sirim, D.; Wagner, F.; Lisitsa, A.; Pleiss, J. The Cytochrome P450 Engineering Database: integration of biochemical properties. *BMC Biochem.* **2009**, *10*.

[202] Sirim, D.; Widmann, M.; Wagner, F.; Pleiss, J. Prediction and analysis of the modular structure of cytochrome P450 monooxygenases. *BMC Struct. Biol.* **2010**, *10*.

[203] Hedegaard, J.; Gunsalus, I. Mixed Function Oxidation. *J. Biol. Chem.* **1965**, *240*, 4038–4043.

[204] Poulos, T. L.; Finzel, B. C.; Gunsalus, I. C.; Wagner, G. C.; Kraut, J. The 2.6-A crystal structure of Pseudomonas putida cytochrome P-450. *J. Biol. Chem.* **1985**, *260*, 16122–30.

[205] Poulos, T. L.; Finzel, B. C.; Howard, A. J. Crystal structure of substrate-free Pseudomonas putida cytochrome P-450. *Biochemistry (Mosc.)* **1986**, *25*, 5314–5322.

[206] Poulos, T. L.; Finzel, B. C.; Howard, A. J. High-resolution crystal structure of cytochrome P450cam. *J. Mol. Biol.* **1987**, *195*, 687 – 700.

[207] Poulos, T. L.; Johnson, E. F. *Cytochrome P450*; Springer International Publishing, 2015; pp 3–32.

[208] Stoddard, B. L. Intermediate trapping and laue X-ray diffraction: Potential for enzyme mechanism, dynamics, and inhibitor screening. *Pharmacol. Ther.* **1996**, *70*, 215–256.

[209] Schlichting, I.; Goody, R. S. *Methods in Enzymology*; Elsevier, 1997; pp 467–490.

[210] Schlichting, I.; Berendzen, J.; Chu, K.; Stock, A. M.; Maves, S. A.; Benson, D. E.; Sweet, R. M.; Ringe, D.; Petsko, G. A.; Sligar, S. G. The Catalytic Pathway of Cytochrome P450cam at Atomic Resolution. *Science* **2000**, *287*, 1615–1622.

[211] Carugo, O.; Carugo, K. D. When X-rays modify the protein structure: radiation damage at work. *Trends Biochem. Sci.* **2005**, *30*, 213–219.

[212] Schmidt, M. Reaction Initiation in Enzyme Crystals by Diffusion of Substrate. *Crystals* **2020**, *10*, 116.

[213] Wilmot, C. M.; Hajdu, J.; McPherson, M. J.; Knowles, P. F.; Phillips, S. E. V. Visualization of Dioxygen Bound to Copper During Enzyme Catalysis. *Science* **1999**, *286*, 1724–1728.

[214] Perkins, A.; Parsonage, D.; Nelson, K. J.; Ogba, O. M.; Cheong, P. H.-Y.; Poole, L. B.; Karplus, P. A. Peroxiredoxin Catalysis at Atomic Resolution. *Structure* **2016**, *24*, 1668–1678.

[215] Rupp, B. *Biomolecular Crystallography*; Garland Science, 2009.

[216] Pike, A. C. W.; Garman, E. F.; Krojer, T.; von Delft, F.; Carpenter, E. P. An Overview Of Heavy-atom Derivatization Of Protein Crystals. *Acta. Crystallogr. D Struct Biol.* **2016**, *72*, 303–318.

[217] Nguyen, R. C.; Yang, Y.; Wang, Y.; Davis, I.; Liu, A. Substrate-Assisted Hydroxylation and *O*-Demethylation in the Peroxidase-like Cytochrome P450 Enzyme CYP121. *ACS Catal.* **2019**, *10*, 1628–1639.

[218] Podgorski, M. N.; Harbort, J. S.; Coleman, T.; Stok, J. E.; Yorke, J. A.; Wong, L.-L.; Bruning, J. B.; Bernhardt, P. V.; Voss, J. J. D.; Harmer, J. R.; Bell, S. G. Biophysical Techniques for Distinguishing Ligand Binding Modes in Cytochrome P450 Monooxygenases. *Biochemistry* **2020**, *59*, 1038–1050.

[219] Coleman, T.; Kirk, A. M.; Chao, R. R.; Podgorski, M. N.; Harbort, J. S.; Churchman, L. R.; Bruning, J. B.; Bernhardt, P. V.; Harmer, J. R.; Krenske, E. H.; Voss, J. J. D.; Bell, S. G. Understanding the Mechanistic Requirements for Efficient and Stereoselective Alkene Epoxidation by a Cytochrome P450 Enzyme. *ACS Catalysis* **2021**, *11*, 1995–2010.

[220] Coleman, T.; Doherty, D. Z.; Zhang, T.; Podgorski, M. N.; Qiao, R.; Lee, J. H. Z.; Bruning, J. B.; Voss, J. J. D.; Zhou, W.; Bell, S. G. Exploring the Factors which Result in Cytochrome P450 Catalyzed Desaturation Versus Hydroxylation. *Chem. Asian J.* **2022**,

[221] Cowieson, N. P.; Aragao, D.; Clift, M.; Ericsson, D. J.; Gee, C.; Harrop, S. J.; Mudie, N.; Panjikar, S.; Price, J. R.; Riboldi-Tunnicliffe, A.; Williamson, R.; Caradoc-Davies, T. MX1: a bending-magnet crystallography beamline serving both chemical and macromolecular crystallography communities at the Australian Synchrotron. *J. Synchrotron Radiat.* **2015**, *22*, 187–190.

[222] Battye, T. G. G.; Kontogiannis, L.; Johnson, O.; Powell, H. R.; Leslie, A. G. W. iMOSFLM: a new graphical interface for diffraction-image processing with MOSFLM. *Acta Crystallogr. D* **2011**, *67*, 271–281.

[223] Evans, P. R.; Murshudov, G. N. How good are my data and what is the resolution? *Acta Crystallogr. D* **2013**, *69*, 1204–1214.

[224] Winn, M. D. et al. Overview of the CCP_4 suite and current developments. *Acta Crystallogr. D* **2011**, *67*, 235–242.

[225] McCoy, A. J.; Grosse-Kunstleve, R. W.; Adams, P. D.; Winn, M. D.; Storoni, L. C.; Read, R. J. Phaser crystallographic software. *J. Appl. Crystallogr.* **2007**, *40*, 658–674.

[226] Emsley, P.; Lohkamp, B.; Scott, W. G.; Cowtan, K. Features and development of Coot. *Acta Crystallogr. D* **2010**, *66*, 486–501.

[227] Adams, P. D. et al. PHENIX: a comprehensive Python-based system for macromolecular structure solution. *Acta Crystallogr. D* **2010**, *66*, 213–221.

[228] Terwilliger, T. C.; Grosse-Kunstleve, R. W.; Afonine, P. V.; Moriarty, N. W.; Adams, P. D.; Read, R. J.; Zwart, P. H.; Hung, L.-W. Iterative-build OMIT maps: map improvement by iterative model building and refinement without model bias. *Acta Crystallogr. D* **2008**, *64*, 515–524.

[229] Afonine, P. V.; Moriarty, N. W.; Mustyakimov, M.; Sobolev, O. V.; Terwilliger, T. C.; Turk, D.; Urzhumtsev, A.; Adams, P. D. FEM: feature-enhanced map. *Acta Crystallogr. D* **2015**, *71*, 646–666.

[230] Bathelt, C. M.; Zurek, J.; Mulholland, A. J.; Harvey, J. N. Electronic Structure of Compound I in Human Isoforms of Cytochrome P450 from QM/MM Modeling. *J. Am. Chem. Soc.* **2005**, *127*, 12900–12908.

[231] Lonsdale, R.; Oláh, J.; Mulholland, A. J.; Harvey, J. N. Does Compound I Vary Significantly between Isoforms of Cytochrome P450? *J. Am. Chem. Soc.* **2011**, *133*, 15464–15474.

[232] Dornevil, K.; Davis, I.; Fielding, A. J.; Terrell, J. R.; Ma, L.; Liu, A. Cross-linking of dicyclotyrosine by the cytochrome P450 enzyme CYP121 from Mycobacterium tuberculosis proceeds through a catalytic shunt pathway. *J. Biol. Chem.* **2017**, *292*, 13645–13657.

[233] Bell, S. G.; Chen, X.; Sowden, R. J.; Xu, F.; Williams, J. N.; Wong, L.-L.; Rao, Z. Molecular Recognition in (+)-α-Pinene Oxidation by Cytochrome P450cam. *J. Am. Chem. Soc.* **2003**, *125*, 705–714.

[234] Atkins, W. M.; Sligar, S. G. The roles of active site hydrogen bonding in cytochrome P-450cam as revealed by site-directed mutagenesis. *J. Biol. Chem.* **1988**, *263*, 18842–9.

[235] Li, H.; Narasimhulu, S.; Havran, L. M.; Winkler, J. D.; Poulos, T. L. Crystal Structure of Cytochrome P450cam Complexed with Its Catalytic Product, 5-exo-Hydroxycamphor. *J. Am. Chem. Soc.* **1995**, *117*, 6297–6299.

[236] Podgorski, M. Investigation of the Mechanism of Multiple Cytochrome P450-catalysed Reactions. M.Sc. thesis, University of Adelaide, 2019.

[237] Pfanzagl, V.; Beale, J. H.; Michlits, H.; Schmidt, D.; Gabler, T.; Obinger, C.; Djinović-Carugo, K.; Hofbauer, S. X-ray–induced photoreduction of heme metal centers rapidly induces active-site perturbations in a protein-independent manner. *J. Biol. Chem.* **2020**, *295*, 13488–13501.

[238] Stohrer, C.; Horrell, S.; Meier, S.; Sans, M.; von Stetten, D.; Hough, M.; Goldman, A.; Monteiro, D. C. F.; Pearson, A. R. Homogeneous batch microcrystallization of proteins from ammonium sulfate. *Acta Crystallogr. D* **2021**, *77*, 194–204.

[239] Hough, M. A.; Owen, R. L. Serial synchrotron and XFEL crystallography for studies of metalloprotein catalysis. *Curr. Opin. Struct. Biol.* **2021**, *71*, 232–238.

[240] Chovancova, E.; Pavelka, A.; Benes, P.; Strnad, O.; Brezovsky, J.; Kozlikova, B.; Gora, A.; Sustr, V.; Klvana, M.; Medek, P.; Biedermannova, L.; Sochor, J.; Damborsky, J. CAVER 3.0: A Tool for the Analysis of Transport Pathways in Dynamic Protein Structures. *PLoS Comput. Biol.* **2012**, *8*, e1002708.

[241] Bailey, L. J.; Fox, B. G. Crystallographic and Catalytic Studies of the Peroxide-Shunt Reaction in a Diiron Hydroxylase. *Biochemistry* **2009**, *48*, 8932–8939.

[242] Duggal, R.; Liu, Y.; Gregory, M. C.; Denisov, I. G.; Kincaid, J. R.; Sligar, S. G. Evidence that cytochrome b5 acts as a redox donor in CYP17A1 mediated androgen synthesis. *Biochem. Biophys. Res. Commun.* **2016**, *477*, 202–208.

[243] Vasaitis, T. S.; Bruno, R. D.; Njar, V. C. CYP17 inhibitors for prostate cancer therapy. *J. Steroid Biochem. Mol. Biol.* **2011**, *125*, 23–31.

[244] Gregory, M. C.; Denisov, I. G.; Grinkova, Y. V.; Khatri, Y.; Sligar, S. G. Kinetic Solvent Isotope Effect in Human P450 CYP17A1-Mediated Androgen Formation: Evidence for a Reactive Peroxoanion Intermediate. *J. Am. Chem. Soc.* **2013**, *135*, 16245–16247.

[245] Liu, Y.; Denisov, I. G.; Grinkova, Y. V.; Sligar, S. G.; Kincaid, J. R. P450 CYP17A1 Variant with a Disordered Proton Shuttle Assembly Retains Peroxo-Mediated Lyase Efficiency. *Chem. Eur. J.* **2020**, *26*, 16846–16852.

[246] Mak, P. J.; Duggal, R.; Denisov, I. G.; Gregory, M. C.; Sligar, S. G.; Kincaid, J. R. Human Cytochrome CYP17A1: The Structural Basis for Compromised Lyase Activity with 17-Hydroxyprogesterone. *J. Am. Chem. Soc.* **2018**, *140*, 7324–7331.

[247] Cho, K.-B.; Moreau, Y.; Kumar, D.; Rock, D.; Jones, J.; Shaik, S. Formation of the Active Species of Cytochrome P450 by Using Iodosylbenzene: A Case for Spin-Selective Reactivity. *Chem. Eur. J.* **2007**, *13*, 4103–4115.

[248] Coleman, T. Utilising CYP199A4 from Rhodopseudomonas palustris HaA2 for investigation of the mechanism of cytochrome P450-catalysed oxidations. Ph.D. thesis, University of Adelaide, 2018.

[249] Miller, J. C.; Lee, J. H. Z.; Mclean, M. A.; Chao, R. R.; Stone, I. S. J.; Pukala, T. L.; Bruning, J. B.; Voss, J. J. D.; Schuler, M. A.; Sligar, S. G.;

Bell, S. G. Engineering C–C Bond Cleavage Activity into a P450 Monooxygenase Enzyme. *J. Am. Chem. Soc.* **2023**,

[250] Aragão, D. et al. MX2: a high-flux undulator microfocus beamline serving both the chemical and macromolecular crystallography communities at the Australian Synchrotron. *J. Synchrotron Radiat.* **2018**, *25*, 885–891.

[251] Berman, H. M.; Westbrook, J.; Feng, Z.; Gilliland, G.; Bhat, T. N.; Weissig, H.; Shindyalov, I. N.; Bourne, P. E. The Protein Data Bank. *Nucleic Acids Res.* **2000**, *28*, 235–242.

[252] Berman, H.; Henrick, K.; Nakamura, H. Announcing the worldwide Protein Data Bank. *Nat. Struct. Mol. Biol.* **2003**, *10*, 980–980.

[253] Chao, R. Utilising CYP199A4 from Rhodopseudomonas palustris HaA2 for Biocatalysis and Mechanistic Studies. M.Sc. thesis, University of Adelaide, 2016.

[254] Okura, I.; Otsuka, K.; Nakada, N.; Hasumi, F. Regeneration of NADH and ketone hydrogenation by hydrogen with the combination of hydrogenase and alcohol dehydrogenase. *Appl. Biochem. Biotechnol.* **1990**, *24-25*, 425–430.

[255] Tutturen, A. E. V.; Holm, A.; Fleckenstein, B. Specific biotinylation and sensitive enrichment of citrullinated peptides. *Anal. Bioanal.Chem.* **2013**, *405*, 9321–9331.

[256] Coleman, T.; Lee, J. Z. H.; Kirk, A. M.; Doherty, D. Z.; Podgorski, M. N.; Pinidiya, D. K.; Bruning, J. B.; Voss, J. J. D.; Krenske, E. H.; Bell, S. G. Enabling Aromatic Hydroxylation in a Cytochrome P450 Monooxygenase Enzyme through Protein Engineering. *Chem. Eur. J.* **2022**, *28*.

[257] Lamb, A. L.; Kappock, T. J.; Silvaggi, N. R. You are lost without a map: Navigating the sea of protein structures. *Biochim. Biophys. Acta - Proteins Proteom* **2015**, *1854*, 258–268.

[258] Petrunak, E. M.; DeVore, N. M.; Porubsky, P. R.; Scott, E. E. Structures of Human Steroidogenic Cytochrome P450 17A1 with Substrates. *J. Biol. Chem.* **2014**, *289*, 32952–32964.

[259] Stevens, C. L.; Glenn, F. E.; Pillai, P. M. Hydroxy ketone rearrangements. II. Kinetics and mechanism of the thermal rearrangements of optically active .alpha.-hydroxy ketones. Example of a cyclic three-component equilibrium. *J. Am. Chem. Soc.* **1973**, *95*, 6301–6308.

[260] Coleman, T.; Kirk, A. M.; Lee, J. H. Z.; Doherty, D. Z.; Bruning, J. B.; Krenske, E. H.; Voss, J. J. D.; Bell, S. G. Different Geometric Requirements for Cytochrome P450-Catalyzed Aliphatic Versus Aromatic Hydroxylation Results in Chemoselective Oxidation. *ACS Catal.* **2022**, *12*, 1258–1267.

[261] Shakunthala, N. New cytochrome P450 mechanisms: implications for understanding molecular basis for drug toxicity at the level of the cytochrome. *Expert Opin. Drug Metab. Toxicol.* **2009**, *6*, 1–15.

[262] Nagano, S.; Poulos, T. L. Crystallographic Study on the Dioxygen Complex of Wild-type and Mutant Cytochrome P450cam. *J. Biol. Chem.* **2005**, *280*, 31659–31663.

[263] Meunier, B.; de Visser, S. P.; Shaik, S. Mechanism of Oxidation Reactions Catalyzed by Cytochrome P450 Enzymes. *Chem. Rev.* **2004**, *104*, 3947–3980.

[264] Feng, Y.; Wang, J.-T.; Liu, L.; Guo, Q.-X. C-H and N-H bond dissociation energies of five- and six-membered ring aromatic compounds. *J. Phys. Org. Chem.* **2003**, *16*, 883–890.

[265] Davico, G. E.; Bierbaum, V. M.; DePuy, C. H.; Ellison, G. B.; Squires, R. R. The C-H Bond Energy of Benzene. *Journal of the American Chemical Society* **1995**, *117*, 2590–2599.

[266] Stok, J. E.; Chow, S.; Krenske, E. H.; Farfan Soto, C.; Matyas, C.; Poirier, R. A.; Williams, C. M.; De Voss, J. J. Direct Observation of an Oxepin from a Bacterial Cytochrome P450-Catalyzed Oxidation. *Chem. Eur. J.* **2016**, *22*, 4408–4412.

[267] Jerina, D. M.; Daly, J. W.; Witkop, B. The role of arene oxide-oxepin systems in the metabolism of aromatic substrates. II. Synthesis of 3,4-toluene-4-d oxide and subsequent "NIH shift" to 4-hydroxytoluene-3-H. *J. Am. Chem. Soc.* **1968**, *90*, 6523–6525.

[268] Koerts, J.; Soffers, A. E. M. F.; Vervoort, J.; Jager, A. D.; Rietjens, I. M. C. M. Occurrence of the NIH Shift upon the Cytochrome P450-Catalyzed in Vivo and in Vitro Aromatic Ring Hydroxylation of Fluorobenzenes. *Chem. Res. Toxicol.* **1998**, *11*, 503–512.

[269] Asaka, M.; Fujii, H. Participation of Electron Transfer Process in Rate-Limiting Step of Aromatic Hydroxylation Reactions by Compound I Models of Heme Enzymes. *J. Am. Chem. Soc.* **2016**, *138*, 8048–8051.

[270] Tomaszewski, J. E.; Jerina, D. M.; Daly, J. W. Deuterium isotope effects during formation of phenols by hepatic monoxygenases. Evidence for an alternative to the arene oxide pathway. *Biochemistry* **1975**, *14*, 2024–2031.

[271] Daly, J. W.; Jerina, D. M.; Witkop, B. Arene oxides and the NIH shift: The metabolism, toxicity and carcinogenicity of aromatic compounds. *Experientia* **1972**, *28*, 1129–1149.

[272] Hanzlik, R. P.; Hogberg, K.; Judson, C. M. Microsomal hydroxylation of specifically deuterated monosubstituted benzenes. Evidence for direct aromatic hydroxylation. *Biochemistry* **1984**, *23*, 3048–3055.

[273] Korzekwa, K. R.; Swinney, D. C.; Trager, W. F. Isotopically labeled chlorobenzenes as probes for the mechanism of cytochrome P-450 catalyzed aromatic hydroxylation. *Biochemistry* **1989**, *28*, 9019–9027.

[274] Bathelt, C. M.; Ridder, L.; Mulholland, A. J.; Harvey, J. N. Mechanism and structure–reactivity relationships for aromatic hydroxylation by cytochrome P450. *Org. Biomol. Chem.* **2004**, *2*, 2998–3005.

[275] Rydberg, P.; Ryde, U.; Olsen, L. Prediction of Activation Energies for Aromatic Oxidation by Cytochrome P450. *J. Phys. Chem. A* **2008**, *112*, 13058–13065.

[276] Bathelt, C. M.; Mulholland, A. J.; Harvey, J. N. QM/MM Modeling of Benzene Hydroxylation in Human Cytochrome P450 2C9. *J. Phys. Chem. A* **2008**, *112*, 13149–13156.

[277] Harlington, A. C.; Shearwin, K. E.; Bell, S. G.; Whelan, F. Efficient *O*-demethylation of lignin monoaromatics using the peroxygenase activity of cytochrome P450 enzymes. *Chem. Commun.* **2022**, *58*, 13321–13324.

[278] Koo, L. S.; Tschirret-Guth, R. A.; Straub, W. E.; Moënne-Loccoz, P.; Loehr, T. M.; de Montellano, P. R. O. The Active Site of the Thermophilic CYP119 from Sulfolobus solfataricus. *J. Biol. Chem.* **2000**, *275*, 14112–14123.

[279] Dangi, B.; Lee, C. W.; Kim, K.-H.; Park, S.-H.; Yu, E.-J.; Jeong, C.-S.; Park, H.; Lee, J. H.; Oh, T.-J. Characterization of two steroid hydroxylases from different *Streptomyces* spp. and their ligand-bound and -unbound crystal structures. *The FEBS Journal* **2018**, *286*, 1683–1699.

[280] Makino, T.; Katsuyama, Y.; Otomatsu, T.; Misawa, N.; Ohnishi, Y. Regio- and Stereospecific Hydroxylation of Various Steroids at the 16α Position of the D

Ring by the Streptomyces griseus Cytochrome P450 CYP154C3. *Appl. Environ. Microbiol.* **2014**, *80*, 1371–1379.

[281] Sivaramakrishnan, S.; Ouellet, H.; Matsumura, H.; Guan, S.; Moënne-Loccoz, P.; Burlingame, A. L.; de Montellano, P. R. O. Proximal Ligand Electron Donation and Reactivity of the Cytochrome P450 Ferric–Peroxo Anion. *J. Am. Chem. Soc.* **2012**, *134*, 6673–6684.

Appendix A Supporting Information for Chapter 2

Chemistry–A European Journal

Supporting Information

Selective Oxidations Using a Cytochrome P450 Enzyme Variant Driven with Surrogate Oxygen Donors and Light

Joel H. Z. Lee, Matthew N. Podgorski, Michael Moir, Alecia R. Gee, and Stephen G. Bell*

Experimental

Abbreviations

P450, cytochrome P450; BSTFA, *N*,*O*-Bis(trimethylsilyl)trifluoroacetamide; δ, chemical shift; DMSO, dimethyl sulfoxide; EDTA, ethylenediaminetetraacetic acid; FAD, flavin adenine dinucleotide; FMN, flavin mononucleotide; GC-MS, gas chromatography-mass spectrometry; IPTG, Isopropyl β-D-1-thiogalactopyranoside; KIE, kinetic isotope effect; LRMS; low resolution mass spectrometry; NADH, reduced nicotinamide adenine dinucleotide; NADPH, reduced nicotinamide adenine dinucleotide phosphate; Pd/C palladium on carbon; PFR, product formation rate; THF, tetrahydrofuran; TLC, thin layer chromatography; TMS, trimethylsilyl; WT, wild-type.

Heme Bleaching:

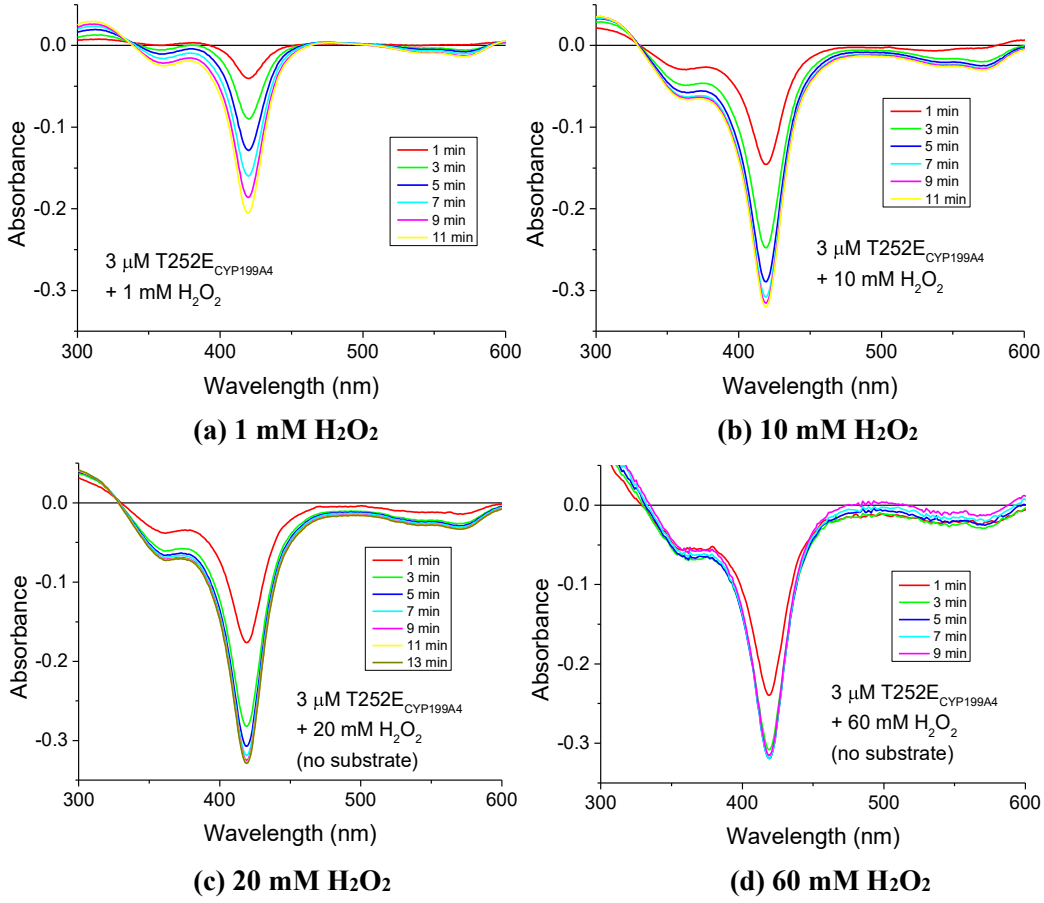

Figure S1 The rate of heme bleaching of substrate-free T252E-CYP199A4 (3 μM) when exposed to (a) 1 mM H_2O_2, (b) 10 mM H_2O_2, (c) 20 mM H_2O_2, and (d) 60 mM H_2O_2. Difference spectra were recorded at 2-minute intervals to monitor the loss of the Soret absorbance band.

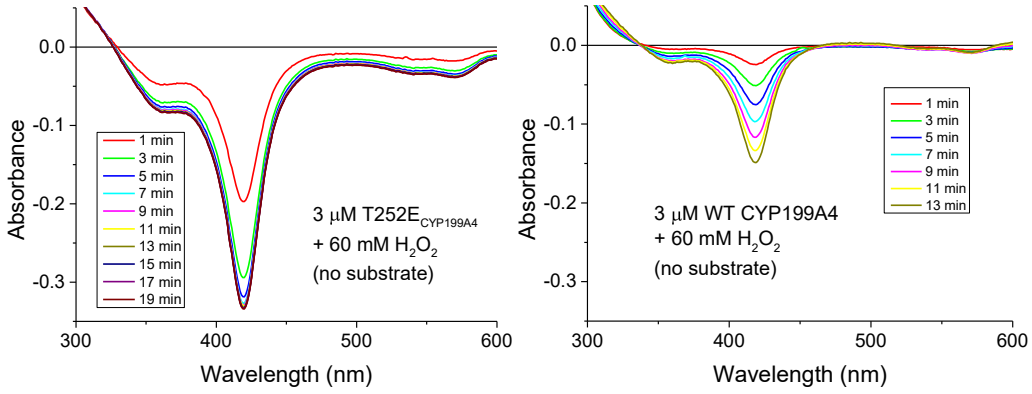

(a) T252E **(b) WT**

Figure S2 Comparison of the rate of heme bleaching of (a) substrate-free T252E-CYP199A4 enzyme (3 μM) exposed to 60 mM H_2O_2, and (b) substrate-free WT CYP199A4 exposed to 60 mM H_2O_2.

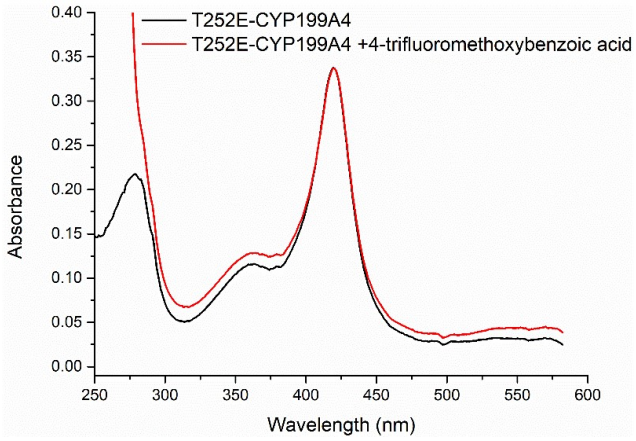

Figure S3 UV-vis spectra of the T252E variant of CYP199A4 before and after the addition of 4-trifluoromethoxybenzoic acid

Figure S4 The Superimposed Cα traces of T252E CYP199A4 bound to 4-methoxybenzoic acid (cyan tube; PDB code: 7REH) and 4-trifluoromethoxybenzoic acid (green tube). The RMSD between Cα atoms is 0.144 Å over all 393 pairs.

Table S1 Structural refinement and data collection statistics for T252E CYP199A4 bound with 4-trifluorobenzoic acid.

	4-trifluoromethoxybenzoic acid + T252E-CYP199A4
PDB code	8D1C
Wavelength (Å)	0.95373
a/b/c (Å)	41.08/51.49/79.62
α/β/γ (°)	90.00/92.25/90.00
Resolution (Å)	43.23-1.95 (2.00-1.95)
<I/σ(I)>	8.3 (0.9)
Unique reflections	24354 (1642)
Completeness	99.6 (95.9)
Redundancy	6.8 (6.7)
R_{merge} (%)	12.7 (166.0)
R_{pim} (%)	5.3 (68.0)
$CC_{1/2}$	99.7 (52.4)
R_{work} (%)	18.81
R_{free} (%)	23.45
Ramachandran plot (%)	
Most favoured	98
Allowed	2
Outliers	0

Table S2 Distances (in angstroms) of key structural features of 4-trifluorobenzoic acid-bound T252E CYP199A4 compared with those of 4-methoxybenzoic acid. W25 is the heme bound aqua ligand.

	Distance (Å)	**Equivalent distance in 4-methoxybenzoic acid-bound T252E**
Fe - OH_2 / OH^- ligand[a]	1.9	2.1
Fe - C358 Sγ	2.3	2.3
Fe - C_{11}	5.4	4.4
Fe - O_{10}	4.9	5.0
Fe - Closest O of E252	4.4	4.2
Fe - F_{12}	5.2	-
Fe - F_{13}	6.8	-
Fe - F_{14}	5.4	-
W25 - Closest O of E252	2.7	2.6
W25 - C_{11}	4.2	3.2
W25 - O_{10}	3.4	3.4
C_{11} - Closest C of F298	5.1	3.4
Angle (°)		
Dihedral (C_{04}-C_{03}-O_{10}-C_{11})	-85.8	-18.3
C_{03}-O_{10}-C_{11}	116.5	-
Occupancies		
4-TrifluoromethoxyBA	91 %	-
F298	81 %	-
W25	85 %	92%

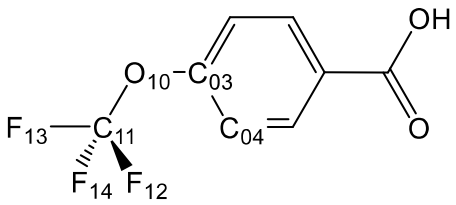

Heme bleaching by H_2O_2 inactivates the P450

To show that the bleached enzyme was inactive, 3 μM substrate-free T252E-CYP199A4 was pre-incubated with 50 mM H_2O_2 for 20 minutes before addition of 1 mM 4-methoxybenzoic acid. No product was generated by the bleached enzyme, demonstrating that it was completely inactive.

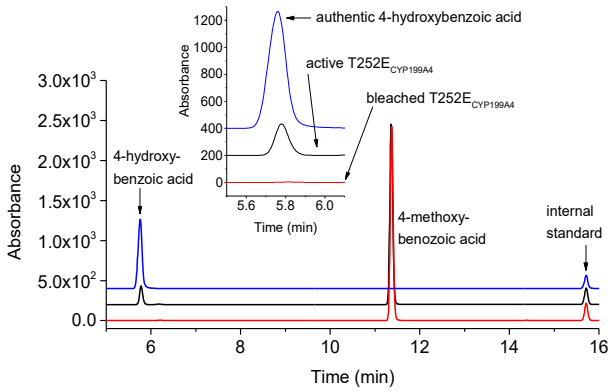

Figure S5 HPLC analysis of a 20-minute reaction of bleached T252E-CYP199A4 (3 μM) with 4-methoxybenzoic acid (red), demonstrating that the bleached enzyme is completely inactive. The T252E enzyme had been bleached by pre-incubation with 50 mM H_2O_2 for 20 mins before addition of substrate. No 4-hydroxybenzoic acid product was generated by the bleached enzyme. For comparison, a 20-min reaction of *active* T252E-CYP199A4 enzyme (3 μM) with 4-methoxybenzoic acid in the presence of 50 mM H_2O_2 is shown in black, which generated product. In blue is authentic 4-hydroxybenzoic acid.

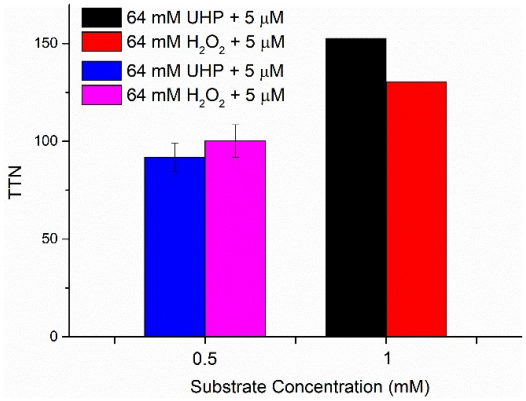

Figure S6 A comparison of the total turnover numbers (TTN) obtained with T252E-CYP199A4 (5 μM) in the presence of 4-methoxybenzoic acid (0.5 mM or 1 mM) and a high concentration of UHP and H_2O_2 (32 mM or 64 mM). Reactions were carried out 16 °C and left for 24 h. Reactions were left for a further 48 h and showed no additional product formation. See **Figure 2** for comparison.

Deuterated Substates:

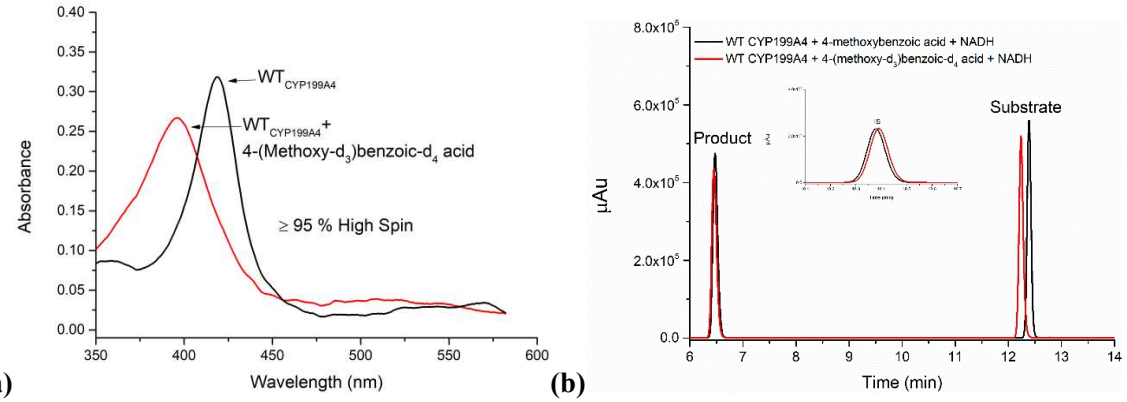

Figure S7 (a) Spin state shift analysis of 4-(methoxy-d_3)benzoic-d_4 acid with WT CYP199A4. The spin state induced by the deuterated substrate is similar to that of the its non-deuterated counterpart (≥ 95 % high spin).[1] **(b)** HPLC analysis of the *in vitro* NADH turnover of 4-methoxybenzoic acid (black) and 4-(methoxy-d_3)benzoic-d_4 acid (red) with WT-CP199A4. Reaction conditions are P450 (0.01 μM), HaPuX (5 μM), HaPuR (0.5 μM) and 1 mM substrate. The NADH consumption rate (given as mol.(molCYP)$^{-1}$.min^{-1} and abbreviated as min^{-1}) was 3540 min^{-1} for 4-methoxybenzoic acid and 3380 min^{-1} for the deuterated derivative. Reactions were left 30 mins before HPLC analysis to ensure complete consumption of NADH.

Table S3 NADH oxidation activity P450 catalysed oxidation reactions.

Substrate	**NADH rate (μM.μM(p450)$^{-1}$ · min^{-1}**
4-methoxyBA	3540
4-(methoxy-d_3)benzoic-d_4 acid	3380
Mixture-of deuterated/non-deuterated 4-methoxyBA	4100 ± 340

When higher concentration of P450 (1 μM) were used the NADH oxidation rate was 1000 ± 10 min^{-1} and 1100 ± 10 min^{-1} for the non-deuterated and deuterated substrates, respectively.

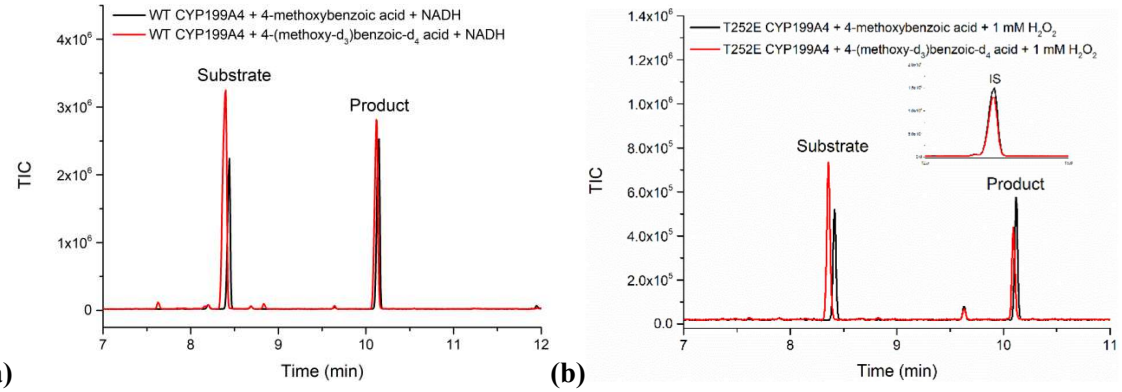

Figure S8 (a) GC-MS analysis of the *in vitro* NADH driven monooxygenase oxidation of 4-methoxybenzoic acid and 4-(methoxy-d_3)benzoic-d_4 acid with WT CYP199A4. **(b)** GC-MS analysis of the *in vitro* peroxygenase oxidation of 4-methoxybenzoic acid and 4-(methoxy-d_3)benzoic-d_4 acid with T252E-CYP199A4 with 1 mM H_2O_2. Substrate concentration used was 100 µM. Reactions were left for 20 h.

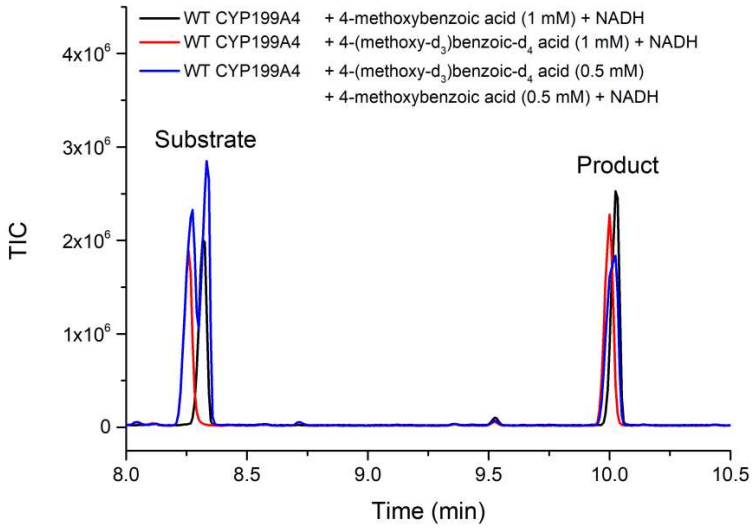

Figure S9 GC-MS analysis of the *in vitro* NADH oxidation of 4-methoxybenzoic acid (black) and 4-(methoxy-d_3)benzoic-d_4 acid (red) and a mixture of these two compounds (blue) by WT CYP199A4. A low concentration (0.01 µM of enzyme was used). HPLC analysis of the sample shown in Figure S7.

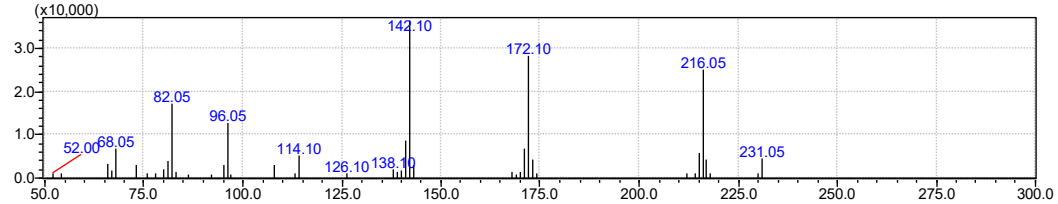

4-(methoxy-d_3)benzoic-d_4 acid (substrate, derivatised, m/z = 231)

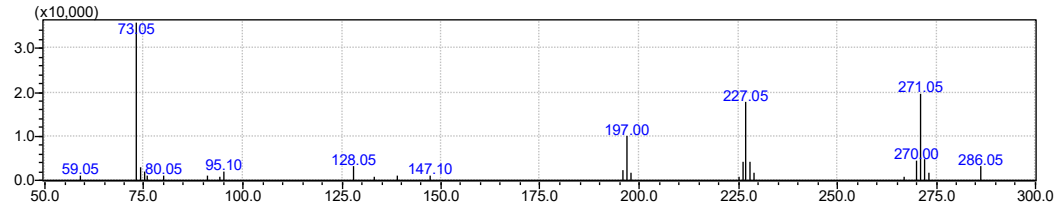

4-hydroxybenzoic-d_4 acid (product, derivatised, m/z = 286)

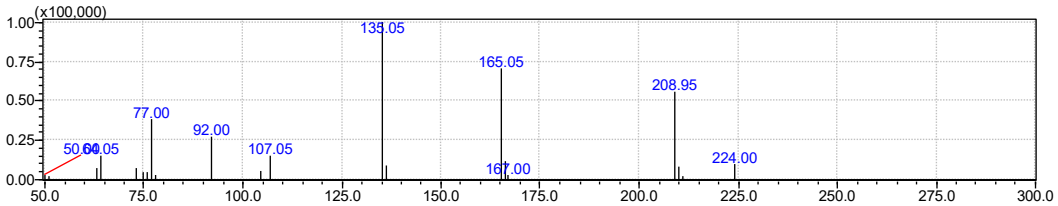

4-methoxybenzoic acid (substrate, derivitised, m/z = 224)

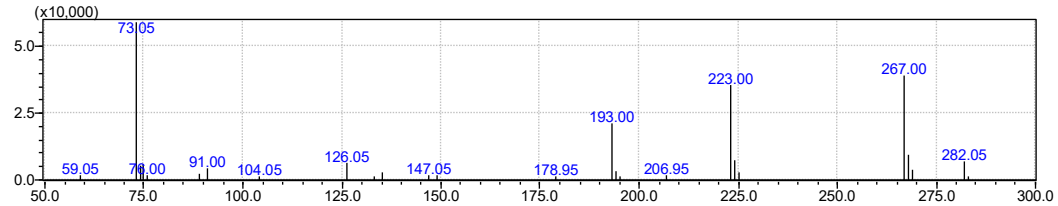

4-hydroxybenzoic acid (product, derivitised, m/z = 282)

Figure S10 MS analysis of 4-(methoxy-d_3)benzoic-d_4 acid and 4-methoxybenzoic acid alongside their product from the oxidation reactions with CYP199A4.

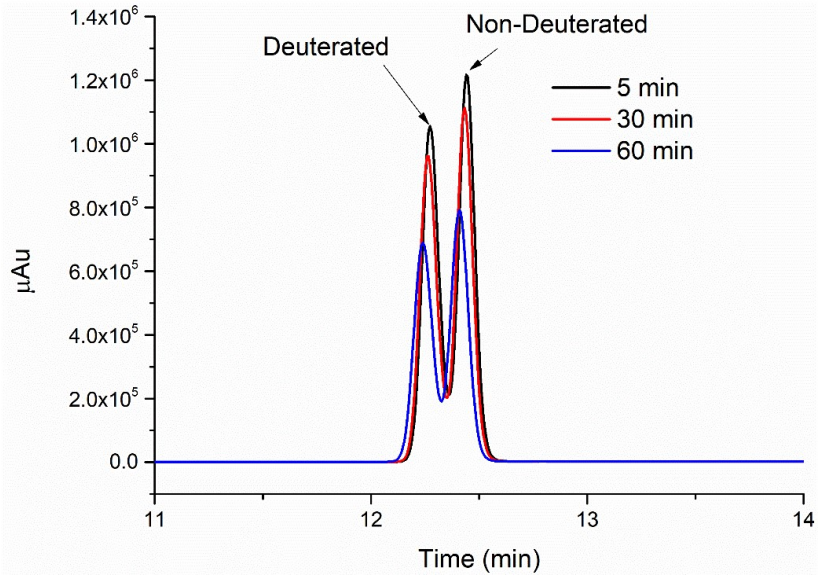

Figure S11 HPLC analysis of the H_2O_2 driven oxidation of a 1:1 mixture of deuterated and non-deuterated 4-methoxybenzoic acid by T252E CYP199A4. The ratio of the areas of each species remains constant throughout the duration of the reaction. Reaction conditions are as follows: T252E-CYP199A4 (1 μM) and 32 mM H_2O_2 with 0.5 mM of each deuterated and non-deuterated substrate. A 132 μL aliquot was taken the times specified for HPLC analysis.

Table S4 Ratio of deuterated to non-Deuterated 4-methoxybenzoic acid substrate in reaction with T252E-CYP199A4 and 32 mM H_2O_2.

Time (min)	Ratio
5	0.894
30	0.905
60	0.894

GC-MS analysis: CYP152A1 (P450$_{BS\beta}$) with Light-Driven Conditions

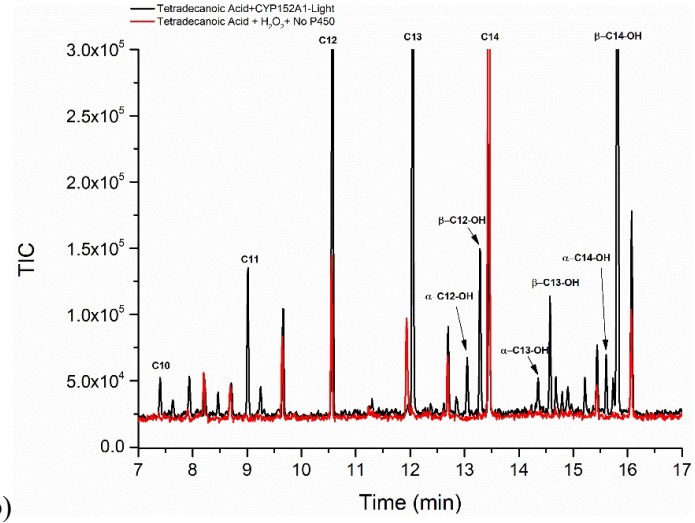

(b)

Figure S12 An enlarged version of the GC-MS Analysis of light driven oxidation of tetradecanoic acid (C14) by CYP152A1 (black, P450$_{BS\beta}$). In red is a control reaction with no P450 added. (

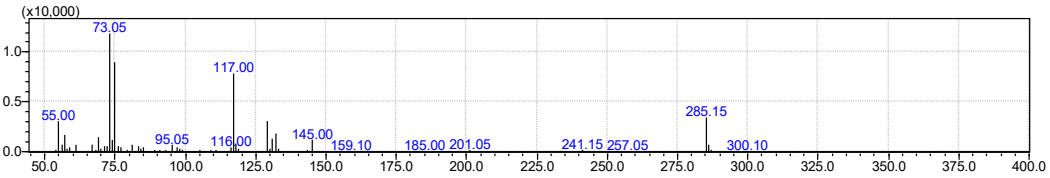

tetradecanoic acid (substrate, derivatised, m/z = 300)

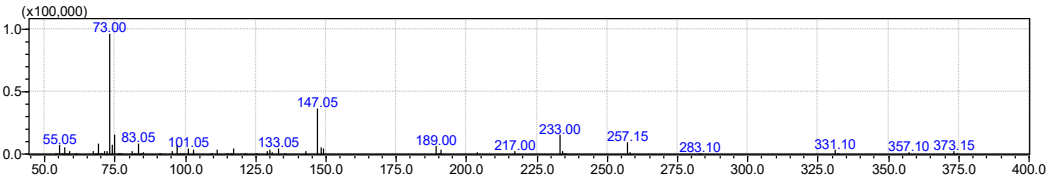

β-hydroxytetradecanoic acid (product, derivatised, m/z = 388)

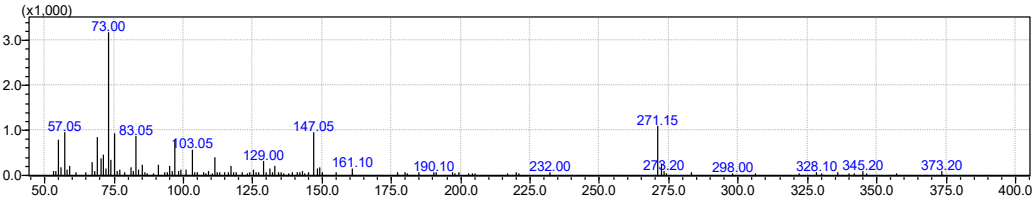

α-hydroxytetradecanoic acid (product, derivatised, m/z = 388)

Figure S13 (a) MS analysis of the tetradecanoic acid and its hydroxylation products as the substrate of P450Bsβ. Mass spectrum of the hydroxy products matches those in the literature.[2]

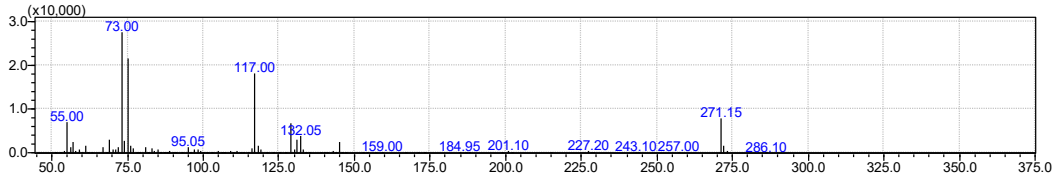

Tridecanoic acid (product, derivatised, m/z = 286)

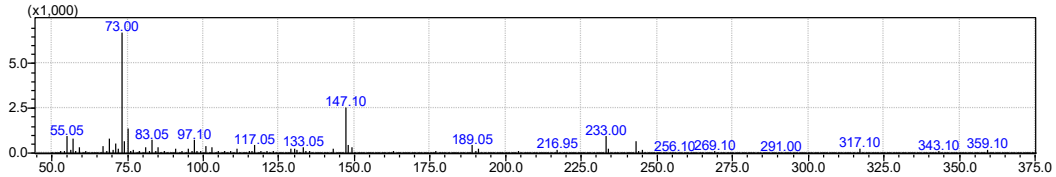

β-hydroxytridecanoic acid (product, derivatised, m/z = 374)

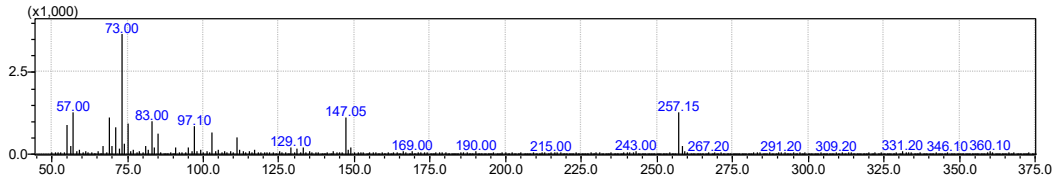

α-hydroxytridecanoic acid (product, derivatised, m/z = 374)

Figure S13 (b) MS analysis of the tridecanoic acid and its hydroxylation products in a reaction with P450Bsβ.

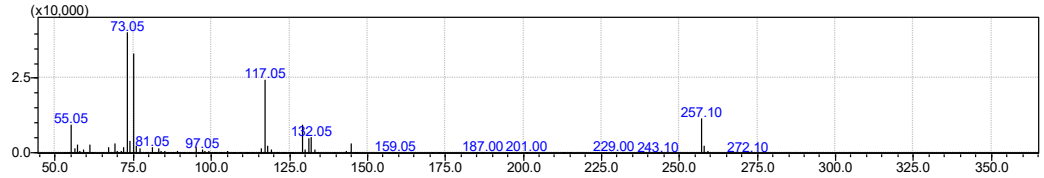

Dodecanoic acid (product, derivatised, m/z = 272)

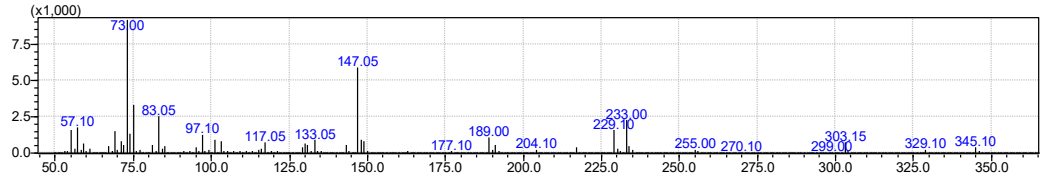

β-hydroxydodecanoic acid (product, derivatised, m/z = 360)

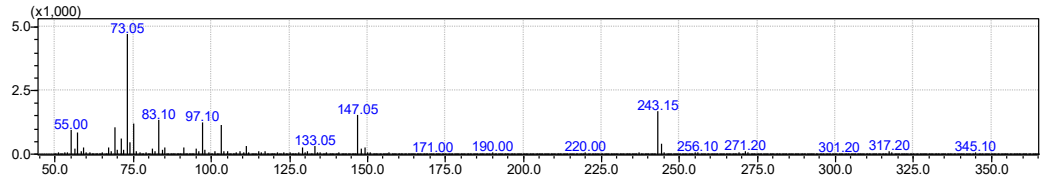

α-hydroxydodecanoic acid (product, derivatised, m/z = 360)

Figure S13 (c) MS analysis of the dodecanoic acid and its hydroxylation products in a reaction with P450Bsβ. Mass spectrum of the β-hydroxy product matched the that of the literature.[3]

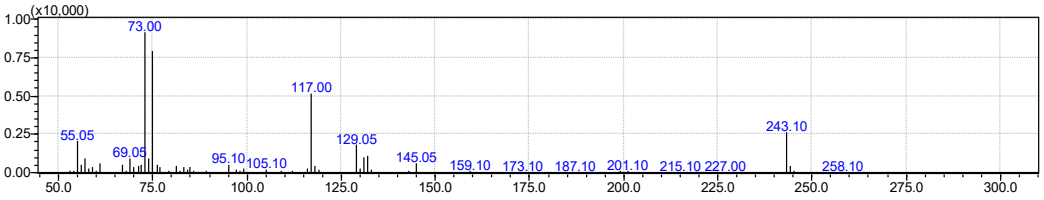

Undecanoic acid (product, derivatised, m/z = 258)

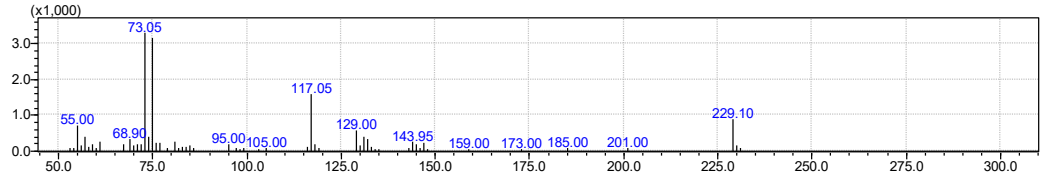

Decanoic acid (product, derivatised, m/z = 244)

Figure S13 (d) MS analysis of the undecanoic acid and decanoic acid as products in a reaction with P450Bsβ.

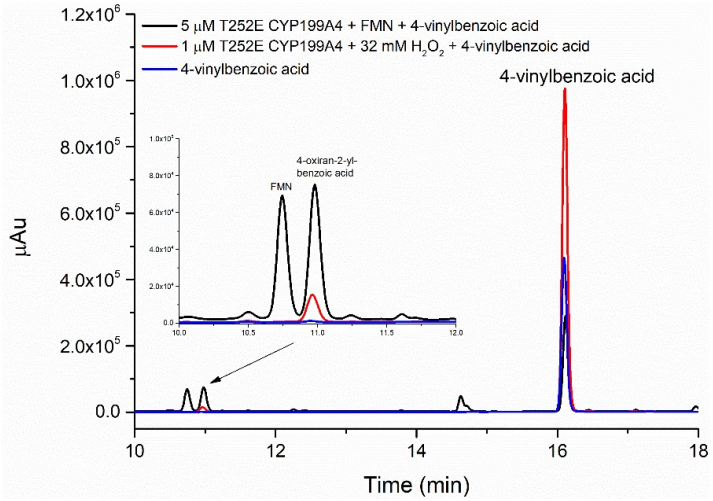

Figure S14 HPLC Analysis of light driven epoxidation of 4-vinylbenzoic acid by T252E-CYP199A4 (black). In red is a control reaction with T252E-CYP199A4 and 32 mM H_2O_2. Conditions used are 5 μM P450, 200 μM FMN, 1 mM EDTA and 200 μM substrate for the light-driven reaction.[4]

References

1. S. G. Bell, R. Zhou, W. Yang, A. B. H. Tan, A. S. Gentleman, L.-L. Wong and W. Zhou, *Chem. Eur. J.*, 2012, **18**, 16677-16688.
2. S. Honda Malca, M. Girhard, S. Schuster, P. Dürre and V. B. Urlacher, *Biochim. Biophys. Acta - Proteins Proteom.*, 2011, **1814**, 257-264.
3. S. N. S. Anis, M. S. Mohamad Annuar and K. Simarani, *Prep. Biochem. Biotechnol.*, 2017, **47**, 824-834.
4. T. Coleman, A. M. Kirk, R. R. Chao, M. N. Podgorski, J. S. Harbort, L. R. Churchman, J. B. Bruning, P. V. Bernhardt, J. R. Harmer, E. H. Krenske, J. J. De Voss and S. G. Bell, *ACS Catal.*, 2021, **11**, 1995-2010.

Appendix B Supporting Information for Chapter 3

B.1 gBlocks for Isothermal DNA Assembly of Oxidase-P450 Fusion Enzymes

gBlock for T252E-CYP199A4

AGTTCTGTTTCAGGGTCCGGGTAGTGGTGGTGGCGGTAGC
catATGGTCAGTAACTCATCGGCGGAGAGTATTAGTGCTCCGCCTAACG
ATTCTACTATCCCTCACCTTGCAATCGATCCATTCTCTTTAGACTTCTTT
GACGACCCATATCCTGATCAGCAAACTTTACGTGACGCGGGGCCGGTTG
TTTACCTGGATAAATGGAACGTCTATGGGGTGGCTCGCTATGCCGAGGT
CCATGCCGTTTTGAATGATCCAACGACATTCTGTTCGTCCCGTGGCGTC
GGATTATCTGACTTTAAGAAGGAAAAACCGTGGCGCCCTCCTAGCCTTA
TCTTAGAGGCAGACCCACCAGCACATACCCGTCCGCGTGCCGTGCTTTC
CAAAGTCCTGTCTCCCGCGACGATGAAAACTATCCGTGACGGGTTCGCT
GCAGCCGCAGACGCCAAGGTCGACGAATTGTTACAGCGTGGTTGTATCG
ACGCGATTGCTGATCTGGCGGAAGCCTATCCACTTTCTGTGTTCCCGGA
CGCAATGGGCTTGAAGCAAGAGGGACGCGAACATTTGCTGCCCTACGCG
GGCCTGGTTTTCAATGCATTCGGCCCACCAAACGAACTGCGCCAGACTG
CGATTGAACGCAGTGCCCCACACCAAGCGTACGTCAATGAACAGTGCCA
ACGTCCAAACTTAGCACCGGGAGGATTCGGCGCCTGCATTCACGCGTTT
ACTGACACAGGAGAGATCACTCCTGACGAGGCACCCCTTTTAGTGCGCT
CGTTGCTGTCAGCGGGTTTGGATGAAACTGTCAACGGCATTGGTGCAGC
AGTCTATTGTTTAGCCCGTTTTCCCGGAGAACTTCAACGTCTTCGTTCCG
ACCCGACTTTAGCTCGTAACGCGTTCGAAGAAGCTGTTCGCTTCGAGTC
TCCTGTTCAGACGTTTTTCCGTACTACGACTCGTGAGGTTGAATTGGGC
GGTGCCGTGATCGGTGAGGGAGAAAAGGTCTTAATGTTCTTGGGTTCTG
CCAATCGCGACCCTCGTCGTTGGAGCGACCCTGATTTATATGATATCAC
TCGTAAAACAAGTGGGCATGTCGGATTTGGTTCAGGTGTGCACATGTGC
GTGGGTCAGCTTGTGGCACGTTTAGAGGGAGAGGTTATGTTGAGTGCCT
TGGCGCGTAAGGTCGCGGCCATTGACATCGATGGCCCTGTAAAGCGTCG
TTTTAACAATACACTTCGCGGCCTGGAATCCTTACCCGTTAAATTAACAC
CGGCCTAATAATAAGGGTTCAGCGCCaagCTT***TGCGGCCGCACTCGAG***
CACCACCACCACCACCACTGAGAT

Figure B1: gBlock containing the DNA sequence of T252E-CYP199A4 used in isothermal DNA assembly. The 5′ end (*italicised*) contains the DNA sequence of the HRV3C amino acid linker that overlaps with the 3′ end in gBlocks for the oxidase enzymes. The 3′ end contains a region of homology with the digested backbone of the pET28 plasmid digested with *NcoI* and *HindIII* (*italicised*). The *NcoI* and *HindIII* restriction sites are underlined.

gBlock for AldOx

tctAGA*AATAATTTTGTTTAACTTTAAGAAGGAGATATACC*ATGCA
CCATCACCATCACCACGGTGAGAATCTTTATTTTCAGGGCATGAGCGACA
TCACCGTGACCAACTGGGCTGGGAACATCACGTACACCGCCAAAGAGTTA
TTACGTCCGCATTCCCTTGATGCTCTTCGTGCCCTTGTGGCGGATAGTGC
GCGTGTGCGTGTCTTGGGTTCCGGACACTCCTTTAATGAGATTGCTGAAC
CGGGCGATGGGGGAGTCCTTTTGTCGCTGGCAGGACTGCCCTCTGTAGTG
GATGTCGATACAGCAGCTCGCACGGTTCGCGTGGGCGGCGGTGTTCGCTA
CGCTGAGCTGGCTCGTGTGGTGCATGCCCGTGGGTTAGCATTGCCGAACA
TGGCCTCTTTGCCGCACATTTCTGTCGCGGGTTCTGTTGCGACAGGCACC
CACGGCTCTGGGGTTGGAAATGGCAGTCTGGCCAGTGTAGTACGTGAGG
TAGAGCTTGTCACTGCAGATGGATCAACCGTTGTCATTGCTCGCGGGGAT
GAACGCTTTGGTGGTGCGGTAACCTCTTTGGGTGCGCTGGGAGTTGTCAC
AAGTTTGACACTTGACTTGGAGCCGGCCTATGAAATGGAGCAACACGTT
TTTACAGAATTACCATTAGCCGGCTTAGACCCGGCTACGTTTGAGACAGT
GATGGCCGCAGCTTACTCAGTAAGTCTGTTTACCGATTGGCGCGCTCCAG
GATTCCGTCAAGTGTGGCTGAAACGTCGTACAGATCGCCCCCTGGACGG
TTTCCCTTATGCGGCACCAGCCGCAGAGAAAATGCATCCAGTACCCGGCA
TGCCAGCCGTAAATTGCACCGAACAGTTTGGCGTCCCTGGACCTTGGCAT
GAACGTCTTCCACATTTTCGCGCCGAATTTACCCCCTCGTCGGGAGCTGA
ACTTCAGTCTGAGTATTTGATGCCGCGTGAACACGCTTTAGCCGCGCTGC
ACGCGATGGATGCAATCCGCGAGACTTTGGCACCCGTTCTGCAAACGTGT
GAAATCCGCACGGTCGCAGCTGACGCACAGTGGCTTTCACCCGCGTATGG
ACGCGACACGGTAGCCGCTCACTTCACGTGGGTGGAAGACACAGCCGCG
GTGCTGCCAGTAGTCCGCCGTTTAGAAGAAGCATTGGTGCCGTTCGCAG
CTCGTCCACATTGGGGGAAGGTATTTACTGTGCCGGCTGGTGAGTTACG
CGCATTATACCCACGCCTTGCGGACTTTGGTGCCTTAGCGGGAGCCCTTG
ATCCTGCTGGCAAATTTACCAACGCATTCGTGCGCGGGGTTCTGGCCGGC
GGTAGTGGTCTGGAAGTTCTGTTTCAGGGTCCGGGTAGTGGTG-
GTGGCGGTAGC

Figure B2: gBlock containing the DNA sequence of alditol oxidase (AldOx) used in isothermal DNA assembly. The 5′ end (*italicised*) contains an overlapping region with the digested backbone of the pET28 plasmid digested with *NcoI* and *HindIII*. The 3′ end (*italicised*) contains the DNA sequence of the HRV3C amino acid linker that overlaps with the 5′ end in the gBlock containing T252E-CYP199A4. The *XbaI* restriction site is underlined.

gBlock for AoFOx

tctAGA*AATAATTTTGTTTAACTTTAAGAAGGAGATATACC* ATGCA
CCATCACCATCACCACGGTGAGAATCTTTATTTTCAGGGCATGGCCACAG
ACGGGTCCCACTTTGATTTCGTAATTGTTGGCGGAGGGACCGCTGGGAAT
ACAGTGGCTGGGCGTCTTGCTGAGAACCCTAACGTAACGGTTTTGATCGT
CGAGGCCGGAATCGGAAATCCTGAGGACATTCCTGAGATCACTACCCCCA
GCTCCGCGATGGATCTTCGCAACTCCAAATACGACTGGGCATACAAGACC
ACGATGGTCCGCCGCGATGATTACGAGCGTATCGAAAAACCAAATACACG
TGGTAAAACGCTGGGTGGGTCGAGTTCCTTGAATTACTTCACCTGGGTGC
CTGGTCATAAAGCAACCTTCGACCAATGGGAAGAATTCGGGGGTAAAGAG
TGGACGTGGGATCCCTTGGTTCCATACCTGCGTAAATCCGCTACTTACCA
TGACGATCCGCGCCTGTATTCTCCAGAACTGGAGAAGATCGGCGGCGGAG
GGCCAATCCCAATCTCACACGCGGAGCTGATTGACGAAATGGCCCCTTTC
CGCGAAAACCTGACGAAGGCGTGGAAGTCTATGGGGCAACCACTTATCGA
GAATATTTACGATGGGGAAATGGATGGTCTGACCCACTGCTGCGACACCA
TTTACCGCGGCCAACGTTCTGGGTCTTTTTTGTTTGTGAAAAACAAACCT
AATATTACAATCGTCCCTGAAGTTCACTCCAAGCGTCTTATTATCAATGA
GGCCGATCGTACTTGCAAAGGAGTGACGGTCGTTACTGCTGCGGGAAAC
GAATTGAATTTCTTCGCTGATCGCGAGGTCATCCTTAGCCAAGGAGTATT
TGAGACCCCTAAACTTTTGATGTTAAGTGGCATCGGACCAACCCGTGAAT
TGTCACGTCACGGGATCAATACAATCGTAGATTCTCGTCATGTTGGCCAG
AACTTAATGGATCACCCAGGCGTGCCTTTTGTCTTGCGCGTGAAGGACGG
ATTTGGTATGGATGATGTCTTATTACGCCACGGCCCGAAGCGTGACGCAG
TGGTGTCTGCTTACAATAAGAATCGTTCAGGGCCCGTTGGTAGTGGGCTT
CTGGAGCTGGTTGGCTTTCCACGTATCGATAAGTATCTGGAGAAGGACGC
TGAATATCGTAAAGCTAAAGCAGCGAATGGGGGGAAGGATCCGTTTAGC
CCGTTAGGGCAACCTCACTTTGAACTGGACTTCGTGTGTATGTTTGGCAC
CGCCTTCCAATGGCACTTTCCTACGCCTAAGACCGGAGATCACCTGACCG
TAGTGGTTGACCTGGTTCGCCCCATCTCTGACCCCGGAGAAGTTACTCTT
AACTCTGCGGACCCGTTTCAACAACCTAACATTAACTTAAACTTTTTTGC
TAATGATCTTGATATCATCGCAATGCGCGAAGGTATTCGTTTCTCGTACG
ACTTGCTTTTCAAAGGAGAAGGGTTTAAGGATCTGGTAGAATCTGAGTAT
CCGTGGGAAATGCCTTTGGATTCTGATAAAGAAATGCATCGTGCGGTGTT
GGATCGCTGCCAGACTGCGTTTCACCCGACAGGTACGGCTCGTTTATCTA
AAAACATTGATCAAGGTGTGGTAGATCCCAAGCTGAAAGTGCATGGTATT
AAAAAACTGCGTGTAGCGGATGCTTCTGTTATCCCAATTATTCCAGACTG
TCGTATCCAAAATTCTGTATATGCCGTGGGAGAAAAATGCGCTGATATGA
TTAAGGCAGAACACAAAGACCTGTAC***GGTAGTGGTCTGGAAGTTCT-***
GTTTCAGGGTCCGGGTAGTGGTGGTGGCGGTAGC

Figure B3: gBlock containing the DNA sequence of formate oxidase (AoFOx) used in isothermal DNA assembly. The 5′ end (*italicised*) contains an overlapping region with the digested backbone of the pET28 plasmid digested with *NcoI* and *HindIII*. The 3′ end (*italicised*) contains the DNA sequence of the HRV3C amino acid linker that overlaps with the 5′ end in the gBlock containing T252E-CYP199A4. The *XbaI* restriction site is underlined.

gBlock for AcC06-AcChOx

tctAGAAATAATTTTGTTTAACTTTAAGAAGGAGATATACCATGCAC
CATCACCATCACCACGGTGAGAATCTTTATTTTCAGGGCATGCACATCGA
TAACATCGAGAATCTGAGCGACCGCGGGTTTGACTACGTTGTAATTGGTG
GTGGAAGCGCAGGCGCAGCAGTAGCCGCGCGCTTATCTGAGGACCCGGA
CGTGTCGGTGGCCTTAGTGGAAGCCGGACCTGACGATCGTAATATTCCGG
AAATCCTGCAACTTGACCGTTGGATGGAACTGCTGGAGAGTGGCTACGA
CTGGGATTACCCGATCGAGCCACAAGAAAACGGCAATTCATTCATGCGCC
ATGCACGCGCCAAAGTCATGGGAGGCTGTAGCTCCCACAATGCGTGCATT
GCTTTCTGGGCACCGCGCGAGGACCTGGATGAATGGGAATCGAAGTACG
GGGCAACCGGCTGGAACGCCGCGAATGCTTGGCCATTGTACAAGCGCCTT
GAAACGAACCAGGACGCTGGTCCTGACGCGCCGCACCACGGGGACTCAG
GTCCCGTGCACCTGATGAATGTTCCGCCAGCGGATCCGAGCGGCGTCGCG
TTGCTTGACGCATGTGAAGAGGCTGGGATTCCTCGCGCCCGTTTTAACAC
GGGTACAACTGTTGTAAACGGGGCAAATTTCTTCCAGATTAATCGTCGTG
GAGATGGGACACGTTCTAGTAGTTCGGTTAGTTATATTCACCCCATTATC
GAGCGTGATAATTTCACATTACTTACAGGATTGCGTGCACGTCAATTAGT
CTTCGATGCCGATAAGCGTTGCACCGGCGTTGAGGTCGTCGGCGGCGCA
CGCGGACGCACTCACCGTTTGACGGCGCGTCATGAAGTAATTCTTTCCAC
AGGAGCTATTGACTCACCGAAACTTCTTATGTTAAGTGGCATTGGTCCTG
CGGAACACTTAGCACAACACGGGATCGAAGTCTTAGTTGATTCTCCAGGG
GTCGGGGAAAATCTTCAAGATCACCCCGAGGGAGTGGTACAATTTGAGG
CAAAGCAGCCGATGGTTCAAACATCAACACAGTGGTGGGAGATTGGAATC
TTCACTCCAACCGAGGATGGATTGGACCGTCCGGATCTTATGATGCATTA
CGGATCTACTCCCCGCGATCGCAACACGCTTCGTCACGGCTATCCTACAA
CGGAAAACGGGTTCTCCTTAACTCCGAATGTTACTCACGCCCGTAGTCGC
GGGACAGTCCGCCTTCGCTCGCGCGACTTTCGCGACAAGCCTATGGTTGA
CCCACGTTATTTTACCGACCCTGAAGGACATGACATGCGTGTAATGGTGG
CCGGCATTCGTAAGGCCCGTGAAATCGCGGCACAACCCGCCATGTCCGCG
TGGACAGGGCGTGAACTTTCGCCGGGCGTTGGGGCCCAAACTGACGAAG
AGTTACAGGATTACATCCGCAAGACACACAACACGGTCTATCATCCGGTG
GGTACAGTACGCATGGGTGCCGATGACGACGGCATGTCCCCATTAGACGC
CCGCCTTCGCGTCAAAGGTGTCACCGGATTACGTGTAGCAGACGCTTCTG
TGATGCCCGAGCATGTAACAGTAAACCCTAATATTACAGTGATGATGATT
GGCGAGCGCTGTGCAGACTTAATTAAAGCTGATTACGCGGGGGCTGATG
CCTTGGAAGAAAAAGAGTTGACAACGAGCTTCGCC***GGTAGTGGTCTG-***
GAAGTTCTGTTT CAGGGTCCGGGTAGTGGTGGTGGCGGTAGC

Figure B4: gBlock containing the DNA sequence choline oxidase (AcC06-AcChOx) used in isothermal DNA assembly. The 5′ end (*italicised*) contains an overlapping region with the digested backbone of the pET28 plasmid digested with *NcoI* and *HindIII*. The 3′ end (*italicised*) contains the DNA sequence of the HRV3C amino acid linker that overlaps with the 5′ end in the gBlock containing T252E-CYP199A4. The *XbaI* restriction site is underlined.

B.2 Sequencing Primers for Oxidase-P450 Enzyme Fusions

The following primer pairs were used to attempt to fully sequence the insert of AldOx + T252E-CYP199A4 in pET28. A map of the binding site for each primer pair is shown also. The direction of PCR amplification for each primer is shown as black arrows.

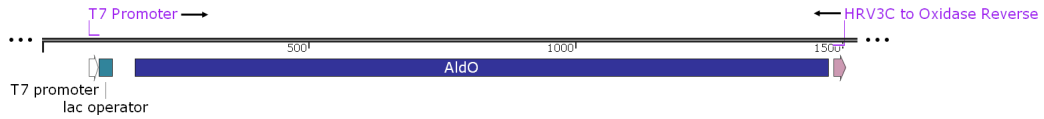

T7 Promoter :

5′-taatacgactcactataggg-3′

HRV3C to Oxidase Reverse:

5′-ccctgaaacagaacttccagac-3′

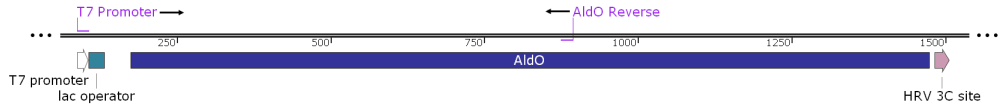

T7 Promoter :

5′-taatacgactcactataggg-3′

AldO Reverse:

5′-cacacttgacggaatcctgg-3′

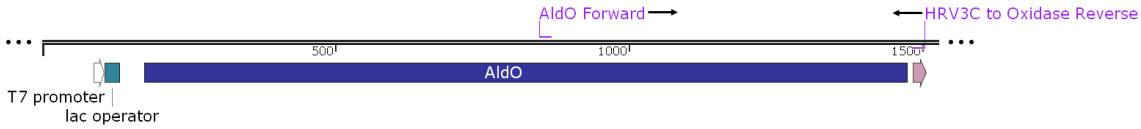

AldO Forward :

5′-gtaagtctgtttaccgattgg-3′

HRV3C to Oxidase Reverse:

5′-ccctgaaacagaacttccagac-3′

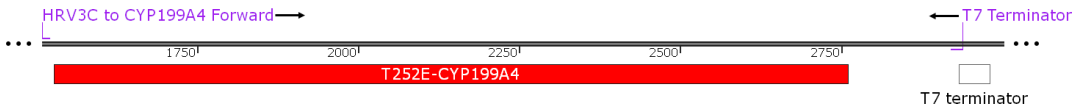

HRV3C to CYP199A4 Forward :

5′-tccgggtagtggtggtggcg-3′

T7 Terminator:

5′-gctagttattgctcagcgg-3′

The following primer pairs were used to attempt to fully sequence the insert of AcChOx + T252E-CYP199A4 in pET28. A map of the binding site for each primer pair is shown also. The direction of PCR amplification for each primer is shown as black arrows.

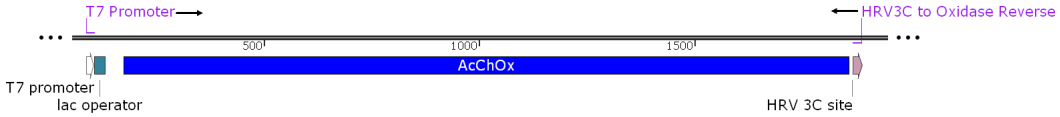

T7 Promoter :

5′-taatacgactcactataggg-3′

HRV3C to Oxidase Reverse:

5′-ccctgaaacagaacttccagac-3′

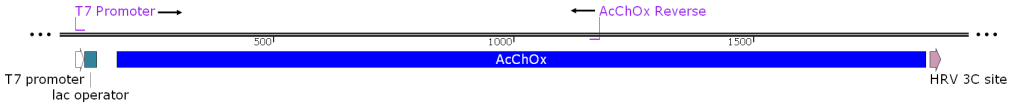

T7 Promoter :

5′-taatacgactcactataggg-3′

AcChOx Reverse:

5′-tttgcctcaaattgtaccact-3′

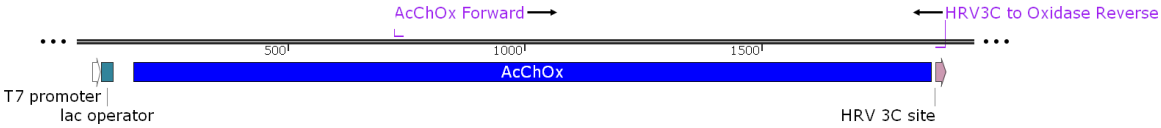

AcChOx Forward :

5′-cgttgcttgacgcatgtgaa-3′

HRV3C to Oxidase Reverse:

5′-ccctgaaacagaacttccagac-3′

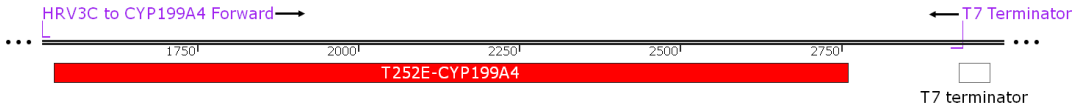

HRV3C to CYP199A4 Forward :

5′-tccgggtagtggtggtggcg-3′

T7 Terminator:

5′-gctagttattgctcagcgg-3′

The following primer pairs were used to attempt to fully sequence the insert of AoFOx + T252E-CYP199A4 in pET28. A map of the binding site for each primer pair is shown also. The direction of PCR amplification for each primer is shown as black arrows.

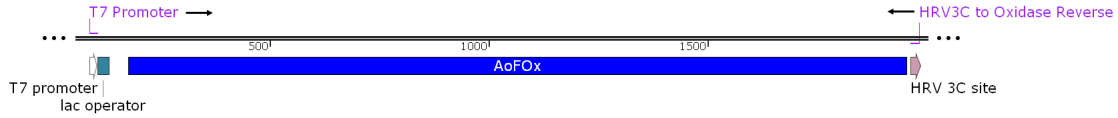

T7 Promoter :

5′-taatacgactcactataggg-3′

HRV3C to Oxidase Reverse:

5′-ccctgaaacagaacttccagac-3′

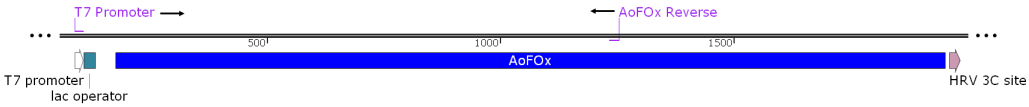

T7 Promoter :

5′-taatacgactcactataggg-3′

AoFOx Reverse:

5′-cgattcttattgtaagcagac-3′

AoFOx Forward :

5′-aatggatggtctgacccact-3′

HRV3C to Oxidase Reverse:

5′-ccctgaaacagaacttccagac-3′

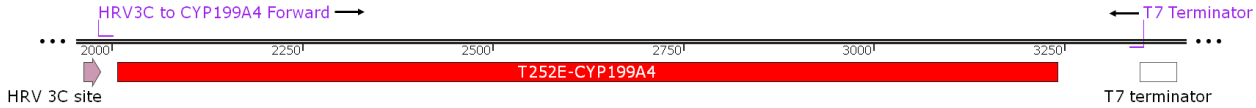

HRV3C to CYP199A4 Forward :

5′-tccgggtagtggtggtggcg-3′

T7 Terminator:

5′-gctagttattgctcagcgg-3′

B.3 Sequence of $P450_{BS\beta}$

ccATGGCGCACCACCACCACCACCACGGAGGCGGTAGCAACGAGCAGATCC
CTCATGATAAATCATTGGACAACTCTCTTACTTTATTAAAAGAGGGCTAC
TTGTTTATTAAAAACCGCACGGAACGTTACAATAGCGACCTGTTTCAAGC
TCGTCTTTTAGGGAAAAATTTCATTTGTATGACTGGAGCGGAAGCAGCGA
AGGTTTTTTACGATACAGACCGTTTCCAACGTCAGAACGCTTTGCCTAAG
CGCGTCCAAAAGTCCTTATTCGGGGTGAATGCCATCCAAGGAATGGATGG
CTCGGCACACATCCACCGTAAAATGCTGTTTCTTAGTCTTATGACGCCGC
CCCACCAAAAGCGCTTGGCTGAGCTTATGACCGAAGAGTGGAAAGCGGCT
GTTACTCGCTGGGAGAAGGCTGATGAAGTAGTGTTGTTTGAAGAGGCTA
AGGAGATTCTTTGCCGTGTCGCATGTTATTGGGCAGGGGTCCCCTTAAAG
GAGACTGAAGTTAAAGAACGTGCTGACGATTTCATCGATATGGTAGACGC
CTTTGGTGCGGTTGGACCACGTCATTGGAAGGGACGCCGCGCCCGTCCAC
GTGCCGAGGAATGGATTGAGGTTATGATCGAGGACGCTCGCGCCGGTCT
GTTGAAGACGACGTCAGGCACCGCACTTCATGAAATGGCATTTCACACCC
AGGAGGATGGCTCGCAATTGGACTCTCGCATGGCTGCGATCGAATTGATT
AACGTATTGCGCCCTATTGTGGCAATCTCTTATTTCCTGGTTTTCTCCGC
TTTGGCTCTTCATGAGCACCCGAAGTACAAGGAATGGTTGCGCAGCGGAA
ATTCACGCGAGCGTGAGATGTTTGTTCAAGAAGTCCGCCGTTACTATCCC
TTTGGGCCTTTCCTTGGTGCGTTGGTCAAGAAAGACTTTGTGTGGAATAA
TTGCGAATTTAAGAAAGGAACATCTGTATTATTGGACTTGTATGGGACCA
ACCATGATCCACGTCTGTGGGATCATCCCGATvGAGTTTCGCCCTGAGCG
TTTTGCAGAGCGTGAAGAGAACTTGTTTGATATGATTCCGCAGGGAGGTG
GGCATGCTGAGAAAGGGCATCGCTGCCCTGGTGAGGGCATTACAATTGA
GGTAATGAAAGCGAGCCTGGATTTTCTGGTACACCAAATCGAATACGATG
TGCCTGAGCAGTCTTTACATTATTCTCTTGCACGTATGCCTAGTTTACCG
GAAAGCGGATTTGTTATGAGCGGAATCCGCCGCAAATCGGAATTCGGAG
GCGGTAGCATGCCCGGACGTGCGCGTGCCCAACGCCAATCTTCTCGCGGG
CGCTAATAAAAGctt

Figure B17: Sequence of $P450_{BS\beta}$. The *NcoI* and *HindIII* restriction sites are underlined. The $3'$ contains the DNA sequence of a silica-binding domain.

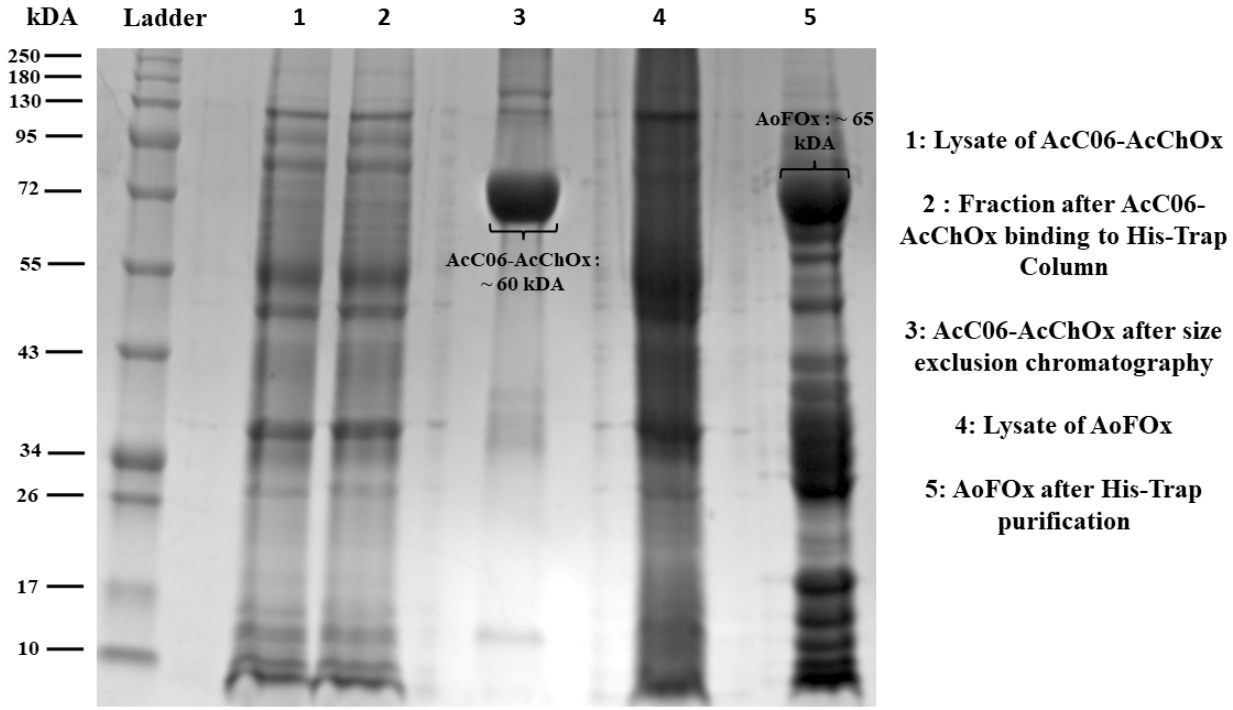

Figure B18: SDS-PAGE analysis of the purification of AcC06-AcChOx and AoFOx. SDS-PAGE was performed with a Mini-PROTEAN TGX gel (Bio-Rad). A broad range protein ladder (10 - 250 kDa) was used.

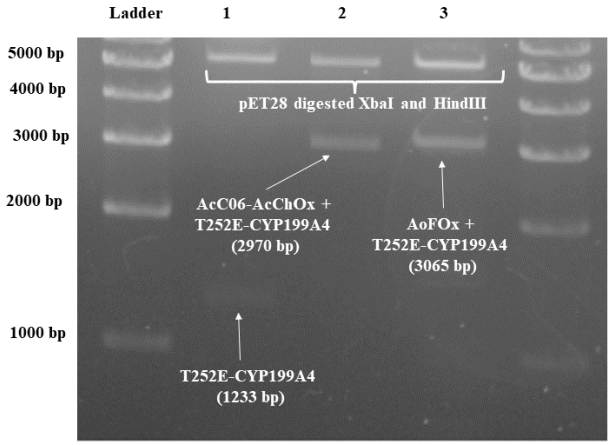

Figure B19: Agarose gel electrophoresis analysis (0.8 % gel) of AcC06-AcChOx + T252E-CYP199A4 (Lane 2) and AoFOx + T252E-CYP199A4 (Lane 3) cloned into pET28 via isothermal DNA assembly. These plasmids were digested at *XbaI* and *HindIII* restriction sites. The same digest was carried out with a pET28 plasmid containing an insert that contains only T252E-CYP199A4 as a control (Lane 1). It can be seen that bands corresponding to the expected size of an insert with both oxidase and T252E-CYP199A4 DNA sequences were observed. A 1 kb DNA ladder from Geneworks was used.

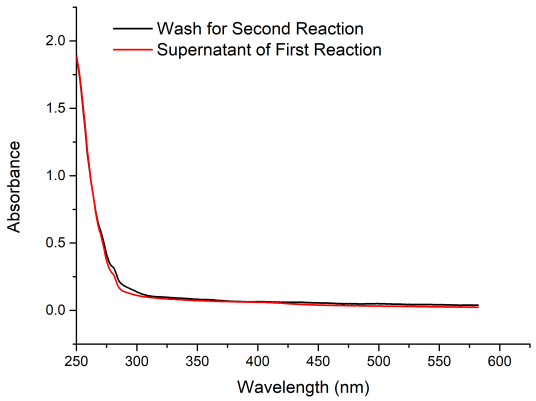

Figure B20: UV-visible spectra for the supernatant of the reaction of immobilised T252E-CYP199A4 and subsequent wash. No P450 enzyme was detected from the reaction and the wash indicating it is still bound to the SOURCE15Q media.

Appendix C Supporting Information for Chapter 4

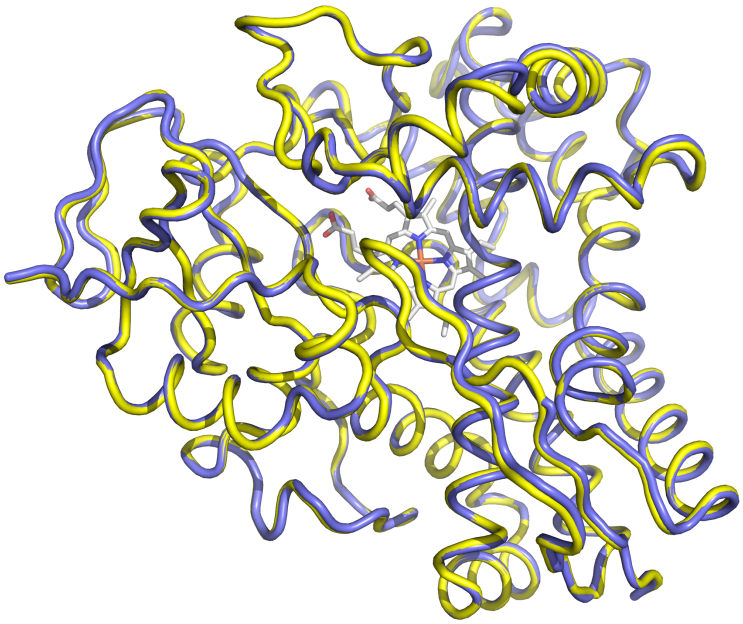

Figure C1: The superimposed structure of T252E-CYP199A4 complexed with 4-hydroxybenzoic acid (yellow tubes) with a structure of T252E-CYP199A4 complexed 4-methoxybenzoic acid (PDB 7REH, navy tubes). The RMSD between the Cα atoms is 0.157 Å over all 393 pairs.

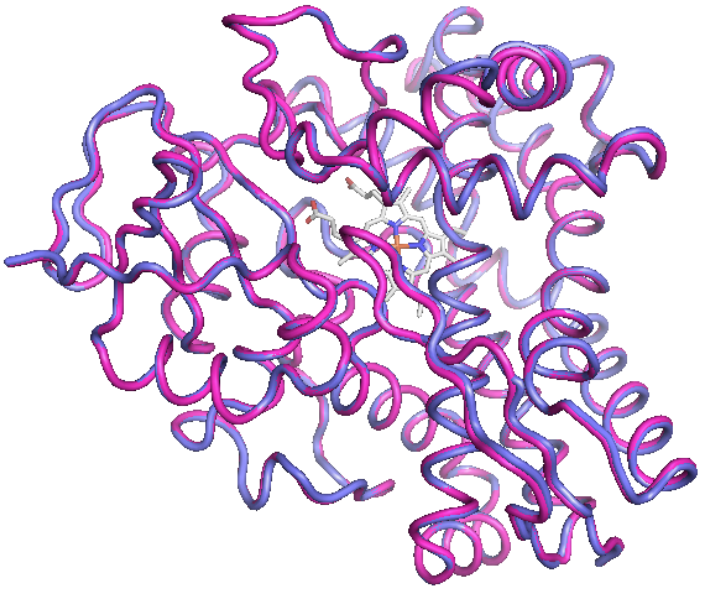

Figure C2: The superimposed structure of T252E-CYP199A4 co-crystallised with 4-methoxybenzoic acid and soaked with 1 mM H_2O_2 for 0 min (magenta sticks) with a structure of T252E-CYP199A4 complexed 4-methoxybenzoic acid (PDB 7REH). The RMSD between the Cα atoms is 0.250 Å over all 393 pairs.

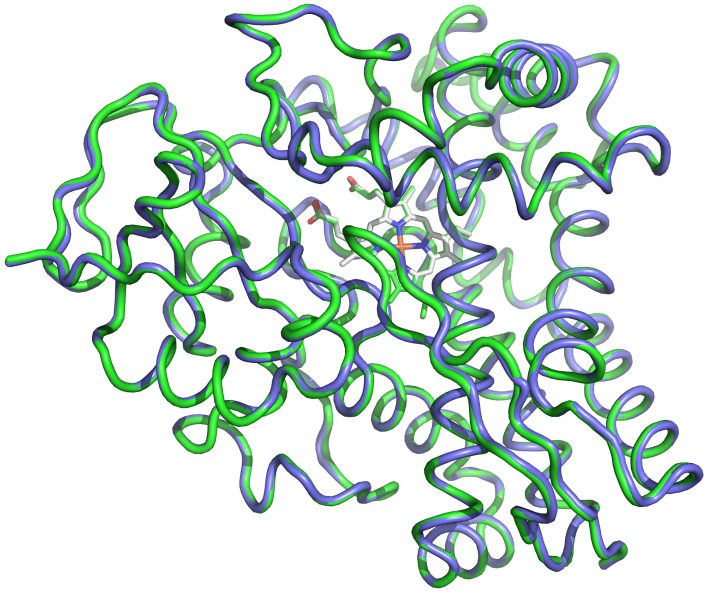

Figure C3: The superimposed structure of T252E-CYP199A4 co-crystallised with 4-methoxybenzoic acid and soaked with 4 mM H_2O_2 for 5 mins with a structure of T252E-CYP199A4 complexed 4-methoxybenzoic acid (PDB 7REH). The RMSD between the Cα atoms is 0.261 Å over all 393 pairs.

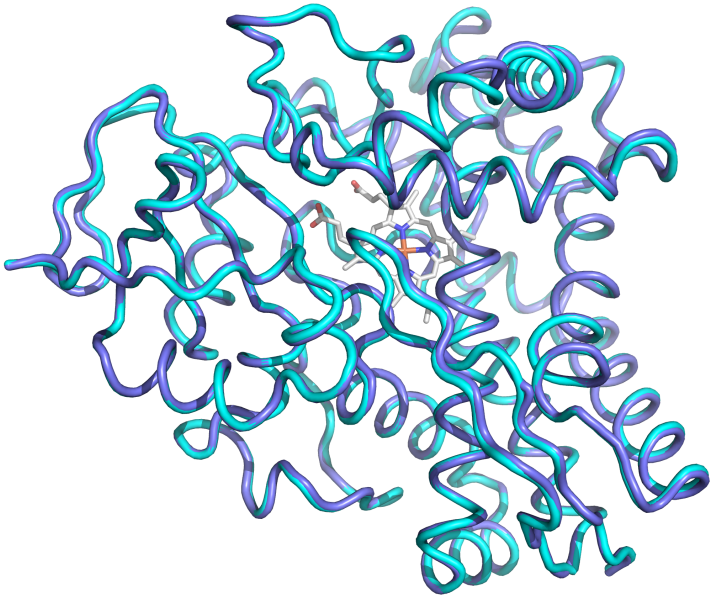

Figure C4: The superimposed structure of T252E-CYP199A4 co-crystallised with 4-methoxybenzoic acid and soaked with 2 mM H_2O_2 for 10 mins with a structure of T252E-CYP199A4 complexed 4-methoxybenzoic acid (PDB 7REH). The RMSD between the Cα atoms is 0.268 Å over all 393 pairs.

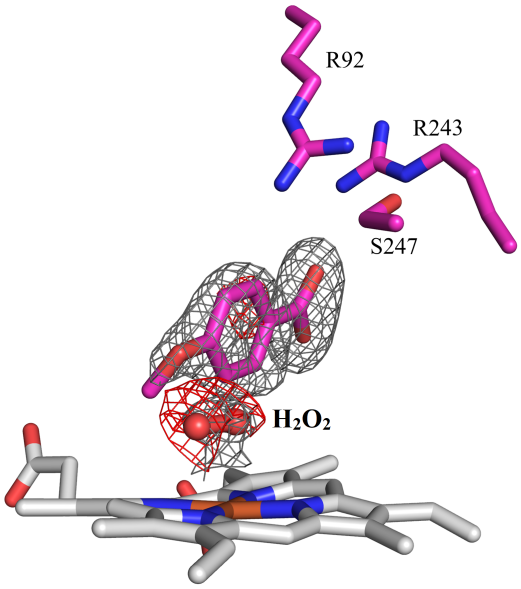

Figure C5: Crystal structure of T252E-CYP199A4 complexed with 4-methoxybenzoic that has been soaked in 1 mM H_2O_2 (magenta sticks). The electron density above the heme centre has been modelled with a hydrogen peroxide molecule (H_2O_2, red sticks). The F_o-F_c map (red mesh, 2.5 σ contour) was shown around the H_2O_2 molecule.

Table C1: Statistics for data collection and refinement of crystal structures of T252E-CYP199A4 complexed with 4-hydroxybenzoic acid and 4-methoxybenzoic acid. Crystals that have been soaked with H_2O_2 is specified . Values in parentheses correspond to the highest resolution (outer) shell.

Initial Ligand/Soaking Condition	4-methoxybenzoic acid + 4 mM H_2O_2 for 5 min	4-methoxybenzoic acid + 2 mM H_2O_2 for 10 min	4-methoxybenzoic acid + 1 mM H_2O_2 for 0 min	4-hydroxybenzoic acid
Final Modelled Ligand	4-hydroxybenzoic acid	4-methoxybenzoic acid	4-methoxybenzoic acid	4-hydroxybenzoic acid
PDB	8GLZ	8GM2	8GM1	8GLY
Beamline	MX1	MX1	MX1	MX1
Wavelength (Å)	0.95	0.95	0.95	0.95
Space group	$P12_11$	$P12_11$	$P12_11$	$P12_11$
a/b/c (Å)	41.17/51.62/78.46	44.37/51.64/79.06	44.17/51.61/79.39	44.19/51.70/79.36
$\alpha/\beta/\gamma$	90.00/92.15/90.00	90.00/92.31/90.00	90.00/92.31/90.00	90.00/92.16/90.00
Resolution (Å)	41.14 - 2.02 (2.07 - 2.02)	44.34 - 2.33 (2.41 - 2.33)	43.26 - 1.85 (1.89 - 1.85)	44.16 - 2.03 (2.08 - 2.03)
$< I/\sigma(I) >$	17.4 (3.1)	11.9 (3)	13.8 (3.6)	10.1 (2.9)
Unique Reflections	21694 (1563)	15455 (1489)	30680 (1850)	23312 (1726)
Completeness	98.3 (96.3)	99.8 (99.6)	99.9 (98.8)	99.8 (99.6)
Redundancy	6.6 (6.5)	6.5 (6.4)	6.6 (5.4)	6.8 (6.1)
R_{merge} (%)	7 (62.2)	13.6 (81.4)	8 (41.6)	15.6 (67.7)
R_{pim}	3.0 (27)	5.8 (35)	3.3 (19.5)	6.4 (29.3)
$CC_{1/2}$ (%)	99.9 (90.7)	99.5 (89.3)	99.8 (91.0)	99.5 (86.8)
R_{work} (%)	19.5	21.1	16.1	16.8
R_{free} (%)	24.7	26.5	20.0	22.6
Ramachandran Plot (%)				
Most Favoured	96	94	96	96
Allowed	4	6	4	4
Outliers	0	0	0	0

Table C2: Distances of notable features within the active site of different crystals of T252E-CYP199A4 soaked with H_2O_2 complexed with 4-methoxybenzoic acid (PDB: 8GLZ and 8GM2). Demethylation of substrate occurred in one of these crystals (PDB: 8GLZ) after soaking with H_2O_2. These crystals were compared to structures of T252E-CYP199A4 complexed to 4-methoxybenzoic acid (PDB: 7REH) and 4-hydroxybenzoic acid (8GM2).

Initial Ligand/Soaking Condition	4-methoxybenzoic acid + 4 mM H_2O_2 for 5 min	4-methoxybenzoic acid + 2 mM H_2O_2 for 10 min	4-hydroxybenzoic acid	4-methoxybenzoic acid
PDB	8GLZ	8GM2	8GLY	7REH
Active Site Ligand	4-hydroxybenzoic acid	4-methoxybenzoic acid	4-hydroxybenzoic acid	4-methoxybenzoic acid
Distance (Å)				
Fe - OH_2 ligand[a]	2.1	2.2	2.0	2.1
Fe=**O**[b] - O_7	3.1	3.4	3.3	3.6
Fe - C358 S_γ[c]	2.4	2.2	2.2	2.3
Fe - O_7[d]	4.7	4.9	4.8	5.0
Fe - closest O of E252	4.2	4.5	4.3	4.2
OH_2 Ligand[a] - O_7	2.7	3.4	3.4	3.4
OH_2 Ligand[a] - C_{Me}		3.3		3.3
amide NH of G249 - closest O of E252	3.0	2.7	2.9	2.7
amide NH of G249 - furthest O of E252	3.2	3.2	3.1	3.1
Angle (°)				
Fe=O-O_7	159.4	154.7	149.7	148.9
Dihedral C_{Me}-O_{10}-C_{03}-C_{04}		-18.3		-25

[a]Heme-bound water ligand [b]Oxygen atom of Cpd I [c]Sulfur atom of heme-bound cysteine thiolate [d]Oxygen atom of the *para-moiety* in 4-hydroxy- and 4methoxybenzoic acid (see below).

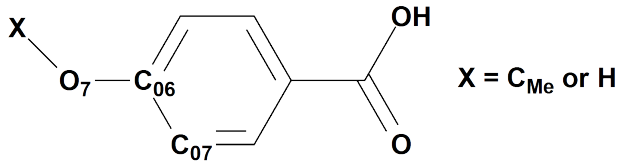

Appendix D Supporting Information for Chapter 5

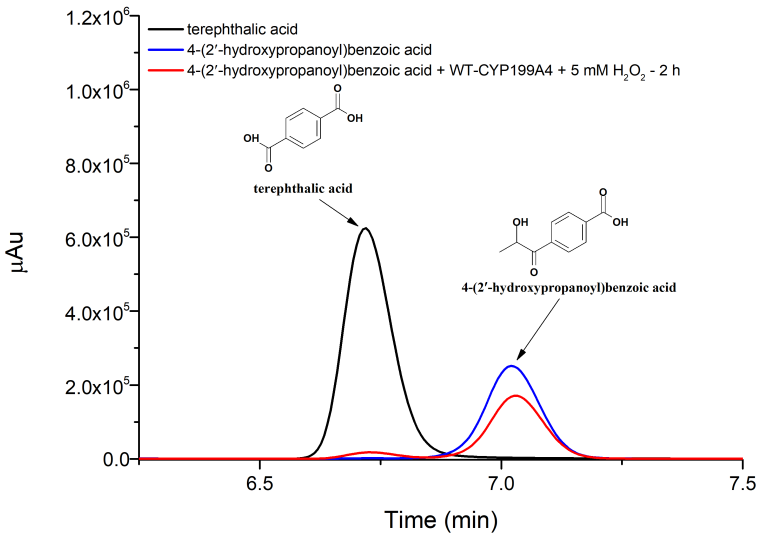

Figure D1: HPLC analysis of the H_2O_2 reaction of WT CYP199A4 with 4-(2′-hydroxypropanoyl)benzoic acid (red) in comparison with terephthalic acid as a control (black) and substrate (blue).

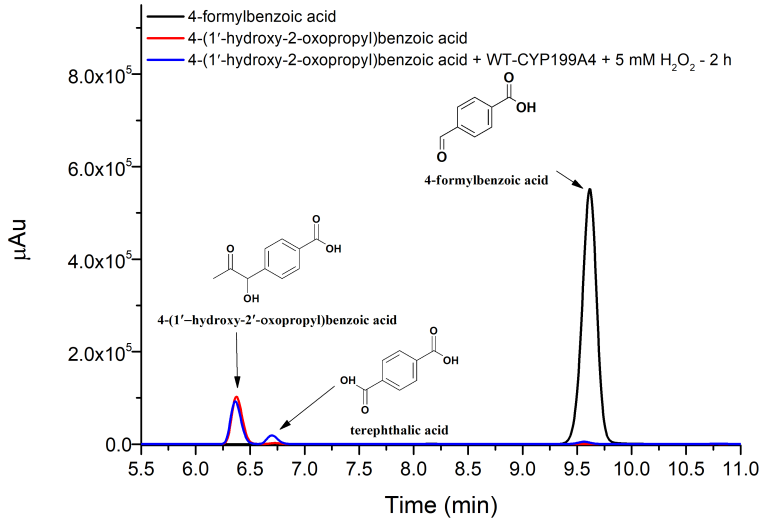

(a)

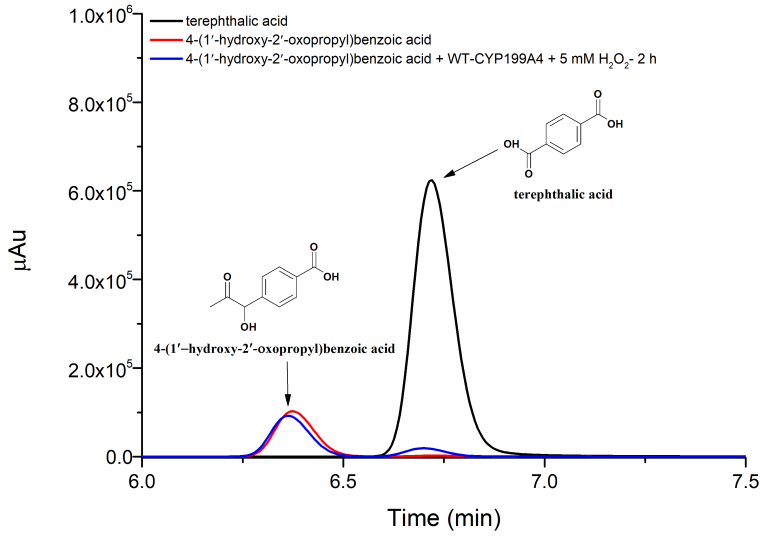

(b)

Figure D2: HPLC analysis of the *in vitro* oxidation reaction of WT CYP199A4 with 4-(1-hydroxy-2′-oxopropyl)benzoic acid in comparison with formylbenzoic acid (a) and 4-terephthalic acid (b) as controls.

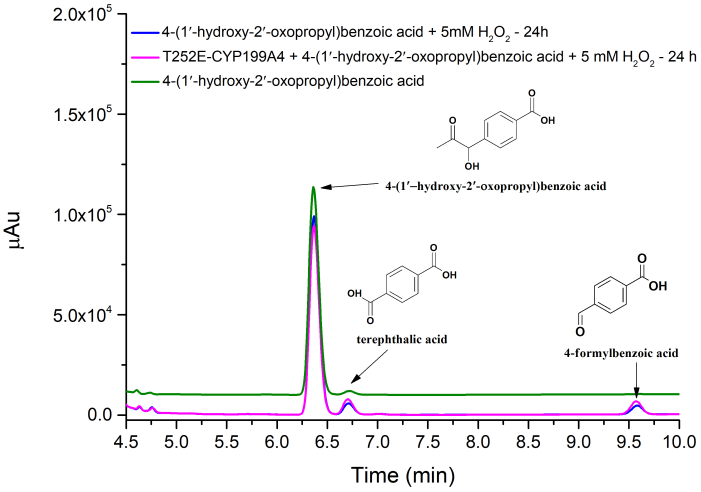

Figure D3: HPLC analysis of the *in vitro* oxidation reactions of T252E CYP199A4 (magenta) with 4-(1′-hydroxy-2′-oxopropyl)benzoic acid ($t_R = 6.4$ min) with 5 mM H_2O_2. A control of 4-(1′-hydroxy-2′-oxopropyl)benzoic acid with 5 mM H_2O_2 (blue) and the substrate control (green, offset in y-axis for clarity) is shown. Further oxidation metabolites is indicated by " * ".

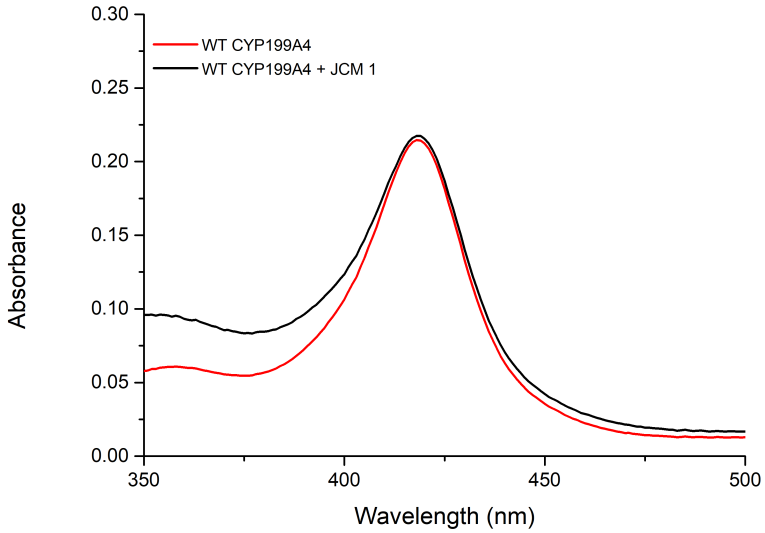

(a)

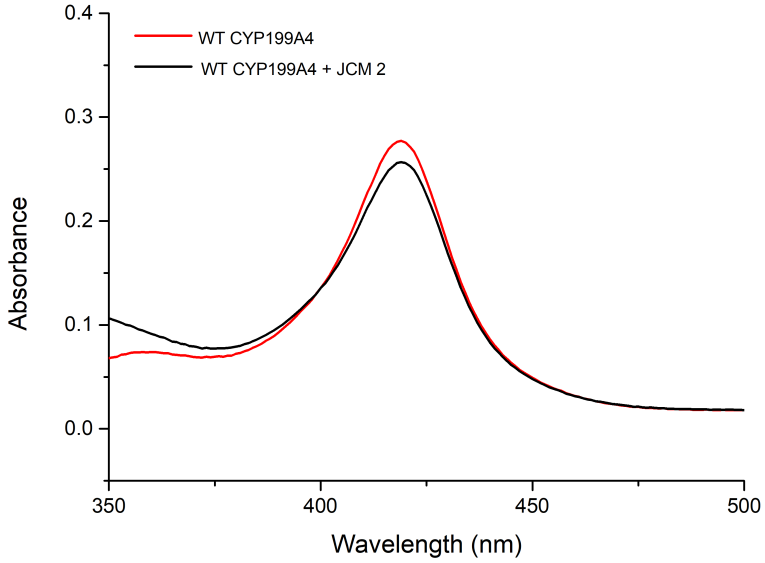

(b)

Figure D4: UV-visible spectra of WT CYP199A4 before and after addition of substrates, JCM 1 (a) and JCM 2 (b). The substrate free form is shown in red and the substrate bound form in black. The Soret maximum for WT CYP199A4 without substrate was 418 nm.

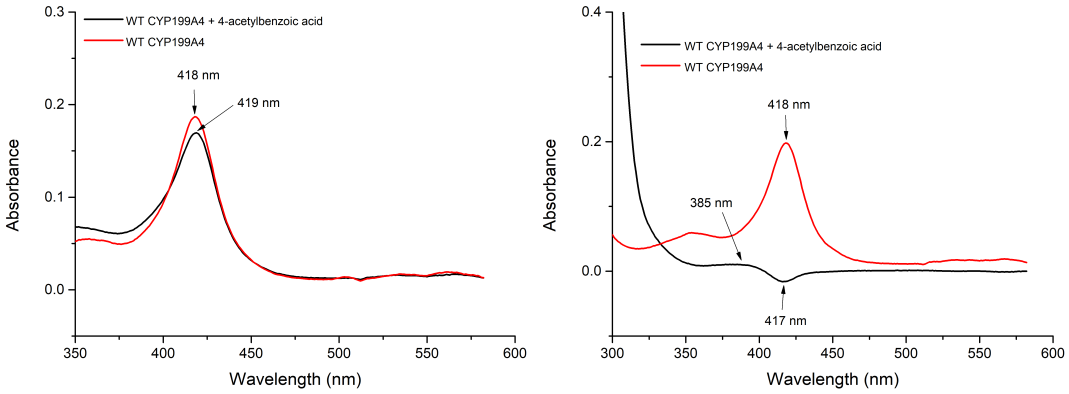

(a) (b)

Figure D5: (a) UV-visible analysis of WT CYP199A4 with 4-acetylbenzoic acid. (b) Difference spectra of WT CYP199A4 with 4-acetylbenzoic acid. The substrate free form is shown in red, and the substrate bound form in black.

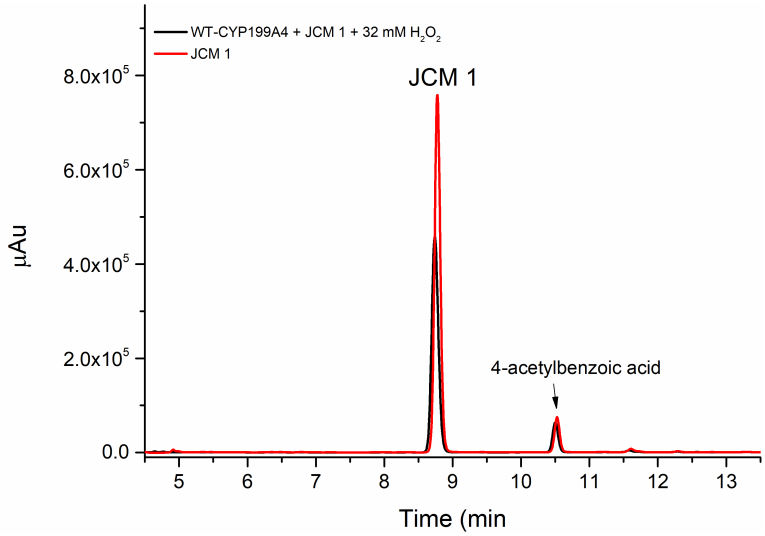

Figure D6: HPLC analysis of the peroxygenase turnover reaction of WT CYP199A4 with JCM 1 and 32 mM H_2O_2 (black) and a JCM 1 substrate control is shown also (red).

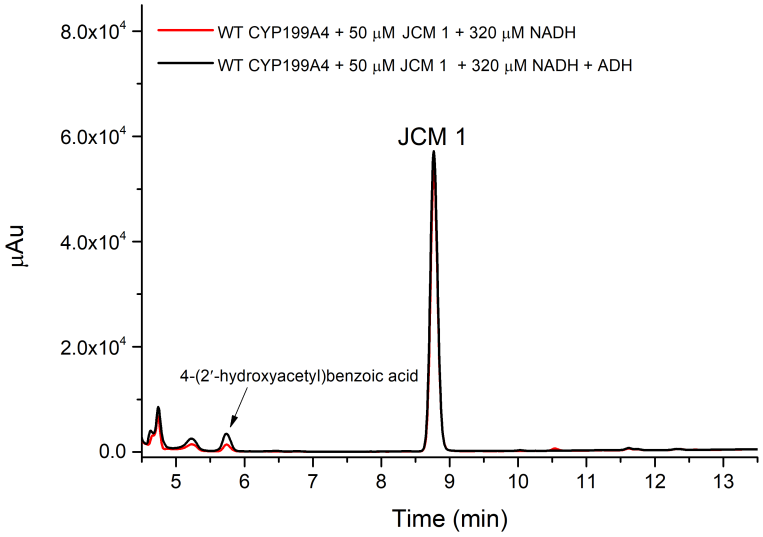

Figure D7: HPLC analyses of the *in vitro* NADH regenerating turnover reaction of WT CYP199A4 with JCM 1 and alcohol dehydrogenase (ADH, black). The same reaction with no alcohol dehydrogenase control is shown also (red). JCM 1 was used at a low concentration (50 µM) as to mitigate the effect of the 4-acetylbenzoic acid impurity, where 4-acetylbenzoic acid will be consumed first and should allow JCM 1 to be oxidised after.

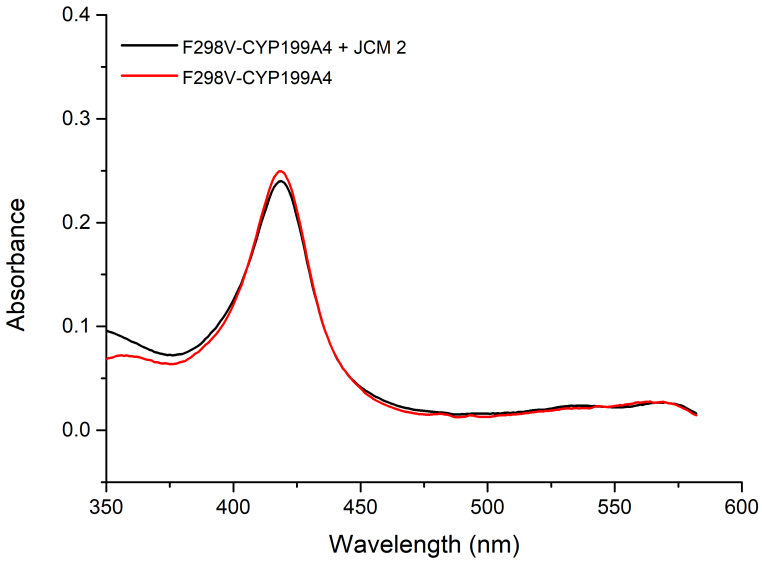

Figure D8: UV-visible spectra of F298V-CYP199A4 before and after addition of JCM 2. The substrate-free form is shown in red and the substrate-bound form in black.

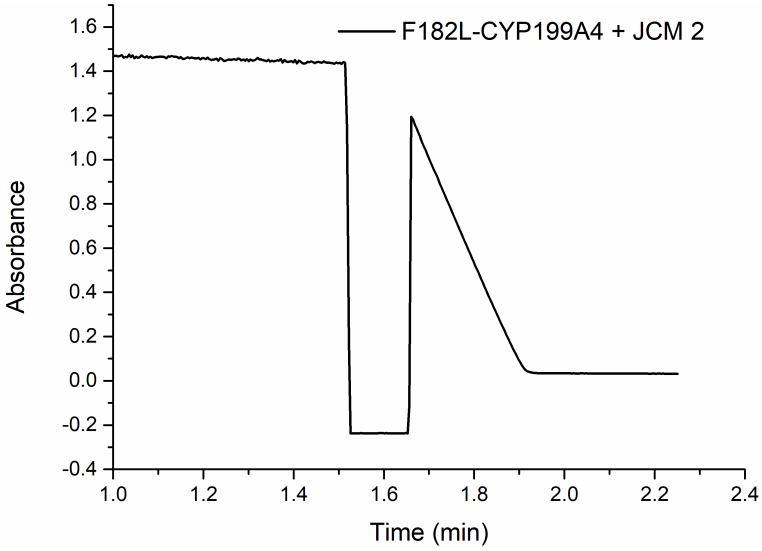

Figure D9: UV-visible analysis of the NADH oxidation reaction of F182L-CYP199A4 with JCM 2.

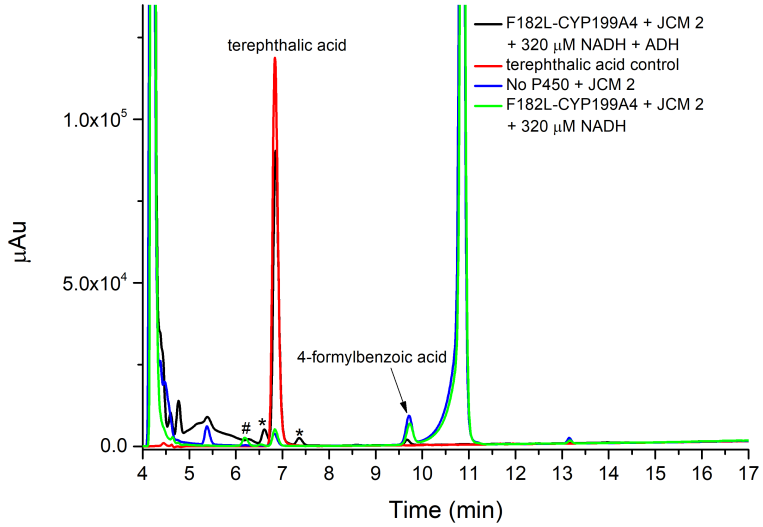

Figure D10: HPLC analysis of the NADH oxidation reaction of F182L-CYP199A4 with JCM 2 with the NADH regenerating system (ADH, black) and without the NADH regenerating system (green). Terephthalic acid standard (red) and a control containing no P450 (blue) is shown also. Unknown metabolites indicated by " # " and " * ".

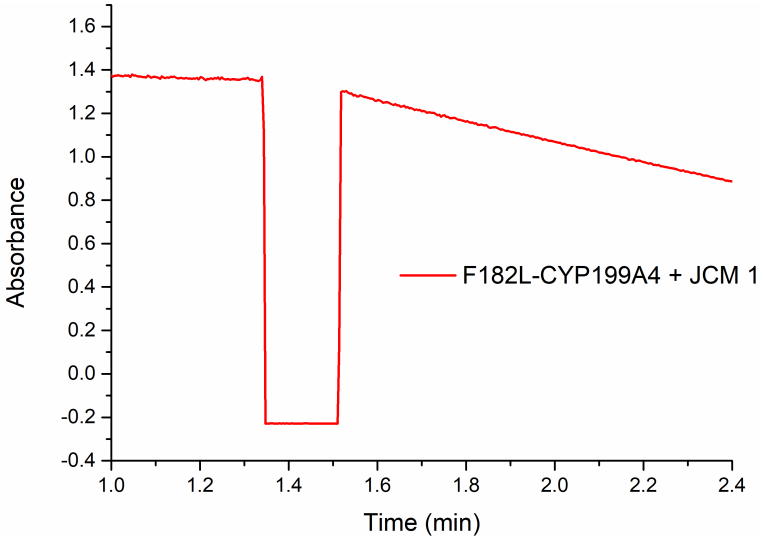

Figure D11: UV-visible analysis of the NADH oxidation reaction of F182L-CYP199A4 with JCM 1.

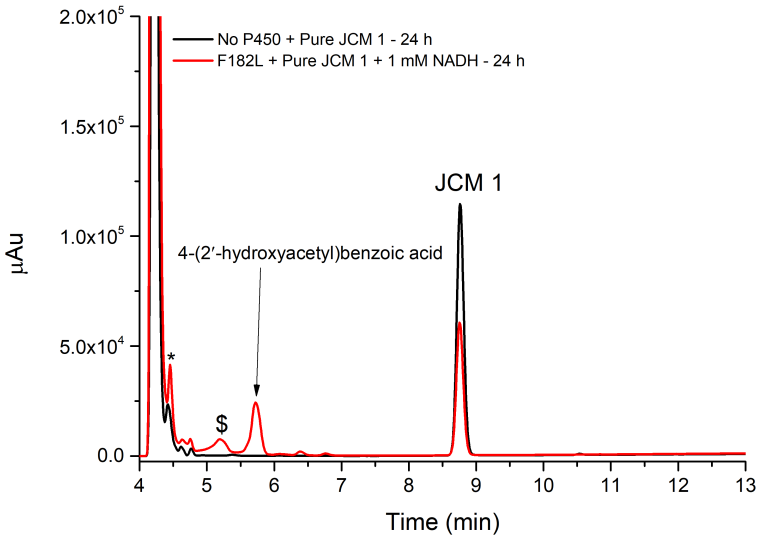

Figure D12: HPLC analysis of the *in vitro* oxidation reaction of F182L-CYP199A4 and purified JCM 1 (red). A no P450 control is shown in black.

GC-MS Analysis: JCM 1 and Products

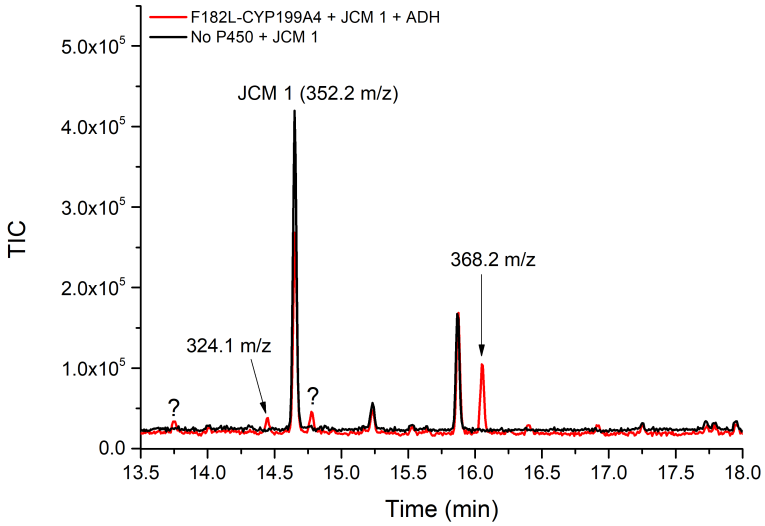

Figure D13: GC-MS analysis of the reaction between F182L-CYP199A4 and JCM1 (red) and a no P450 control with JCM 1 is shown also (black). The m/z value for product peaks is as labelled. Unknown product peaks are labelled with " ? ".

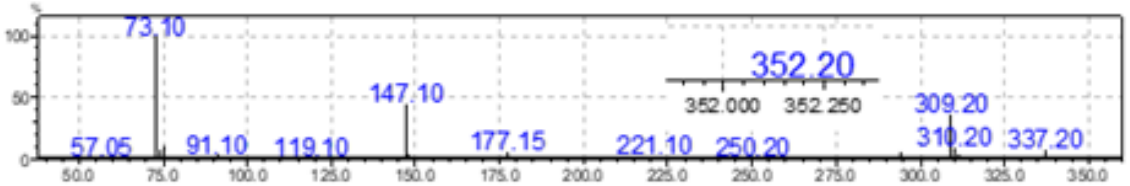

(a) Mass spectra of JCM 1, with m/z = 352.2 and t_R = 14.4 min

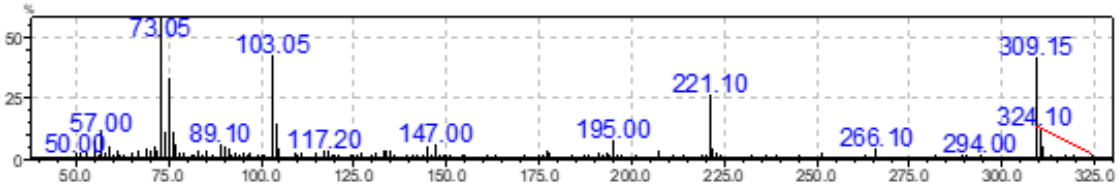

(b) Mass spectra of 4-(2′-hydroxyacetyl)benzoic acid with m/z = 324.1 and t_R = 14.4 min

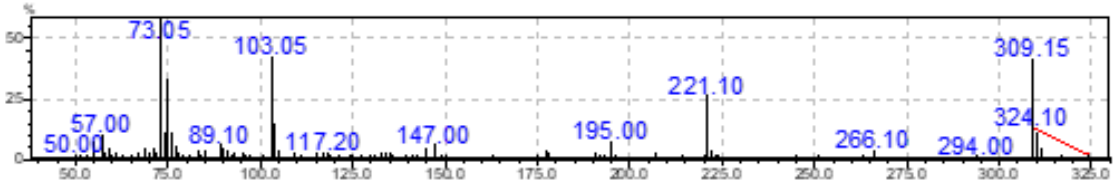

(c) Mass spectra of a potential hydroxylation product of JCM 1 (" & ", doubly derivitised) with m/z = 368.2 and t_R = 16.1 min

Figure D14: Mass spectra of JCM 1 reaction with F182L-CYP199A4.

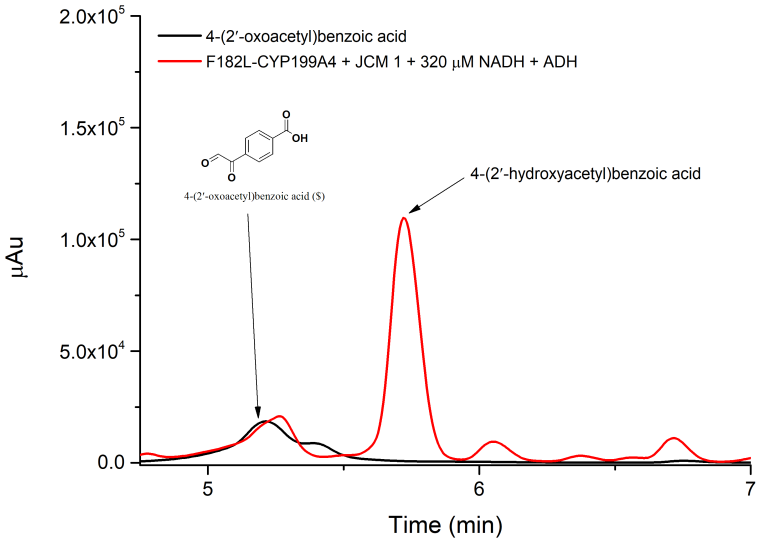

(a)

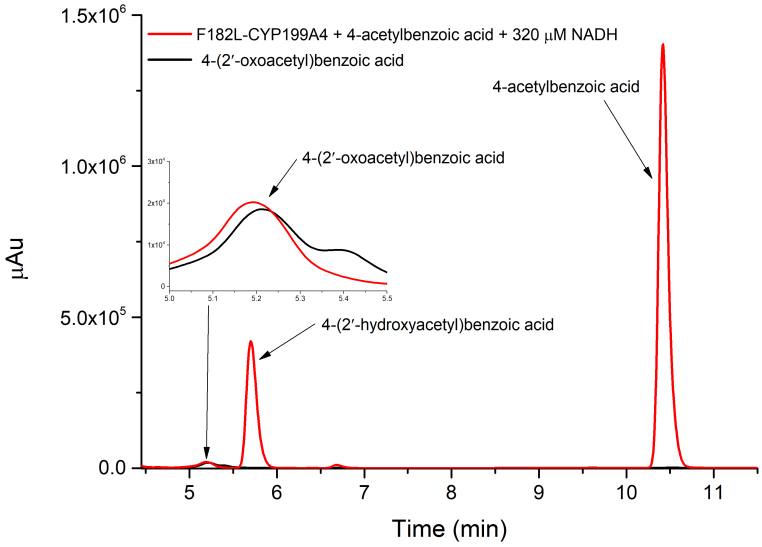

(b)

Figure D15: HPLC analysis of the co-elution experiment of 4-(2′-oxoacetyl)benzoic acid (black) with the NADH oxidation reaction of F182L-CYP199A4 with JCM 1 (a) and 4-acetylbenzoic acid (b), both shown in red.

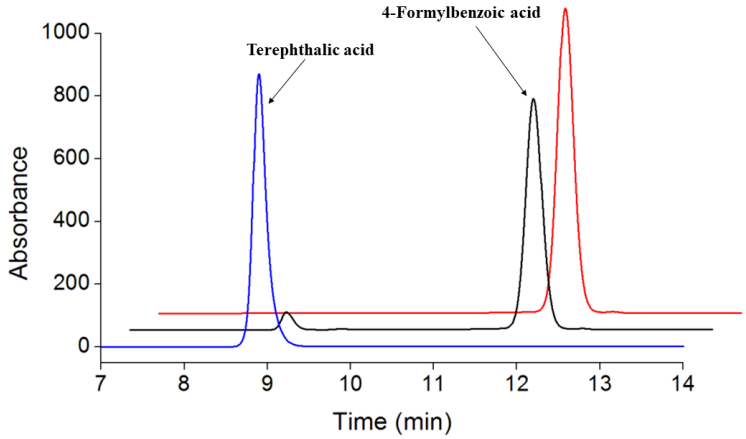

Figure D16: HPLC analysis of the reaction of WT CYP199A4 with 4-formylbenzoic acid (black) provided by Rebecca Chao co-eluted with terephthalic acid (blue) and 4-formylbenzoic acid (red).[253]

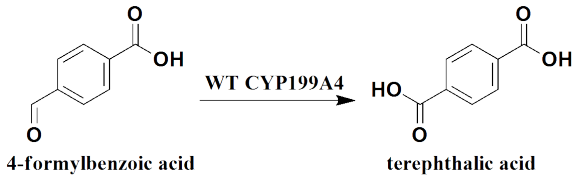

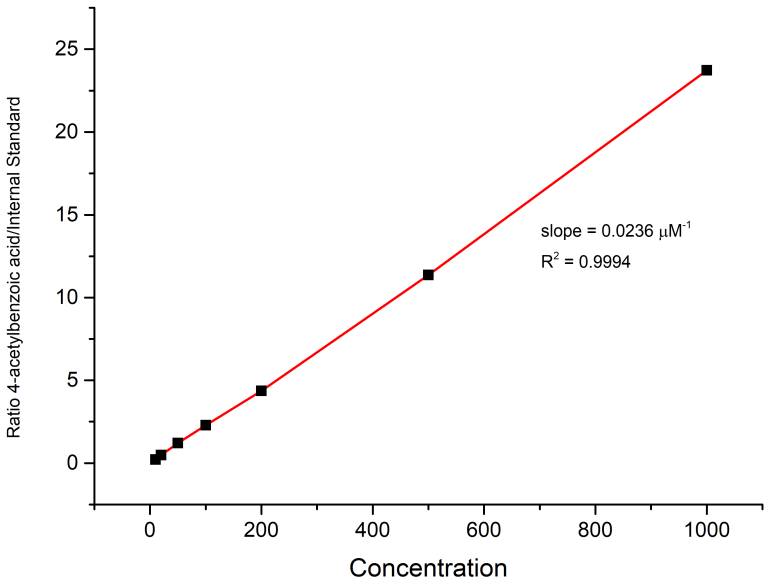

Figure D18: Calibration curve of 4-acetylbenzoic acid.

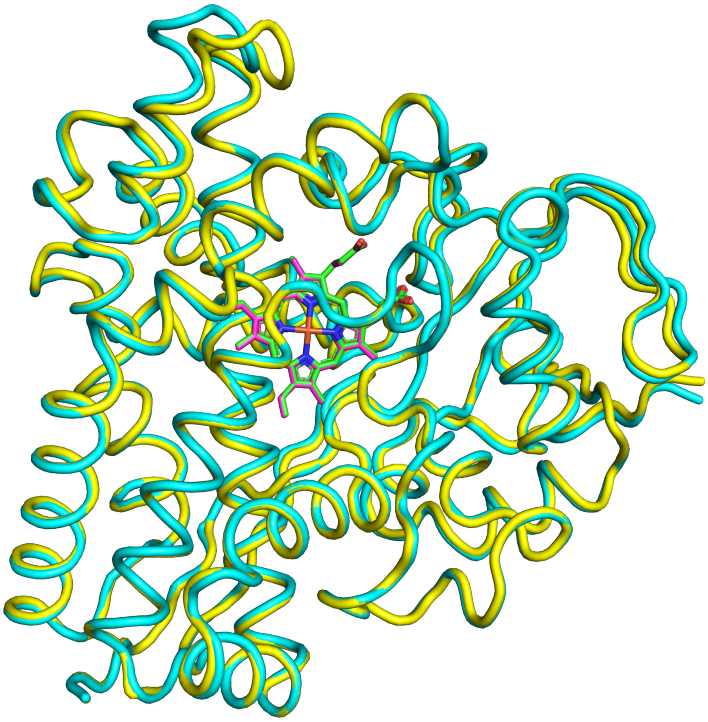

Figure D19: The superimposed structure of F182L-CYP199A4 complexed with (*S*)-JCM 1 (PDB: 8G35) with a structure of WT CYP199A4 complexed 4-methoxybenzoic acid. The RMSD between the Cα atoms is 0.492 Å over all 393 pairs.

Figure D20: The superimposed structure of F182L-CYP199A4 complexed with terephthalic acid (PDB: 8G36) with a structure of WT CYP199A4 complexed 4-methoxybenzoic acid. The RMSD between the Cα atoms is 0.597 Å over all 393 pairs.

Table D.1: B-factor comparison between W291, W267, W107 and W255 with their respective closest residues in F182L-CYP199A4.

Water Molecule	B, water	Average B, Closest Residue
W291	22.8	26.0 (T252)
W267	24.3	26.7(A243)
W107	29.36	30.4 (D251)
W255	28.2	22.478 (L182)

Table D1: Statistics for data collection and refinement of crystal structures of The F182L mutant of CYP199A4 in complex with JCM1 and JCM2.

	F182L-CYP199A4 + JCM 1	F182L-CYP199A4 + JCM 2[a]
PDB Code	8G35	8G36
Beamline	MX1	MX1
Wavelength (Å)	0.95373	0.95373
Space group	$P12_11$	$P12_11$
a/b/c (Å)	44.29/51.35/78.69	44.32/51.41/78.91
$\alpha/\beta/\gamma$	90.00/92.62/90.00	90.00/92.47/90.00
Resolution (Å)	44.25 - 2.00 (2.05 - 2.00)	44.28-2.10 (2.16-2.10)
$< I/\sigma(I) >$	12.1 (2.3)	3.4 (0.9)
Unique Reflections	23987 (1761)	20827 (1594)
Completeness	99.7 (99.9)	99.3 (94.2)
Redundancy	6.8 (6.8)	6.8 (6.6)
R_{merge} (%)	10.5 (88.5)	41.7 (192)
R_{pim}	4.3 (36.7)	17.2 (79.2)
$CC_{1/2}$	99.7 (85.7)	96.7 (41)
R_{work} (%)	17.43	20.0
R_{free} (%)	22.17	25.52
Ramachandran Plot (%)		
Most Favoured	96	96
Allowed	4	4
Outliers	0	0

[a]The electron density within the active site was more readily modelled as a terephthalic acid molecule instead of JCM 2.

Appendix E Supporting Information for Chapter 6

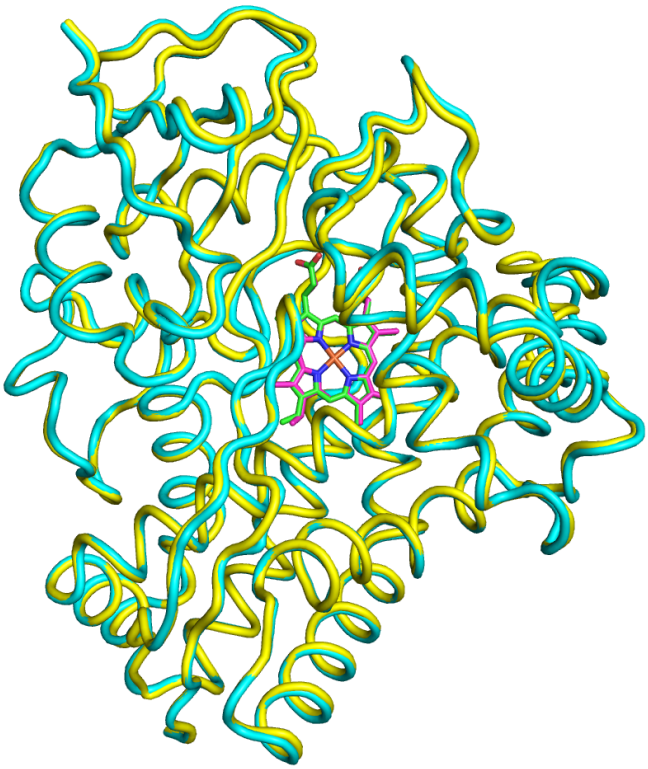

Figure E1: The superimposed structure of WT CYP199A4 complexed with 4-phenylbenzoic (7JW5) acid with a structure of WT CYP199A4 complexed 4-ethylbenzoic acid (PDB: 4EGM). The RMSD between the Cα atoms is 0.518 Å over all 393 pairs.

Table E1: Statistics for data collection and refinement of crystal structures of WT CYP199A4 in complex with 4-phenylbenzoic acid.

	WT CYP199A4 + 4-phenylbenzoic acid
PDB Code	7JW5
Beamline	MX2
Wavelength (Å)	0.95
Space group	$P12_11$
a/b/c (Å)	44.5/51.5/78.7
$\alpha/\beta/\gamma$	90.00/92.14/90.00
Resolution (Å)	44.48 - 1.53 (1.53 - 1.55)
$< I/\sigma(I) >$	8.9 (0.8)
Unique Reflections	53158 (2365)
Completeness	97.7 (87.8)
Redundancy	6.7 (5.5)
R_{merge} (%)	10.8 (147)
R_{pim}	4.5 (66.9)
$CC_{1/2}$	99.8 (43.2)
R_{work} (%)	16.6
R_{free} (%)	19.8
Ramachandran Plot (%)	
Most Favoured	97.4
Allowed	2.6
Outliers	0

GC-MS Analysis: 4-Phenylbenzoic Acid Metabolites

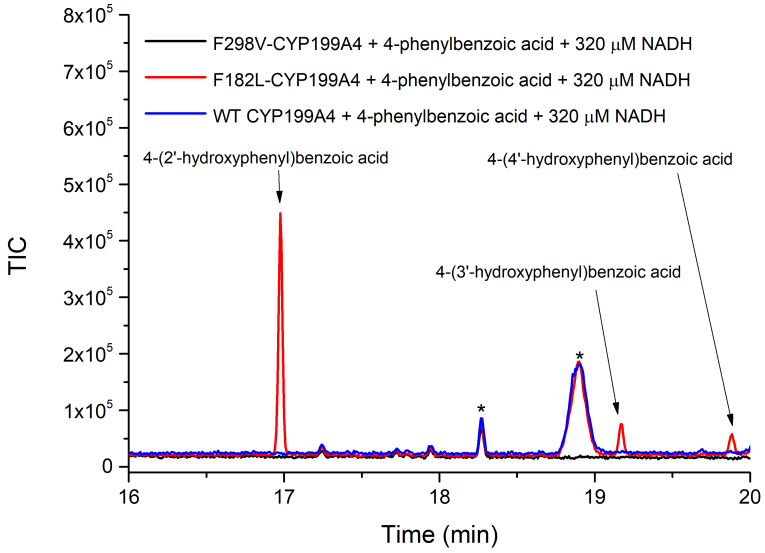

Figure E2: (a) GC-MS analysis of the NADH oxidation reaction with WT CYP199A4 and 4-phenylbenzoic acid (blue). The same reactions with CYP199A4 mutants, F182L (red) and F298V (black) can be seen also. Three different metabolites were detected in the reaction with the F182L mutant. These metabolites were identified as 4-(4′-hydroxyphenyl)benzoic acid (t_R = 19.9 min), 4-(3′-hydroxyphenyl)benzoic acid (t_R = 19.2 min) and 4-(2′-hydroxyphenyl)benzoic acid (t_R = 17.0 min). All samples were derivatised with excess BSTFA/TMCS (99:1).

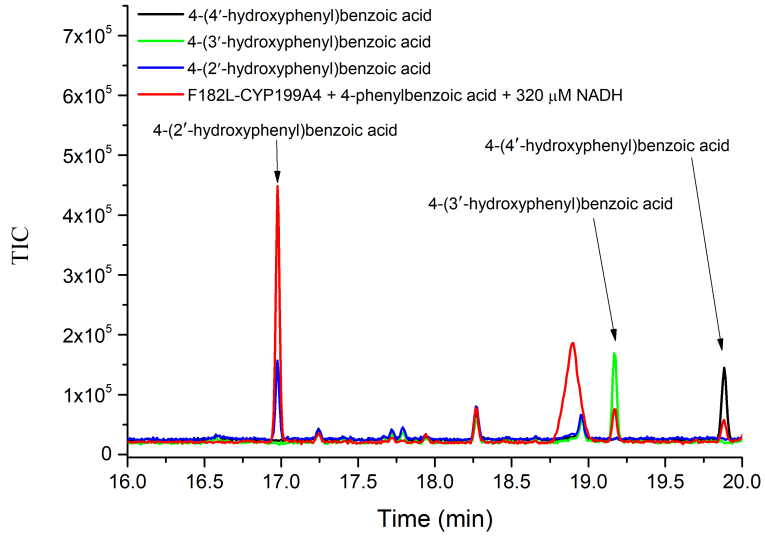

Figure E3: GC-MS analysis of the reaction between F182L-CYP199A4 and 4-phenylbenzoic acid (red). Co-elution with standards of 4-(4′-hydroxyphenyl)benzoic acid (black, t_R = 19.9 min), 4-(3′-hydroxyphenyl)benzoic acid (green, t_R = 19.2 min) and 4-(2′-hydroxyphenyl)benzoic acid (blue, t_R = 17.0 min). All samples were derivatised with excess BSTFA/TMCS (99:1).

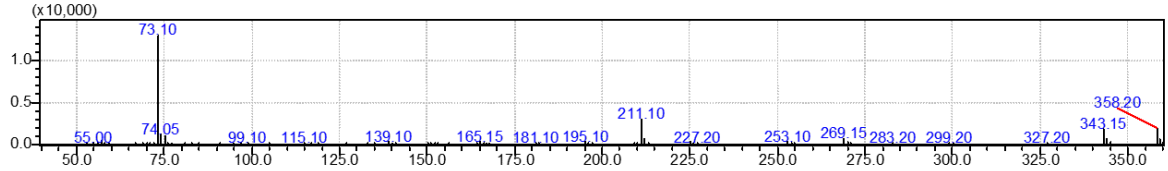

(a) Mass spectra of TMS-derivatised 4-(2′-hydroxyphenyl)benzoic acid, with m/z = 358.2 and t_R = 17.0 min

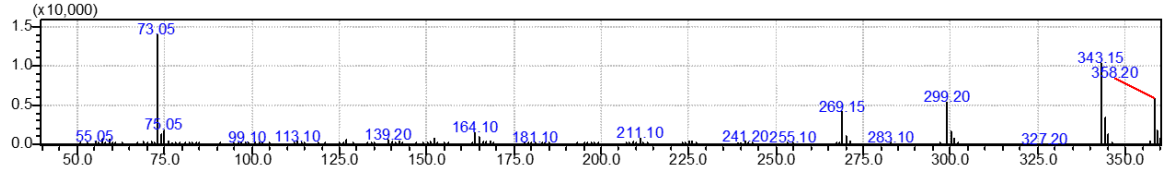

(b) Mass spectra of TMS-derivatised 4-(3′-hydroxyphenyl)benzoic acid with m/z = 358.2 and t_R = 19.2 min

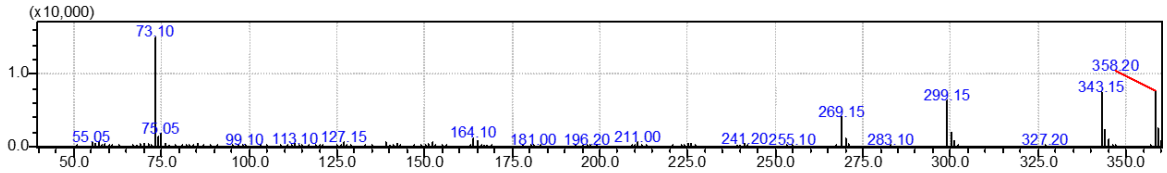

(c) Mass spectra of TMS-derivatised 4-(4′-hydroxyphenyl)benzoic acid with m/z = 358.2 and t_R = 19.9 min

Figure E4: Mass spectra of products from the 4-phenylbenzoic acid reaction with F182L-CYP199A4.

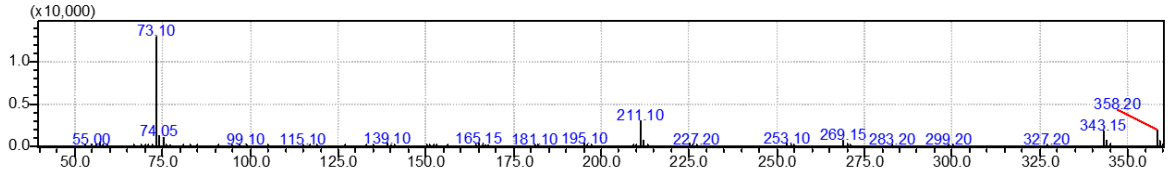

(a) Mass spectra of authentic standard of TMS-derivitised 4-(2′-hydroxyphenyl)benzoic acid, with m/z = 358.2 and t_R = 17.0 min

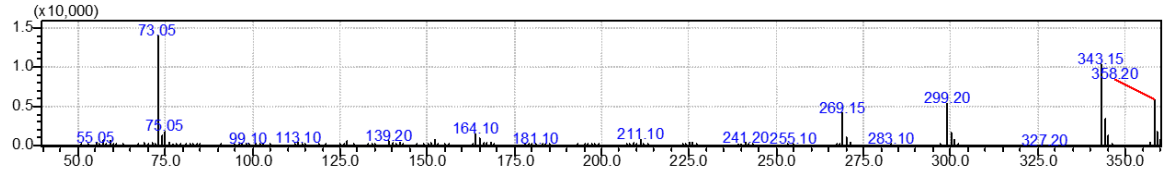

(b) Mass spectra of authentic standard of TMS-derivatised4-(3′-hydroxyphenyl)benzoic acid with m/z = 358.2 and t_R = 19.2 min

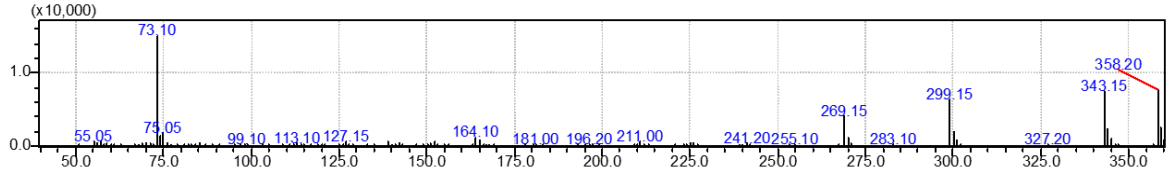

(c) Mass spectra of authentic standard of TMS-derivatised4-(4′-hydroxyphenyl)benzoic acid with m/z = 358.2 and t_R = 19.9 min

Figure E5: Mass spectra of authentic standards of hydroxylated 4-phenylbenzoic acid metabolites.

GC-MS Analysis: 4-Cyclohexylbenzoic Acid Metabolites

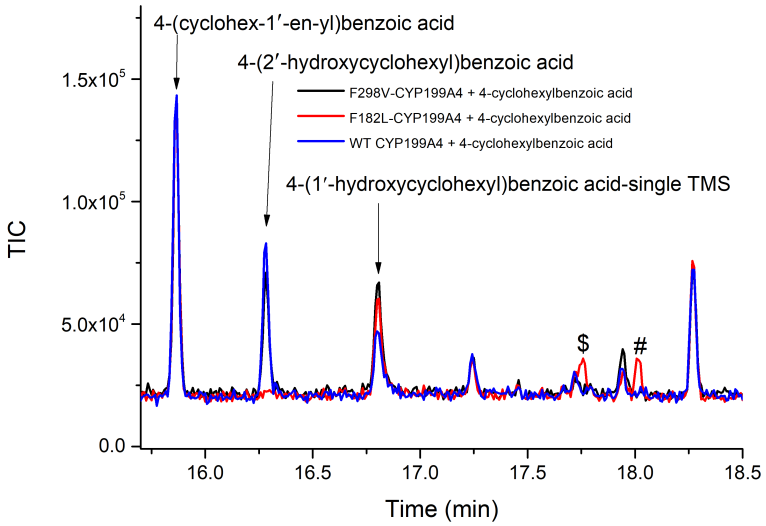

Figure E6: (a) GC-MS analysis of the NADH oxidation reaction with WT CYP199A4 and 4-cyclohexylbenzoic acid (blue). The same reactions with CYP199A4 mutants, F182L (red) and F298V (black) can be seen also. Metabolites detected and confirmed via mass spectra include 4-2′-hydroxycyclohexylbenzoic acid (t_R = 16.3 min) and and 4-(cyclohex-1′-en-yl)benzoic acid (t_R = 15.7 min). A peak potentially belonging to singly TMS-derivatised 4-(1′-hydroxycyclohexyl)benzoic acid (t_R = 16.8 min was detected also. Two unknown metabolites " $ " (t_R = 17.8 min) and " # " (t_R = 18.0 min) were detected also. MS spectra of these unknown metabolites corresponded to singly and doubly hydroxylated metabolites. All samples were derivatised with excess BSTFA/TMCS (99:1).

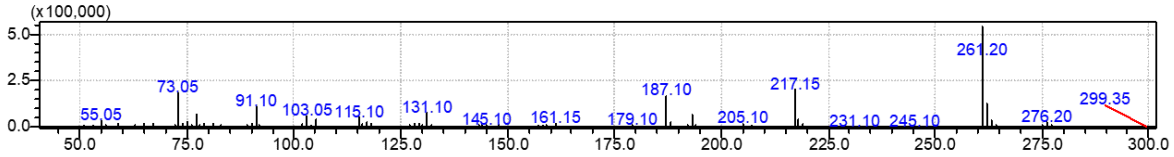

(a) Mass spectra of double TMS-derivatised 4-cyclohexylbenzoic acid as the substrate, with observed m/z = 276.2 (expected 276 m/z) and t_R = 14.8 min.

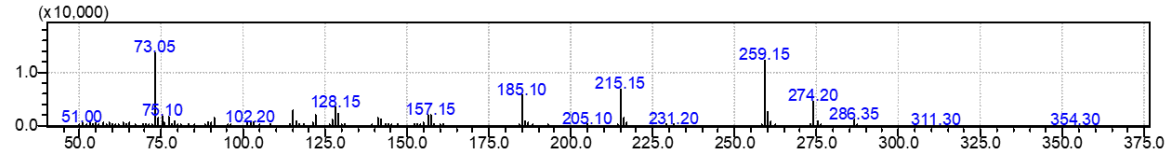

(b) Mass spectra of double TMS-derivatised 4-(cyclohex-1′-en-yl)benzoic acid with m/z = 274.2 (expected 274 m/z) and t_R = 15.7 min.

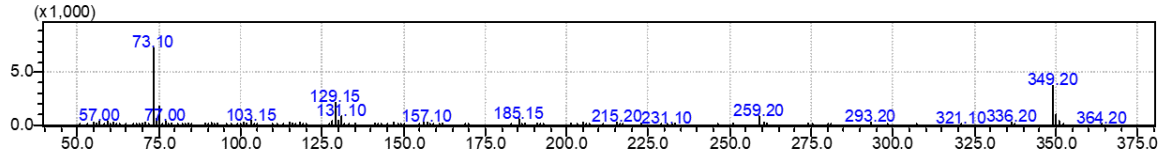

(c) Mass spectra of double TMS-derivatised 4-(2′-hydroxycyclohexyl)benzoic acid with m/z = 364.2 (expected 364.1 m/z) and t_R = 16.3 min.

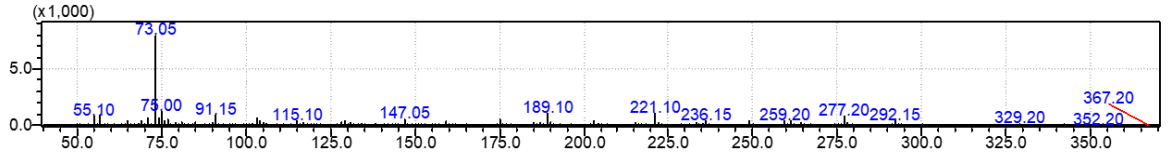

(d) Mass spectra of single TMS-derivatised 4-(1′-hydroxycyclohexyl)benzoic acid with m/z = 292.15 (expected 292.1 m/z) and t_R = 16.3 min. Metabolite was derivatised with a single TMS rather than two expected.

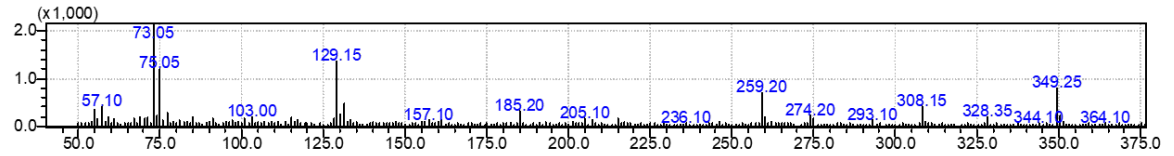

(e) Mass spectra of the peak at t_R =17.8 min with m/z = 364.1 (“ $ ”). The mass spectrum corresponded to the singly hydroxylated 4-cyclohexylbenzoic acid that has been derivatised with a single TMS. Possible identity of this metabolite could be 4-(3′-hydroxycyclohexyl)benzoic acid or 4-(4′-hydroxycyclohexyl)benzoic acid.

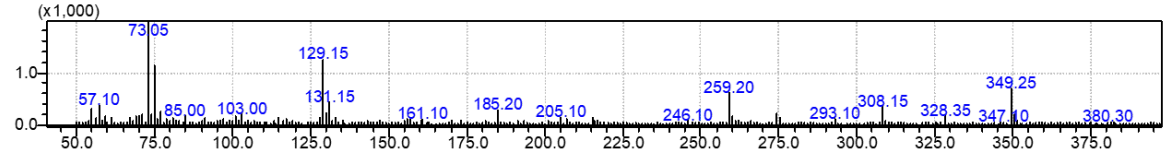

(f) Mass spectra of the peak at t_R =18 min (“ # ”) with m/z = 380. The m/z value of 380 could correspond to the doubly hydroxylated 4-cyclohexylbenzoic acid that has been derivatised twice with TMS.

Figure E7: Mass spectra of products from the 4-cyclohexylbenzoic acid reactions with CYP199A4 variants.